Interplay between Wnt signalling and SOX6 in the development of substantia nigra pars compacta (SNc) midbrain dopaminergic neurons

Thesis submitted for the degree of

Doctor of Philosophy

at the University of Leicester

by

Emma Moles-Garcia

MRC Toxicology Unit

University of Leicester

October 2020

Interplay between Wnt signalling and SOX6 in the development of substantia nigra pars compacta (SNc) midbrain dopaminergic neurons

Emma Moles-Garcia

Abstract

In Parkinson's disease (PD), degeneration of substantia nigra pars compacta (SNc) midbrain dopaminergic (mDA) neurons causes motor impairments in patients suffering from this illness. Yet, the reasons behind the selective degeneration of neuronal subpopulations and the specific mechanisms triggering PD are still unknown. However, research in mice identified Sox6 as a possible intrinsic determinant of SNc mDA neurons and their vulnerability. This thesis aims to disclose whether Sox6 plays a role in the selective vulnerability of SNc mDA neurons and to study its implication in the development of mDA neurons. To achieve this objective, this thesis established two hESC platforms generating subpopulations of SNc-like Sox6^{+} and VTA-like Otx2^{+} mDA neurons that are vulnerable and resistant to parkinsonism toxins, respectively. One platform generates Sox6^{+}mDA neurons by inhibiting Wnt signalling and was used to investigate the interplay between Sox6 and Wnt singalling. The other platform gives rise to this vulnerable subpopulation by overexpressing Sox6 and was used to determine potential Sox6 downstream targets. In addition, this thesis also characterised a new *Sox6*^{GFPCreERT} mouse line which was used for Sox6 lineage tracing to better understand the role of this transcription factor in the development of mDA neurons *in vivo*. Thus, my work was able to determine cell culturing conditions that favoured the generation of hESC-derived SNc-like mDA neurons, demonstrated that low Wnt signalling levels promoted a SNc mDA neuronal fate and identified a possible mechanism by which Sox6 could make SNc mDA neurons vulnerable.

Acknowledgments

First, I would like to thank Dr. Lia Panman for giving me the opportunity to undertake this project in her lab. Thank you to my colleagues: Dr. Pedro Garcao, Dr. Clement Soleilhavoup, Dr. Kieran Patrick and Marco Travaglio for their support, endless chats, and scientific discussions. Also, I would like to acknowledge Dr. Tony Oosterveen for the training I received culturing hESC.

I am particularly grateful to Prof. Marion MacFarlane who acquired a supervisory role while I was writing the thesis and offered me guidance and proofread the thesis.

Equally, I am especially thankful to Prof. Andrew Smith, the director of the Integrative Toxicology Training Partnership (ITTP), the PhD program that funded my PhD project. Thank you for your support throughout the PhD and for the organisation of the ITTP weeks which allowed me to meet many interesting scientists and encouraged interesting scientific debates with other PhD students.

A big thank you to Dr. Lucia Pinon in the MRC Toxicology Unit who helped me with the FACS sorting of neurons.

I would like to thank Dr. Mariah Lelos and her team, the PhD student Charlotte Bridge and Rachel Hills in the University of Cardiff, for the transplantation studies. In addition, I would like to acknowledge Valerie Labas and Lucie Combes-Soia from University of Tours in France for performing the mass spectrometry.

I finally would like to thank my mum whom support has been invaluable and always encouraged me to persevere and pursue my dreams.

Statement of contribution

This thesis is my own work and contains nothing which is the outcome of work done in collaboration with others, except as specified bellow.

In chapter III figure 3.2 shows the images of in-situ hybridisations of human embryonic tissue. I contributed to this work by synthetising the human *CORIN* in-situ probe that was used for the in-situ hybridisations done by Dr. Clement Soleilhavoup and imaged by Dr. Lia Panman. Figure 3.3 the immunohistochemistry and their imaging were done by my colleague Dr. Kieran Patrick.

In chapter IV figure 4.14 and the appendix show a western blot done by my colleague Dr. Clement Soleilhavoup. Figures 4.15 and 4.16 show mass spectrometry results. Mass spectrometry was performed by Valerie Labas and Lucie Combes-Soia from the Universite of Tours (France) in viral transfected hESC-derived mDA neurons that were cultured by my colleague Dr. Tony Oosterveen. I contributed to the mass spectrometry by performing the pathway and gene ontology analysis from the list of proteins that were identified by mass spectrometry. Figure 4.18 and figure 4.19 show images of lentiviral transduced and IWP2 exposed hESC-derived mDA neurons grafted in rats. I contributed to this work by differentiating hESC into neurons with the IWP2 and the lentivirus protocol. In addition, I dissociated the neurons in single cells for their transplantation. In the lab of Dr. Mariah Lelos at the University of Cardiff, late neuronal progenitors were transplanted into rat striatum by Dr. Mariah Lelos, Rachel Hills and Charlotte Bridge. The staining and imaging were done by Charlotte Bridge in the University of Cardiff.

In chapter V figure 5.3 was imaged and immunostained by Marco Travaglio.

Table of contents

List of tables

List of figures

Abbreviations

AD	Alzheimer's disease
ALDH1A1	Aldehyde Dehydrogenase 1 Family Member A1
ALS	Amyotrophic lateral sclerosis
BARHL1	BarH-like 1 homeobox protein
BMP4	Bone morphogenetic protein 4
BNST	stria terminalis
CALB1	Calbindin 1
Ci	Caudal linear nucleus
CNPY1	Protein canopy homolog 1
CNS	Central nervous system
CORIN	Atrial natriuretic peptide-converting enzyme
CRABP	Cellular retinoic acid-binding protein
CRD	Cysteine rich domain
DA	Dopamine
DAT	Dopamine transporter
DC	Destruction complex
DKK1	Dickkopf-related protein 1
Dvl	Dishevelled
ECAR	extracellular acidification rate
EN1	Engrailed 1
ENO	Enolase
ESC	Embryonic stem cell
ETV5	ETS translocation variant 5
FF	Fast fatigable
FGF8	Fibroblast growth factor 8
FOXA2	Hepatocyte nuclear factor 3-beta
FZD	Frizzled
GABA	Gamma-aminobutyric acid
GAD	Glutamate decarboxylase
GEF	Guanine nucleotide exchange factor
GIRK2	G protein-activated inward rectifier potassium channel 2
GLI1	Zinc finger protein GLI1
GSK	Glycogen synthase kinase-3
HD	Huntinghton's disease
hESC	Human embryonic stem cell
ICM	Inner cell mass
IF	Interfascicular nucleus
iPSC	Induced pluripotent stem cell
IsO	Isthmus organiser
IWP2	Inhibitor of Wnt production 2

IWR1	Inhibitor of Wnt response 1
JNK	Jun N-terminal kinase
LDHB	Lactate dehydrogenase B
LMO3	LIM domain only protein 3
LMX1A	LIM homeobox transcription factor 1
LRP	Low density lipoprotein receptor related protein
LRRK	Leucine-rich repeat kinase
mDA	Midbrain dopaminergic
MHB	Midbrain hindbrain boundary
NKX2.1	NK2 Homeobox 1)
NURR1	Nuclear receptor related 1
OTX2	Orthodenticle Homeobox 2
PBP	Parabrachial nuclei
PCP	Planar cell polarity
PD	Parkinson's disease
PDIA	Proein disulfide isomerase
PITX3	Pituitary homeobox 3
PKA	Protein kinase A
PKC	Protein kinase C
PN	Paranigral nuclei
PRDX	Peroxiredoxin
Rac	Ras-related C3 botulinum toxin substrate 1
RLi	Rostral linear nucleus of the raphe
RRF	Retrorubral field
SAG	Shh agonist
SATB1	SATB Homeobox 1
SERPINH	Serpin Family H Member 1
SHH	Sonic hedgehog
SNc	Substantia nigra pars compacta
SNl	Substantia nigra pars lateralis
SNr	Substantia nigra pars reticulata
SOX6	*SRY*-related HMG-box genes
SPRY	Sprouty RTK Signaling Antagonist 1
STN	Subthalamic nucleus
TF	Transcription factor
TGFβ3	Transforming growth factor beta
TH	Tirosyne hydroxylase
TKNS	Tankyrase
TPI	Triose phosphate isomerase
UPR	Unfolded protein response
Vglut2	Vesicular glutamate transporter 2
vMB	Ventral midbrain
VTA	Ventral tegmental area

Chapter 1

Introduction

Chapter 1 Introduction

1.1 Cell diversity of the nervous system

The mammalian brain is composed of a complex interconnected array of glia and neurons processing sensory information, mediating motor and cognitive behaviour as well as being able to create memories. Glia and neurons are two large and highly diverse cell populations. Glial cells consist of oligodendrocytes (produce myelin in the central nervous system), Schwann cells (produce myelin in the peripheral nervous system), astrocytes (support synaptic signalling), ependymal, choroid plexus cells (produce cerebrospinal fluid) and microglia (play a key role in the immunological response of the CNS. All the former glial cell types derive from the neuroectodermal lineage, except microglia that develops from the mesoderm (Barres, 2008; Kandel *et al.*, 2012b). Neurons can be classified into different subpopulations depending on their neurotransmitter, their function, their developmental origin, their anatomy and their molecular identity. Indeed, many studies successfully employ single-cell RNA sequencing to decipher new cell types in the nervous system based on their genetic identity (Usoskin *et al.*, 2015; Tasic *et al.*, 2016; Zeisel *et al.*, 2018). Based on the neurotransmitter they use, neurons can be grouped into glutamatergic (glutamate), GABAergic (gamma-Aminobutyric acid), glycinergic (glycine), cholinergic (acetylcholine), dopaminergic (dopamine), noradrenergic (noradrenaline), adrenergic (adrenaline), serotonergic (serotonin), histaminergic (histamine), or nitric oxidergic (nitric oxide) (Kandel *et al.*, 2012a; Zeisel *et al.*, 2018). The correct functioning of the nervous system depends on intricate protein interaction networks that regulate the proper development and functional activity of different regions of the brain. Dysregulation of this machinery due to genetic and environmental factors results in protein aggregation and subsequent neuron degeneration leading to neurodegenerative diseases such as Alzheimer's disease (AD), Parkinson's disease (PD), Amyotrophic lateral sclerosis (ALS) or Huntington's disease (HD) (Pourhaghighi *et al.*, 2020). In PD, reduced dopamine levels in the basal ganglia result in motor and cognitive impairments. Thus, research in dopaminergic neurons is key for the understanding of the disease and development of PD treatments.

1.2 Dopaminergic neurons

Research on dopaminergic neurons has been burgeoning since the early 1960s when Arvid Carlsson and colleagues identified dopamine as a neurotransmitter, they uncovered its role in motor function, mapped in greater detail dopamine neurons in the central nervous system and suggested the use of the dopamine precursor L-DOPA as a therapy to alleviate the symptoms in Parkinson's disease patients by restoring the levels of dopamine (Carlsson and Waldeck, 1958; Bertler and Rosengren, 1959; Dahlstrom and Fuxe, 1965). The neurotransmitter dopamine belongs to a group of monoamine transmitters called catecholamines characterised by a 3,4-dihydroxilated benzene ring and it is involved in the regulation of reward and voluntary movement. In the site of its release, dopamine biosynthesis is catalysed by the rate-limiting enzyme tyrosine hydroxylase (TH) that converts the essential amino acid L-tyrosine into L-DOPA, which in turn is decarboxylated by L-DOPA decarboxylase producing dopamine and CO_2. Dopaminergic neurons are among the seventeen groups of catecholaminergic neurons previously classified in the rat brain as A1-A17. In particular, the dopaminergic system is formed by ten different neuronal populations localised in the midbrain (A8, A9 and A10), hypothalamus zona incerta (A11 and A13), hypothalamus neuroendocrine system (A12, A14 and A15), olfactory bulb (A16) and retina (A17) (Figure 1.1; Dahlstrom and Fuxe, 1965).

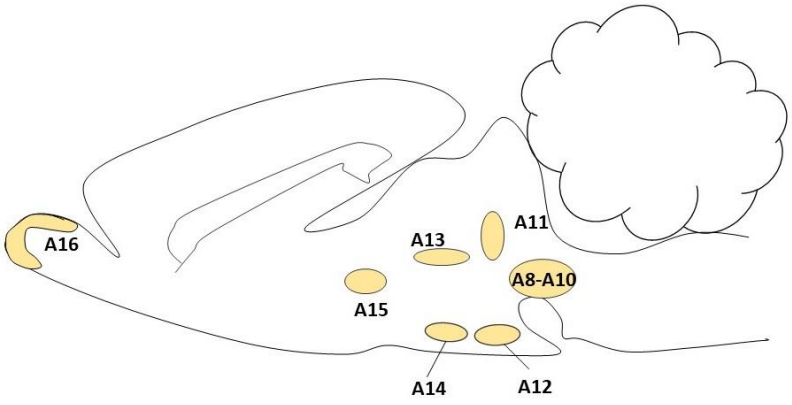

Figure 1.1 Sagittal representation of the dopaminergic neurons in the mouse brain.

1.3 Midbrain dopaminergic neurons

1.3.1 Heterogenicity of midbrain dopaminergic neurons

Midbrain dopaminergic (mDA) neurons are the largest group of DA releasing cells in the central nervous system expressing TH. This neuronal group comprises the retrorubral field (RRF), substantia nigra (SN) and ventral tegmental area (VTA), identified as A8, A9 and A10 respectively (Figure 1.2 and Figure 1.3).

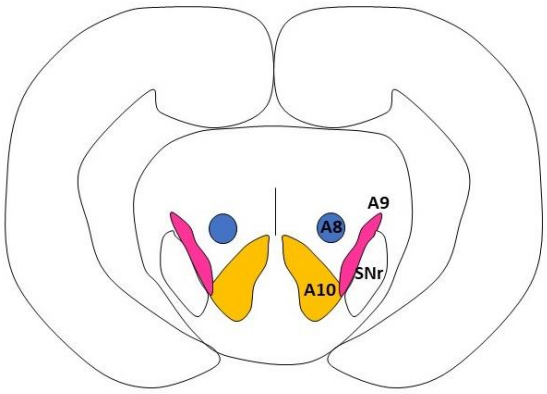

Figure 1.2 Schematic representation of the mouse midbrain and the localisation of the mDA neuronal populations. A8: RRF; A9: SNc; A10: VTA and SNr: substantia nigra pars reticulata. Adapted from Arenas et al., 2015.

The A8 group is a heterogeneous neuronal population that contains dopaminergic neurons expressing TH intermingled with GABAergic (expressing glutamate decarboxylase mRNA) and glutamatergic (expressing vesicular glutamate transporter 2 mRNA) neurons. (McRitchie, Hardman and Halliday, 1996; Nair-Roberts *et al.*, 2008; Yamaguchi, Wang and Morales, 2013). TH immunohistochemistry in the rostral midbrain of the rat, revealed that the A8 dopaminergic neurons appear as a group of cells forming a bridge that crosses from the rostral-lateral SN to the lateral VTA. In a more caudal region of the midbrain, two aggregates of A8 dopamine neurons can be distinguished. The dorsal part of the A8 group can be differentiated from the ventral part. A similar organisation has been described in macaques and monkeys, with the cell bridge also present. In humans, RRF neurons are situated dorsally and medial to the medial lemniscus (Deutch *et al.*, 1988). The study of projections in rat revealed that the RRF dopaminergic neurons contribute to the mesolimbic innervation by projecting to the hippocampus (Gasbarri *et al.*, 1996), amygdala, the striatum (nucleus accumbens

and particularly the ventral lateral area of the caudate putamen), bed nucleus of the stria terminalis, olfactory tubercle, along with their mesocortical projections to the prefrontal cortex (Figure 1.4). The DA neurons in the RRF reach the diencephalon by passing through the SN and VTA regions and connect with other DA neurons in the VTA (Deutch *et al.*, 1988). On the other hand, the GABAergic neuronal population of the RRF projects to the parvicellular reticular formation and receives the innervation of the central amygdaloid nucleus (von Krosigk *et al.*, 1992; Tsumori *et al.*, 2010). Because of their connections with the limbic areas of the brain, the RRF dopaminergic neurons control emotional behaviour, natural motivation, reward, cognitive functions and are being involved in a variety of psychiatric diseases.

SN neurons are laterally located neighbouring the VTA neuronal population. They are anatomically divided into the SN pars compacta (SNc), a dense compacted neuronal region, displaying a dorsolateral extension known as SN pars lateralis (SNl), and the SN pars reticulata (SNr) consisting of sparsely organised neurons situated ventrally between the SNc and the cerebral peduncles (Figure 1.3)(Falck *et al.*, 1962; Richards, Shiroyama and Kitai, 1997; González-Hernández and Rodríguez, 2000; Bentivoglio and Morelli, 2005; Yamaguchi, Wang and Morales, 2013). In humans and primates, SNc and SNl neurons are distinguished from SNr by the presence of neuromelanin, a brown pigment enclosed in cytoplasmatic granules. In contrast, there is scarcely a difference between these neuronal types in rodents, given that neuromelanin is not present (Yelnik *et al.*, 1987; Halliday *et al.*, 2006). As with the RRF neuronal population, SN and VTA neuronal populations are constituted by different types of neurons. Studies in rat showed that the SNr neuronal population comprises a mixture of GABAergic neurons, localised in the rostromedial region, expressing the GABA synthetizing enzyme GAD and dopaminergic neurons (around 20%), expressing TH, in the caudal area (Richards, Shiroyama and Kitai, 1997; González-Hernández and Rodríguez, 2000; Ding, Wei and Zhou, 2011). Interestingly, these GABAergic and DA neurons present a compartmentalised and complementary distribution, with clusters of only TH or GAD expressing neurons (González-Hernández and Rodríguez, 2000). Moreover, a glutamatergic neuronal population, expressing VGlut2, has been reported in the dorsal SNr with no TH coexpression (Yamaguchi, Wang and Morales, 2013). On the other hand,

the SNc subdivision is mainly constituted of dopaminergic neurons expressing TH. However, other neuronal types have also been identified. For instance, it has been described a population of glutamatergic neurons expressing Vglut2 but lacking TH expression in the SNc of rat, primates and humans. In the rat SNc, VGlut2 expressing neurons are mostly located in the dorsal and lateral areas and only a very small proportion of VGlut2 neurons expresses TH (Yamaguchi, Wang and Morales, 2013; Poulin *et al.*, 2018). In the rat SNl, the number of VGlut2 neurons increases in the caudal levels (Yamaguchi, Wang and Morales, 2013). In the marmoset and the human, SNc is dominated by dopaminergic neurons expressing only TH, with a small population of VGlut2 neurons located in the ventral part of the human SNc. The SNl of human and marmoset contains VGlut2 neurons intermingled with TH neurons and only a small percentage coexpress Vglut2 and TH (Root *et al.*, 2016). The different subpopulations in the SN project to distinct targets so they can regulate specific functions. Dopaminergic neurons located in the ventral tier of the SNc control motor functions by innervating the caudate-putamen (dorsolateral striatum) via the nigrostriatal pathway. In contrast, dopaminergic neurons localised in the dorsal tier contribute to the projection of the nucleus accumbens. Furthermore, a dopaminergic subpopulation expressing VGlut2 in the lateral SNc contributing to the innervation of the amygdala has been recently discovered (Figure 1.4; Poulin *et al.*, 2018). Although SNc neurons have been normally linked to motor functions, a dorsolateral SNc neuronal population responding to reward and aversive stimuli and neurons located ventromedial in the SNc responding to only reward stimuli have been identified in nonhuman primates (Matsumoto and Hikosaka, 2009). These results support the idea of functional diversity in the SNc, with the dorsolateral SNc neuronal population corresponding to the glutamatergic neurons located in the SNl as previously described in the marmosets (Root *et al.*, 2016).

The VTA neuronal population is medially located in the midbrain, flanked by SN neurons. It consists of two main lateral nuclei (parabrachial (PBP) and paranigral nuclei (PN)) and three midline nuclei (caudal linear nucleus (Cli), interfascicular nucleus (IF) and rostral linear nucleus of the raphe (RLi; Figure 1.3).

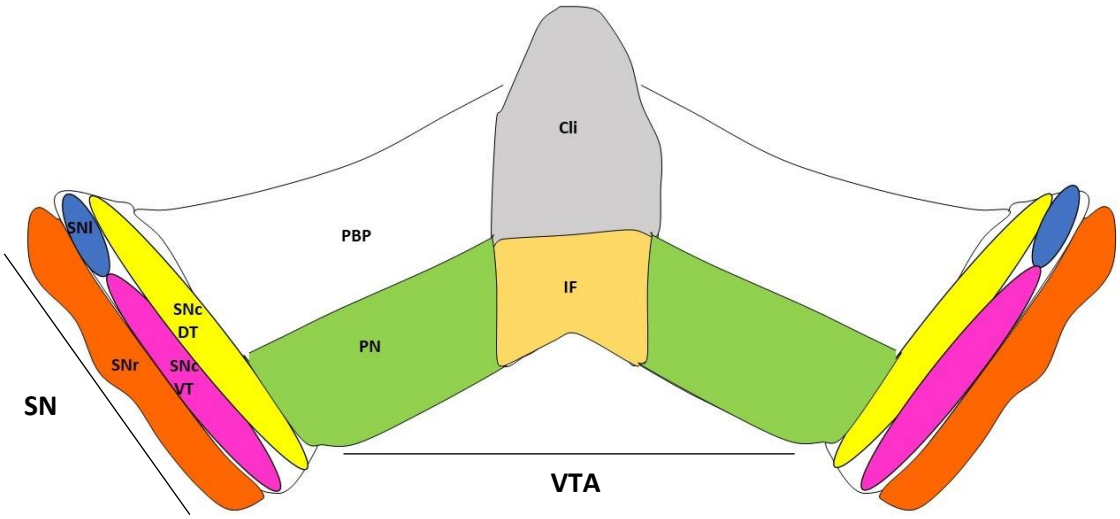

Figure 1.3 Coronal view of the mouse midbrain and the distinct neuronal populations. Coronal illustration of the mDA neuronal subpopulations. Medial VTA: Cli, Caudal linear nucleus; IF, Interfascicular nucleus and Rli, Rostral linear nucleus of the raphe (caudal nucleus not represented). Lateral VTA: PBP, parabrachial nuclei and PN, paranigral nuclei. SN: SNc DT and VT, substantia nigra pars compacta dorsal tier and ventral tier, respectively; SNl: substantia nigra pars lateralis and SNr: substantia nigra pars reticulata.

Just as the A8 and A9 groups, the VTA population comprises GABAergic, glutamatergic and dopaminergic neurons. However, this population also presents some neurons displaying combinatorial neurotransmitter characteristics. In fact, it has been reported that some VTA neurons co-release dopamine and glutamate, dopamine and GABA or glutamate and GABA. Neurons co-expressing TH and VGlut2, and releasing dopamine and glutamate, represent a small percentage of the total VTA dopaminergic or glutamatergic neurons and are principally localised in the midline nuclei of the VTA (Stuber *et al.*, 2010). The proportion of glutamate and glutamate-dopamine neurons is lower in the marmosets, which present a dominance of dopamine only neurons, in comparison to mice and rats (Root *et al.*, 2016). Although a small number of co-labelled TH and GAD VTA neurons has been identified in rats and mice, only GABA but no dopamine release has been detected in these TH-GAD neurons (Stamatakis *et al.*, 2013). The VTA also contains neurons that do not express TH but show co-expression of *VGlut2* and *GAD* mRNA by in-situ hybridisation and release GABA and glutamate. Interestingly, these neurons are the main constituent of the VTA innervation to the lateral habenula (Root *et al.*, 2014). Furthermore, VTA dopaminergic neurons project to the hippocampus, nucleus accumbens (ventromedial striatum) and amygdala forming the mesolimbic pathway and they innervate the prefrontal cortex via the mesocortical

pathway (Stott and Ang, 2013; Morales and Margolis, 2017). They also target the stria terminalis (BNST), olfactory tubercle (OT) and locus coeruleus (Figure 1.4; Morales and Margolis, 2017). Given the fact that these neurons innervate the cortex and limbic system, they play a role in cognitive functions. Evidence suggests that the A10 neuronal population, is involved in regulating reward and aversion, motivation, learning as well as its implication in psychiatric disorders such as drug addiction. Research showed that VTA mDA neurons signal learning about reward-predicting cues. When the learning starts and the association cue-reward is weak, VTA mDA neurons are activated by unpredicted reward stimuli. As learning improves, VTA dopaminergic neurons activate to cues that predict the reward, instead of being activate by the reward stimuli. Another study showed that VTA dopaminergic neurons can be inhibited by a spontaneous or predicted stimuli and suggested that these neurons could play a role in learning to approach rewards and avoid aversive stimuli (Matsumoto and Hikosaka, 2009; Morales and Margolis, 2017).

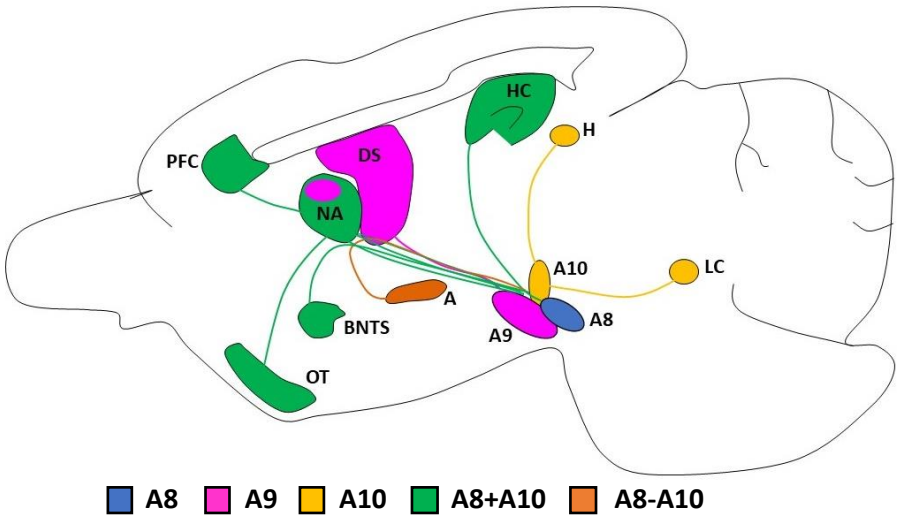

Figure 1.4 Diagram illustrating the projections of mDA neurons in the adult mouse brain. Sagittal view of the mDA neuronal populations and their projections. A8: retrorubral field; A9: substantia nigra; A10: ventral tegmental area; A8+A10: regions innervated by A8 and A10 neuronal populations; A8-A10: regions innervated by A8, A9 and A10 neuronal populations. Adapted from Arenas et al., 2015.

1.3.2 Parkinson's disease and selective vulnerability of SNc dopaminergic neurons

Parkinson's disease is a common and complex neurodegenerative disorder first described by James Parkinson in 1817. Patients suffering from this condition are diagnosed because of the motor symptoms they present including bradykinesia, rigidity, tremor, or postural instability. Although, these are the most well-known clinical signs of the disease, patients also present an onset of non-motor symptoms some of which are characteristic of a pre-motor period (that can last more than 20 years) such as constipation, REM sleep behaviour disorder, depression or hyposmia. The origin of the disease continues to be unidentified, yet it is understood to result from an interplay of genetic and environmental factors disturbing neuronal processes (Kalia and Lang, 2015). In some patients, there is an inheritable predisposition to suffer from this illness. Indeed, several genetic mutations linked to an autosomal dominant or recessive form of Parkinson's disease have been identified. For example, duplications and triplications in the *SNCA* gene coding for α-synuclein or missense mutations in the *LRRK2* gene have been related to the autosomal dominant form of Parkinson's disease, whereas mutations in *Parkin* are associated to the autosomal recessive form of it (Kitada *et al.*, 1998; Singleton *et al.*, 2003; Chartier-Harlin *et al.*, 2004; Zimprich *et al.*, 2004). It has also been described that exposure to certain environmental factors, such as herbicides, pesticides or heavy metals can also cause parkinsonian symptoms. One of the most studied chemical compound is the MPTP, a by-product issued from the production of an injectable synthetic drug that was discovered to be causing parkinsonism in drug addicts in the early 1980s. MPTP can cross the brain barrier to be metabolised into MPP^+ which is subsequently transported into the dopaminergic neurons by DAT and inhibits the complex I of mitochondria (Przedborski and Vila, 2001). In addition to MPTP, some pesticides, such as rotenone, have also been shown to inhibit the complex I of the mitochondria. Although a direct association between Rotenone and Parkinson's disease in humans has not been demonstrated, it has been shown to reproduce certain parkinsonian clinical signs such as rigidity or tremor in rats, along with pathological features like SNc dopaminergic neuronal degeneration and presence of Lewy bodies-like structures in these neurons (Betarbet *et al.*, 2000). The heavy metal manganese

(Mn) has also a clear association with Parkinson's disease symptoms as was seen in drug addicts that injected high doses of this metal. Intoxication with Mn, resulted in individuals presenting clinical symptoms similar to the ones suffered by Parkinson's disease patients such as tremor or bradykinesia, but individuals did not respond to L-DOPA therapy and presented normal levels of dopamine in the striatum (Neal and Guilarte, 2013).

The motor impairments that Parkinson's disease patients experience, are caused by a degeneration of dopaminergic neurons localised in the ventrolateral tier of the SNc and the loss of striatal dopamine in the caudate-putamen. Interestingly, the neighbouring developmentally related VTA dopaminergic neurons remain relatively spared (Kordower *et al.*, 2013; Surmeier, Obeso and Halliday, 2017). The investigation of a set of post-mortem human brains determined that SNc neurons which were TH positive decreased markedly by 50%-90% over the course of the disease, as well as the melanized neurons (30%-80%). In the putamen, a 35%-75% loss of TH and dopamine transporter fibre density was reported during the first three years, reaching 90% by the fifth year, after Parkinson's disease diagnosis (Kordower *et al.*, 2013). Another pathological feature of Parkinson's disease is the presence of Lewy bodies resulting from the assembly of α-synuclein misfolded monomers into toxic oligomeric forms, which in turn aggregate into Lewy bodies (Kovacs *et al.*, 2012). Even though, several hypotheses have arisen to explain the selective vulnerability of SNc dopaminergic neurons in Parkinson's disease, this question remains unsolved. One of the theories is the Braak model which considers that misfolded α-synuclein could act as a prion by moving from the enteric nervous system to the central nervous system via the preganglionic fibres of the vagal nerve. According to this hypothesis Lewy pathology follows a coherent pattern with temporal and spatially related stages (Braak, Rüb, *et al.*, 2003). It starts at stage 1 in the dorsal motor nucleus and olfactory system, continuing to the pons (locus ceruleus, medullary raphe nuclei and giganto cellular nucleus) in stage 2, attaining the midbrain (SNc dopaminergic neurons) at stage 3, progressing to the mesocortex, allocortex and limbic system in stage 4 and finally reaching the neocortex in stages 5 and 6 (Braak, Del Tredici, *et al.*, 2003). Different studies in mice support Braak's theory. For instance, by showing that the microbially produced short-chain fatty acids metabolites play a role in

promoting α-synuclein pathology, neuroinflammation and motor dysfunction (Sampson *et al.*, 2016). Another example is the recent research demonstrating that injection of α-synuclein preformed fibrils in mice gut can spread to their brain, causing SNc dopaminergic neuronal degeneration and that this phenomenon could be stopped by truncal vagotomy or in *Snca* knockout mice (Kim *et al.*, 2019). Additional hypotheses include the association of T lymphocyte neural inflammation with neuronal death in Parkinson's disease (Sommer *et al.*, 2018) or that the selective vulnerability of SNc is linked to a high basal metabolic rate. These neurons contain an elevated density of mitochondria and possess large axonal arborisations. Therefore, their energy demands are increased along with their basal oxidative stress resulting in a higher vulnerability of SNc mDA neurons to many factors such as aging, toxic insults or genetic mutations (Pacelli *et al.*, 2015). Besides the previous theories, research also focuses in deciphering the molecular mechanisms involved in neuronal degeneration. For instance, the special AT-rich sequence-binding protein 1 (SATB1) has been identified as a neuroprotective factor which is highly expressed in the SNc vulnerable subpopulation (Brichta *et al.*, 2015). This DNA-binding protein is required for the survival of mature hESC derived midbrain dopaminergic neurons and to avoid p21 induced senescence *in vivo* in the PD vulnerable dopaminergic subpopulation (Riessland *et al.*, 2019). Thus, understanding the development of mDA neurons is key to gain an insight into the selective sensitivity of SNc mDA neurons which are affected in Parkinson's disease and will help to decipher the molecular basis of this illness.

1.4 Development of SN and VTA dopaminergic neurons

1.4.1 Gastrulation and establishment of the neural plate

In the developing embryo, the formation of the anterior-posterior axis takes place alongside with the establishment of the three germ layers (endoderm, mesoderm and ectoderm) during the gastrulation. Indeed, it has been observed in chick that before this process occurs, the hypoblast (layer of cells derived from the inner cell mass and in contact with the blastocoel) expresses FGF which seems to sensitise the epiblast to

neuronal induction factors, such as BMP antagonists (Streit *et al.*, 2000). In chick, gastrulation initiates with the invagination of the cells in the epiblast in the posterior part of the embryo leading to the formation of the primitive streak. The migrating cells undergo an epithelial-to-mesenchymal transformation forming the endoderm, mesoderm, and ectoderm (Gilbert and Barresi, 2016). The presumptive endoderm progressively moves the hypoblast to the anterior end of the embryo, allowing the elongation of the streak (Bertocchini and Stern, 2002). In gastrulation, the node, a thickening of epiblast cells localised in the anterior part of the streak, is responsible for the anterior-posterior patterning of the mouse. The posterior region of the embryo is defined by a gradient (progressively decreases in the anterior area) of the signalling molecules, Nodal, FGFs, Wnts, BMPs and retinoic acid, while in the anterior part of the embryo the node secretes Wnt and BMP inhibitors (Gilbert and Barresi, 2016). Another phenomenon that occurs during gastrulation is the decision of the ectoderm to adopt an epidermal fate. It has been found that the bone morphogenesis protein 4 (Bmp4), which is strongly expressed in the ectoderm during gastrulation, is a potent inducer of the epidermis (Wilson and Hemmati-Brivanlou, 1995). Therefore, for the ectoderm to become the neural plate, Bmp4 activity must be inhibited by chordin and noggin, two organiser factors expressed in the node (Wilson and Hemmati-Brivanlou, 1995; Bachiller *et al.*, 2000). Thereafter, the neural plate folds into a tubular structure, the neural tube, and its patterning is directed by the establishment signalling centres instructing the positioning of the cells throughout the dorsal-ventral and anterior-posterior axes.

1.4.2 The morphogens Shh, Wnt and FGF8 govern the development of mDA neurons

In the midbrain, two signalling centres are formed: the floor plate and the isthmus organiser (IsO), situated in the midbrain-hindbrain boundary (MHB). The floor plate secretes the morphogen Sonic Hedgehog (Shh), which patterns the dorsoventral axis, while the IsO secretes the factors FGF8 and Wnt-1 establishing the rostral-caudal axis (McMahon and Bradley, 1990; Martí *et al.*, 1995; Ye *et al.*, 1998; Jeong and Epstein, 2003). Indeed, the combined action of these morphogens alongside with transcription

factors are essential for the development of mDA neurons (Ye *et al.*, 1998; Prakash *et al.*, 2006). The localisation and establishment of the IsO is governed by the reciprocal repression of Otx2 and Gbx2 which also mark the development of the midbrain and the hindbrain, respectively (Wassarman *et al.*, 1997; Broccoli, Boncinelli and Wurst, 1999; Millet *et al.*, 1999). In addition to Gbx2, FGF8 is also crucial for the maintenance of the MHB. This factor acts as a gradient, being highly expressed in the anterior hindbrain close to the IsO and progressively decreasing towards the caudal hindbrain (Sunmonu *et al.*, 2011). In contrast, Wnt-1 is secreted in the midbrain and its expression is maintained by FGF8 (Figure 1.5; Chi *et al.*, 2003).

Another major event involved in the development of the midbrain is the establishment of the floor plate. This signalling centre is ventrally located in the midline of the neural tube and extends from the diencephalon to the spinal cord. Interestingly, the floor plate is a very heterogeneous organising centre with its constituting cells presenting molecular and morphological differences. In addition, the specification processes as well as the origin of the distinct anterior-posterior floor plate levels differ (Placzek and Briscoe, 2005). This organising centre, is induced by the expression of a Shh gradient, highly expressed ventrally and gradually decreasing towards the roof plate. Interestingly, in chick embryos, Shh secreted from the prechordal mesoderm (cluster of axial mesoderm cells situated in front of the notochord) seems to be essential for the induction of the floor plate cells in the midbrain (Patten *et al.*, 2003). In mice, Shh activates FOXA2, which subsequently promotes the expression of Shh in the ventral midbrain (vMB; Figure 1.5; Mavromatakis *et al.*, 2011).

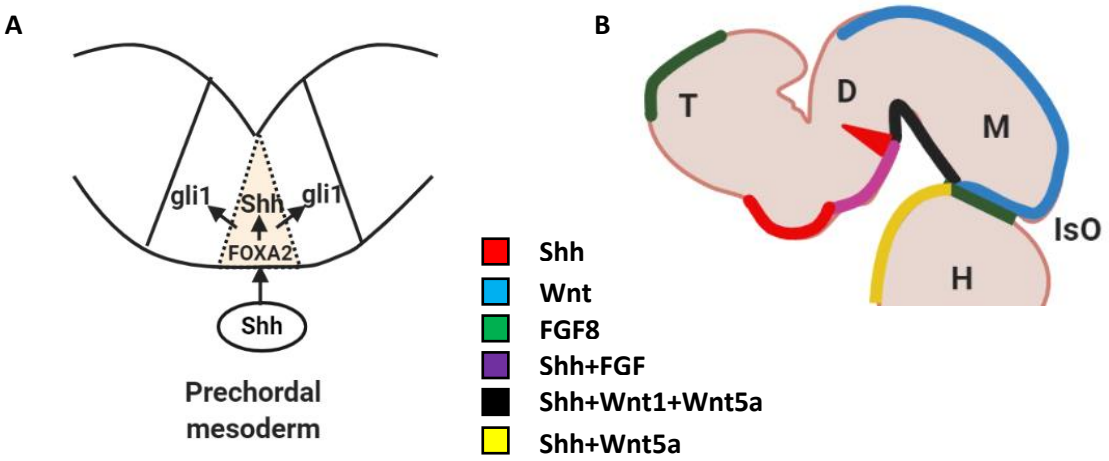

Figure 1.5 Schematic representation of the initial processes directed by the floor plate and the isthmus organiser (IsO) for the development of mDA neurons in mouse. (A) Coronal view of the floor plate at E8.5. Shh which is expressed in the prechordal mesoderm, activates FOXA2, which in turn induces Shh expression in the medial floor plate of the midbrain. Interestingly, Gli1 expression is laterally located to Shh in the medial floor plate, with no overlap. During the development of the mouse, Gli1 and Shh expression will move laterally in the ventral midbrain, always next to each other. (B) Sagittal view of an E11.5 mouse embryo localising the expression of the morphogens involved in the patterning of the ventral midbrain. In the IsO, FGF8 is expressed in the hindbrain whilst Wnt is induced in the midbrain leading to the patterning of the two regions. D, diencephalon; H, hindbrain; M, midbrain; T, telencephalon. Figure 1.5 B adapted from Arenas et al. 2015.

1.4.3 Understanding Wnt and Shh signalling pathways

1.4.3.1 Canonical and non-canonical Wnt signalling pathways

Wnt proteins are growth factors which orchestrate developmental processes. They induce cell proliferation by stimulating the expression of factors, such as cyclin D1, that regulate the cell cycle (Tetsu and McCormick, 1999). At the same time, Wnt proteins act as organisers, patterning the embryonic axis (Nordström, Jessell and Edlund, 2002; Kitajima *et al.*, 2013) inducing cell polarity (Goldstein *et al.*, 2006) and differentiation (Chung, Leung, B. Han, *et al.*, 2009). Multiple genes codify for this large family of proteins in different animal species ranging from invertebrates to humans. In invertebrates, 11 Wnt genes have been identified in *Hydra,* 7 in *Drosophila* and 5 in *C.Elegans*. In vertebrates, 19 Wnt genes have been identified in human, 19 in mouse, *Xenopus* and 23 in Zebrafish (Nusse, 2001). Interestingly, individual Wnts seem to have specific functions and their elimination causes the appearance of distinctive morphological phenotypes matching their area of expression. For instance, some

studies determined that in Wnt1 (which is expressed in the MHB and throughout the midbrain as a gradient) mutant mice the midbrain and anterior hindbrain failed to develop (Figure 1.5; McMahon and Bradley, 1990), while in Wnt4 (ventrally expressed in the metanephric mesenchyme) mutants, metanephric development is impaired (Stark *et al.*, 1994). In addition, Wnt proteins are evolutionarily conserved and orthologs can be found through the animal phyla. For example, *Drosophila* Wnt proteins wg, DWnt6, and DWnt10, which are encountered adjacent to each other forming a cluster, present orthologs in humans called WNT1, WNT6 and WNT10 respectively. Intriguingly, this cluster has been preserved in humans in two chromosomes organised as WNT1-WNT10B and WNT6-WNT10A (Nusse, 2001).

Wnt proteins are 40kDa in size and very hydrophobic, partly due to the post-translational modification by the attachment of a lipid (Willert *et al.*, 2003). In the endoplasmic reticulum, the acyltransferase Porcupine, transfers an acyl group called palmitoleic acid to the conserved serine and cysteine of Wnt3a (Tanaka, Kitagawa and Kadowaki, 2002; Takada *et al.*, 2006). Indeed, it has been suggested that palmitoleoyl CoA, obtained from the conversion of palmitoyl CoA by the enzyme stearoyl CoA desaturase, is used by Porcupine as a substrate being able to transfer the unsaturated fatty acid to Wnt (Rios-Esteves and Resh, 2013). Once lipidated, the Wnt protein binds to the transmembrane protein Wntless/Evi (WIs) in order to be secreted on exocytic vesicles (Korkut *et al.*, 2009; Gross *et al.*, 2012). In this model, WIs are crucial for the transport of Wnt, which travels anchored externally to the exosome via this transmembrane protein (Figure 1.6; Korkut *et al.*, 2009). In order to exert their functions, Wnt proteins regulate three distinct pathways: the canonical Wnt/β-catenin pathway as well as the non-canonical Wnt/planar cell polarity (PCP) and Wnt/calcium (Ca^{2+}) pathways.

The Wnt/β-catenin pathway is activated with the binding of Wnt to the receptor complex of two molecules, Frizzled (FZD) and the Low-density lipoprotein receptor related proteins 5 and 6 (LRP5/6). The receptor FZD, is formed by a 7 transmembrane domain with a cysteine-rich domain (CRD) linked to it (Bhanot *et al.*, 1996). It has been found that Wnt binds with the receptor FZD throughout the CRD domain. In *Xenopus*, Wnt8 (XWnt8), interacts with two binding sites of the CRD domain. In one site, the

palmitoleic acid group attached in the serine of Wnt projects to a groove in the CRD. In the other binding site, hydrophobic aminoacids make the contact XWnt8-CRD (Janda *et al.*, 2012). In the active Wnt/β-catenin pathway the cytoplasmatic protein β-catenin is translocated to the nucleus to regulate gene expression. This depends on the stability of β-catenin which is controlled by the destruction complex (DC). This complex is composed by the protein axin which acts as a scaffold, binding to β-catenin, the protein APC and two serine-threonine kinases (CK1 and GSK3). Another protein required for the activation of the pathway is Dishevelled (Dvl) which binds, throughout its 3 conserved domains PDZ, DEP and c-terminus, to the FZD receptor c-terminal. The Dvl DIX domain, does not attach to FZD, being able to interact with possible downstream targets (Tauriello *et al.*, 2012). When the receptors FZD/LRP are ligand free, CK1 and GSK3, consecutively phosphorylate β-catenin. Firstly, β-catenin N-terminal is phosphorylated by CK1-Axin complex at the Ser45 residue and subsequently GSK3 phosphorylates at the Th41, Ser37 and Ser33 residues (Amit *et al.*, 2002; Liu *et al.*, 2002). This phenomenon causes the recognition of β-catenin by the protein β-TRCP, which couples the β-catenin phosphorylation-ubiquitination process resulting in proteasomal degradation of β-catenin (Hermann *et al.*, 1997; Liu *et al.*, 1999). In the nucleus, TCF is inactive by binding to Groucho and acting as a transcriptional repressor (Cavallo *et al.*, 1998). Conversely, the binding of Wnt with the CRD domain of FZD, triggers the heterodimerization of FZD and LRP5/6, which are located in close proximity (Janda *et al.*, 2017). Consequently, LRP5/6 is phosphorylated at its PPPSP motif, located in its cytoplasmatic end, being able to bind Axin (Tamai *et al.*, 2004). In addition, the phosphorylated LRP could also inhibit GSK3 directly leading the stabilisation of β-catenin (Stamos *et al.*, 2014). Thus, the intracellular concentration of β-catenin increases being able to translocate to the nucleus where it displaces Groucho from TCF. This turns TCF into a transcriptional activator (Figure 1.6; Daniels and Weis, 2005). Results suggest that upon activation of Wnt/β-catenin pathway, TCF induces the transcription of axin2, a Wnt/β-catenin downstream target, by binding to its promoter. Subsequently, high levels of axin2 downregulate β-catenin via a negative feedback loop to limit the duration and intensity of the Wnt signalling pathway (Jho *et al.*, 2002). Given the fact that, *axin2* levels increase

with Wnt/β-catenin pathway induction this gene is used as a marker for Wnt/β-catenin signalling activation (Yan *et al.*, 2001).

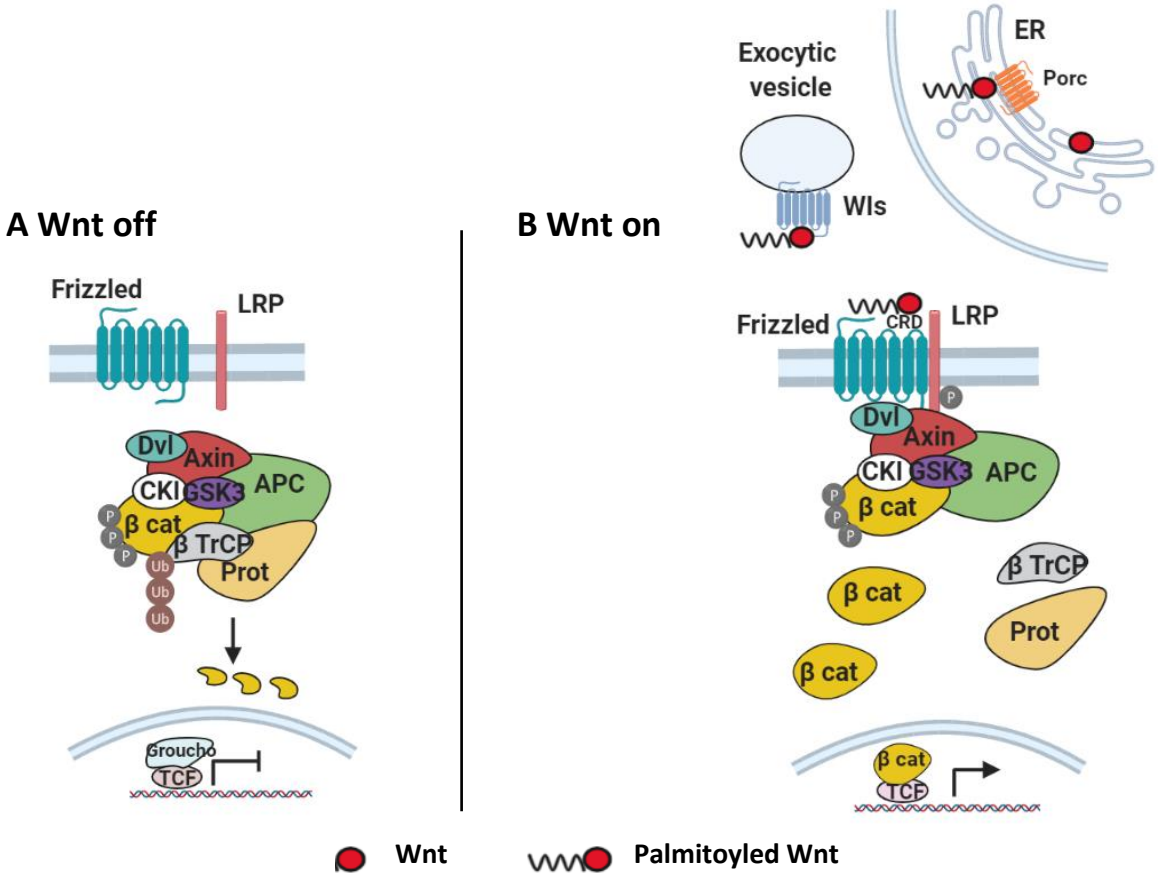

Figure 1.6 Diagram illustrating the Wnt/β-catenin signaling pathway. (A) In the absence of Wnt protein, the receptors Frizzled (Frz) and LRP are not interacting. In the cytoplasm β-catenin is phosphorylated and degraded by the proteasome (Prot) not being able to translocate into the nucleus. Therefore, Groucho binds to TCF, inhibiting gene transcription. (B) In the endoplasmic reticulum (ER), Porcupine (Porc) modifies Wnt by the addition of a palmitoyl. The lipidated Wnt is transported to its receptor Frz, bound in an exocytic vesicle via Wntless/Evi (Wls). The attachement of Wnt to Frz, triggers the dimerization of Frz with its phosphorylated coreceptor LRP, the stabilisation of the destruction complex and subsequent translocation of β-catenin (β-cat) in the nucleus to regulate gene expression via its attachment to TCF.

The Wnt/planar cell polarity signalling pathway is the most studied non-canonical pathway. It was identified in *Drosophila* where it is involved in the establishment of planar cell polarity (PCP), a process that consists in the synchronised orientation of cells throughout the plane of the tissue they form (Vinson and Adler, 1987). Core components specific for the PCP pathway in *Drosophila*, such as Van Gogh (Vangl), Frizzled, Diego and Flamingo, appear to be conserved in vertebrates playing a common role in cell polarisation (Seifert and Mlodzik, 2007). This complex signalling pathway

contains among its core components Rho family GTPases such as Rho and Rac. One of the branches of the PCP pathway, involve the activation of Rho, via the Dvl/Daam1/Fzd complex. When the receptor Fzd is activated, Daam1 binds to the PDZ/DEP domains of Dvl and activates RhoA via a guanine nucleotide exchange factor (GEF). Subsequently, Rho-GTP can activate ROCK kinase which will induce cytoskeletal changes (Habas, Kato and He, 2001). In another PCP pathway, the binding of the receptor Fdz to its ligand, forms the complex Dvl/Rac1/Tiam1, where Rac1 associates with Dvl through the DIX N-terminal domain, while Tiam1 does it in the Dvl C-terminal proline rich domain (Cajanek *et al.*, 2013). Thereafter, Tim1 acts as a GEF forming a Rac1-GTP complex, which in turn activates c-Jun N-terminal kinase (JNK) to regulate processes such as dendritic development (Rosso *et al.*, 2005).

The less studied Wnt/calcium (Ca^{2+}) non-canonical signalling pathway has been identified in *Xenopus* and zebrafish (Slusarski *et al.*, 1997; Kühl *et al.*, 2000). In *Xenopus*, this pathway is involved in the specification of ventral cell fate and it has been seen to participate in the regulation of neural progenitor, cell proliferation and differentiation (Kühl *et al.*, 2000; Huang *et al.*, 2011). Upon the binding of Wnt to the receptor FZD, the induction of the heterotrimeric pertussis-toxin sensitive G-protein causes intracellular Ca^{2+} release (Slusarski, Corces and Moon, 1997) and subsequent activation of protein kinase C (PKC) as well as calmodulin- dependent protein kinase II (CamKII; Sheldahl *et al.*, 1999; Kühl *et al.*, 2000). This, in turn, dephosphorylate the transcription factor NFAT, causing its translocation to the nucleus to activate target genes (Saneyoshi *et al.*, 2002). Although Wnt pathways have been historically classified into canonical and non-canonical groups, results suggest that a same Wnt protein is able to activate different Wnt signalling pathways and that the various types of interact with each other. For instance, NFAT inhibits Wnt/β-catenin signalling by interfering with the interaction of β-catenin with Dvl (Huang *et al.*, 2011). Also, wnt5a, which has been largely accepted as a non-canonical signalling activator, has been shown to induce β-catenin expression in a 293T cell line overexpressing the mouse frizzled receptor (mFz4; Mikels and Nusse, 2006).

1.4.3.2 Wnt 1 and Wnt5a are crucial for the development of mDA neurons

Wnt1 and Wnt5a play a crucial role in the regulation of mDA neuronal development throughout the activation of the Wnt/ β-catenin and the Wnt/PCP-Rac1 pathway respectively (Andersson *et al.*, 2008; Chung, Leung, B. Han, *et al.*, 2009) . In cell culture, Wnt1 promotes neurogenesis of midbrain dopaminergic and non-dopaminergic neurons by stimulating the proliferation of progenitors. On the other hand, Wnt5a, promotes the differentiation of precursors expressing Nurr1 into DA neurons which are TH^+ (Castelo-Branco *et al.*, 2003). Interestingly, in Wnt1 knockout mice ($Wnt1a^{-/-}$), mDA neurons development was impaired resulting in their death (cCASP3 was detected) indicating that Wnt1 expression is necessary for the development of mDA neurons *in vivo* (Prakash *et al.*, 2006). Conversely, Wnt5a knockout mice ($Wnt5a^{-/-}$), showed a mild and transient differentiation phenotype, with only some temporary effects that were recovered at later embryonic stages. However, Wnt5 limits proliferation and is involved in the morphology and positioning of neurons in the ventral midbrain (Andersson *et al.*, 2008). The two Wnt pathways Wnt1 and Wnt5a activated, show a complex interaction to regulate mDA neuronal development. Wnt1 and Wnt5a double knockout mice ($Wnt1a^{-/-}$; $Wnt5a^{-/-}$) presented a greater loss of $Nurr1^+$ cells and TH^+ neurons than $Wnt1a^{-/-}$ mice. For instance, the anterior-posterior distribution of TH^+ neurons in the midbrain was reduced of 55% in $Wnt1a^{-/-}$ mice versus 85% in $Wnt1a^{-/-}$; $Wnt5a^{-/-}$. Thus, Wnt1 induced β-catenin and Wnt5a induced PCP pathways cooperate to regulate mDA development *in vivo* (Figure 1.5; Andersson *et al.*, 2013).

1.4.3.3 Wnt signalling inhibitors

During embryonic development, there are some molecules that repress Wnt signalling in the anterior part of the embryo. They permit the development of the forebrain and midbrain as well as the head formation in vertebrates (Kim *et al.*, 2000). Dickkopf-1 (Dkk1) is member of a family of secreted proteins and has been identified as a Wnt signalling antagonist. Dkk proteins are codified by 4 genes in human (*DKK1*, *DKK2*, *DKK3* and *DKK4*) and 3 genes in mouse (*Dkk1*, *Dkk2* and *Dkk3*; Fedi *et al.*, 1999; Krupnik *et al.*, 1999; Wu *et al.*, 2000). Although, it has been identified that Dkk1 is expressed in the

Spemann organiser (the node of amphibians) and functions as a head inducer in *Xenopus*, the role that play other Dkk proteins is still unknown (Glinka *et al.*, 1998). However, it has been reported that Dkk2 activates Wnt/β-catenin pathway (Wu et *al.*, 2000). Experiments in HEK293T cells showed that dkk1 binds to the co-receptor LRP5/6, in a different domain of interaction than the receptor FZD, resulting in the repression of the Wnt/β-catenin pathway (Figure 1.7; Bafico *et al.*, 2001; Mao *et al.*, 2001).

Apart from proteins that occur naturally to inhibit Wnt signalling during embryogenesis, there are some synthetic chemicals that have been found to repress this pathway. Inhibitors of Wnt production (IWP) and inhibitors of Wnt response (IWR), are small molecules that were identified in a mouse L-Wnt-STP cell line that was constitutively expressing Wnt/β-catenin signalling pathway. The L-Wnt-STP cells were transfected with a Wnt/β-catenin pathway-responsive firefly luciferase reporter plasmid, an expression construct encoding for the protein Wnt3a as well as a control reporter for cell death, and were exposed to different chemical compounds. After several tests to identify potential compounds with minimal cytotoxicity and with specificity to repress the Wnt/β-catenin signalling pathway, 4 IWP compounds along with 5 IWR were determined. Particularly, IWP2 and IWR1 were seen to inhibit Wnt/β-catenin pathway induced by Wnt1. IWP2 interacts with Porcupine, reduces the palmytoilation of Wnt protein thus Wnt cannot be released from the ER. Contrarily, IWR promoted the stabilisation of the destruction complex by increasing Axin levels and therefore maintaining β-catenin phosphorylation (Figure 1.7; Chen *et al.*, 2009).

Another study identified the small molecule XAV939 as an inhibitor of the Wnt/β-catenin pathway by prolonging the half-life of axin and promoting the degradation of β-catenin via the inhibition of tankyrases (TNKS). TKNS1 and TKNS2 act jointly, directly PARsylating axin-1 and axin-2, which bind to the TKNS via the tankyrase binding domain (TBD), to promote their ubiquitination and subsequent degradation. When the inhibitor XAV939 binds to the catalytic (PARP) domains of TKNS1 and TKNS2, the PARsylation of axin-1 and axin-2 is repressed, thus axin protein is stabilised as well as the destruction complex resulting in the degradation of β-catenin. Interestingly, this study suggested that IWR-1 could also promote axin stabilisation throughout the inhibition of TKNS (Figure 1.7; Huang *et al.*, 2009).

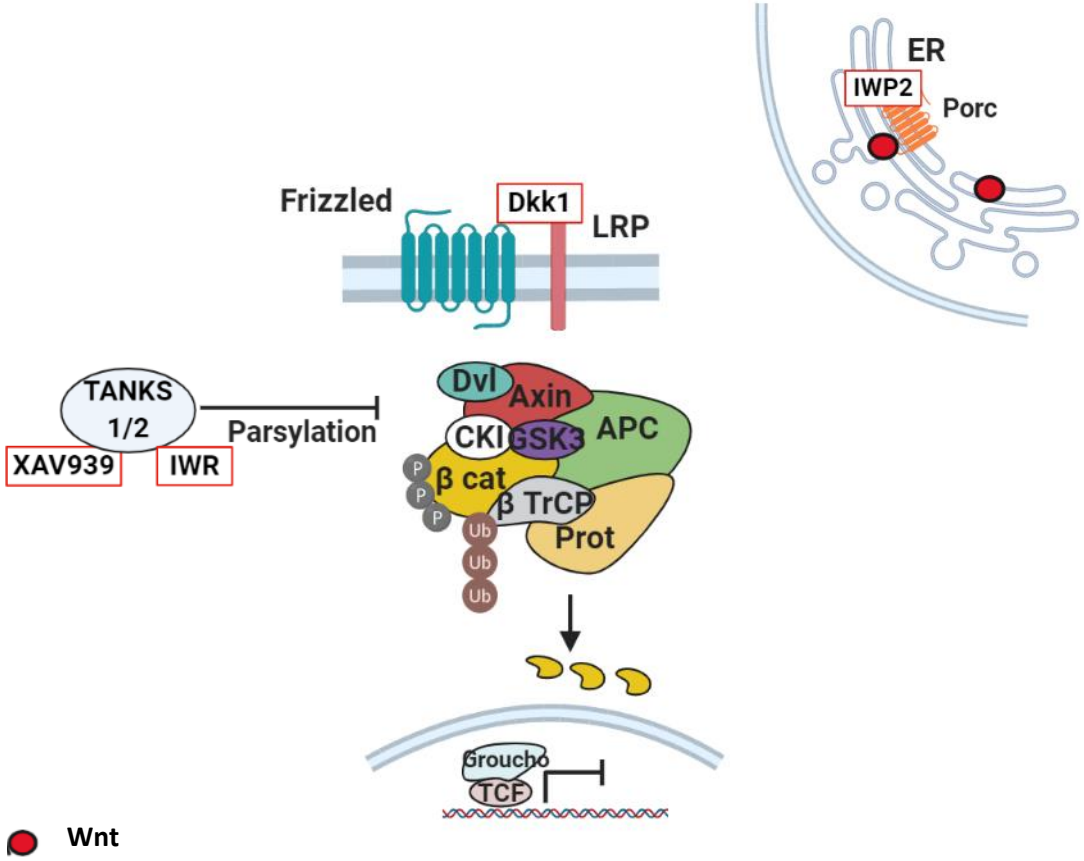

Figure 1.7 Schematic representation of the Wnt/β-catenin repression mechanism undertaken by the inhibitors Dkk1, IWP2, XAV939 and IWR. IWP2 inhibits the palmytoilation of Wnt protein, so Wnt cannot leave the endoplasmic reticulum (ER) to bind to its receptor. Dkk1 attaches to LRP repressing the heterodimerization with Frizzled. XAV939 and IWR inhibit the Tankyrases 1 and 2 (TANKS 1/2) parsylation of Axin, stabilising the destruction complex.

1.4.3.4 Shh signalling

The gene Hedgehog (HH) was identified for the first time in *Drosophila*, as a homozygous mutation affecting the larvae segment number and polarity (Nusslein-Volhard and Wieschaus, 1980). Later, three type of mammalian HH were identified in mouse: *Desert hedgehog (Dhh), Indian hedgehog (Ihh)* and *Sonic hedgehog (Shh)* (Echelard *et al.*, 1993). Shh is expressed in signalling centres which are involved in the development of the embryo, Dhh plays a role in spermatogenesis and Ihh is involved in cartilage differentiation (Echelard *et al.*, 1993; Bitgood, Shen and McMahon, 1996; Vortkamp *et al.*, 1996; Szczepny, Hime and Loveland, 2006). The HH proteins are synthesised as ~45KDa precursor proteins that experience cleavage. During biosynthesis in the ER, the HH precursor protein is activated via autoproteolysis in the Gly-Cys-Phe sequence, between Gly 257-Cys 258. The C-terminal domain of the unprocessed peptide

undergoes a rearrangement replacing the Gly -Cys linkage by a thioester which suffers a nucleophilic attack resulting in a N-terminal and a C-terminal fragment (Lee *et al.*, 1994; Porter *et al.*, 1995). Another consequence of the autocatalytic process is the acquisition of a cholesterol in the C terminus of the N-fragment (Porter *et al.*, 1996; Porter, Young and Beachy, 1996). *In vitro*, studies showed that the C-terminal moiety resulting from the fragmentation, gets degraded via the ER-associated degradation (ERAD; Chen *et al.*, 2011). Subsequently, the acyltransferase, coded by the gene *sightless,* attaches a palmitic acid in the N terminus of N-terminal peptide (Pepinsky *et al.*, 1998; Chamoun *et al.*, 2001). Although this process has been elucidated in *Drosophila*, it is conserved in vertebrates (Lee *et al.*, 1994; Porter *et al.*, 1995). The lipidation of HH proteins, anchor them to the plasma membrane and restrict their mobility showing that their secretion should be actively performed (Peters *et al.*, 2004). For instance, once Shh is anchored to the plasma membrane, it can be secreted through the synchronised action of Dispatched (Disp), a multispanning membrane protein, and Scube2, a secretion protein that binds Shh via the cholesterol anchor allowing its solubility (Tukachinsky *et al.*, 2012). Shh signalling is one of the most studied HH pathways but it remains poorly defined. It has been observed that the correct functioning of the pathway relies on the primary nonmotile cilium, a microtubule-based structure that projects from the plasma membrane and that can function as a key signalling organelle (Caspary, Larkins and Anderson, 2007). The primary cilium contains nine doublets of microtubules forming the axoneme and which are anchored to a basal body formed by nine triplets of microtubules. Intraflagellar transport (IFT) is required to maintain and assemble the primary cilium by transporting ciliary cargoes along the axoneme. In the absence of Shh, the receptor patched (Ptc) is localised in the cilium and, inhibits the translocation into the cilia of the transmembrane protein smoothed (Smo). Although it is still not clear, some results suggest that Smo could be trafficked in and out of the primary cilium via IFT. At this point, the full-length protein Gli3 is phosphorylated by PKA and subsequently processed to a shortened repressor form by the proteasome. The Gli3 repressor protein translocates within the nucleus and inhibits gene transcription (Wang, Fallon and Beachy, 2000). Similarly, the full-length protein Gli2 is phosphorylated by PKA and subsequently degraded by the proteasome

(Pan *et al.*, 2006). In addition, suppressor of fused protein (SuFu) forms a complex with the residual full-length proteins in the cytosol inactivating them (Tukachinsky, Lopez and Salic, 2010). When Shh binds to Ptc, Smo inhibition stops and it is translocated to the cilia. Moreover, Shh signalling induces the stabilisation of Gli2 and its protein transcription activity (Pan *et al.*, 2006). Shh signalling also triggers the dissociation of the complex SuFu-Gli and the inhibition of Gli3 cleavage (Wang, Fallon and Beachy, 2000; Tukachinsky, Lopez and Salic, 2010). Active Gli translocates to the nucleus to induce the Gli1 mediated Shh signalling. For example, Gli3 can activate the transcription of Gli1 by binding to the Gli1 promoter (Figure 1.8; Dai *et al.*, 1999).

The morphogen Shh, which is expressed in the floor plate, is crucial for the induction of mDA neurons (Prakash *et al.*, 2006). A study in mice, revealed that *Shh* expression is dynamic in the ventral midbrain and with *Gli 1* (used as readout for elevated levels of Shh expression) being induced one day before than *Shh*. Interestingly, they identified that progenitors laterally located in the ventral midbrain expressing Gli1 after E9.5 were giving rise mainly to VTA midbrain dopaminergic neurons. Thus, the duration of Shh signalling and the timing could have an impact in the differentiation of mDA neurons. At a later stage of the development (between E10.5 and E11.5), Wnt inhibits Shh in the ventral midbrain allowing neurogenesis. Although high levels of Shh are needed in the early midbrain development, Wnt/β-catenin signalling supresses the *Shh* expression in the ventromedial midbrain promoting neurogenesis (Figure 1.9; Joksimovic *et al.*, 2009).

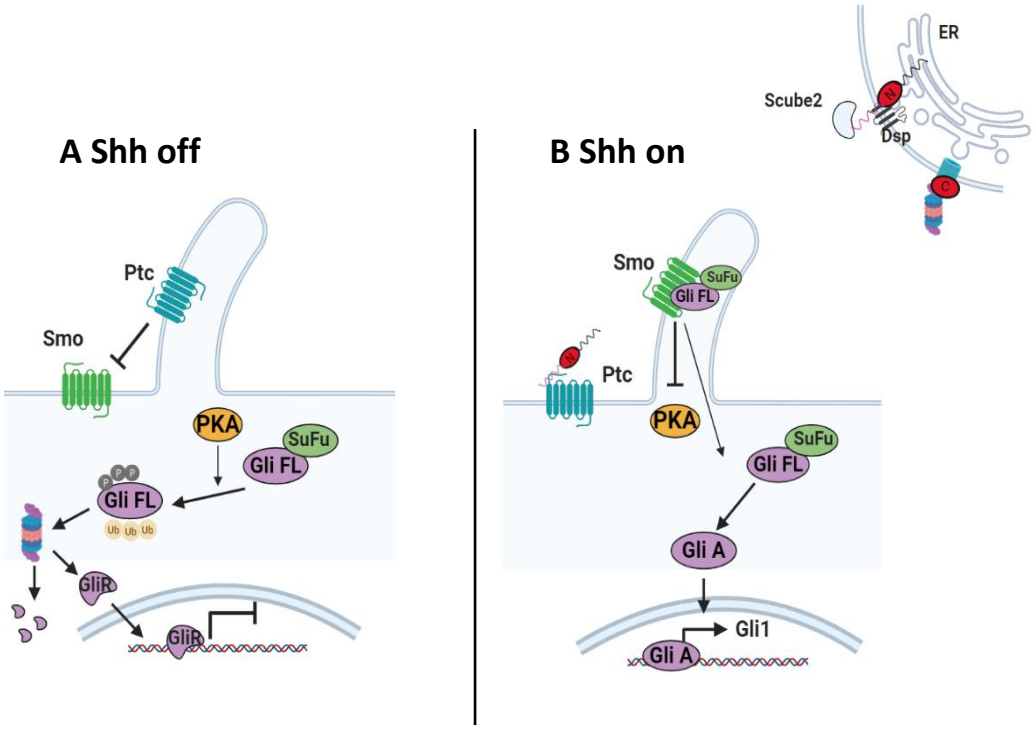

Figure 1.8 Model of Shh signalling. (A) In absence of the ligand, the receptor Pitched (Ptc) inhibits smoothened (Smo). The protein kinase A (PKA) promotes by phosphorylation the processing and cleavage of the Gli3 and Gli2 full length (Gli FL) proteins respectively. This results in a modified Gli3 repressor (GliR) protein which translocates to the nucleus blocking gene transcription. (B) During the synthesis, Shh undergoes autoproteolysis in the endoplasmic reticulum (ER) leading to a N-terminal and C-terminal fragment. The C-terminal fragment is degraded, while the N-terminal fragment is processed having attached a cholesterol in its C-terminus and a palmitoyl in its N-terminus. The cholesterol bins to Dispatched (dsp) and Scube 2 so it can be transported to its target. Once Shh binds to Ptc, Smo along with the complex GliFL-SuFu are translocated to the primary cilia causing the dissociation of the complex, repression of PKA and the actives Gli (GliA) translocate to the nucleus so the transcription of gene targets, such as *Gli1*, is activated.

1.4.4 Role of the transcription factors in mDA neuron development

1.4.4.1 Transcription factors and morphogens interact to orchestrate mDA neuronal development

Transcription factors (TF) are proteins that bind to DNA in a sequence specific manner, through DNA binding domains, in order to regulate gene transcription. Particularly, TF attach to binding sites located in regulatory domains that are necessary for transcription control. Some of these regulatory sequences are promoters that help the polymerase with the initiation of the transcription, others are silencers that block the promoter to prevent the transcription and there are also enhancers that control spatial, temporal and gene expression rate. The regulation of developmental process is done by many different TF that recognise binding sites within the enhancers (Vaquerizas *et al.*, 2009). An enhancer contains a set of binding sites, where diverse transcription factors can attach and allows the expression of a gene in a specific cell type. One gene present multiple enhancers, so the same gene will be induced in various cell types depending on the TF recognising the different enhancers (Zinzen *et al.*, 2009).The are several ways in which a TF functions once bound to its regulatory domain. The attachment of the TF can trigger the recruitment of cofactors (other TF or proteins) throughout the protein-protein interaction domain, resulting in the activation of histone modifying enzymes making the binding sites more accessible to other TF. Furthermore, they can form bridges by creating chromatin loops so the TF bound to the enhancers can be in contact with the promoters for transcription regulation. Interestingly, some TF seem to be intrinsic determinants of cell fate, being sufficient to differentiate cells into a specific cell type. For example, only the expression of four genes (*Oct3/4, Sox2, c-Myc and Klf4*) coding for TF is necessary for the reprograming of adult mouse and human fibroblasts into mouse and human embryonic stem cells respectively (Takahashi and Yamanaka, 2006; Takahashi *et al.*, 2007). Another study showed that forced expression of Lmx1a, in permissive cultures of mouse and human embryonic stem cells, resulted in an efficient production of mDA neurons. In addition, the grafted mouse Lmx1a-derived mDA neurons were indistinguishable from the authentic mDA neurons in the host mouse (Friling *et al.*, 2009).

The development of mDA neurons has been extensively studied in mouse. Their correct differentiation depends on a complex process that involves the interaction of the morphogens Shh and FGF8/Wnt, released from the signalling organisers floor plate and IsO respectively, with multiple TFs. mDA neurons originate from glial-like cells apically located in the medial floor plate of the midbrain (Bonilla *et al.*, 2008). These floor plate cells possess neurogenic potential and give rise to neural progenitors, which express the transcription factor FOXA2 required, for the induction of Shh signalling in the ventral midbrain (Ono *et al.*, 2007; Bonilla *et al.*, 2008; Mavromatakis *et al.*, 2011). Shh signalling, in turn, will stimulate throughout the activation of FOXA2, the expression of Lmx1a, a TF that acts as an intrinsic determinant of mDA and it is essential for their induction (Elisabet Andersson *et al.*, 2006; Metzakopian *et al.*, 2012). Independently of Shh, Wnt-1 directly activates Lmx1a via the β-catenin complex and vice versa, Lmx1a induces Wnt-1, resulting in an autoregulatory loop (Chung, Leung, B. Han, *et al.*, 2009). Although, induction of Shh signalling is necessary for the establishment of mDA neurons by promoting Lmx1a expression and expanding the progenitor pool, in the later embryonic development, it hampers mDA neurogenesis (Elisabet Andersson *et al.*, 2006). Therefore, Wnt/β-catenin pathway inhibits Shh levels at the midline of the midbrain floor plate, generating permissive conditions for neurogenesis in floor plate cells (Joksimovic *et al.*, 2009). In addition, Wnt1 activation of the Wnt/β-catenin also induces the expression of Otx2 which is required to confer neurogenic potential to midbrain floor plate cells and to establish a mDA progenitor domain (Prakash *et al.*, 2006; Ono *et al.*, 2007). Lmx1a, which expression is maintained in the ventral midbrain by Wnt/β-catenin signalling, activates Msx1, a Groucho/TLE dependent homeodomain repressor, which in turn upregulates neurogenin 2 (Ngn2), a proneural gene, involved in the differentiation of mDA neurons. Thu Msx1 seems to be involved in the suppression of alternative fates and the switch of glial-like cells to mDA progenitors, facilitating the differentiation of mDA neurons (Figure 1.9; E. Andersson *et al.*, 2006; Elisabet Andersson *et al.*, 2006).

Factors regulating the generation and survival of mDA neurons start to be expressed in early post-mitotic neurons. The Lmx1a and structurally related Lmx1b (its expression induced by FOXA2) TFs directly increase the expression of the post-mitotically induced

Nurr1 and Pitx3. Although in mutant mice for Lmx1b$^{-/-}$, TH neurons expressing Ptx3 were lost, in embryonic stem cells, Lmx1a and Lmx1b compensate each other expression, and only when expression of both TFs is downregulated, Nurr1 and Pitx3 significantly decreased (Figure 1.9; Smidt *et al.*, 2000; Chung, Leung, B. Han, *et al.*, 2009). Nurr1$^{-/-}$ mutant mice lack TH expression, showing that Nurr1 is required for TH expression. In fact, Nurr1 induces genes encoding the storage (vesicular monoamine transporter 2), transport (dopamine transporter) and synthesis (tyrosine hydroxylase) of the neurotransmitter dopamine (Smits *et al.*, 2003). Pitx3 is highly expressed in mDA neurons and it has been suggested that it is involved in the development of SNc. This subpopulation is selectively lost in Pitx3-/- mutant mice, suggesting that this transcription factor plays a role in the development of the lineage. However, the transcription factor Pitx3 is not expressed in mDA progenitors at E11.5, but its expression is detected from E12.5 in the mouse brain indicating that Pitx3 is involved in later stages of the differentiation being key for the generation of SNc (Smidt *et al.*, 2004). The survival of mDA neurons depends on the TFs En1 and E2. En1 and En2 are expressed from progenitors to post-mitotic neurons. En1 is expressed at high levels in SN and in VTA neurons all along the development while En2 levels are high in a subset of cells. While in mice mutants for En1$^{-/-}$/En2$^{-/-}$ there is a complete loss of mDA neurons due to apoptosis induction, homozygous mutants for En1 or En2 present minimal alterations in the midbrain. Interestingly, in mice mutants for En1$^{+/-}$/En2$^{-/-}$ only one En1 allele is sufficient to have a phenotype similar to wild type, while in mice En1$^{-/-}$/En2$^{+/-}$ that only express one En2 allele it is not (Simon *et al.*, 2001; Albéri, Sgadò and Simon, 2004).

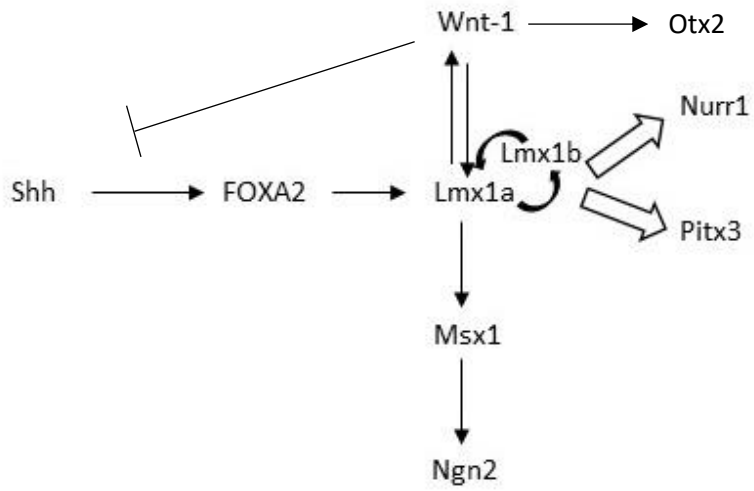

Figure 1.9 Schematic representation of the interactions between the morphogens and TFs involved in mDA neuronal development. Shh induces FOXA2 levels which in turn activates Lmx1a expression in the ventral midbrain promoting the formation of mDA progenitors. Independently, Wnt1 stimulates Lmx1a and vice versa, forming an autoregulatory group. In addition, it inhibits Shh signalling inducing neurogenesis in the ventral midbrain. Lmx1b and Lmx1a act in coordination and both promote Nurr1 and Pitx3 expression. Lmx1a activates Msx1 which induces Neurogenin 2 (Ngn2) levels. Msx1 and Ngn2 promote the maturation of mDA progenitors and neurogenesis, respectively. Nurr1 and Pitx3 are post-mitotic TFs that promote the differentiation and maturation of mDA neurons.

1.4.4.2 Single-cell transcriptomics molecularly define subpopulations of SN and VTA dopaminergic neurons

In the last decade, advances in the field of single-cell transcriptomics and bioinformatics have permitted the identification of gene expression profiles in individual cells. This made possible to describe distinct neuronal subpopulations constituting the SN and the VTA. As a result, many different markers have been identified, demonstrating that these regions of the midbrain are much more heterogeneous and complex than previously thought. Traditionally, there were some markers that were used to differentiate SN and VTA neuronal subpopulations. The G protein-activated inward rectifier potassium channel 2 (Girk2), encoded by the human gene *KCNJ6*, has been used as a marker for SNc DA neurons presumably. However, it has recently been observed in mice and humans that Girk2 is widely expressed at different levels in VTA and SN DA neurons (Reyes *et al.*, 2012). The calcium binding protein, calbindin, has been generally used for the determination of populations of DA neurons, such as the VTA, in models for PD. However, no differences in vulnerability were found in a mouse model for PD that was

Calb$^{-/-}$. Studies in mice and humans, show that calbindin is expressed in the VTA and the dorsal population of SNc DA neurons (Poulin *et al.*, 2018). Another marker of the most vulnerable SNc DA subpopulation in PD is Aldehyde dehydrogenase 1 (Aldh1a1). In mice, it is expressed in the ventral part of SNc, and in a group of VTA DA neurons (Poulin *et al.*, 2018). In addition to the former SN and VTA markers, a study identified the TFs Sox6 and Otx2 which have been important to understand the development of SN and VTA DA neurons. Sox6 is expressed in medially located progenitors in the ventral midbrain giving rise to the SNc DA neurons from the ventral tier, while the Otx2 progenitors are laterally situated, neighbouring Sox6 and originating the VTA DA neurons. Post-mitotic SNc and VTA will continue to express Sox6 and Otx2 respectively (Panman *et al.*, 2014).

Molecular heterogenicity of dopaminergic neurons has been analysed in several studies in an effort to organize, based on gene expression, the distinct subpopulations forming the midbrain. Recently, it has been proposed by Poulin et al., 2020, that the different dopaminergic neuronal subpopulations contained in the SN and the VTA can be molecularly defined in seven groups based on the results of five single-cell transcriptomics studies (Figure 1.10). Interestingly, Sox6, Otx2 and Aldh1a1 are some of the markers used to define the molecular signatures of these groups.

Rostrally, the subpopulation of neurons expressing Sox6^{+}/Aldh1a1^{+} are Calb1^{-} and projecting to the dorsolateral caudate-putamen have been located in the ventral tiers of the SNc (Poulin *et al.*, 2018). They correspond to the neuronal group that degenerates in PD (Panman *et al.*, 2014; Poulin *et al.*, 2018). Lmo3 has also been detected in this neuronal subpopulation by single cell-sequencing and has been validated by immunohistochemistry in this ventral SNc neuronal subpopulation (Figure 1.10; La Manno *et al.*, 2016).

Dorsally in the SNc there is another dopaminergic subpopulation being Sox6^{+}/Aldh1a1^{-}/Calb1^{+} which has also been detected in the PBP bordering with SNc. Interestingly the neuronal group located dorsally in the SNc, projects to the ventromedial caudate - putamen. The neuronal group located in the VTA is Otx2^{-} and innervate the nucleus accumbens (Figure 1.10; Poulin *et al.*, 2018).

A group of Vglut2$^{+/}$Calb1^{+} population of dopaminergic neurons was detected the study of Poulin et., 2014. In an analysis that was done later, it was seen that this experiment

probably detected two types of neuronal subpopulations. In the VTA, this neuronal population is located in the lateral (PBP) and medial (Rli and IF) (Yamaguchi *et al.*, 2011; Poulin *et al.*, 2018). Another group of dopaminergic neurons expressing Vglut2 has been identified in the dorsolateral area of the SNc being Calb1$^+$ and innervating the caudate putamen (Figure 1.10; Poulin *et al.*, 2018).

The Vgat$^+$ subpopulation of mDA neurons is localised mainly in the IF and some can also be detected in the PBP. It has been observed that some of them innervate the lateral habenula, and although being TH$^+$ they only release of GABA has been detected in the lateral habenula (Figure 1.10; Stamatakis *et al.*, 2013).

The population of neurons coexpressing Aldh1a1, Otx2 and Calb1 has been detected in different studies (Di Salvio *et al.*, 2010; Poulin *et al.*, 2014, 2018; La Manno *et al.*, 2016). They are located ventral-laterally in the VTA and although in an analysis with in-situ hybridisation it has been shown that a low number of TH$^+$ neurons located in this area are Vglut2$^+$, Poulin et al., 2018 showed that there was quite a high number of these neurons expressing Vglut2. These neurons project to the nucleus accumbens and olfactory tubercle (Figure 1.10; Poulin *et al.*, 2018).

Several studies identified mDA neurons expressing Vip (Poulin *et al.*, 2014; La Manno *et al.*, 2016; Tiklová *et al.*, 2019). These neuronal population is located very caudal in the periaqueductal gray and dorsal raphe (Poulin *et al.*, 2018; Tiklová *et al.*, 2019). They project to the bed nucleus of the stria terminalis (BTS) and the amygdala (Figure 1.10; Poulin *et al.*, 2018).

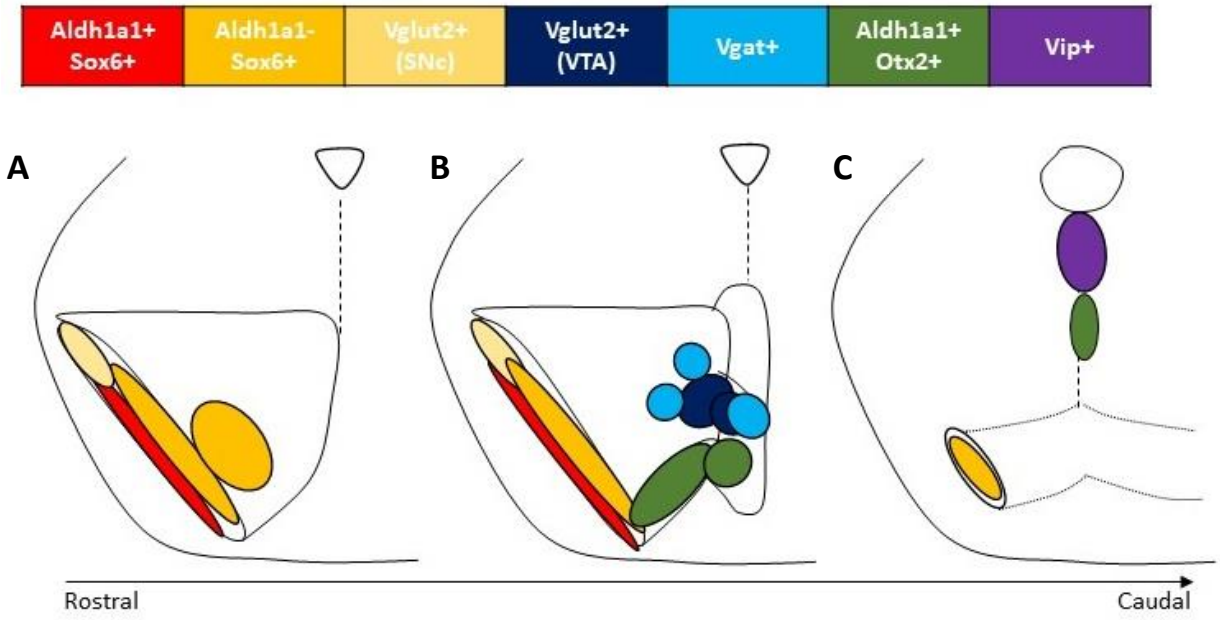

Figure 1.10 Classification of mDA neuronal subpopulations based on their molecular identities. (A) The neuronal subpopulations Aldh1a1^{+}/Sox6^{+}, Aldh1a1^{-}/Sox6^{+} and Vglut2^{+} are localised in the ventral tier, dorsal tier, and lateral area of the SNc, respectively. A neuronal subpopulation Aldh1a1-/Sox6+ is also present in the VTA. (B) Vglut2^{+} and Vgat^{+} neurons are located medially in the VTA while the neuronal subgroup expressing Aldh1a1/Otx2 is medio-ventrally positioned in the VTA. (C) The most caudal subpopulation expresses Vip and is localised in the periaqueductal gray and dorsal raphe (PAG/DR). Adapted from Poulin et al., 2020.

1.4.5 The transcription factor Sox6 is involved in the development of SN dopaminergic neurons

The TF Sox6, is a member the SOX family characterised by the presence of a conserved HMG DNA binding domain (Bowles, Schepers and Koopman, 2000). SOX genes are involved in many cell fate decisions during developmental processes such as Sox2 which is crucial in maintaining pluripotency in mouse and human embryonic stem cells (Takahashi and Yamanaka, 2006; Takahashi *et al.*, 2007). In mammals there are 20 SOX genes that, by phylogenetic study and sequence comparison, have been classified in the following ten groups: A, B (B1/B2), C, D, E, F, G, H and I, Sox6 being a SOXD gene (Bowles, Schepers and Koopman, 2000; Schepers, Teasdale and Koopman, 2002). In mouse Sox6 has being involved in chondrogenesis, oligodendrocyte and cortical interneurons development (Lefebvre, Li and De Crombrugghe, 1998; Stolt *et al.*, 2006; Azim *et al.*, 2009; Batista-Brito *et al.*, 2009). A study in the mouse myelin-forming oligodendrocytes showed that Sox6 along with Sox5 and other SoxE genes keep progenitors in

undifferentiated states, preventing terminal differentiation. Thus, their expression is downregulated in post-mitotic neurons so oligodendrocytes can reach maturity (Stolt *et al.*, 2006). In the forebrain, Sox6 is expressed in progenitors located in the subpallial medial (MGE) and caudal ganglionic eminences (CGE). Post-mitotically, Sox6 is expressed in most of MGE derived interneurons in the mature brain. Its expression is necessary for the cortical migration and laminar positioning as well as for the establishment of interneuron subtype diversity (Azim *et al.*, 2009; Batista-Brito *et al.*, 2009). Apart from the forebrain, the analysis done in mouse by Panman et *al*., 2014, showed that Sox6 is involved in the development of SNc DA neurons, while the homeodomain protein Otx2 induces VTA DA neurons in the midbrain. Interestingly, Sox6 is expressed in progenitors giving rise to SNc that are medially located in the vMB and Corin^{+}. In contrast, progenitors originating VTA neurons express Otx2 and Nolz1 and are laterally localized. Both groups of progenitors were also expressing Lmx1a, an intrinsic determinant of mDA neurons. When progenitors exit the cell cycle, at E13.5, early post-mitotic SNc and VTA neurons undergo radial migration from the ventral zone to the intermediate zone. Once in this region, they start tangential migration, so SNc and VTA early post-mitotic DA neurons reach their laterally and medially final destinations, respectively (Panman *et al.*, 2014). This migration is mediated by the extracellular matrix molecule, Reelin, that promotes the fast tangential migration of the neurons (Vaswani *et al.*, 2019). The laterally located mature SNc neurons express the markers of Aldh1a1, Girk2, Sox6 and the glycosilated active form of the dopamine transporter (Glyco-DAT). Conversely, the markers for the medially located VTA neurons are Calbindin, Otx2 and Nolz1. In neonatal mice (4 and 8 months old) DatCre;Sox6$^{fl/fl}$, the TH innervation to the dorsal-lateral part of the striatum was reduced as well as the dopamine and its metabolites (DOPAC and HVA), proving that Sox6 is involved in the fate determination of SNc mDA neurons (Panman *et al.*, 2014). The TH^{+}/Sox6^{+} subpopulation of SNc mDA neurons has been validated, in mouse, by a recent study that employed 3 different intersectional strategies to genetically mark mDA neurons. Interestingly, they found a subpopulation of mDA neurons Sox6^{+}/TH^{+}/Aldh1a1^{+}, localised in the ventral tier of the SNc and projecting to the dorsolateral striatum (Poulin *et al.*, 2018). In addition, similarly to another study done by Di Salvio et *al*., 2010 where they described a subpopulation of

$Otx2^+/TH^+/Aldh1a1^+$ mDA neurons, Poulin et *al*., 2018 identified another subpopulation of mDA neurons located in the VTA that were $TH^+/Otx2^+/Vglut^+$ $/Aldh1a1^+$. This neuronal subpopulation projected to the nucleus accumbens as previously seen with the $Otx2^+/TH^+$ mDA neurons described in Panman et *al*., 2014. It has been hypothesised that Sox6 could confer sensitivity to the mDA neurons located in the ventral tier of the midbrain that degenerate during PD. Indeed, the expression of Sox6 has been analysed in healthy and PD human post-mortem tissue. In the healthy samples, Sox6 coexpressed with neuromelanin neurons that were TH^+, while its expression was clearly reduced in the neuromelanin expressing neurons from PD samples (Panman *et al.*, 2014). In addition, it has been shown that Sox6 is key for the development of gastric neurons TH^+ and that the loss of Sox6 causes a reduction of gastric mobility. This supports the Braak hypothesis that PD initiates in the gut and progresses to the brain, as PD patients suffer from constipation (Memic *et al.*, 2018). Conversely, Otx2 could have a protective function in the VTA mDA neurons and mice lacking Otx2 are more sensitive to the PD related MPTP toxin (Di Salvio *et al.*, 2010).

1.5 Human embryonic stem cells: a new paradigm

Current therapies for PD are mainly focused on the alleviation of the motor symptoms suffered by patients. Treatments involving the dopamine precursor L-DOPA or deep brain stimulation (DBS) are commonly used. However, L-DOPA is metabolised to dopamine in cells that are non-dopaminergic leading to many side effects. Another cell therapy with many drawbacks is the dopamine neuronal transplantation from human embryos into the striatum of PD patients. A study that followed up PD patients transplanted with foetal tissue revealed that parkinsonism signs in patients improved after a few months of the surgery, with a patient having the dose of L-DOPA reduced 30% (Mendez *et al.*, 2005). However, transplantations are not always successful, as happened with three patients presenting increased dystonia after the procedure (Hagell *et al.*, 2002). The engrafted foetal ventral midbrain's dopamine content is only 5-10% and contains other neuronal types such as GABAergic neurons which in ventral midbrain-grafted mice considerably participate in graft-host connectivity (Thompson,

Kirik and Björklund, 2008). In addition, this procedure involves the use of several human embryos (3 to 4 embryos per procedure) which raises technical complications and ethical concerns (Mendez *et al.*, 2005). Thus, the use of high number of embryos, the heterogeneity of the grafted cell population and their low survival rate, arises the need to find alternative therapies. Human embryonic stem cells (hESC) and human induced pluripotent stem cells (hiPSC) offer relevant platforms for disease modelling and prospective solutions for the treatment of PD.

hESC are derived from the inner cell mass (ICM) of the blastocyst. At this stage, the ICM as well as the blastocoel are formed and the cells in the ICM become pluripotent, being able to generate the three embryonic layers (endoderm, mesoderm and ectoderm) (Gilbert and Barresi, 2016). Once in culture, hESC form colonies that display a uniform, flat undifferentiated morphology and that are not derived by single-cell clonal expansion (Thomson *et al.*, 1998). Although being derived from the pre-implantation ICM, X-chromosome inactivation occurs in one of the two chromosomes in female cells. Furthermore, their pluripotent stage depends on the presence of the growth factors activin, Nodal and FGF2 (Brons *et al.*, 2007). hiPSC are generated by reprogramming human fibroblasts into a pluripotent state with the TF Oct3/4, Sox2, Klf4, and c-Myc. These cells are very similar to the hESC in their morphology, proliferation or gene expression, however there are still epigenetic differences between cell lines (Takahashi *et al.*, 2007). The advantage of hESC and iPSC is that they can be differentiated into the cell type of interest. This allows the generation of platforms that can be used for disease modelling (Devine *et al.*, 2011), for cell therapy (Kikuchi *et al.*, 2017; Doi *et al.*, 2020) and for developmental studies (Elisabet Andersson *et al.*, 2006; Chung, Leung, B. S. Han, *et al.*, 2009). There are many relevant published protocols that differentiate hESC into mDA neurons (Kriks *et al.*, 2011; Kirkeby *et al.*, 2012; Nolbrant *et al.*, 2017). However, it remains unclear which subpopulations of mDA neurons are generated. Thus, further investigations need to be performed to be able to obtain pure cultures of vulnerable SNc mDA neurons that could be used for transplantation or to gain a better insight into PD.

1.6 Aims of the project

In PD patients, SNc mDA neurons degenerate causing motor impairments, while the neighbouring population of VTA mDA neurons remain relatively spared. However, it remains poorly understood why SNc mDA neurons are selectively vulnerable in PD. A previous study in mice observed that the transcription factor Sox6 plays a role in the development of SNc mDA neurons and its expression is significantly decreased in neuromelanin expressing neurons of PD patients (Panman *et al.*, 2014). Overall, this thesis aims to investigate whether Sox6 is sufficient and required to induce SNc fate and to further study its function in the development of mDA neurons.

In chapter 3, the objective will be to identify culturing conditions that will generate hESC-derived SNc-like mDA neurons expressing Sox6. This will be done by modulating Wnt signalling, one of the most important pathways orchestrating the development of mDA neurons.

In chapter 4, the aim will be to investigate whether Sox6 expressing neurons obtained in the former established protocol (chapter 3) present a SNc-like phenotype by studying the expression of SNc key markers and their vulnerability to toxins causing Parkinsonism. Furthermore, this research envisages to identify possible Sox6 downstream targets.

The final purpose of this project will be to characterise the *Sox6*$^{GFP\text{-}Cre\text{-}ERT2}$ mouse line and to use it for Sox6 lineage tracing overtime via tamoxifen exposure. Thus, the function of Sox6 in the development of mDA neurons can be further studied.

Chapter 2

Materials and methods

Chapter 2 Materials and methods

2.1 Human embryonic stem cells (H9)

2.1.1 Maintenance of human embryonic stem cells in pluripotent stage

The human ES cell line WA09 (H9) used in this thesis was obtained from the company WiCell. The WA09 cell line from WiCell was approved for research purposes by the Steering Committee for the UK Bank and for the Use of Stem Cell Lines. This committee ensures that the human embryonic stem cell lines have been ethically sourced with fully informed and free donor consent. Human ES cells H9 (WA09, passage 32-48; Thomson *et al.*, 1998) were cultured with Essential8 medium on 6 well plates coated with Geltrex™ (Gibco; Chen *et al.*, 2011). Following the manufacturer's protocol, plates were incubated for 1 hour at 37°C with Geltrex (diluted 1:100 times in DMEM). Cells were passaged every 3 days by splitting 1 well into 6 wells. The reagent EDTA (0.5mM) (Gibco) was used for the splitting of cells. Note that the Essential8 medium was changed daily. For maintenance of iPS cells, 10 µM of Rock inhibitor (Tocris) was added to the medium after the split.

2.1.2 Differentiation of hES cells into midbrain dopaminergic neurons

A revised version of the midbrain dopaminergic neuron protocol (Kriks *et al.*, 2011) was employed in order to undertake a floor plate mediated dopaminergic differentiation. The neuronal induction was initiated with the transfer of a confluent well from a 6 well plate into a well of a 24 well plate which was previously coated with Geltrex at 37°C for 1 hour. As previously described, cells were split with 0.5mM EDTA. The day after (day 1 of the differentiation), the medium was replaced with a 1:1 ratio mixture of N2 and B27 neural induction medium (Shi, Kirwan and Livesey, 2012) supplemented with 100 nM LDN193189 (StemMacs) and 10 µM SB431542 (Tocris). The medium was changed and was made fresh every day. The growth factors were added in a time point as detailed in the Kriks et al., 2011 protocol: at day 2 and day 3 the neural induction medium contained C24II (R&D), Purmorphamine (Calbiochem) and FGF8 (R&D) in addition to LDN and SB, at day 4 and day 5 CHIR (Stemgent) was added and from day 6 to day 7 SB was removed

from the medium. On day 8, progenitors were dissociated with dispase (Life Technologies; Shi, Kirwan and Livesey, 2012) and plated in a 24 well plate at a 1:2 ratio (1 well into 2 wells). At this point, progenitors were cultured with neural induction media supplemented with LDN and CHIR until day 10. From day 11 until maturation, early post-mitotic neurons were cultured in neural maintenance medium which was made with a mixture of N2/B27 (1:1 ratio) enriched with the following survival promoting factors: BDNF (R&D; 25 ng/ml), GDNF (R&D; 25 ng/ml), TGFβ3 (R&D; 1 ng/ml), ascorbic acid (Sigma; 200 µM), DAPT (Sigma; 10 µM) and db-cAMP (Sigma; 500 µM). From day 11, the protocol can be continued in two different ways: with lentiviral infection or with the exposure to IWP2.

a. Lentivirus transduction

At d18-d20 of differentiation, depending on their degree of maturation, the cultures were split at a 2:3 ratio (2 wells into 3 wells from a 24 plate) using non diluted Accutase (Millipore). Cells were subsequently plated on 24 well plates previously coated at room temperature during 3 hours in a PBS solution with laminin (Sigma), fibronectin (Sigma) and poly-L-ornithine (Sigma; Kriks *et al.*, 2011). The day after the Accutase split (d19-d21), early post-mitotic neurons were transduced with the control, SOX6 and OTX2 viruses over a period of 48 hours resulting in 70% infection and analysed at day 35.

b. IWP2 induction of substantia nigra like neurons

The IWP2-mediated induction of substantia nigra like dopaminergic neurons was based on alterations in the differentiation protocol previously depicted. The modifications comprised the type of SHH agonist used, the elimination of the Accutase split and the activation time of Wnt signalling.

Progenitors were exposed to SHH C24II+purmorphamine or to two different concentrations of the smoothened agonist SAG (Calbiochem; 100nM or 200nM) at the same time points described in the former neuronal induction protocol. To explore the role that Wnt signalling plays in the development of midbrain dopaminergic neurons, progenitors were treated with different IWP2 (Tocris) concentrations (0.5µM, 1µM, 2µM and 4µM) at several time points: IWP2 d11-d16 or IWP2 d11-d18 (CHIR was added until d11 followed by IWP2 exposure), IWP2 d12-d16 (CHIR was added until d11 and IWP2 exposure started at d12), IWP2 d13-d16 (CHIR was added until d11 and IWP2

exposure started at d13) and CHIR d4-d11+IWP2 d13-d16 (CHIR was added until d13 followed by IWP2 exposure). Progenitors in the CHIR and control conditions were not treated with IWP2. In the CHIR condition progenitors were exposed to CHIR until day 13 whilst in the control condition progenitors were exposed to CHIR until day 11.

2.1.3 Chemical exposure

Post-mitotic neurons (hESC) at day 35 formerly infected with lentivirus were exposed to rotenone (Sigma; 50nM and 100nM) for 24 hours and to MPP^+ (Sigma; 20µM and 50µM) for 96 hours. Similarly, neurons at day 35 differentiated in presence of 0.5µM IWP2, 1 µM IWP2 and with either SAG (200nM) or SHH C24II+purmorphamine, were exposed to rotenone (50nM and 100nM) for 48 hours and MPP^+ (50µM) for 96 hours.

2.2 Human embryonic kidney 293T cells

Human embryonic kidney 293T (HEK 293T) cells were cultured in 175mL flasks with expansion medium consisting in high-glucose DMEM enriched with 10% FBS, 1mM sodium pyruvate, 0.1mM non-essential amino acids, 2mM L-glutamine, 1% penicillin/streptomycin and 0.6% G418 (geneticin). They were split when confluent with TrypleE Express enzyme (Gibco) into new flasks.

For lentivirus production, $30x10^6$ 293T cells/dish were cultured overnight with expansion medium into four 15cm dish. The dishes were previously coated for 1hour at room temperature with a coating solution containing 0.11% acetic acid and collagen diluted in H_2O.

2.3 Human tissue

Human foetal tissue at Canergie stage 16 in figure 3.2 was imported from Erik Sundström and the staff at the gynecology clinic, Karolinska University Hospital, Huddinge. Human embryos were collected after elective routine abortions with consent given by the pregnant women and approval from the Regional Human Ethics Committee, Stockholm. Human foetal tissue at week 20 post conception was obtained from the Developmental Biology Resource (HDBR). The HDBR functions as a Research

Tissue Bank under the approval of the National Research Ethics Service (NRES) and complies with the Human Tissue Act (HTA; 2004). Human tissue at CS 16 and 20 was fixed for 3 hours and human tissue at 18 weeks was fixed overnight in 4% PFA at 4°C, followed by 30% glucose incubation and mounted in tissue-tek. Cryosections of 12 µm for CS 16 and 20 embryos and 14 µm sections of 20-week post-conception embryos were made. Sections used for immunohistochemical analysis were incubated for 20 minutes at 98°C in 10mM citric acid pH 6.0. for antigen retrieval.

2.4 Mouse lines

2.4.1 Animal welfare statement

All mice were kept in standard conditions with food and water ad libitum and maintained on the C57BL/6J genetic background. Mice stayed in the animal house in the University of Leicester, on a 12-hour light/dark cycle, at 50±100% humidity and at 21±1°C. All animal procedures followed the guidelines and legislation as regulated under the Animals Scientific Procedures Act 1986 (ASPA) and were approved by the Animal Welfare and Ethical Review Body (AWERB) from the University of Leicester. Maintenance of the colonies was done by breeding males and females with the selected genotype to keep the transgenic lines. For time mating, females and males were chosen for breeding based on their genotypes. Plugs were checked daily for 3 days and when a plug was detected, females were separated from males. Once females reached the required embryonic stage, they were killed following schedule 1 by cervical dislocation and the embryos were isolated for further analysis.

2.4.2 Genotyping

2.4.2.1 DNA extraction

Adult mice earsnips (colony maintenance) and embryonic biopsy, were used for genotyping. Samples were digested overnight at 56°C with 400µL (270µL for embryos) of tail buffer containing proteinase K (1mg/mL). The next day, volume was completed with tail buffer to reach 750µL solution (400µL for embryos) and mixed with NaCl (2M).

After 10min centrifugation at maximum speed, supernatant was collected. Note that if needed, the supernatant can be centrifuged again to remove possible precipitate residues. Subsequently, DNA was precipitated for 10min at maximum speed following isopropanol (62%) addition. Supernatant was discarded and the pellet was washed with 80% Ethanol. Precipitated DNA was left to dry and was afterwards resuspended in 450µL (250µL for embryos) of TE buffer (10mM Tris pH=8.0 + 0.1mM EDTA pH=8 + water) and kept at 4°C for analysis.

2.4.2.2 PCR

The extracted DNA was amplified by PCR for genotyping of the mouse line. Mastermix was prepared following the Q5 High-fidelity DNA polymerase manufacturer's protocol. For each sample, 50µL of reaction mix was prepared comprising 4µL of sample (DNA extracted), 0.5µL (20mM dNTPs), 5µL primer mixture (10µM), 10µL Q5 High GC Enhancer, 5µL Q5 High-Fidelity DNA polymerase and 25.5µL of nuclease-free H_2O. The PCR reaction conditions for the *Sox6*^{GFPCreERT} and the Gt(ROSA)26 mouse line are described in Table 2.1 and Table 2.2, respectively.

Step	Temperature (°C)	Time (seconds)	Cycles
Initial denaturation	94	120	1x
Denaturing	94	30	35x
Annealing	65	30	
Extension	70	60	
Completion	68	480	1x

Table 2.1 PCR reaction conditions for the *Sox6*^{GFPCreERT} mouse line.

Step	Temperature (°C)	Time (seconds)	Cycles
Initial denaturation	98	120	1x
Denaturing	98	10	35x
Annealing	65	30	
Extension	72	30	
Completion	72	120	1x

Table 2.2 PCR reaction conditions for the Gt(ROSA)26 mouse line.

2.4.3 Tissue preparation

Mouse embryo brains were isolated at the desired embryonic stage and fixed on ice, shaking, in 4% paraformaldehyde (PFA). Note that the time of fixation depended on the embryonic stage (Table 2.3). After, they were incubated in 30% sucrose overnight at 4˚C and subsequently embedded coronally in OCT Compound (VWR). Cryosections (12µM) of mouse embryonic brain were made and stored on superfrost mounting slides (Thermofisher) at -80°C.

Embryonic stage	Fixation time
11.5 - 12.5	1hr
13.5 - 15.5	1hr 30min
17.5 – 18.5	3hr

Table 2.3 Time of fixation depending on the embryonic stage.

2.4.4 *Sox6*^{GFPCreERT} and Gt(ROSA)26 mouse lines

In the *Sox6*$^{GFP\text{-}Cre\text{-}ERT2}$ mouse line the function of the *Sox6* gene is disrupted by the insertion of the eGFP/CreER^{T2} cassette under the control of an ATG codon localised in the exon 8 of the gene (Figure 2.1).

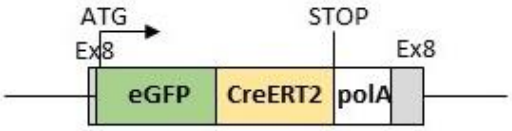

Figure 2.1 Schematic representation of the *Sox6* knock-in locus containing the eGFP/CreER^{T2} cassette. polA (polyA tail), Exon 8 (Ex8).

Females heterozygous (*Sox6*$^{eGFP\text{-}Cre\text{-}ERT2/+}$) were crossed with males heterozygous (*Sox6*$^{eGFP\text{-}Cre\text{-}ERT2/+}$) in order to characterise the mouse line. The embryos wild type (*Sox6*$^{+/+}$), heterozygous (*Sox6*$^{eGFP\text{-}Cre\text{-}ERT2/+}$) and mutants (*Sox6*$^{eGFP\text{-}Cre\text{-}ERT2/eGFP\text{-}Cre\text{-}ERT2}$) were analysed by immunohistochemistry at E11.5, E15.5 and E18.5.

In the ROSA26R^{LacZ} mouse line a stop codon flanked by two *loxP* sites blocks the expression of the *LacZ* gene localised downstream. When crossed with *Sox6*$^{eGFP\text{-}Cre\text{-}ERT2/+}$ mice, and after administration of tamoxifen, CreER^{T2} induces the recombination of the *loxP* sites and therefore allows the constitutive expression of *LacZ* (Figure 2.2).

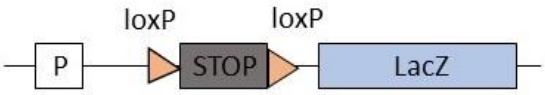

Figure 2.2 Schematic representation of the R26R reporter allele. A loxP site flanked stop codon, under the control of a broadly expressed promoter (P) prevents the downstream expression of LacZ.

Females *Sox6*$^{eGFP\text{-}Cre\text{-}ERT2/+}$ were crossed with males homozygous for the R26R reporter allele (R26R$^{LacZ/LacZ}$) for lineage tracing with tamoxifen administration.

2.4.5 Tamoxifen administration

Pregnant females (Sox6$^{GFPCreERT/+}$), crossed with a homozygous male for the R26R reporter allele, were exposed by oral gavage to 4mg of tamoxifen (10mg/mL), diluted in corn oil, for two or three consecutive days. The exposures as well as the analysis of the embryos were done at different embryonic stages (Table 2.4)

Tamoxifen exposure (embryonic stage)	Fixation embryo (embryonic stage)
8.5+9.5	11.5
10.5+11.5+12.5	18.5
8.5+9.5+10.5	18.5

Table 2.4 Table displaying the embryonic stages of tamoxifen exposure and the stage they were analysed.

2.4.6 Probe synthesis and in-situ hybridisation

2.4.6.1 Probe synthesis

Two different methods were used to produce the in-situ probes of interest either from a plasmid carrying the sequence of interest or from PCR products. The human in-situ probes *AXIN2, LMX1A* and *WNT1* were generated *in vitro* from linearised plasmids. The human and mouse in-situ probes *CORIN* were produced from PCR products.

From all the in-situ probes mentioned before I produced the human in-situ probe *CORIN*. Briefly, the PCR method requires the generation of primers which were selected from the mouse brain Atlas (http://developingmouse.brain-map.org). Then, the gene of interest was amplified by PCR (the PCR protocol used is described in Table 2.2) from hESC derived mDA progenitors (day 13). This was followed by transcription to anti-sense RNA (20µL reaction mixture diluted in water containing 1X transcription buffer, 0.02M DTT, DIG RNA nucleotides 1mM, PCR product 4µg, SP, T7 or T3 RNA polymerase 10U/µL). Then, the mixture was incubated in the water bath at 37°C for 2 hours followed by addition of 100µL TE, 10µL 5MLiCl, 300µL ethanol. Next, samples were incubated overnight at -20°C so the DNA could precipitate. The next day, RNA was centrifuged for 20min at 4°C, the pellet was washed with 70% ethanol and subsequently dried. After resuspending the pellet in 100µL TE the probe was stored at -20°C for further use.

2.4.6.2 In-situ hybridisation

In-situ hybridisation for mouse *Corin* probe was performed on cryosections of E11.5 Sox6GFPCreER^{T} mouse brain from heterozygous mice (Sox6GFPCreER^{T}/WT) and

mutants (Sox6GFPCreER^T/ Sox6GFPCreER^T). The sections were fixed for 10 min with 4% PFA made fresh the same day and washed with 3 washes of PBS. Subsequently, slides were incubated in Proteinase K solution (1µg/mL Proteinase K in 50mM TRIS-Cl pH7.5+ 5mM EDTA in water). After 5 minutes, the fixation and washing steps were repeated. Then, samples were exposed to acetylation solution (1.3% Triethanolamine+0.06% HCl+0.25% acetic anhydride in water) for 10 minutes followed by 2 hours incubation with hybridisation buffer (50% formamide+5X SSC solution+50X Denhart's solution+250µg/mL Baker's yeast RNA+500µg/mL salmon sperm DNA+blocking reagent 20mg/mL in water) in a humidified chamber with a 5X SCC+20% formamide solution. Notice that washes with PBS were done in between these steps. The corin probe was diluted (3µL to 5µL depending on the efficiency of the probe) in 150µL of hybridisation buffer and warmed up in the water bath at 80°C for 5 min. Once cooled down, the probe was added on top of the slides, in the humidified chamber, and were covered with a cover slide to be incubated overnight at 70°C. The next day, cover slides were removed with the help of a 5X SSC solution and incubated for 2 hours in a 0.2X SSC solution. Notice that both solutions are at 70°C. Then, slides, were incubated in a water humidified chamber with 10% heat inactivated FCS diluted in B1 buffer for 1 hour. Afterwards, 0.5mL of anti-DIG antibody (1:5000 dilution in B1 containing 1% FCS) was added on each slide and the humidified chamber was placed at 4°C overnight. When the incubation was finished, the antibody was washed with B1 and B3 buffer and samples were exposed to a solution of 10% PVA (10% polyvinyl alcohol, 100mM Tris pH9.5, 100mM Nacl diluted in water) supplemented with 5 mM $MgCl_2$, NBT, B-CIP and 1X Levamisol. Samples were incubated in the dark for 24 hours, however they could stay in solution from 3 hours to 3 days depending on the probe. Excess of PVA solution was washed off with tap water and mounted with Aquatex. Images of the in-situ hybridisation were taken with the Axiovert.

2.5 Lentivirus production

2.5.1 Lentiviral constructs

Lentiviral constructs were formerly made in the laboratory by cloning cDNAs encoding human *SOX6*, human *OTX2* and GFP into the lentiviral vector pRRL SIN.cPPT.PGK-GFP.WPRE (Addgene) under the regulation of a PGK promoter. The lentiviral vector without insertion was used as a control.

2.5.2 Transfection and collection of the lentiviral particles

The transfection was performed in 293T cells plated at 80% confluency the previous day (refer to 2.1.2 for details). Initially, the viral mixture was prepared by combining the reagents from two different tubes (tube 1 and tube 2) (Table 2.) for 10 minutes at room temperature. During the incubation period of the reagents, 293T cells were washed once with transfection medium (DMEM supplemented with 1mM sodium pyruvate and 0.1mM non-essential amino acids). Next, cells in each dish were incubated with 12mL of transfection media and 6.8mL of viral solution for 4 hours at 37°C. Once time had elapsed, the medium was replaced with 30mL/dish of collection medium (high-glucose DMEM enriched with 10% FBS, 1mM sodium pyruvate, 0.1mM non-essential amino acids, 2mM L-glutamine, 1% Penicillin/Streptomycin, 0.6% G418 (geneticin) and 0.37% sodium bicarbonate). Two days later, the medium containing lentiviral particles was collected, stored in the fridge and replaced with new collection medium (30mL/dish). The following day, the stored and new collection medium were combined, then filtered to remove any debris through a 0.45 µL filter unit. Subsequently, lentiviral particles were concentrated and collected by using an ultracentrifuge (25000rpm for 4 hours). Supernatant was discarded and lentiviral particles were resuspended in 1200 µL of collection media and kept at -80°C in 1.5mL microcentrifuge tubes (100 µL virus/tube) for further use.

Tube 1		Tube 2	
Reagents	**Amount**	**Reagents and plasmids**	**Amount**
Lipofectamine	150µL	Expression vector (SOX6, OTX2, GFP and control)	13.5µg
OptiMEM	4375µL	pLP1	13.5µg
		pLP2	13.5µg
		VSVG	4.5 µg
		optiMEM	2187.5 µL
		PLUSreagent	43.75 µL

Table 2.5 Reagents and plasmids used for the transfection. Notice that pLP1/pLP2/VSVG are packaging plasmids (Invitrogen).

2.6 Immunocytochemistry

Cells were washed once with PBS before fixing them with 2% PFA for 20 min. After two PBS washes, non-specific binding was prevented by incubating cells with blocking solution for 1 hour at room temperature. Then, cells were exposed overnight at 4°C to 500 µL of primary antibodies diluted in blocking solution. The next day, they were washed three times with PBS and incubated with secondary antibodies, diluted in PBS, for 1h at room temperature. After several PBS washes, samples were mounted on a glass slide with mounting solution (Vectashield) and analysed under the confocal microscope.

SOX6 was detected in hESC-derived neurons by using the anti-mouse SOX6 and anti-rabbit SOX6 antibodies. The specificity of the antibodies was characterised by staining 293T cells transfected with increasing quantities of the human SOX6 lentivirus (0µL, 1µL, 5µL, 10µL, 15µL and 20µL).

2.7 Immunohistochemistry

Cryosections were washed once with PBS before exposure to blocking solution (5% donkey serum, 0.25% Triton diluted in PBS) for 1 hour at room temperature. Then, the tissue was incubated overnight at 4°C, in a PBS humidified chamber, with primary

antibodies which were diluted in blocking solution. The next day, the sections were washed three times with PBS and incubated with the secondary antibodies (diluted in PBS) for 1h at room temperature. After several PBS washes, samples were mounted with mounting solution (Vectashield) and analysed under the confocal microscope.
SOX6 was detected in mouse tissue by using the anti-guinea pig SOX6 antibody. The specificity of the antibody was analysed by staining the mouse midbrain and ensuring that the expression of SOX6 in this area was correctly localised.

2.8 RNA extraction

Genetic content from progenitors and post-mitotic neurons was released with 350µL/well of lysate buffer containing β-mercaptoethanol diluted (100X) in RLT buffer. Lysates were collected and centrifuged at room temperature (2 min at maximum speed) in homogenizer tubes (QIAshredder, Qiagen) to filter the debris. Then, total RNA was extracted from lysates by following the protocol in the Qiagen RNeasy micro kit (Qiagen). The process started by adding the same volume of 70% ethanol in the lysates (for RNA precipitation) and this mixture was transferred to the RNeasy MinElute spin column provided with the kit. After a wash with RW1 buffer, samples were incubated for 15min with RDD buffer and DNAse to degrade DNA. Then, samples were washed with RPE buffer and subsequently with 80% ethanol to collect possible RNA trapped in the membrane of the column. Finally, the pellet of RNA was eluted in 14µL of nuclease-free water before measuring its concentration and purity with the nanodrop. RNA samples were stored at -80°C.

2.9 cDNA synthesis and qPCR

cDNA was synthesized from mRNA by using oligodT as a primer (Invitrogen) and the reverse transcriptase III (SuperScipt III from Invitrogen). RNA (500ng) was diluted in nuclease-free water, oligodT and dNTPs. This mixture was warmed up at 65°C for 5 minutes to ensure that RNA was single stranded and to help annealing the RNA with the primer. Subsequently, the mixture comprising the buffer, DTT, RNase inhibitor and SuperScript III, was added to the RNA solution and incubated in the water bath at 50°C. After 50 minutes, the DNA polymerisation was stopped, and the enzyme was

deactivated by heating the solution at 85°C in the heating plate. The cDNA was diluted 17X in nuclease free water and stored at -20°C.

For real time PCR (qPCR) primers of interest (forward and reverse; 100 µM) were diluted in nuclease-free water 10X and stored at -20°C. When performing the qPCR a mixture combining SYBRgreen mastermix and the diluted primers (10X dilution) was made fresh the same day. Previously diluted cDNA was loaded (4.5µL/well) in a 96 multiwell plate along with the primers/SYBRgreen mixture (5.5µL/well) obtaining a primer final concentration of 50nM. Gene expression values were normalized against RPL19 and fold change was calculated using the $2^{-\Delta\Delta CT}$ method (Livak and Schmittgen, 2001).

2.10 ATP assay

The CellTiter-Glo Luminescent cell viability assay (Promega) was employed to determine the ATP content within lentiviral transduced neurons (control, sox6 and otx2) treated with rotenone. Reagents were prepared as described in the protocol provided by the manufacturer. Neuronal temperature was equilibrated at room temperature for 30min with 400µL/well of maintenance media without the survival factors BDNF and GDNF. Subsequently, 400µL/ well of CellTiter-Glo reagent was mixed with the media for 10 minutes at room temperature to allow cell lysis. In order to measure the luminescent signal, 200µL of cell lysate was transferred as triplicates to an opaque 96 well plate (Greiner bio-one) and readings were performed with the GloMax 96 microplate luminometer (Promega). Notice that a control well with no cells was used to determine the luminescence background. In addition, an ATP standard curve was performed in the same 96 well plate by plating different concentrations of ATP stock solution (10µM, 1µM, 0.1µM and 0.01µM) diluted in medium.

2.11 Mitosox assay and fluorescence activated cell sorting

Mature lentiviral transduced (GFP, SOX6, OTX2 and control) dopaminergic neurons exposed to 50nM rotenone for 24 hours, were incubated with 5µM MitoSOX red reagent (Invitrogen) at 37ºC for 30 min, in order to detect mitochondrial superoxide. After three washes with HBSS/Ca/Mg buffer (Gibco), neurons were dissociated with Accutase and centrifuged at 200g for 10 min in 1.5mL microtubes filled with buffer.

Finally, the pellet was resuspended in PBS (Gibco) and samples were analysed by fluorescence activated cell sorting using a BD FACSCanto II Flow Cytometer.

2.12 Cytotoxicity assay

The amount of viable IWP2 derived midbrain dopaminergic neurons and lentiviral infected (control, SOX6 and OTX2) 293T cells treated with 100nM rotenone for 48 hours and 24 hours respectively, was determined by using the cell counting kit-8 (CKK-8) (Dojindo). According to the manufacturer's instructions, neurons were incubated with 500 µL of maintenance medium without BDNF and GDNF and HEK 293T with expansion medium, containing 10% of CCK-8 solution during 1h at 37˚C. The absorbance from distinct samples was measured as triplicates (100 µL/well) in a 96 well microplate reader (Tecan Infinite M200 Pro) at 450nm. Significance was determined by the two-tailed student's t-test.

In the experiment with HEK 293T, cells were plated in a 24 well plate (25000 cells/well). The next day, they were infected during a time period of 48 hours with lentiviral particles (control, SOX6 and OTX2) and subsequently treated for 24 hours with 100nM Rotenone. The same protocol and kit as used with the neurons was employed to measure cell viability of the 293T cells after chemical exposure.

2.13 Seahorse assay

hESC derived neurons, previously infected with control, Sox6 and Otx2 lentiviruses, were plated at day 30, in a 96 well Seahorse plate by using Accutase (100 000 neurons/well). Five days later, at day 35, the Seahorse XF glycolysis stress test was performed by following the manufacturer's protocol. Before starting the measurements, neurons were washed three times with 180µL of sugar-free media, and placed in a CO_2-free incubator for 45 min. In the meantime, glucose (20mM), oligomycin (2µM) and 2-Deoxy-D-glucose (60mM) were loaded in the sensor cartridge which had been previously hydrated with Seahorse XF Calibrant at 37°C in a CO_2-free incubator overnight. The extracellular acidification rate (ECAR) was measured with the Agilent Cell Analysis software in three separate experiments. Notice that the results were normalised to the number of live cells, which were quantified with an automated cell

counter (Bio-Rad). Live cells from dead cells were discriminated by the addition of trypan blue.

2.14 Quantitative mass-spectrometry analysis

Sample preparation: hESC derived mDA neurons infected with empty (control), SOX6 and OTX2 lentivirus were cultured in the laboratory. At day 35, Dr. Clement Soleilhavoup collected and prepared the samples, as follows, for mass spectrometry analysis. Three independent samples for each condition (Control, Sox6 and Otx2) and protein concentration was determined by using Bradford Ragent (Sigma). Each sample was migrated on a 10% SDS-PAGE gel (50V for 30 minutes) and 40µg protein/lane was loaded. The gel was stained with Comassie blue, each lane was isolated and digested with bovine trypsin (Roche). Subsequently, peptides were dried using the SpeedVac.

Nanoflow liquid chromatography tandem mass-spectrometry (NanoLC-Ms/MS): Mass-spectrometry analysis was performed by the University of Tours (France). Peptide extract (5µL) was loaded on a trap column for desalting and separated using a nano-column. Mass spectrometry was done in a dual linear ion trap Fourier transform mass spectrometer (FT-MS) LTQ Orbitrap Velos (Thermo Fisher Scientific) coupled to an Ultimate® 3000 RSLC Ultra High-Pressure Liquid Chromatographer (Dionex).

Protein identification and validation: The University of Tours processed the raw data file with the Proteome Discoverer software (version 2.1; Thermo Fisher Scientific). To generate the peak lists the parameters were a precursor mass range of 350-500 Da and signal to noise ratio of 1.5. They employed the MS/MS ion search from Mascot search engine (version 2.6, Matrix science) coupled to the NCBInr database (mammalia taxonomy, 2017) to identify fragmented ions. Mascot results were analysed with the Scaffold software (version 4.8.9, Proteome Software) by employing the protein cluster analysis feature (proteins that share similar peptides were grouped into clusters). Peptide prophet was utilised to determine confidence in identified spectra. Thus peptide identification was considered correct if the determined probability was higher than 95%. Similarly, protein identifications were considered as correct if the determined proabibility was higher than 95% and they contained at least two identified peptides.

The quantity of identified peptides within samples was predicted by calculating the Exponentially Modified Protein Abundance Index (EMPAI) and the False Discovery Rate (FDR) was <0.01%.

Protein quantification: The University of Tours applied two different quantitative systems: the spectral counting (SC) quantifies and compares the number of fragment spectra detecting peptides of a given protein. The average precursor intensity (API) measures and compares the mass spectrometric signal intensity of peptide precursor ions belonging to a protein. Scaffold Q+ software was used by the University of Tours to calculate the Student's t-test for the SC and API quantifications so the significance between the different conditions L-SOX6 and L-OTX2 as well as L-SOX6 and L-control was determined.

Pathway analysis and gene ontology: To detect proteins differentially expressed I calculated the fold changes between L-SOX6/L-OTX2 and L-SOX6/L-control by using the average of Normalised Weighted Spectra (NWS). I considered only the proteins which averages of NWS were ≥5 and a protein was differentially expressed if the fold change between conditions was >1.5. Results obtained were significant if t-test was >0.05. For pathway analysis I used ToppGene Server to identify pathway enrichment based on the proteins differentially expressed between L-SOX6 and L-OTX2 as well as L-SOX6 and L-control conditions.

2.15 Transplantation studies

Neuronal differentiation: I differentiated hESC into neurons by following the IWP2 and lentiviral protocol (see 2.1.2 for further details).

Cell suspension preparation: Once in Cardiff I performed the following protocol to obtain cell suspension for transplantation. Early post-mitotic neurons were washed two times with PBS to discard the dead and floating cells. Subsequently, neurons were incubated with 500µL/well of accutase during 10 minutes at 37°C for their dissociation, and the reaction was stopped with high glucose tissue culture medium. Then, neurons were centrifuged for 5 minutes at 400X g and the pellet was resuspended in 1mL of HBSS medium supplemented with 1:6 Dornase Alpha as well as 100µL of tissue culture medium. Cells were quantified and the medium was replaced, after centrifugation, with

the correct amount of HBSS + 1:6 Dornase Alpha to achieve 250000 cells/µL. The resulting cell suspension was then left on ice until the transplantation.

Transplantation: Transplantations were performed by Dr. Mariah Lelos research group from the University of Cardiff. Suspension of hESC derived neurons (day 18) exposed to 0.5 µM IWP2 and 1 µM IWP2, as well as control, were transplanted in rats (n=4) lesioned striatal hemispheres. The lentiviral overexpressed Sox6 and Otx2 hESC derived neurons were grafted in rats (n=2) lesioned and unlesioned striatal hemispheres. Six weeks after grafting, brains were perfused and subsequently fixed with 4% PFA for 24 hours. Then, they were stored in 20% sucrose until being sectioned (30µm sections) with a freezing microtome.

2.16 Imaging

Images in figure 3.18, figure 3.21, figure 4.7 figure 4.10 and all the images in chapter 5 except figure 5.3 and figure 5.4 were taken with the confocal microscope Zeiss LSM 880 AiryScan equipped with an Argon 405nm, 458nm, 488nm and 514nm, as well as a HeNe 561nm and 633nm laser. Lateral and axial (Z) resolution being 140nm and 400nm respectively. These images were taken with a x20 objective. The rest of confocal images in the thesis and images in figure 5.3 and figure 5.4 were taken with the confocal microscope Zeiss LSM510 Meta equipped with a MaiTai multiphoton laser, an Argon 488nm, 514nm as well as a HeNe 543nm and 633nm laser. These images were taken with a water immersion x25 objective. Bright-field images for *in-situ*hybridisations were taken with a x10 objective using the Axiovert inverted microscope.

2.17 Data analysis

To assess statistical differences in between two and more than two groups that presented a Gaussian distribution the two tail Student's t-test and the one-way ANOVA have been used, respectively. Data that did not present a normal distribution was analysed with the non-parametric Kruskal-Wallis test. Shapiro-Wilk normality test was used to assess whether the samples presented a Gaussian distribution. Inferential

statistical analysis was done with GraphPad Prism 7 and data was presented as mean values with error bars indicating ± standard deviation (SD).

Neuronal quantifications were done with the help of the software package Photoshop to ensure that cells were counted only once. DAPI stained cells were counted automatically with ImageJ. Neuronal cell bodies expressing TH were used to discriminate neurons from other cell types in tissue cultures. For quantifications of neurons exposed to toxins, $TH^+/DAPI^+$ neurons were counted in 2x2 tile scans (25X objective) from experiments stained with anti-mTH and anti-rbSOX6 antibodies. $SOX6^+/TH^+$ neurons were counted in 4 single scans (25X objective) from experiments stained with anti-mTH and anti-rbSOX6 antibodies. $OTX2^+/TH^+$ neurons were counted in 2X2 tile scans (25X objective) from experiments stained with anti-mTH and anti-gOTX2 antibodies. The quantifications of dopaminergic markers LMX1A and FOXA2 were done by counting neurons expressing FOXA2/TH and LMX1A/TH in 4 single scans (25X objective) from experiments stained with anti-mTH, anti-rbLMX1A and anti-gFOXA2 antibodies. The quantifications of the dopaminergic marker NURR1 were done by counting neurons expressing NURR1/TH in 4 single scans (25X objective) from experiments stained with anti-mTH, anti-rbNURR1 and anti-gFOXA2 antibodies. The quantifications of the marker GIRK2 were done by counting neurons $GIRK2^+/TH^+$ in 3 single scans (25X objective) from experiments stained with anti-gGIRK2, anti-mTH and anti-rbSOX6. The quantifications of the marker CALB1 were done by counting neurons $CALB1^+/TH^+$ in 3 single scans (25X objective) from experiments stained with anti-rbCALB1 and anti-mTH.

2.18 Tables of antibodies and PCR/qPCR primers

Mouse line	Primer name	Primer sequence 5'-3'	Expected size of PCR product		
			WT	+/-	-/-
Sox6$^{GFP\text{-}Cre\text{-}ERT2}$	141551cof-PLI1	GAACGCTGTCCCAGTCAGCATCTTG	760bp	486 + 760bp	486bp
	141553cof-PLI1	ATTGGTGTGCGGTCTGCCACTCA			
	141561-cof-PLI1	AGGCTGGTCTCCAACTCCTAATCTCAGG			
Gt(ROSA)26	oIMR8052	GCGAAGAGTTTGTCCTCAACC	650bp	340 + 650bp	340bp
	oIMR8545	AAAGTCGCTCTGAGTTGTTAT			
	oIMR8546	GGAGCGGGAGAAATGGATATG			

Table 2.6 List of PCR primers used for genotyping the Sox6$^{GFP\text{-}CreERT2}$ mouse line.

Gene	Primer sequence	
hCORIN	ATGGTGACGAGGACTGCAAG	TCACTCACCTAAGCAGCCTGA

Table 2.7 PCR primer used for the hCORIN in-situ probe.

Antigen	Species	Company (cat.n°)	Dilution
ß-galactosidase	Goat	AbD Serotec (4600-1409)	1:5000
CALBINDIN	Rabbit	Swant (CB38)	1:500
CORIN	Rat	R&D Systems (MAB2209)	1:500
FOXA2	Goat	R&D Systems (AF2400)	1:500
GFP	Goat	Abcam (ab6673)	1:500
GFP	Rabbit	Abcam (ab6556)	1:500
GIRK2 (KCNJ6)	Goat	Abcam (ab65096)	1:500
LMX1A	Rabbit	Merck Millipore (AB10533)	1:1000
NESTIN	Mouse	BD Biosciences (611658)	1:1000
NURR1	Rabbit	Santa Cruz (sc-990)	1:1000
OTX2	Goat	R&D Systems (AF1979-SP)	1:500
SATB1	Rabbit	Abcam (ab7004)	1:250
SOX6	Mouse	Santa Cruz (sc-393314)	WB 1:1000 IH: 1:500
SOX6	Rabbit	Atlas Antibodies (HPA001923)	1:1000
SOX6	Guinea pig	gift from Jonas Muhr	1:1500
TH	Mouse	Merck Millipore (MAB318)	1:1000
TH	Rabbit	Pel-Freez (P40101-150)	1:1000
TH	Sheep	Pel-Freez (P60101-150)	1:1000

Table 2.8 List of primary antibodies.

Antigen	Species	Company (cat. no)	Dilution
Anti-Goat Alexa Fluor 488	Donkey	Invitrogen (A-11055)	1:500
Anti-Goat Alexa Fluor 555	Donkey	Invitrogen (A-21432)	1:500
Anti-Goat Alexa Fluor 647	Donkey	Invitrogen (A-21447)	1:500
Anti-Mouse Alexa Fluor 488	Donkey	Invitrogen (A-21202)	1:500
Anti-Mouse Alexa Fluor 555	Donkey	Invitrogen (A-31570)	1:500
Anti-Rabbit Alexa Fluor 488	Donkey	Invitrogen (A-21206)	1:500
Anti-Rabbit Alexa Fluor 555	Donkey	Invitrogen (A-31572)	1:500
Anti-Rat Alexa Fluor 488	Donkey	Invitrogen (A-21208)	1:500
Anti-Sheep Alexa Fluor 555	Donkey	Invitrogen (A-21436)	1:500
Anti-Guinea pig Cy5	Donkey	Stratech (706-175-148-JIR)	1:400

Table 2.9 List of secondary antibodies.

Chapter 3

Wnt signalling inhibition induces Sox6 expression

Chapter 3 Wnt signalling inhibition induces Sox6 expression

3.1 Introduction

As described in chapter 1, iPSC and hESC derived platforms can be differentiated into the desired cellular type, making this technology a promising tool for cell therapy in neurodegenerative diseases, such as Parkinson's disease, but also in drug screenings, toxicological research, or disease modelling. Although previous published protocols differentiate hESC into mDA neurons, it is unclear whether distinct subpopulations are present in the neuronal culture. Yet, the correct modulation of signalling pathways involved into the development of neuronal subtypes could give rise to hESC derived cultures of SN-like or VTA-like mDA neurons.

Wnt signalling has been involved in regulating different aspects of the mDA neuronal development. For instance, Wnt1 has been involved in the positioning of the midbrain-hindbrain boundary and neurogenesis of mDA neurons, while Wnt5a is implicated in later differentiation of mDA neurons. It has been hypothesised that Wnt signalling might be implicated in defining different domains of mDA progenitors and could play a role in the establishment of mDA neuronal diversity. Studies in mice suggest that mDA progenitors, which coexpress Lmx1a and FOXA2 in the ventral midbrain, can be classified, based on the differential expression of Wnt1, into two regions giving rise to distinct populations of mDA neurons. In E11.5 mice embryos laterally located mDA precursors express Wnt-1, Axin2 along with high levels of Otx2 and favourably generate VTA mDA neurons. In contrast, the medially located midbrain progenitors show Corin as well as Sox6 expression and preferentially induce SNc mDA neurons (Figure 3.1 A, B, C, D and E; Panman *et al.*, 2014). Particularly, the study of dynamic changes in Gli and Shh expression in the ventral mesencephalon of mouse embryos, identified that at E11.5, the progenitors laterally located in the developing ventral midbrain generate the ventral medial PN and the IF . Interestingly, an *in vivo* analysis of mice (*Shh::cre;Ctnnb1*$^{lox(ex3)}$) experiencing excessive Wnt/β-catenin signalling in the ventral midbrain, found an increase in the number of Otx2^{+} laterally located progenitors, which expanded into the

medial progenitor domain. Indeed, ablation of Otx2 in the ventral midbrain of mouse embryos (E11.5) results in a lateral expansion of the Sox6 expressing precursor domain (Tang *et al.*, 2010). This suggests that Wnt induces Otx2 expression laterally in the developing ventral midbrain, which in turn restricts Sox6 expression, in the neighbouring, medially located, progenitor domain.

Post mitotically, SNc and VTA mDA neurons express Sox6 and Otx2, respectively. These neuronal post-mitotic subpopulations have also been characterised in different single-cell transcriptomic studies. Interestingly, although in mice showing constitutive expression of Wnt/β-catenin signalling in the ventral midbrain, there is a decrease in the number of mDA neurons, SNc mDA neurons are more severely reduced, in comparison to the VTA mDA neurons (Tang *et al.*, 2010; Nouri *et al.*, 2015).

Therefore, the aim of chapter 3 is to determine promising culturing conditions to differentiate hESC into SNc-like or VTA-like mDA neurons by analysing the interplay between Wnt signalling, Sox6 and Otx2 expression.

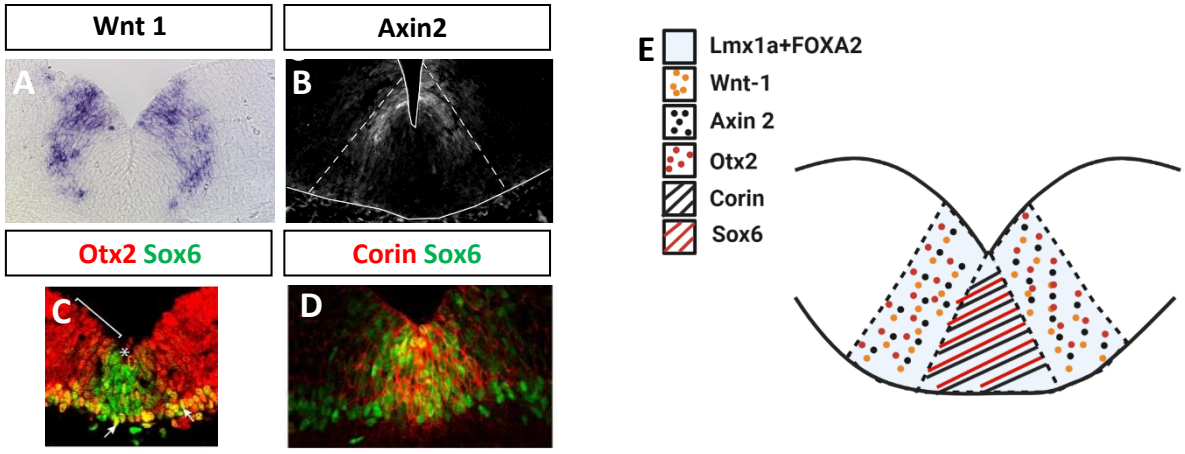

Figure 3.1 Characterisation of two distinct progenitor domains in the developing ventral midbrain. Analysis of (A) Wnt1, (B) Axin2, (C) Otx2 and Sox6 and (D) Corin and Sox6 expression in the mouse ventral midbrain (E11.5). (E) The developing ventral midbrain region giving rise to mDA neurons in mouse (E11.5), characterised by Lmx1a and FOXA2 coexpression, can be divided in two different domains: the lateral domain showing Wnt1, Axin2 as well as Otx2 expression and the medial domain expressing Corin and Sox6. Note that the gene expression analysis has been done by Anderegg et al., 2013 (A and B) and Panman et al., 2014 (C and D).

3.2 Results

3.2.1 SNc and VTA mDA neurons express SOX6 and OTX2 respectively in the human brain

In order to decipher the role that Wnt signalling might play in the differentiation of hESC into SNc-like or VTA-like mDA neurons, it is important to study its pattern of expression in the human brain. Immunohistochemistry and in-situ hybridisation were performed in human midbrain tissue at the Carnegie stages (CS) 16 and 20, which correspond to the postconception (PC) week 6 and 8, respectively. TH immunoreactivity in the mesencephalon, starts to be seen after 6.5 weeks PC (CS18-19) in the region adjacent to the ventricular zone (Freeman *et al.*, 1991). Therefore, expression of SOX6 and LMX1A, as well as the RNA levels of *LMX1A*, *CORIN*, *WNT1* and *AXIN2* were analysed in human mDA progenitors at CS 16 (Figure 3.2). In-situ hybridisation confirmed that in the progenitors expressing *LMX1A*, the medial progenitor domain expresses *CORIN* while the lateral mDA progenitor domain expressed *WNT1* (Figure 3.2 A, B, and C).

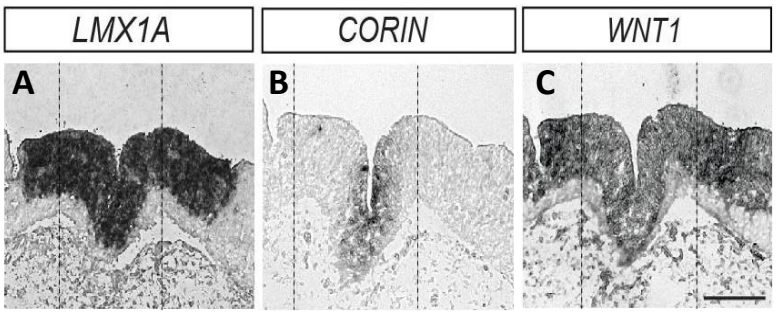

Figure 3.2 Characterisation of the DA medial and lateral progenitor domains in the human midbrain at CS16 (A, B and C) In situ hybridisation in the mDA progenitor domain, as showed by *LMX1A* levels, describes the expression pattern of *CORIN* and *WNT1*. Dash lines separate the medial progenitor from the lateral progenitor domain. (Scale bar: 50µm). Immunohistochemistry and pictures were done by Dr. Clement Soleilhavoup (A, B and C).

At week 20 post conception, the foetal period of development, the expression of SOX6 and OTX2 in mDA neurons was examined in the human midbrain (Figure 3.3 A). Similarly to the mouse, it was observed that TH^+ neurons in the SN and VTA expressed SOX6 and OTX2 respectively (Figure 3.3 B-B'' and C-C''). The expression of SOX6 and OTX2 in mDA

neurons was complimentary and a few VTA mDA neurons expressed SOX6 (Figure 3.3 C'-C'').

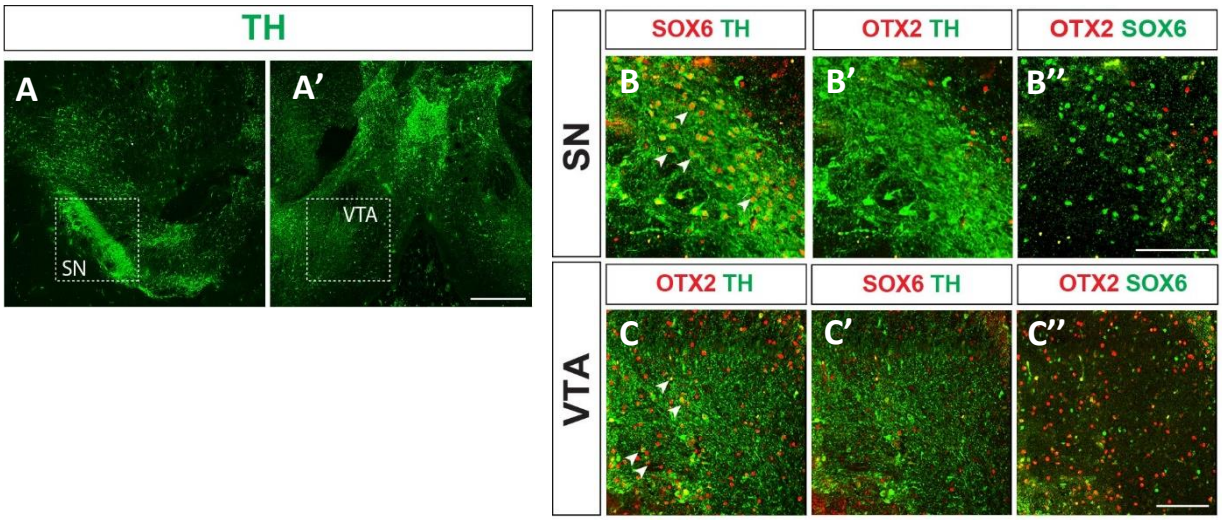

Figure 3.3 SOX6 and OTX2 are expressed in SN and VTA mDA neurons respectively in the human midbrain at week 20. (A and A') Confocal micrograph of human midbrain section stained with anti-mTH antibody (green) shows the localisation of SN and VTA mDA neurons. (Scale bar: 500µm). (B-B'') Confocal micrographs show magnified region denoted by hatched box in A. (B) Confocal micrographs of human midbrain section stained with anti-mTH and anti-gSOX6 antibodies, (B') anti-mTH and anti-gOTX2 antibodies and (B'') anti-gOTX2 and anti-rbSOX6 antibodies. (Scale bar: 100µm). (C-C'') Confocal micrographs show magnified region denoted by hatched box in A'. (C) Confocal micrographs of human midbrain section stained with anti-mTH and anti-rbSOX6 antibodies, (C') anti-mTH and anti-gOTX2 antibodies and (C'') anti-gOTX2 and anti-rbSOX6 antibodies. (Scale bar: 200µm). Arrowheads point to (B) $SOX6^{+}/TH^{+}$ neurons and (C) $OTX2^{+}/TH^{+}$ neurons. Immunohistochemistry and images were done by Dr. Kieran Patrick.

Given that, in the human brain, SNc and the VTA mDA neurons express SOX6 and OTX2 respectively, the expression of these TFs was investigated in the hESC derived mDA neurons obtained with the previous published protocol from Kriks et al., 2011. Immunohistochemistry showed that at day 25 of maturation, mDA neurons expressed high levels of OTX2 and low levels (always overlapping with OTX2) of SOX6 (Figure 3.4).

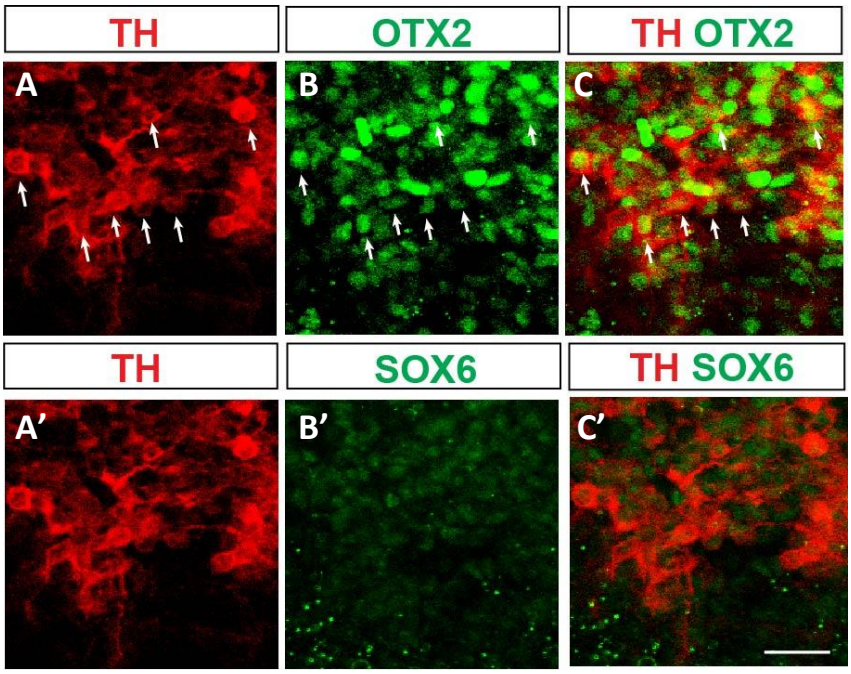

Figure 3.4 hESC derived mDA neurons express OTX2. (A-C') Confocal micrographs of a monolayer of hESC derived neurons at day 25. Images show neurons stained with (A and A'), anti-mTH antibody, (B) anti-gOTX2 antibody, (C) anti-mTH and anti-gOTX2 antibodies, (B') anti-rbSOX6 antibody and (C') anti-mTH and anti-rbSOX6 antibodies. Arrows point at TH+/OTX2+hESC derived mDA neurons (scale bar: 50µm).

3.2.2 Modelling Wnt signalling to obtain SOX6 expressing hESC derived mDA neurons

The midbrain comprises distinct subpopulations of dopaminergic neurons characterised by the expression of different markers. *In vivo* analysis in mouse and human midbrain histological studies, showed that SNc mDA neurons are $SOX6^+$ while the VTA mDA neurons are $OTX2^+$. However, previous published protocols differentiate hESC into mDA neurons that express OTX2 or show SOX6/OTX2 coexpression. Therefore, the next step will be to mimic *in vivo* conditions by generating distinct subpopulations of hESC derived mDA neurons that will express either SOX6 or OTX2.

Based on the previous results, SOX6 expressing mDA neurons are developed from medial progenitor domains in the vMB depleted of Wnt/β-catenin signalling. Thus, it can be hypothesised that inhibiting Wnt signalling in the progenitor stage, will give rise to $SOX6^+$ mDA neurons.

As previously detailed in the introduction, the production of mDA neurons requires the induction of Shh and Wnt signalling in the early stage. In the Krik et al., 2011 protocol, progenitors were exposed to C24II+Purmorphamine and to CHIR for Shh and Wnt signalling activation respectively. The molecule C24II, is the Shh protein-N-terminus, that recognises the Ptc receptor and consequently activates the receptor Smo. At the same time, the molecule purmorphamine binds to Smo, and the activity of both molecules results in a strong induction of Shh signalling. On the other hand, CHIR, inhibits GSK3, subsequently stabilising the expression of β-catenin and triggering Wnt signalling. To generate $SOX6^{+}$ mDA neurons, CHIR treatment was reduced for two days (day 3 to day 11) followed by the inhibition of Wnt signalling with different IWP2 concentrations (0.5µM, 1µM, 2µM and 4µM) during 5 or 7 days. Note that, as detailed in the introduction, IWP2 represses the palmitoylation of Wnt and blocks the exit of the molecule from the ER. The CHIR (CHIR treatment day 3 to day 13) and the control conditions (CHIR treatment day 3 to day 11) were subjected to high and to low levels of Wnt signalling respectively (Figure 3.5 A).

In early post-mitotic neurons (day 25) exposed to the conditions described in Figure 3.5 A, the expression of SOX6 and OTX2 was analysed by immunocytochemistry. Results showed that there was no reduction of OTX2 or increase of SOX6 levels in any of the conditions (Figure 3.5 B).

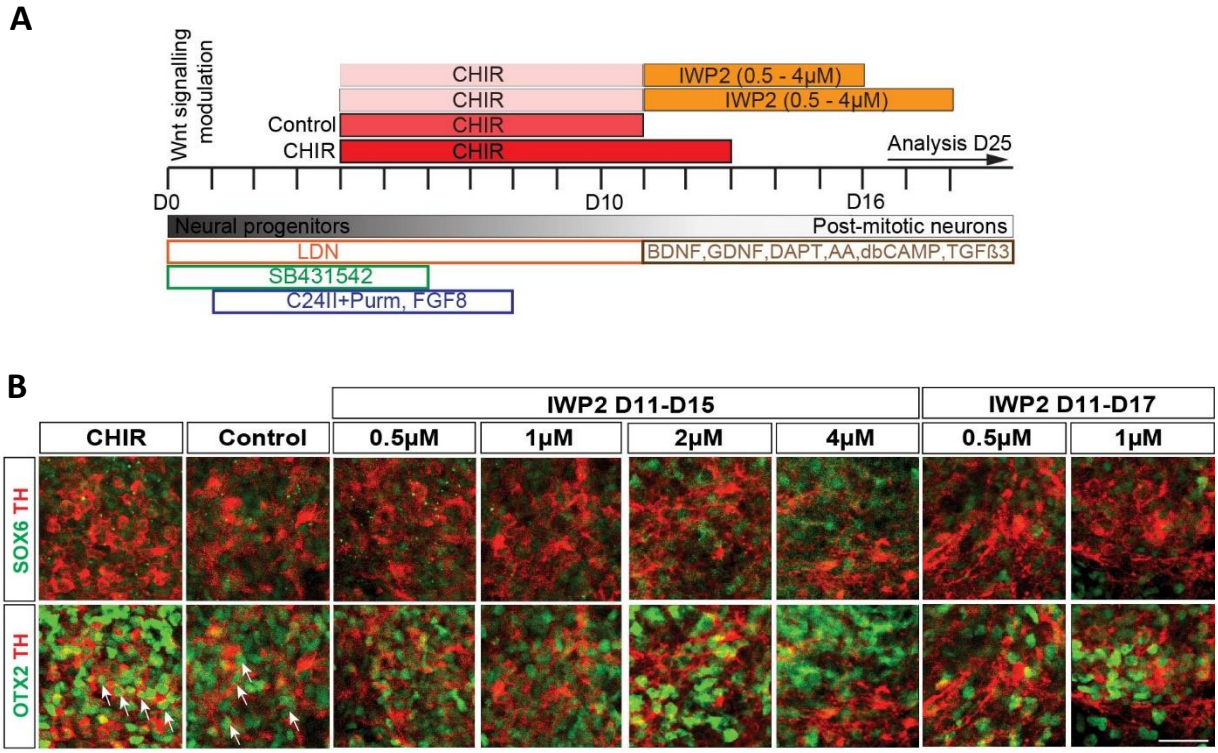

Figure 3.5 SOX6 expression is not increased in C24II+Purmorphamine treated mDA neurons (day 25) upon Wnt signalling inhibition with IWP2. (A) Diagram illustrating the modifications that have been done in the Kriks et al., 2011 protocol to differentiate hESC into mDA neurons. (B) Confocal microscope images of monolayer cultures of hESC derived mDA neurons differentiated with C24II+Purmorphamine and stained with anti-mTH, anti-gOTX2 and anti-rbSOX6 antibodies. Inhibition of Wnt signalling has been done with different IWP2 concentrations (0.5µM-4µM) and at diverse timepoints (for 5 and 7 days) (scale bar: 50µm). D: days. Arrows point to $OTX2^{+}/TH^{+}$ neurons.

Subsequently, the relative expression of *SOX6, OTX2* and *TH* was studied by qPCR and was always compared to the control. *SOX6* expression did not increase in neurons treated for 5 days with 0.5µM, 1µM, 2µM and 4µM IWP2, while *OTX2* expression decreased in neurons exposed to 2µM and 4µM IWP2 for 5 days (Figure 3.6 A). In contrast, long IWP2 exposure (7 days) resulted in an upregulation of *SOX6* expression, which was significant in neurons exposed to 0.5µM IWP2, however *OTX2* levels were maintained and only downregulated in the 1µM IWP2 condition (Figure 3.6 B). Analysis of *TH* indicated that its expression was reduced by 50% at high IWP2 concentrations (2µM and 4µM) and by 30% when exposed to this molecule for a prolonged period of time (7 days). Interestingly, in the presence of high Wnt signalling levels (CHIR condition), *SOX6* expression was downregulated while *OTX2* levels were unchanged (Figure 3.6 A and B).

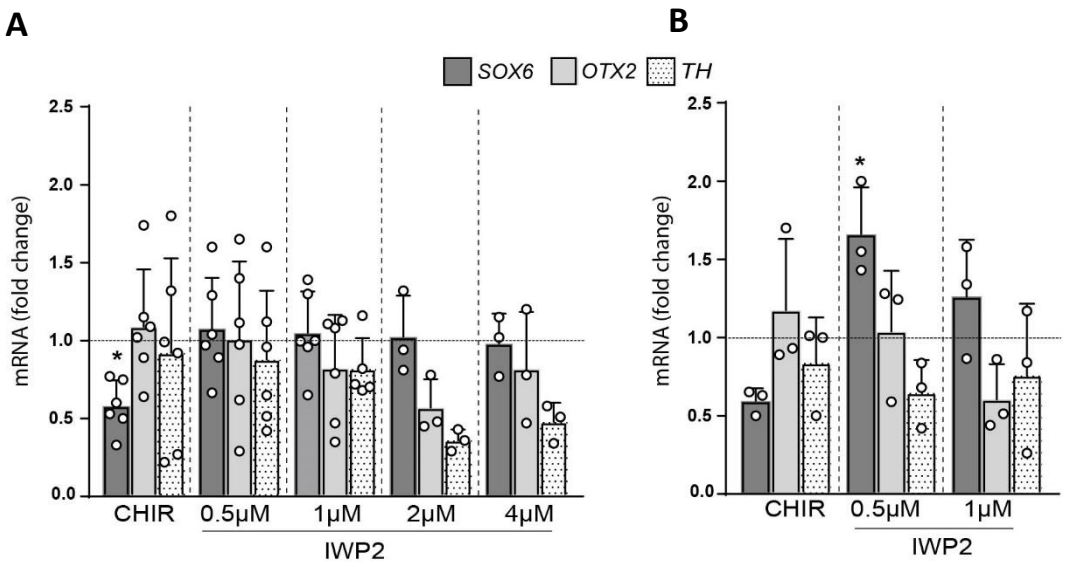

Figure 3.6 Analysis of *SOX6*, *OTX2* and *TH* expression in early post-mitotic neurons at day 25 treated with CHIR or IWP2. (A) Gene expression was examined by qPCR in neurons exposed to CHIR for 10 days and to different IWP2 concentrations (0.5µM-4µM) for 5 days (from d11 until d15); Mean values ± SD; one-way ANOVA (Sidak) and Kruskall-Wallis (Dunn); experimental replicates; n=6/3. (B) Gene expression was examined by qPCR in neurons exposed to CHIR for 10 days and to different IWP2 concentrations (0.5µM-1µM) for 7 days (from d11 until d17). Relative *SOX6*, *OTX2* and *TH* mRNA levels were compared to the control condition (normalized to 1). Mean values ± SD; one-way ANOVA (Sidak) and Kruskall-Wallis (Dunn); experimental replicates; n=3. *p < 0.05, **p < 0.01 and ***p< 0.001.

Given that there was no significant increase in SOX6 or decrease in OTX2 expression, the activation of Wnt signalling was studied in the progenitors by examining the levels of the Wnt/β-catenin downstream targets *AXIN2* and *SP5*. Note that these TFs are upregulated when Wnt signalling is activated. qPCR results showed that upon Wnt signalling repression by IWP2 exposure, *AXIN2* expression was not significantly reduced. *SP5* expression presented a 2-fold decrease when compared to the control, but the reduction was not significant. As expected, in the CHIR condition, the levels of *AXIN2* and *SP5* were significantly upregulated, 2-fold and 5-fold increase respectively, suggesting that these progenitors had been exposed to higher levels of Wnt signalling in comparison to the control (Figure 3.7).

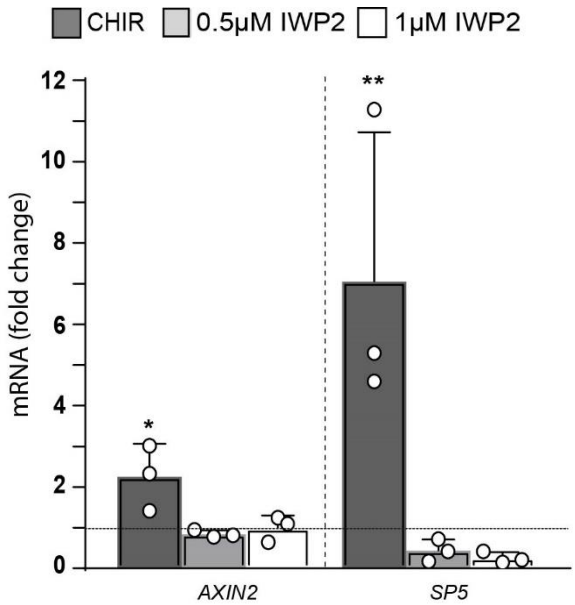

Figure 3.7 Wnt signalling is feebly repressed in C24II+Purmorphamine treated mDA progenitors exposed to IWP2. Relative *AXIN2* and *SP5* mRNA levels were quantified by qPCR and compared to the control condition (normalized to 1). Mean values ± SD; one-way ANOVA (Dunnett); experimental replicates; n=3. *p < 0.05 and **p < 0.01.

Analysis of *SOX6* and *OTX2* expression in progenitors revealed that *SOX6* levels were increased but *OTX2* levels were unchaged in the IWP2 treated cells, in comparison to the control condition. When comparing the CHIR with the control condition, it was observed that *SOX6* expression was barely reduced, while *OTX2* expression was significantly increased in the presence of high levels of Wnt signalling. Although *SOX6* levels were increased upon Wnt signalling repression, *OTX2* levels did not vary between conditions. Surprisingly, a reduction in *SOX6* expression was not observed in the CHIR condition when compared to the control (Figure 3.8). All together, these results suggest that IWP2 blocks Wnt signalling in Shh+purmorphamine treated progenitors because *SP5* levels are reduced in the progenitors exposed to IWP2. However, the repression might be inefficient given that *AXIN2* is only slighlty downregulated when the Wnt pathway is repressed in the IWP2 treated progenitors.

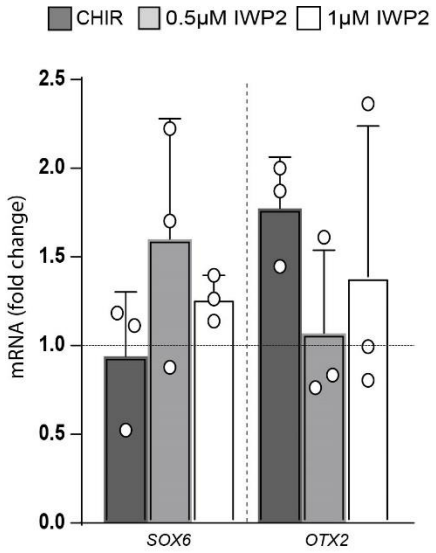

Figure 3.8 C24II+Purmorphamine derived mDA progenitors (day 13) do not present a reduction of *OTX2* levels upon Wnt signalling inhibition with IWP2. Relative *SOX6* and *OTX2* mRNA levels were quantified by qPCR and were compared to the control condition (normalized to 1). Mean values ± SD; one-way ANOVA (Dunnett); experimental replicates; n=3.

3.2.3 Shh signalling levels are critical for the efficient induction of hESC derived mDA neurons expressing SOX6

With the aim to understand why Wnt signalling is not very successfully repressed in the former protocol, the interaction between Shh signalling and SOX6 was examined. As described in the introduction, Shh pathway induces Lmx1a expression which in turn activates Wnt signalling forming an autoregulatory loop (Wnt pathway activates Lmx1a expression). Therefore, high Shh signalling levels strongly stimulate Lmx1a expression which consecutively activates the Wnt pathway impairing its inhibition by IWP2.

According with this hypothesis, Shh levels were decreased in the differentiation protocol, in order to create the optimal conditions to efficiently repress the Wnt pathway. This was achieved by replacing the Shh signalling activators C24II and purmorphamine with an inducer of the receptor Smo, the smoothened agonist (SAG). Analysis of the Shh signalling downstream target *GLI1* confirmed that its expression was 70% lower in early progenitors (day 8) exposed to 100nM SAG than in the Shh+purmorphamine treated mDA precursors (Figure 3.9).

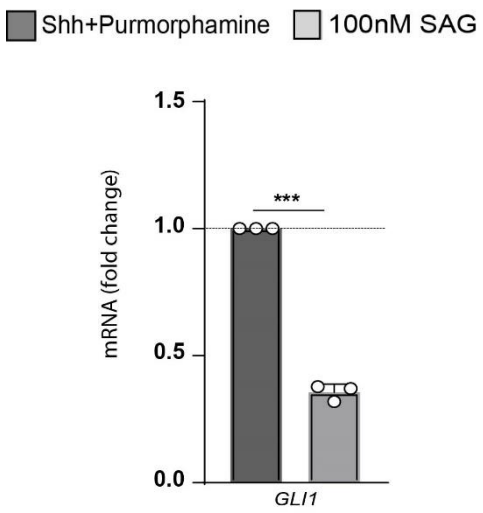

Figure 3.9 *GLI1* expression is reduced in 100nM SAG treated mDA progenitors at day 8. Relative *GLI1* mRNA levels in progenitors from the 100nM SAG protocol were quantified by qPCR and compared to the C24II+Purmorphamine condition (normalized to 1). Mean values ± SD; unpaired t-test (Welch); n=3. ***p < 0.001.

In the modified protocol, 100nM SAG replaced C24II and purmorphamine. The inhibition of Wnt signalling by IWP2 was done at different time points to determine the best condition for SOX6 induction. Because of the loss of *TH* expression in neurons exposed to IWP2 for 7 days and at high IWP2 concentrations, differentiation was performed under 0.5µM and 1µM IWP2 for 5 days. In addition, later exposure was investigated, by adding IWP2 from day 13. Similarly, to the C24II and purmorphamine protocol, CHIR treatment was reduced 2 days, except for the condition in which CHIR was kept until day 13 followed by IWP2 addition (Figure 3.10 A). Study of SOX6 and OTX2 expression by immunocytochemistry in early post-mitotic neurons (day 25) exposed to 100nM SAG, revealed that $SOX6^+/TH^+/OTX2^-$ mDA neurons were present when Wnt signalling was inhibited (0.5µM and 1µM IWP2 were added at day 11 and day 13). In addition, the amount of $OTX2^+/TH^+$ neurons was reduced when compared to the control and the CHIR conditions. When IWP2 was added at day 13 without shortening CHIR exposure, no difference was observed in comparison with the control condition (Figure 3.10 B).

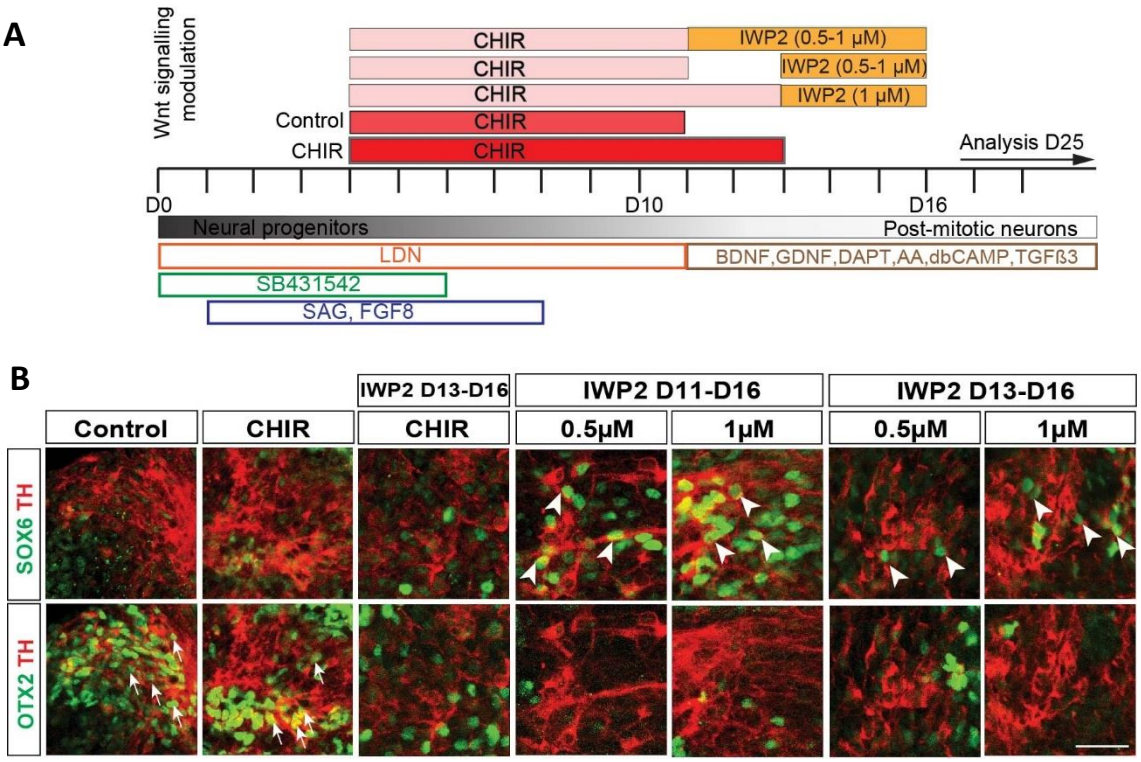

Figure 3.10 Low Shh signalling levels and inhibition of Wnt signalling are crucial for SOX6 induction in early post-mitotic mDA neurons (day 25). (A) Diagram illustrating the modifications that have been done in the Kriks et al., 2011 protocol to differentiate hESC into mDA neurons. (B) Confocal microscopy images of monolayer cultures of hESC derived mDA neurons differentiated with SAG and stained with anti-mTH, anti-gOTX2 and anti-rbSOX6 antibodies. Inhibition of Wnt signalling has been done with different IWP2 concentrations (0.5µM-1µM) and at diverse timepoints (for 3 and 5 days) (scale bar: 50 µm). D: days. Arrowheads point to $SOX6^+/TH^+$ neurons. Arrows point to $OTX2^+/TH^+$ neurons.

SOX6 and *OTX2* gene expression was determined by qPCR and normalised to the control in early post-mitotic neurons at day 25, exposed to IWP2 for 5 (from day 11 to day 15) and 3 days (from day 13 to day 15). Results revealed that post-mitotic neurons treated with 0.5µM and 1 µM IWP2 for 5 days showed a 1.2-fold increase in SOX6 levels, while neurons having Wnt signalling activated (CHIR condition) presented a 2.5-fold reduction in SOX6 expression (Figure 3.11 A). Conversely, OTX2 levels were significantly decreased by 50% in all the conditions, including CHIR (Figure 3.11 A and B). Neurons treated with IWP2 for 3 days, did not show a significant increase or decrease in SOX6 and OTX2 levels, respectively (Figure 3.11 B). Therefore, based on the former immunocytochemistry and gene expression results, the best conditions for the induction of hESC derived mDA $SOX6^+/TH^+$ neurons are the combination of weak Shh signalling induction, via SAG, and the inhibition of Wnt signalling with IWP2 for 5 days (from day 11 to day 15).

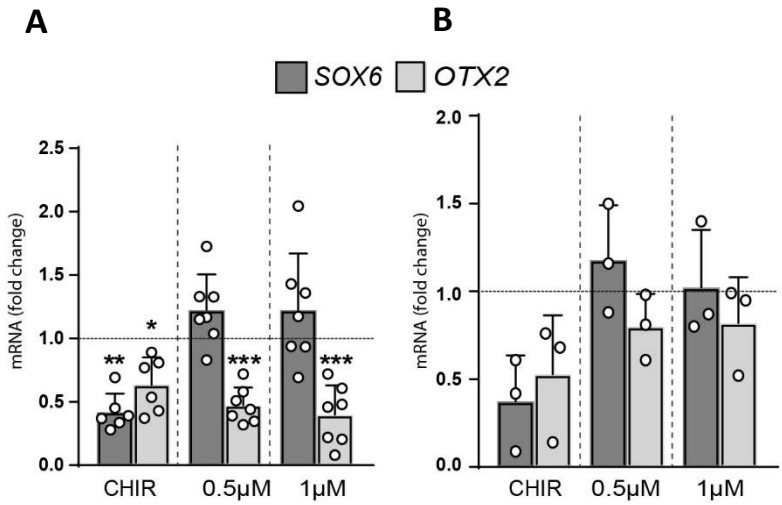

Figure 3.11 Analysis of *SOX6* and *OTX2* expression in early mDA post-mitotic neurons at day 25 differentiated with 100nM SAG. (A) Gene expression was examined by qPCR in neurons exposed to different IWP2 concentrations (0.5µM-1µM) for 5 days (from d11 until d15); Mean values ± SD; one-way ANOVA (Sidak); experimental replicates; n=6/7. (B) Gene expression was examined by qPCR in neurons exposed to different IWP2 concentrations (0.5µM-1µM) for 3 days (from d13 until d15); Mean values ± SD; one-way ANOVA (Sidak); experimental replicates; n=3. Relative *SOX6* and *OTX2* mRNA levels were quantified by qPCR and compared to the control condition (normalized to 1). *p < 0.05, **p < 0.01 and ***p< 0.001.

Next, *FOXA2* and *LMX1A* expression was analysed in precursors, at day 13, differentiated in presence of low Shh signalling levels (100nM SAG). Results showed that, their expression was unchanged when antagonising Wnt signalling in comparison to CHIR and the control (Figure 3.12).

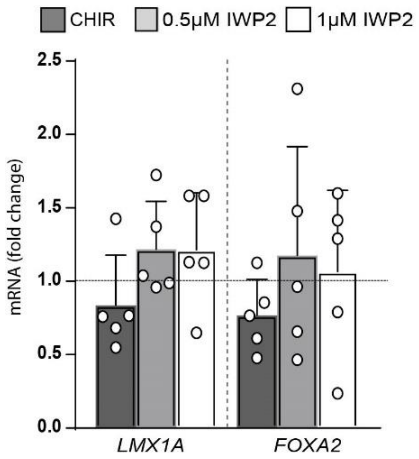

Figure 3.12 *LMX1A and FOXA2* expression is maintained throughout the different conditions in 100nM SAG derived mDA progenitors (day 13). Relative *LMX1A* and *FOXA2* mRNA levels in progenitors exposed to 0.5µM and 1µM IWP2 were quantified by qPCR and compared to the control condition (normalized to 1). Mean values ± SD; one-way ANOVA (Dunnett); experimental replicates; n=5.

Although midbrain dopaminergic identity was maintained when repressing Wnt signalling, immunocytochemistry revealed that most of the NESTIN$^+$ progenitors were not LMX1A$^+$ and FOXA2$^+$ (Figure 3.13 A). Therefore, LMX1A and FOXA2 gene expression from progenitors exposed to 100nM SAG was compared with precursors differentiated with C24II + purmorphamine. Results showed that LMX1A and FOXA2 levels were dramatically downregulated (34-fold decrease) in progenitors exposed to 100nM SAG (Figure 3.13 B). Overall, this suggests that midbrain dopaminergic identity is lost in progenitors exposed to low levels of Shh signalling.

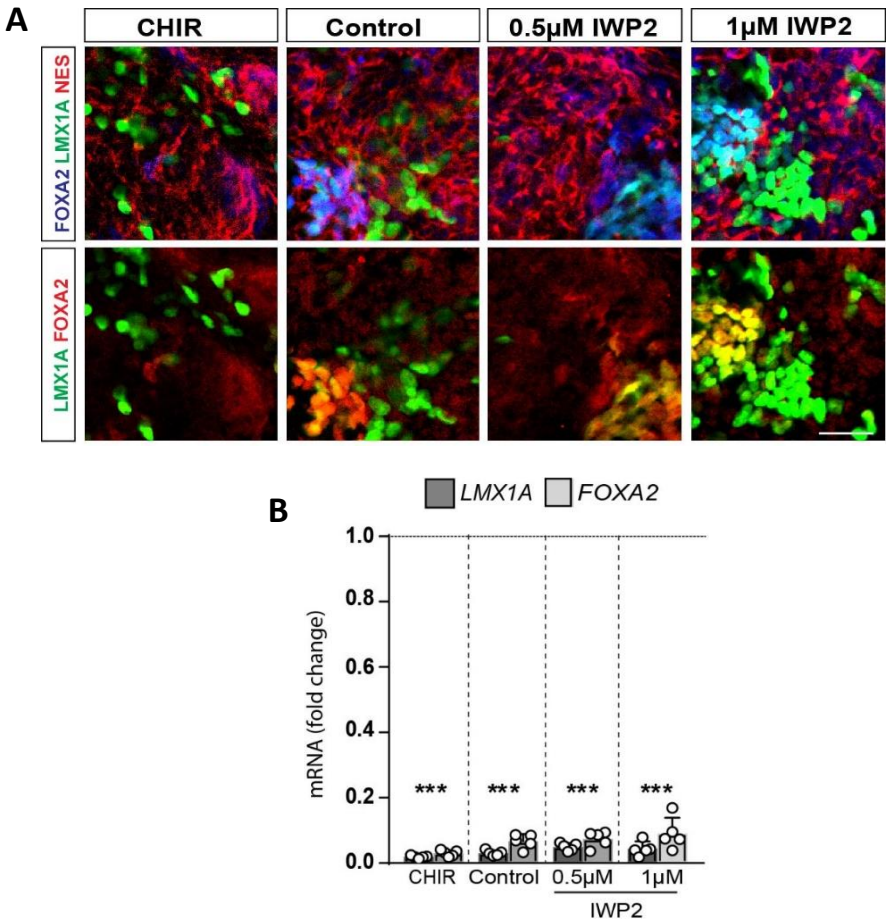

Figure 3.13 Expression of midbrain dopaminergic markers LMX1A and FOXA2 is dramatically decreased in progenitors (day 13) exposed to 100nM SAG. (A) Confocal microscopy images of monolayer cultures of hESC derived mDA progenitors stained with anti-rbLMX1A, anti-gFOXA2 and anti-mNESTIN antibodies. Progenitors were treated with IWP2 and exposed to 100nM SAG (Scale bar: 50µm). (B) Relative *LMX1A* and *FOXA2* mRNA levels in progenitors from the 100nM SAG protocol were quantified by qPCR and compared to the C24II+Purmorphamine condition (normalized to 1). Mean values ± SD; one-way ANOVA (Dunnett); experimental replicates; n=5. ***p < 0.001.

To obtain optimal Shh signalling levels permitting efficient Wnt pathway repression without losing midbrain dopaminergic identity, the concentration of SAG was doubled (200nM). Gene expression analysis by qPCR demonstrated that progenitors exposed to 200nM SAG, presented a 1.4-fold increase in *GLI1* levels in comparison to the precursors treated with 100nM SAG (Figure3.14 A). However, Shh signalling levels in 200nM SAG progenitors remained 2-fold lower when compared with the C24II+Purmorphamine progenitors (Figure 3.14 B).

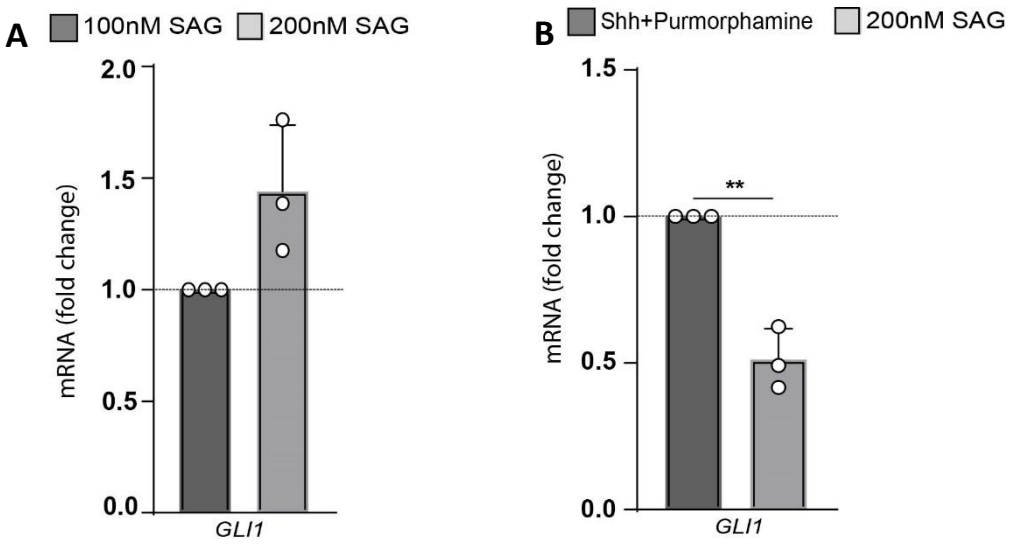

Figure 3.14 *GLI1* expression is increased in mDA progenitors (day 8) differentiated with 200nM SAG. (A) Relative *GLI1* mRNA levels in progenitors from the 200nM SAG protocol were quantified by qPCR and compared to the 100nM SAG condition (normalized to 1). (B) Relative *GLI1* mRNA levels in progenitors from the 200nM SAG protocol were quantified by qPCR and compared to the C24II+Purmorphamine condition (normalized to 1). Mean values ± SD; unpaired t-test (Welch); technical replicates; n=3. **p < 0.01.

Then, mDA identity was assessed throughout the quantification of *LMX1A* and *FOXA2* gene expression by qPCR. Data revealed that, as with the other protocol (100nM SAG), *LMX1A* and *FOXA2* levels were maintained when Shh signalling was inhibited (Figure 3.15).

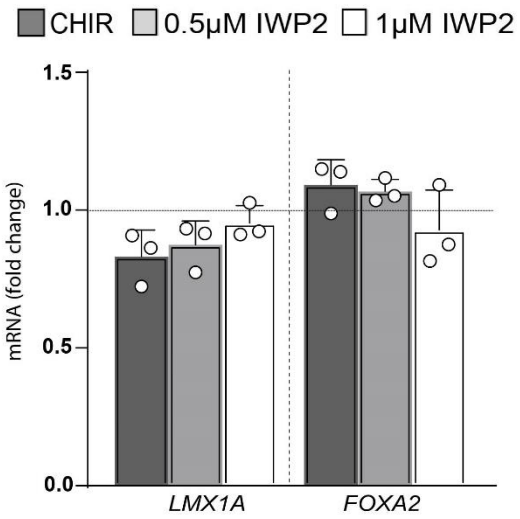

Figure 3.15 *LMX1A* and *FOXA2* expression is conserved upon IWP2 exposure in mDA progenitors (day 13) differentiated with 200nM SAG. Gene expression was examined by qPCR in precursors exposed to different IWP2 concentrations (0.5µM-1µM) for 5 days (from d11 until d15). Relative *LMX1A* and *FOXA2* mRNA levels were compared to the control condition (normalized to 1); Mean values ± SD;one-way ANOVA (Dunnett); technical replicates; n=3.

Further study of LMX1A and FOXA2 by immunocytochemistry showed that the number of precursors NESTIN^{+} coexpressing LMX1A and FOXA2 was significantly higher in the 200nM SAG than in the 100nM SAG protocol. However, some progenitors remained negative for LMX1A and FOXA2 (Figure 3.16 A). Interestingly, results showed that *LMX1A* and *FOXA2* expression was increased 3 to 4-fold in progenitors exposed to 200nM SAG, when compared to the precursors differentiated in presence of 100nM SAG (Figure 3.16 B).

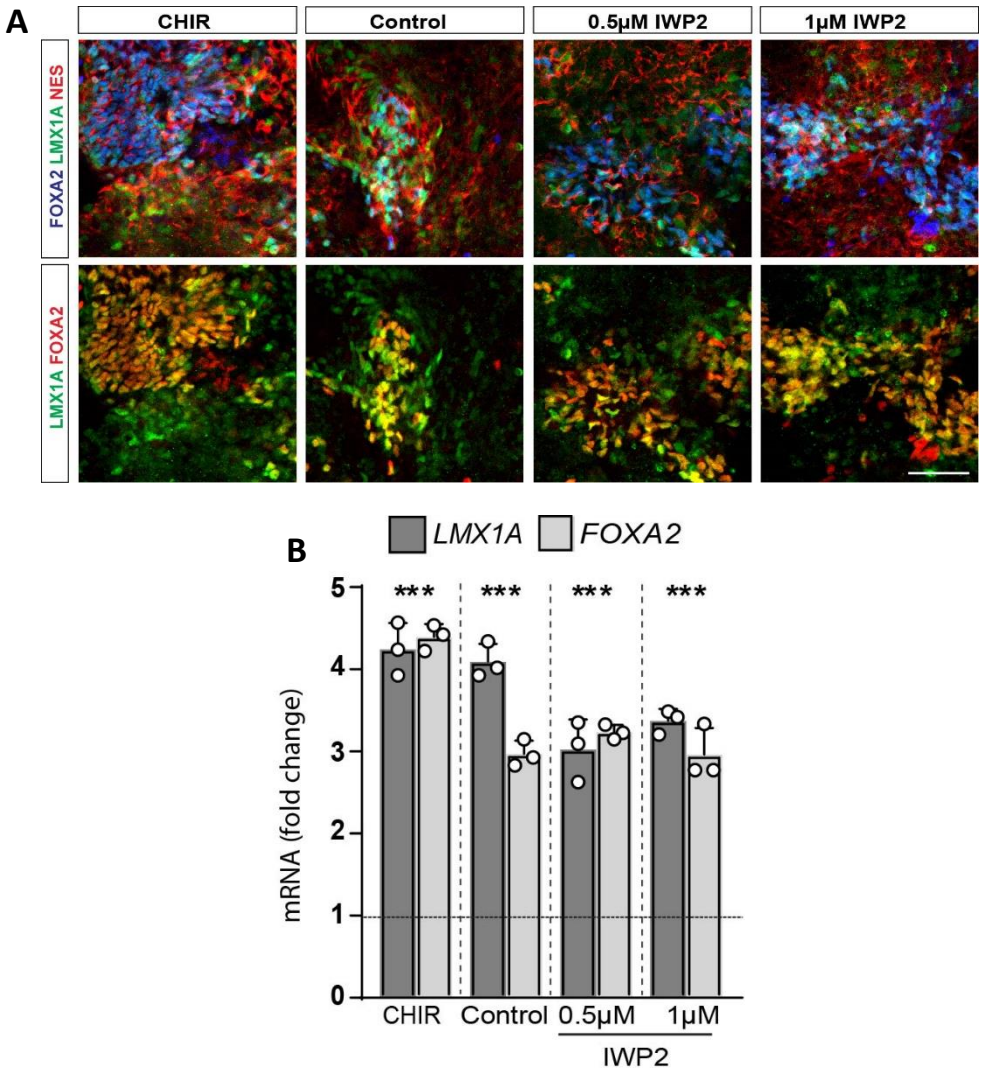

Figure 3.16 Expression of midbrain dopaminergic markers LMX1A and FOXA2 increases in progenitors (day 13) exposed to 200nM SAG. (A) Confocal microscopy images of monolayer cultures of hESC derived mDA progenitors stained with anti-rbLMX1A, anti-gFOXA2 and anti-mNESTIN antibodies. Progenitors were treated with IWP2 and exposed to 200nM SAG (B) Quantification by qPCR of the relative *LMX1A* and *FOXA2* mRNA levels in progenitors, exposed to 200nM SAG were compared to the 100nM SAG condition (normalized to 1); Mean values ± SD;one-way ANOVA (Dunnett); experimental replicates; n=3. ***p< 0.001.

Further examination of the *SOX6, OTX2, AXIN2*, *SP5* and *CORIN* levels was done in the progenitors exposed to 200nM SAG by qPCR. Interestingly, *SOX6* and *CORIN* were upregulated, 1.5-fold and 3-fold respectively, while *OTX2* and *SP5* were significantly downregulated, 1.5-fold and 5-fold respectively, in the IWP2 treated progenitors when compared to the control. *AXIN2* levels were 2-fold decreased although the downregulation was not significant. Conversely, *SOX6* and *CORIN* were downregulated,

1.5-fold and 6.5-fold decrease respectively, while *OTX2, AXIN2* and *SP5* were upregulated, 1.3-fold, 1.5-fold and 2-fold increase respectively, in the CHIR condition when compared to the control. Indeed, the variations observed in *SOX6, OTX2* and *CORIN* levels, were also detected by immunostainings (Figure 3.17 A, B and C). This data indicates that Wnt signalling was effectively inhibited in progenitors exposed to IWP2, and that the levels of this pathway were higher in the CHIR condition than in the control. Furthermore, these results support the idea that Wnt signalling antagonises SOX6 as well as CORIN expression.

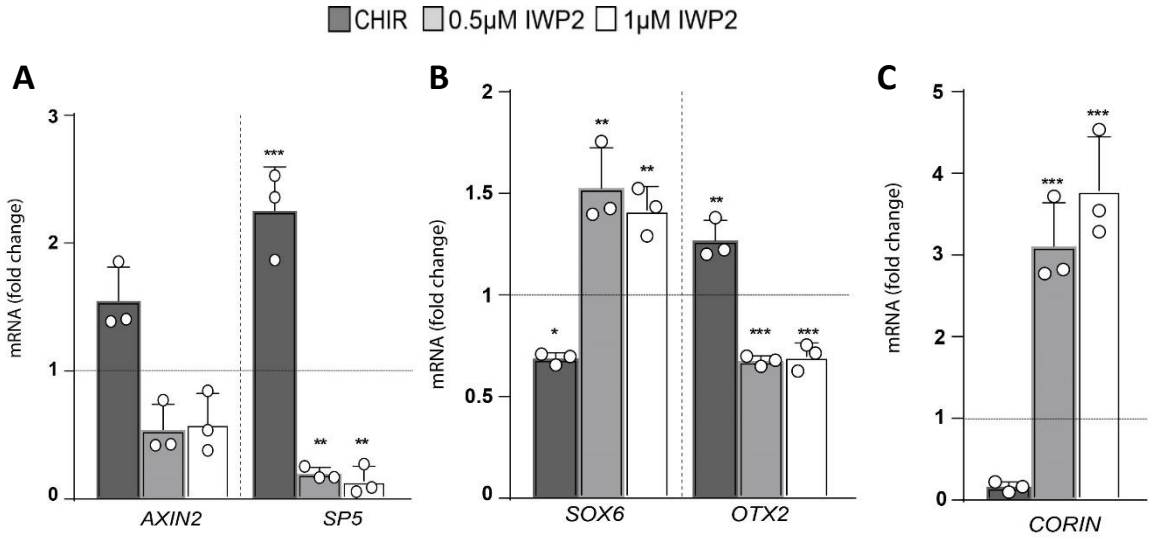

Figure 3.17 Progenitors (day 13) differentiated with the 200nM SAG protocol show an efficient repression of Wnt signalling. (A) *AXIN2* and *SP5* expression was quantified by qPCR upon Wnt signalling activation (CHIR) and inhibition (IWP2). (B and C) *SOX6*, *OTX2* and *CORIN* expression was quantified by qPCR upon Wnt signalling activation (CHIR) and inhibition (IWP2). Relative *AXIN2, SP5, SOX6, OTX2 and CORIN* mRNA levels in progenitors exposed to 0.5µM and 1µM IWP2, were compared to the control condition (normalized to 1); Mean values ± SD; one-way ANOVA (Dunnett) and Kruskall-Wallis (Dunn); technical replicates; n=3. *p<0.05, **p<0.01 and ***p< 0.001.

Subsequently, SOX6 and OTX2 expression was analysed in early post-mitotic neurons at day 25. Quantifications of $TH^+/SOX6^+$ and of $TH^+/OTX2^+$ neurons revealed that in presence of IWP2 the number of TH neurons expressing SOX6 was significantly increased, reaching 35%, in comparison to the control and CHIR conditions. In contrast, the amount of IWP2 treated neurons coexpressing TH and OTX2 was 50% lower than in the control and CHIR mDA neurons (Figure 3.18 A and B). Thus, Wnt signalling inhibition

together with the optimal Shh signalling levels, gives rise to hESC derived mDA neurons expressing $TH^+/SOX6^+/OTX2^-$.

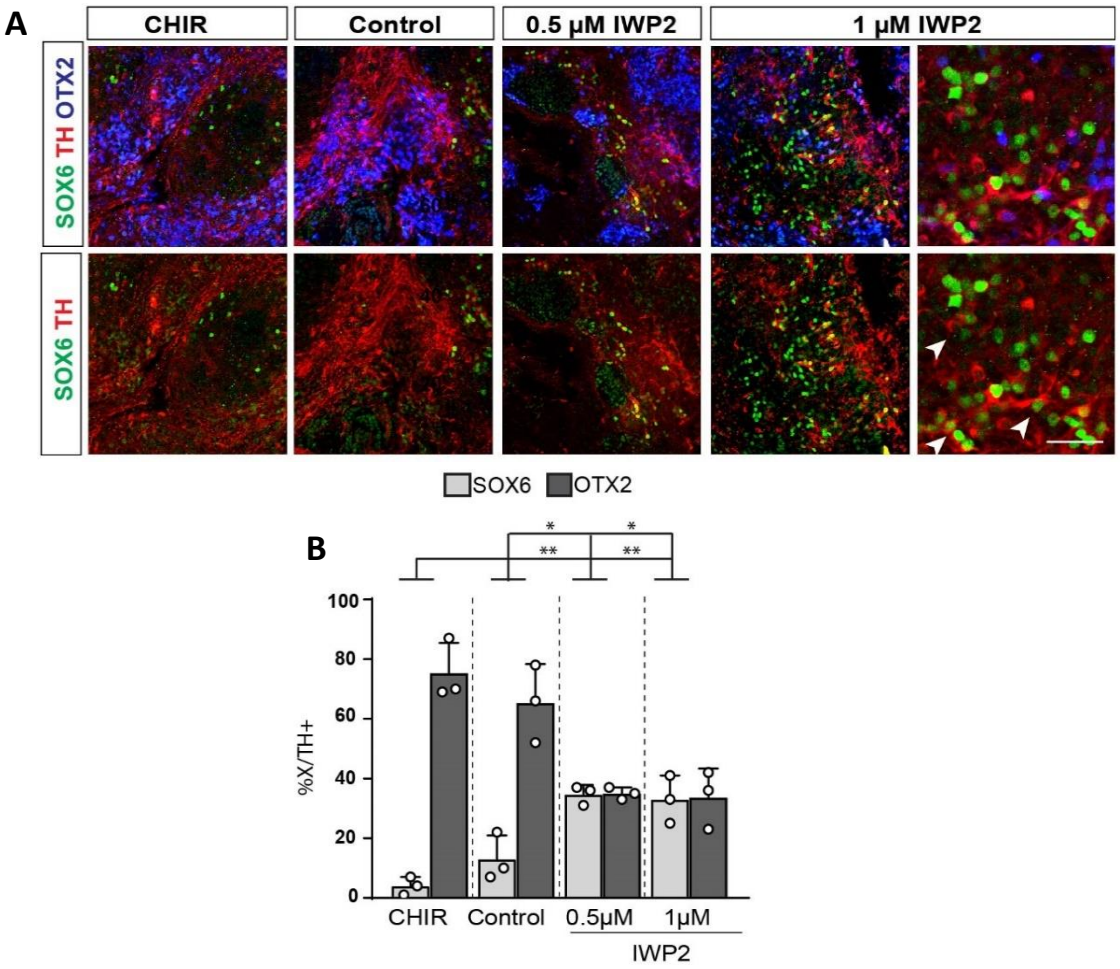

Figure 3.18 Wnt signalling inhibition with IWP2 gives rise to mDA neurons expressing SOX6 differentiated with 200nM SAG. (A) Confocal microscopy images of monolayer cultures of hESC derived mDA progenitors stained with anti-mTH, anti-rbSOX6 and anti-gOTX2 antibodies. (Scale bar: 50µm). Arrowheads indicate $TH^+/SOX6^+$ derived mDA neurons. (B) Number of $TH^+/SOX6^+$ and $TH^+/OTX2^+$ mDA neurons. Mean values ± SD;one-way ANOVA (Sidak); experimental replicates; n=3. *p<0.05 and **p<0.01.

3.2.4 Investigation of Wnt signalling antagonism by IWR1, dkk1 and XAV939

To confirm that SOX6 induction was due to the inhibition of Wnt signalling and was not a consequence of an IWP2 related mechanism, the repressors IWR1, DKK1 and XAV939 were used to antagonise Wnt signalling. As detailed in the introduction, IWR1 and XAV939 act by stabilising the destruction complex in the Wnt/β-catenin pathway leading to the degradation of β-catenin. On the other hand, DKK1 binds to the coreceptor

LRP5/6 resulting in the inhibition of Wnt/β-catenin signalling (for more detail see Chapter I).

Consistent with the IWP2 treatment, repressors were added for 5 days (from day 11 to day 15) previous CHIR reduction and the conditions CHIR as well as control were the same as previously described in the IWP2 protocol. However, because of time constraints, DKK1 and IWR were tested in the 100nM SAG protocol while XAV939 was analysed in the 200nM SAG protocol.

Analysis of SOX6 expression in early post-mitotic neurons at day 25 showed that while repression of Wnt signalling by DKK1 induced SOX6 expression (similar to the IWP2 treatment), IWR treatment was not able to generate such neuron types (Figure 3.19).

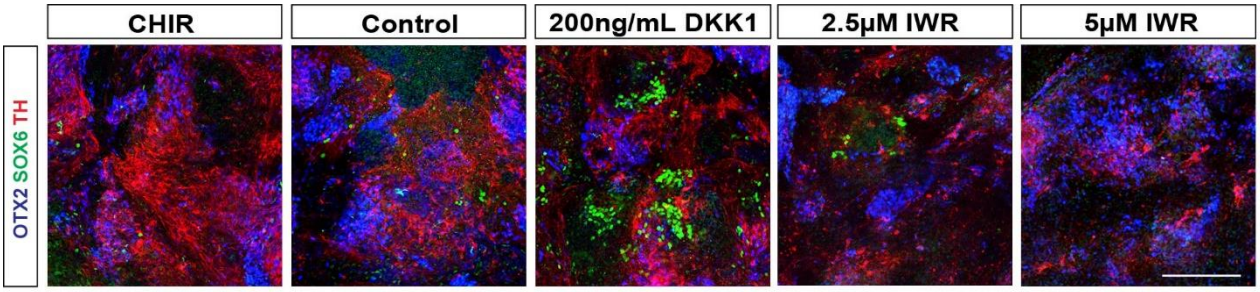

Figure 3.19 SOX6 expression is induced when inhibiting Wnt signalling with DKK1 in early post-mitotic neurons (day 25) differentiated with 100nM SAG. Confocal microscopy tile scans of monolayer cultures of hESC derived mDA neurons stained with anti-mTH, anti-rbSOX6 and anti-gOTX2 antibodies. Neurons were exposed to the Wnt inhibitors dkk1 and IWR. (Scale bar: 50µm).

Next, gene expression in precursors (day 13) exposed to DKK1, was analysed. Interestingly, *AXIN2* levels were not downregulated while *SP5* levels presented a 1.5-fold decrease when compared to the control (Figure 3.20 A). Similarly, to the IWP2 treatment, *SOX6* and *CORIN* levels were upregulated whilst *OTX2* levels were downregulated in comparison to the control (Figure 3.20 B and C). Overall, these results suggest that, as shown by the downregulation of *SP5*, Wnt signalling was inhibited. Although, a decrease in *AXIN2* expression could not be detected, the inhibition was robust enough to cause a decrease in *OTX2* and an increase in *SOX6* as well as in *CORIN* expression.

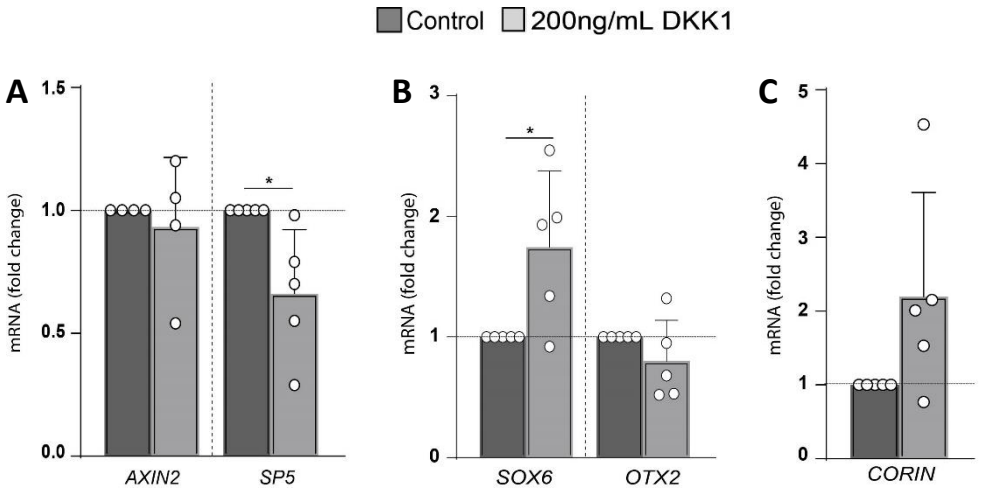

Figure 3.20 Wnt signalling inhibition by DKK1 (200ng/mL) is sufficient to upregulate *SOX6* levels in progenitors (day 13) differentiated with the 100nM SAG protocol. (A) *AXIN2* and *SP5* levels were quantified by qPCR upon Wnt signalling inhibition (DKK1); Mean values ± SD; one-way ANOVA (Sidak); experimental replicates; n=4/5. (B and C) *SOX6*, *OTX2* and *CORIN* expression was quantified by qPCR upon Wnt signalling inhibition (DKK1). Relative *AXIN2, SP5, SOX6, OTX2 and CORIN* mRNA levels in progenitors exposed to dkk1, were compared to the control condition (normalized to 1). (B) Mean values ± SD; one-way ANOVA (Dunnett); n=5; *p<0.05. (C) Mean values ± SD; unpaired ttest (Welch); n=5;

Different concentrations of XAV939 were tested in the 200nM SAG protocol. Analysis at day 25 showed that SOX6 levels were induced in post-mitotic mDA neurons treated with 5µM XAV939 (Figure 3.21).

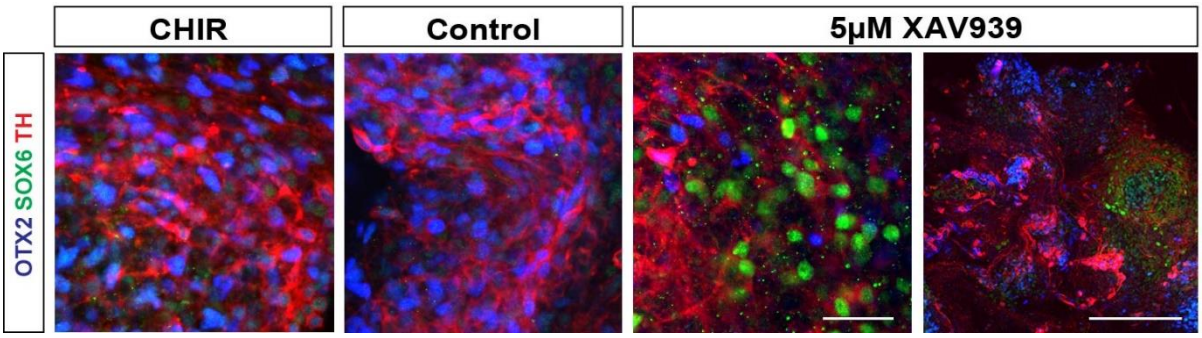

Figure 3.21 SOX6 levels are induced when inhibiting Wnt signalling with XAV939 in early post-mitotic neurons differentiated with 200nM SAG. Confocal microscopy images of monolayer cultures of hESC derived mDA neurons stained with anti-TH, anti-SOX6 and anti-OTX2 antibodies. Neurons were exposed to the Wnt inhibitor XAV939. (Scale bar: 50µm).

indicating that Wnt signalling was efficiently repressed (Figure 3.22 A). The analysis of *SOX6* and *CORIN* expression in progenitors exposed to XAV939 revealed that *SOX6* was upregulated (1.8-fold increase) while *CORIN* presented a slight increase (1.3-fold). In

contrast, analysis of *OTX2* expression showed that its levels were marginally downregulated (1.2-fold; Figure 3.22 B and C).

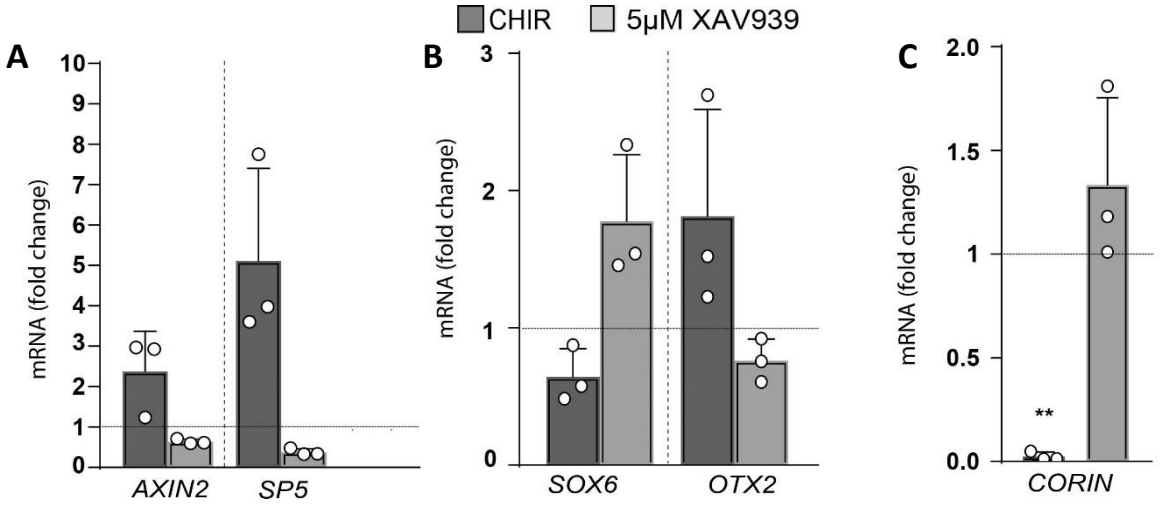

Figure 3.22 XAV939 (5 µM) efficiently inhibits Wnt signalling in progenitors (day 13) exposed to 200nM SAG. (A) *AXIN2* and *SP5* mRNA levels were quantified by qPCR upon Wnt signalling inhibition (XAV939); Mean values ± SD; Kruskal Wallis (Dunn). (B) Progenitor domain markers *SOX6* and, *OTX2* expression was quantified by qPCR upon Wnt signalling inhibition (XAV939); Mean values ± SD;one-way ANOVA (Dunnett); n=3. (C) Progenitor domain marker *CORIN* expression was quantified by qPCR upon Wnt signalling inhibition (XAV939); Mean values ± SD; unpaired t-test (Welch); n=3. **p<0.01. Relative *AXIN2, SP5, SOX6, OTX2 and CORIN* mRNA levels in progenitors, were compared to the control condition (normalized to 1).

This data suggests that, although less efficently, Wnt signalling repressors DKK1 and XAV939, have similar effects than IWP2. Therefore, OTX2 repression as well as SOX6 and CORIN induction, are due to Wnt signalling inhibition. Taken all together, these results support the idea that Wnt signalling antagonises SOX6 as well as CORIN expression and gives rise to a lateral progenitor domain $OTX2^{+}$. In absence of Wnt, SOX6 and CORIN are expressed in the medial progenitor domain devoid of OTX2 expression.

3.3 Discussion

My work established a protocol that obtains two hESC derived neuronal types, SOX6 and OTX2 expressing mDA neurons, that are generated from two different groups of progenitors. Firstly, SOX6 expressing mDA neurons are derived from progenitors CORIN$^+$ and SOX6$^+$. Secondly, OTX2 expressing mDA neurons are derived from progenitors that are OTX2$^+$. Similarly to the mouse, these two types of progenitors mimic the SOX6$^+$ medially and OTX2$^+$ laterally located progenitor domains in the midbrain of the mouse, which in turn give rise to the SOX6$^+$ SNc and OTX2$^+$ VTA mDA neurons, respectively.

The histological analysis of human embryonic midbrain in this work revealed that, although SNc and VTA mDA neurons express SOX6 and OTX2 respectively, the progenitor domain was OTX2$^+$ at week 8 and only some scattered SOX6$^+$ cells were medially localised, overlapping with the CORIN expressing region, at week 6. Interestingly, the TH$^+$/SOX6$^+$ neuronal population at week 8 was located medially in the midbrain, while the TH$^+$/OTX2$^+$ neuronal population was located laterally in the midbrain. Thus, akin to the mouse, human SNc mDA neurons expressing SOX6, could be generated earlier than VTA mDA neurons from the SOX6$^+$/CORIN$^+$ domain and subsequently undertake tangentially migration to reach their lateral location in the midbrain at week 20. Indeed, it has been hypothesised that SNc mDA neurons are born earlier than the VTA mDA neurons in mouse.

As detailed in the introduction, the TF OTX2 is induced by Wnt signalling and OTX2 inhibits SOX6 expression in the mouse (Panman *et al.*, 2014). In addition, this work showed that the lateral located progenitor domain in the human midbrain (week 6) coexpresses high levels of *WNT1* and *AXIN2*. Based on these results, Wnt signalling has been inhibited to generate SOX6 expressing mDA neurons and the degree of repression has been determined by quantifying the levels of the Wnt/β-catenin downstream targets *AXIN2* and *SP5*. These markers have been chosen since their expression is induced in a dose-dependent manner by the activator of Wnt/β-catenin signalling CHIR (Huggins *et al.*, 2017). This work results revealed that this pathway is poorly repressed in hESC derived progenitors exposed to the Wnt inhibitor IWP2 and treated with C24II+Purmorphamine (high Shh levels) since *OTX2* and *AXIN2* levels were not

downregulated when compared to the control (low Wnt signalling levels) condition. This could be explained by the fact that Shh induces LMX1A expression which is crucial for the development of mDA neurons and in turn activates Wnt signalling. Therefore, if Wnt is inhibited but Shh is strongly induced, LMX1A levels are high enough to continue the activation of Wnt signalling resulting in an ineffective repression of the pathway (Figure 3.23 A). This has been demonstrated when progenitors differentiated with low Shh signalling levels (SAG) have been exposed to the Wnt signalling repressor IWP2 showed a significant downregulation of *AXIN2*, *SP5* and *OTX2* levels compared to the control (low Wnt signalling levels) condition (Figure 3.23 B).

In addition, results from this chapter clearly demonstrated that Wnt represses *SOX6* and *CORIN* expression. In the CHIR condition (high Wnt signalling levels) *SOX6* and *CORIN* expression are downregulated in progenitors when compared to the control. Conversely, these transcription factors are upregulated when inhibiting Wnt signalling with diverse repressors of the pathway, such as DKK1, IWP2 and XAV939, in comparison to the control condition (Figure 3.23 A and B).

Analysis of Wnt inhibition in the progenitors showed that the relative *SP5* expression (compared to the control) was higher in the DKK1 and XAV939 treated progenitors (2-fold decrease) than in the IWP2 treated progenitors (5-fold decrease). This indicated that IWP2 was the most powerful inhibitor while DKK1 and XAV939 mildly repressed the pathway. Changes in the relative *AXIN2* expression (compared to the control) were less dramatic than with the *SP5* levels. Even though Wnt signalling repression was strong enough to induce *SOX6* and *CORIN* expression, progenitors exposed to DKK1 did not present any downregulation of *AXIN2*. This is consistent with the fact that upon Wnt signalling activation, *AXIN2* is induced at lower levels than *SP5*. In addition, *AXIN2* is only momentarily expressed while *SP5* expression remains steady overtime (Huggins *et al.*, 2017).

In the post-mitotic neurons (day 25) SOX6 expression is also downregulated in the CHIR condition in comparison to the control condition. However, why OTX2 expression in the CHIR condition (day 25) of the 100nM agonist protocol was downregulated? Wnt signalling levels are controlled by its downstream targets, such as AXIN2 and SP5, which act as negative regulators of the pathway. Therefore, after a constant activation of Wnt

signalling with CHIR, negative regulators downregulate Wnt signalling leading to a decrease in OTX2 expression. Because of Shh signalling levels being lowered, LMX1A expression also drops, resulting in a decrease in Wnt signalling levels and subsequently in OTX2 expression.

This research supports the hypothesis that Wnt signalling is involved in the specification of mDA neuronal diversity since modulating this pathway gives rise to two types of neuronal population. Indeed, low levels of Wnt signalling are necessary to obtain $SOX6^+$ mDA neurons, while high levels of Wnt signalling give rise to $OTX2^+$ mDA neurons. Thus, the next step will be to investigate whether the $SOX6^+$ and the $OTX2^+$ mDA neurons that are obtained in this protocol are SNc-like and VTA-like mDA neurons, respectively.

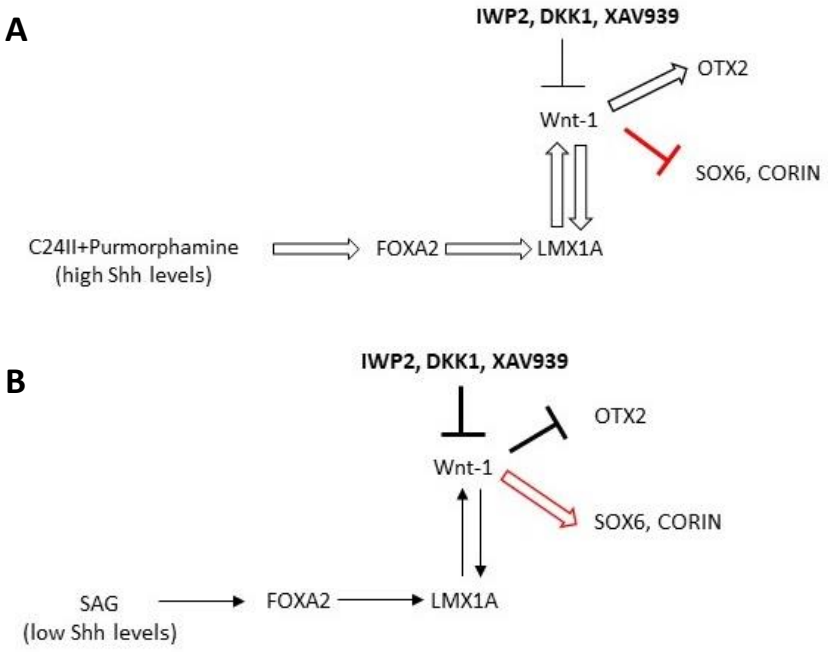

Figure 3.23 Schematic representation of how the interaction between Wnt and Shh signalling influences in the inhibition of Wnt pathway, with IWP2, DKK1 and XAV939, in hESC derived mDA neurons. (A) Wnt signalling is inefficiently inhibited in mDA neurons differentiated with high levels of the Shh pathway, resulting in an induction of OTX2 levels. (B) Wnt signalling is effectively repressed in mDA neurons differentiated with low levels of the Shh pathway, resulting in an induction of SOX6 and CORIN levels. Block and regular arrows indicate strong and weak induction, respectively. Bold and regular inhibitory sign indicates strong and weak repression, respectively. Red signs are the new discovered interaction between SOX6, CORIN and Wnt signalling.

Chapter 4

hESC derived mDA neurons expressing SOX6 display SN-like characteristics

Chapter 4 hESC derived mDA neurons expressing SOX6 display SN-like characteristics

4.1 Introduction

As described in Chapter I, mDA neurons are formed by distinct neuronal subpopulations with different molecular identities. The most vulnerable subpopulation in PD is the ventral tier of the SNc which is characterised by the expression of ALDH1A1, SOX6, LMO3 and SATB1 in mouse (Poulin *et al.*, 2014, 2018; Brichta *et al.*, 2015; La Manno *et al.*, 2016) . Interestingly, a subpopulation with this molecular identity has also been identified by RNA sequencing in human (Brichta *et al.*, 2015; La Manno *et al.*, 2016). Conversely, VTA mDA neurons contain the subpopulation positive for CALB1, OTX2 and ALDH1A1 in mouse and human, which appears relatively unaffected in PD patients (Di Salvio *et al.*, 2010; La Manno *et al.*, 2016; Poulin *et al.*, 2018).

It is unknown the reason why SNc mDA neurons selectively degenerate causing motor impairments in patients suffering from PD. Interestingly, SOX6 is seen as a candidate for the development and maintenance of SN features and previous investigations suggested its involvement in the selective vulnerability of SNc mDA neurons (Panman *et al.*, 2014). In humans, SOX6 is expressed in neuromelanin SNc neurons that degenerate in PD patients (Panman *et al.*, 2014). In addition, a SOX6 mutation caused parkinsonism symptoms, such as resting tremor in all 4 limbs, oculomotor apraxia and slowness of speech, in a 4-year old girl (Scott *et al.*, 2014).

Therefore, the aim of this chapter is to investigate whether hESCderived $SOX6^+$ and $OTX2^+$ mDA neurons, obtained with the protocol developed in chapter 3, present a SNc-like and a VTA-like phenotype, respectively. Furthermore, it will be examined whether SOX6 acts as an intrinsic determinant of SNc mDA neurons. To achieve this objective, the expression of specific markers for the ventral tier of SNc and VTA mDA neurons will be examined. In addition, selective vulnerability will be studied by exposing these neuronal subpopulations to toxins, such as MPTP or Rotenone, causing parkinsonism in humans.

4.2 Results

4.2.1 SOX6$^+$mDA neurons express SN markers

First the identity of the progenitors giving rise to the SOX6$^+$ neurons was further analysed. It has been previously described, in mouse and humans, that mDA and subthalamic nucleus (STN) neuronal lineages present a close developmental origin (Kee *et al.*, 2017). Indeed, progenitors coexpressing LMX1A and FOXA2 do not only generate mDA neurons, but also STN neurons which are localised in the diencephalon and display a glutamatergic phenotype. Investigations revealed that the TF BARHL1 promotes STN neuronal lineage by inhibiting mDA neuronal fate. Consequently, two progenitor domains have been established in the ventral midbrain. The rostral progenitor domain LMX1A$^+$/FOXA2$^+$/OTX2$^+$/PITX2$^+$/BARHL1$^+$, generates glutamatergic STN neurons. The caudal progenitor domain LMX1A$^+$/FOXA2$^+$/OTX2$^+$/EN1$^+$/CNPY1$^+$ gives rise to mDA neurons (Kee *et al.*, 2017). To determine the identity of the progenitor domain obtained with the IWP2 protocol, the expression of *BARHL1*, *NKX2.1* (diencephalic precursor marker) and *PAX6* (dorsal forebrain precursor marker) was analysed by qPCR. Results showed that *BARHL1* levels present a 6-fold decrease while *NKX2.1* and *PAX6* levels are unchanged in the IWP2 condition in comparison to the control. In the CHIR (high Wnt levels) condition, gene expression for both markers is unchanged when compared to the control. This suggests that progenitors exposed to IWP2 do not present a more rostral identity than the control and CHIR condition (Figure 4.1).

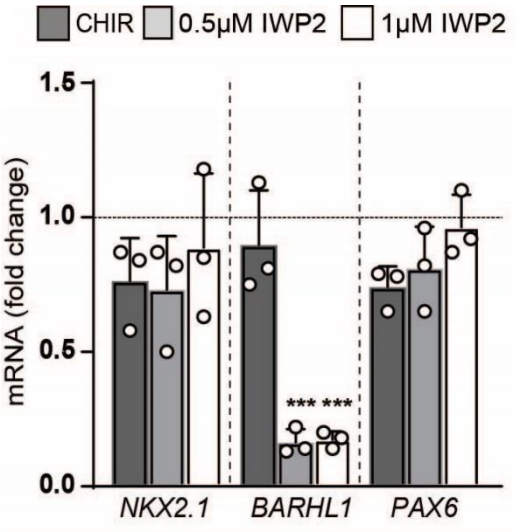

Figure 4.1 Rostral phenotype is not enhanced in progenitors (day 13) having Wnt signalling inhibited (IWP2). *NKX2.1, BARHL1* and *PAX6* expression was quantified by qPCR. Relative *NKX2.1, BARHL1* and *PAX6* mRNA levels of progenitors in the CHIR, 0.5µM and 1µM IWP2 conditions were compared to the control condition (normalized to 1). Mean values ± SD;one-way ANOVA (Dunnett); technical replicates; n=3. ***p<0.001.

Other studies identified that hESC-derived progenitors expressing a set of markers enriched in the caudal midbrain, such as EN1, SPRY1, ETV5, PAX8 and CNPY1, give rise to dopaminergic-rich grafts and extensively innervate the host brain being able to provide a functional recovery of motor impairments in a PD rat model. Therefore, the expression of these transcription factors in the progenitors was analysed by qPCR. Unsurprisingly, the expression of *EN1*, *SPRY1*, *ETV5*, *PAX8* and *CPNY1*, was from 2 to 4-fold lower in the IWP2 treated progenitors than the control condition. In contrast, *EN1*, *SPRY1*, *ETV5*, *PAX8* expression was increased 2-fold and *CNPY1* expression was increased 9-fold, in the CHIR condition when compared with the control (Figure 4.2 A and B). Thus, although inhibiting Wnt signalling with IWP2 does not generate progenitors displaying a more rostral identity than the control and CHIR conditions, levels of caudal markers are significantly reduced. This suggests that progenitors obtained with this protocol have a more rostral identity than those obtained with the previous published protocols.

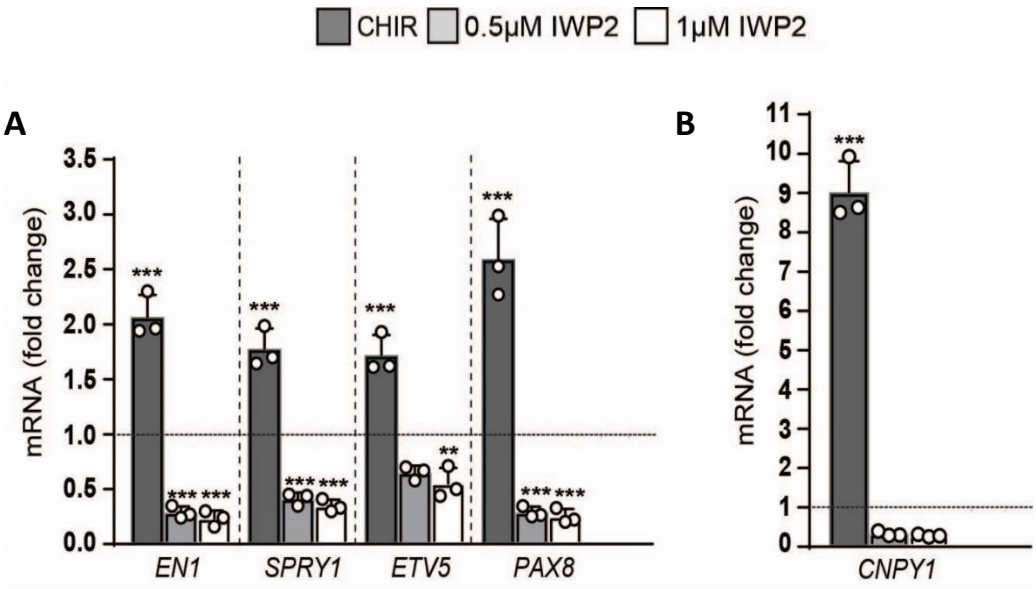

Figure 4.2 The expression of caudal ventral midbrain progenitor markers is downregulated in progenitors (day 13) having Wnt signalling inhibited (IWP2). The expression of caudal ventral midbrain markers is upregulated in progenitors with high levels of Wnt signalling (CHIR) when compared to progenitors exposed to low levels of Wnt (control). (A) Relative *EN1, SPRY1, ETV5, PAX8* mRNA levels in progenitors were quantified by qPCR in the CHIR, 0.5µM and 1µM IWP2 conditions and compared to the control condition (normalized to 1). Mean values ± SD;one-way ANOVA (Dunnett); technical replicates; n=3. **p<0.01 and ***p< 0.001. (B) Relative *CNPY1* mRNA levels in progenitors were quantified by qPCR in the CHIR, 0.5µM and 1µM IWP2 conditions and compared to the control condition (normalized to 1). Mean values ± SD; unpaired t-test (Welch); technical replicates; n=3. ***p< 0.001.

Expression of the midbrain dopaminergic markers LMXA1, FOXA2 and NURR1 was examined with immunocytochemistry in post-mitotic neurons at day 25. Around 70% of the TH^+ neurons expressed LMX1A, FOXA2 and NURR1 and these levels were maintained in the IWP2 treated neurons when compared with the CHIR and the control conditions. This demonstrates that post-mitotic neurons treated with IWP2 keep mDA identity (Figure 4.3 and Figure 4.4).

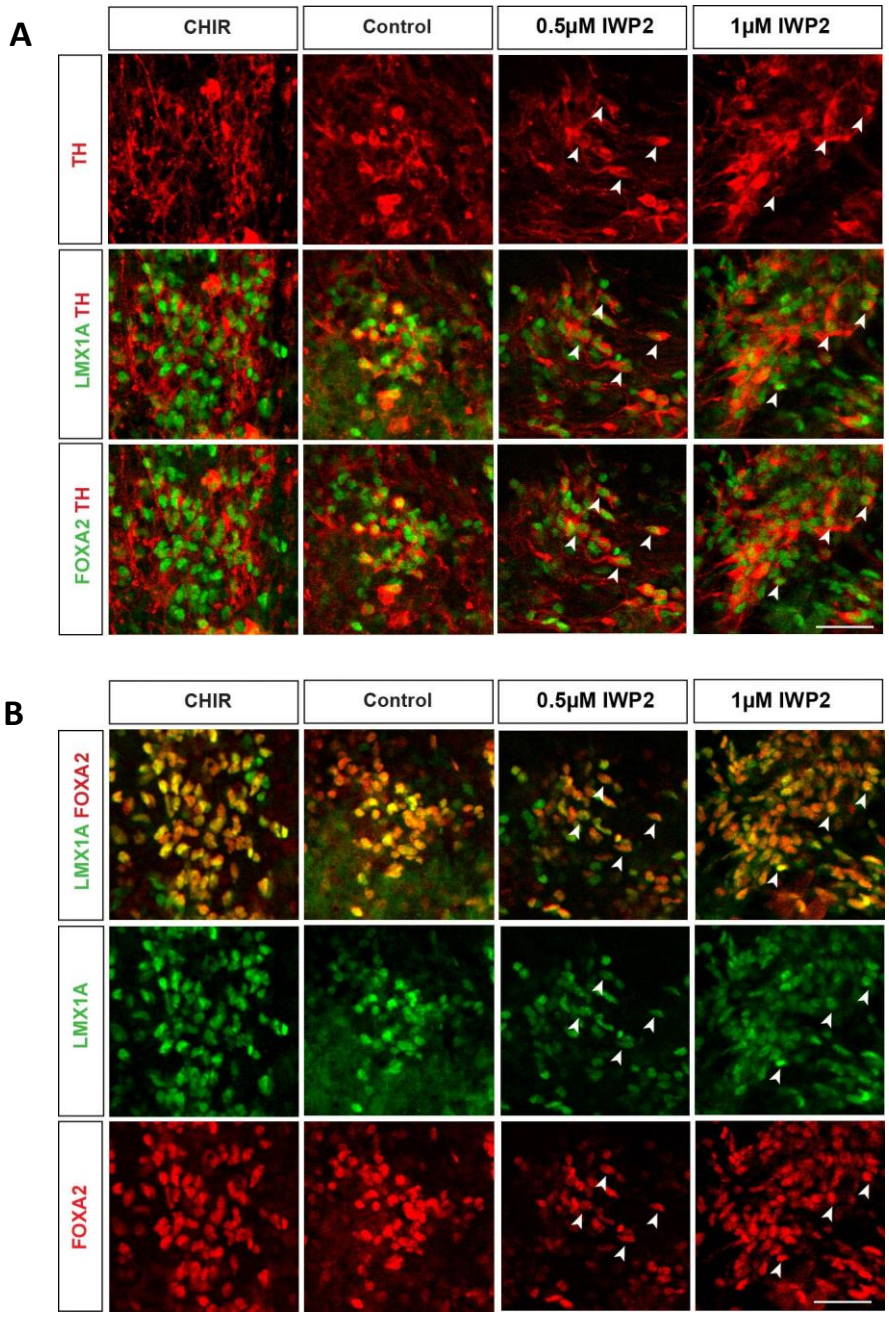

Figure 4.3 Midbrain dopaminergic identity is maintained in the IWP2 treated neurons at day 25. (A) Confocal micrographs of a monolayer of hESC derived neurons at day 25 with no exposure to IWP2 (CHIR and control) and exposed to IWP2 (0.5μM and 1μM IWP2). Images show neurons stained with anti-mTH, anti-rbLMX1A and anti-gFOXA2 antibodies. Arrowheads point to neurons LMX1A$^+$/TH$^+$ and FOXA2$^+$/TH$^+$(scale bar: 50μm). (B) Confocal micrographs of a monolayer of hESC derived neurons at day 25 with no exposure to IWP2 (CHIR and control) and exposed to IWP2 (0.5μM and 1μM IWP2). Images show neurons stained with anti-rbLMX1A and anti-gFOXA2 antibodies. Arrowheads point to neurons LMX1A$^+$, FOXA2$^+$ and neurons coexpressing LMX1A and FOXA2 (scale bar: 50μm).

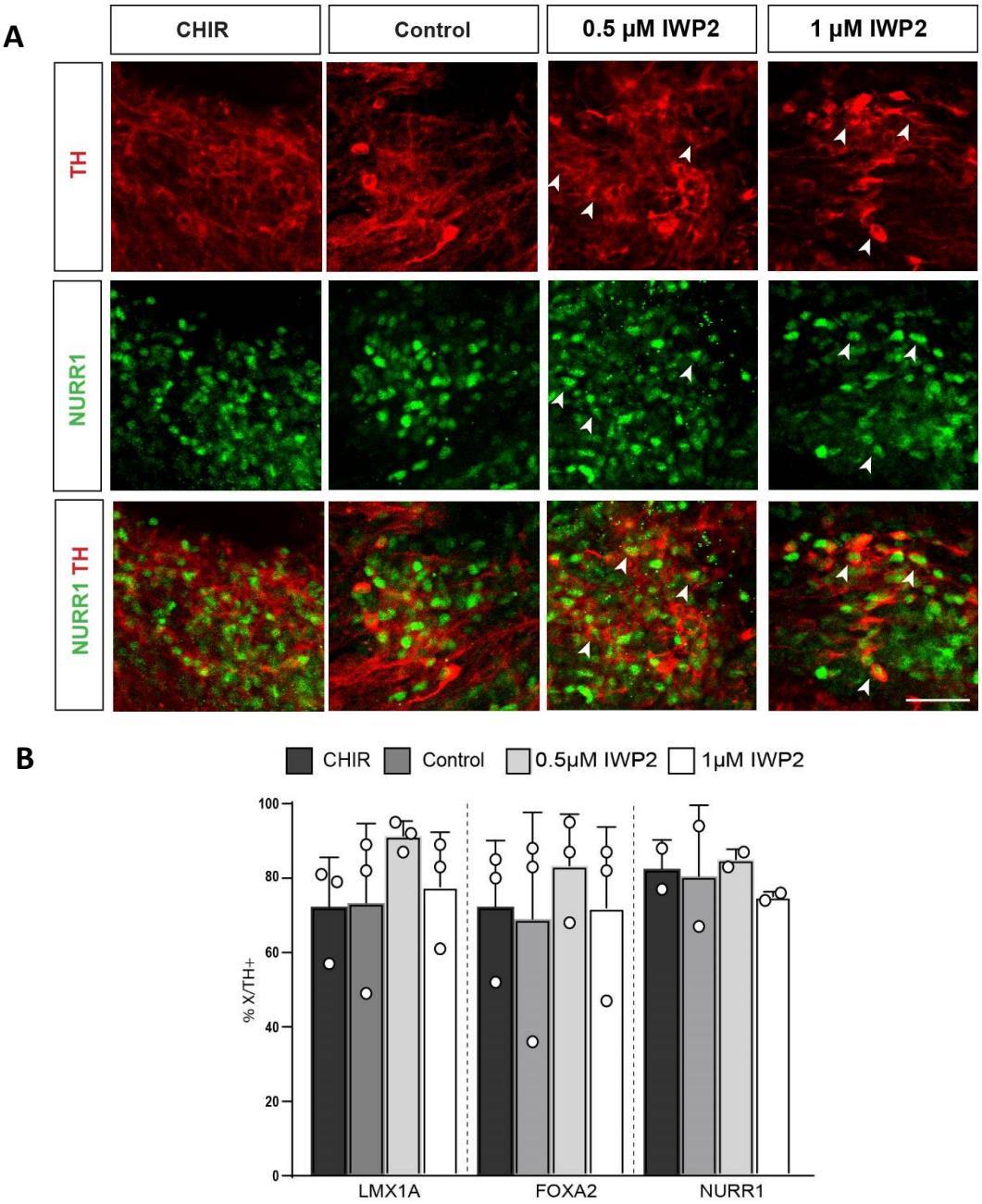

Figure 4.4 IWP2 exposed neurons express the midbrain dopaminergic marker NURR1. (A) Confocal micrographs of a monolayer of hESC derived neurons at day 25 with no exposure to IWP2 (CHIR and control) and exposed to IWP2 (0.5µM and 1µM IWP2). Images show neurons stained with anti-mTH and anti-rbNURR1. (Scale bar: 50µm). Arrows point to neurons $NURR1^{+}/TH^{+}$. (B) Quantification of TH neurons expressing LMX1A, FOXA2 and NURR1 in each condition (CHIR, control, 0.5µM and 1µM IWP2). Mean values±SD; one-way ANOVA (Sidak); experimental replicates; n=3/2.

In order to determine whether SOX6$^+$/TH$^+$ and OTX2$^+$/TH$^+$ neurons present SNc-like and VTA-like characteristics, respectively, the SNc marker GIRK2 and the VTA marker CALBINDIN1 (CALB1) were analysed. Immunocytochemistry results showed that the number of TH$^+$/GIRK2$^+$ neurons was increased, being 40% of the TH neurons positive for GIRK2 in the IWP conditions when compared with the control (Figure 4.5 A and Figure 4.6 A). In contrast, the number of TH$^+$/CALB1$^+$ neurons was significantly reduced 30% in the IWP2 treated neurons in comparison with the control condition (Figure 4.5 B and Figure 4.6 A). In addition, analysis of SOX6 expression showed that TH$^+$/SOX6$^+$ neurons coexpressed GIRK2 (Figure 4.5 A).

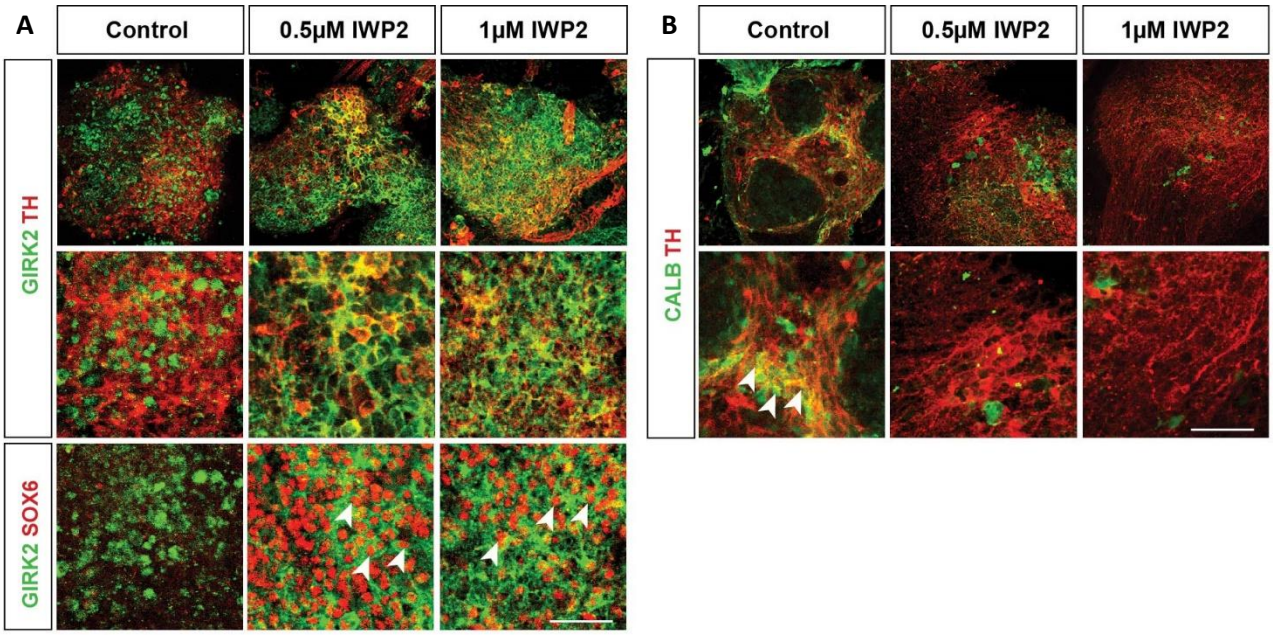

Figure 4.5 hESC derived IWP2 treated post-mitotic neurons SOX6$^+$ are GIRK2$^+$. (A) Confocal micrographs of a monolayer of hESC derived neurons at day 35 with no exposure to IWP2 (CHIR and control) and exposed to IWP2 (0.5µM and 1µM IWP2). Images show neurons stained with anti-mTH, anti-gGIRK2 and anti-rbSOX6. Arrowheads point to neurons coexpressing GIRK2 and SOX6 (Scale bar: 50µm). (B) Confocal micrographs of a monolayer of hESC derived neurons at day 35 with no exposure to IWP2 (CHIR and control) and exposed to IWP2 (0.5µM and 1µM IWP2). Images show neurons stained with anti-mTH and anti-rbCALB. (Scale bar: 50µm). Arrowheads indicate TH$^+$/CALB$^+$ neurons (scale bar: 50µm).

Next, GIRK2 and CALB1 gene expressions were quantified by qPCR. Results showed a *GIRK2* levels were significantly increased 1.5 fold in the 1µM IWP2 condition when compared with the control. However, *CALB1* levels were significantly reduced 2-fold in neurons exposed to IWP2 in comparison with the control (Figure 4.6 B). Thus, hESC-

derived neurons that have been treated with IWP2, present an upregulation of the SNc marker GIRK2 and a downregulation of the VTA marker CALB1.

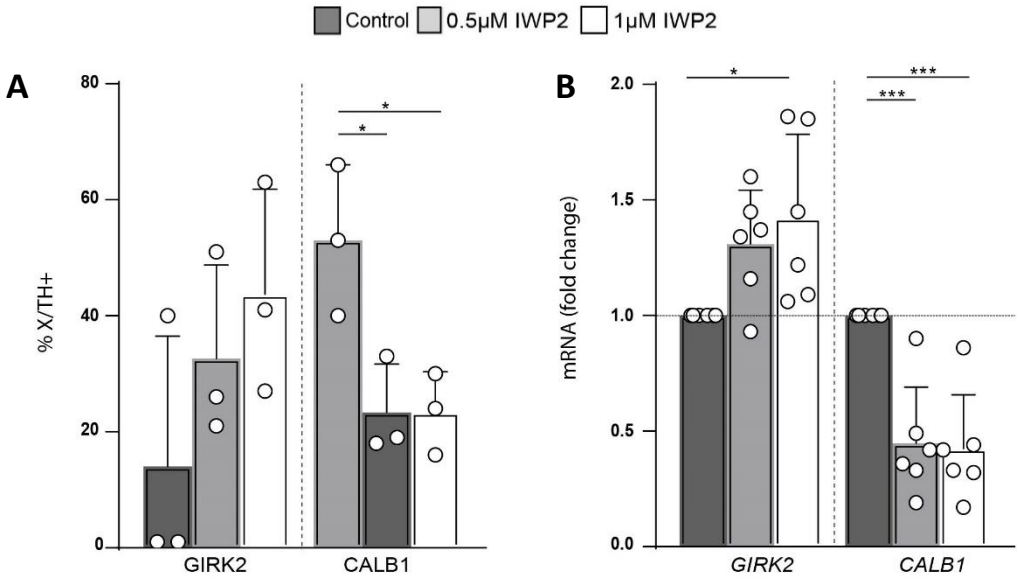

Figure 4.6 Inhibition of Wnt signalling induced GIRK2 expression in presumptive mDA neurons IWP2 treated. (A) Quantification of $TH^+/GIRK2^+$ and $TH^+/CALB1^+$ in IWP2 treated neurons. Mean values±SD; one-way ANOVA (Sidak); *p<0.05. (B) qPCR analysis of the *GIRK2* and *CLAB1* expression in IWP2 treated neurons. Relative *GIRK2* and *CALB1* mRNA levels were quantified by qPCR in neurons treated with 0.5µM and 1µM IWP2 and compared to the control condition (normalized to 1). Mean values ± SD;one-way ANOVA (Dunnett); experimental replicates; n=6. *p<0.05 and ***p<0.001.

As mentioned in the introduction, GIRK2 is expressed in all the mDA neurons but its expression is higher in the SNc neurons of human tissue. Therefore, to further characterise the hESC-derived neuronal populations previously obtained, it was necessary to examine additional SNc mDA neuronal markers by immunocytochemistry. Single cell RNA sequencing permitted to identify new SNc markers, such as SATB1, which expression is higher in SNc mDA neurons in comparison with the VTA neuronal population. Therefore, in addition to GIRK2 and CALB1, the marker SATB1 was analysed by immunocytochemistry. Although, SATB1 expression was detected in the control condition, these neurons did not express SOX6. In contrast in $TH^+/SOX6^+$ coexpressed SATB1 in the IWP2 conditions (Figure 4.7 A, B and C).

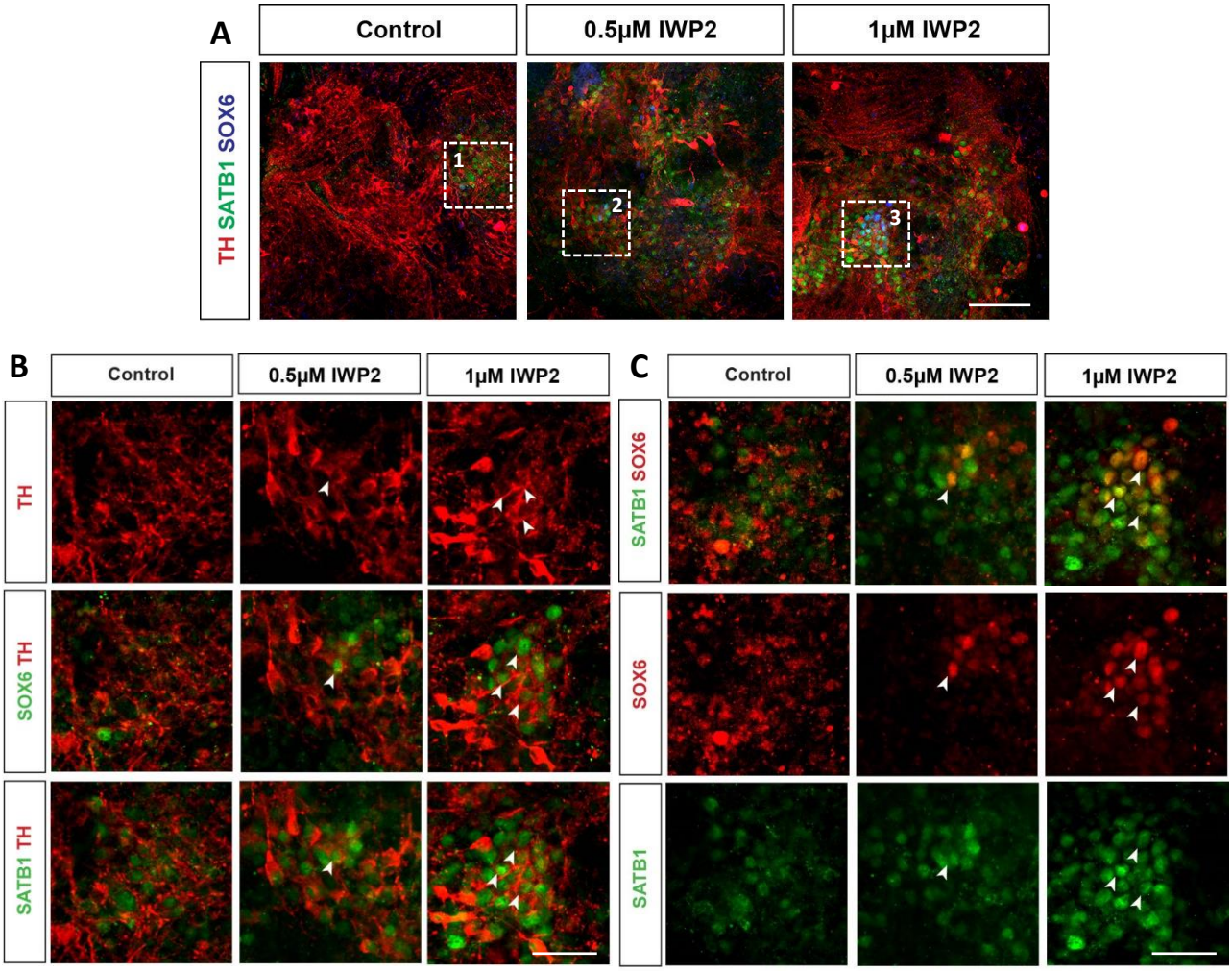

Figure 4.7 hESC derived mDA neurons SOX6$^+$ express SATB1 (day 25) in IWP2 exposed neurons. (A) Confocal micrographs of a monolayer of hESC derived neurons at day 25 with no exposure to IWP2 (control) and exposed to IWP2 (0.5μM and 1μM IWP2). Images show neurons stained with anti-shTH (red), anti-rbSATB1(green) and anti-mSOX6 (blue) antibodies. (B and C) Zoom of the section defined with dashed square in A. Sections defined with dashed squares 1, 2 and 3 are zoomed in the control, 0.5μM and 1μM conditions, respectively. (B) Images show neurons stained with anti-shTH, anti-mSOX6 and anti-rbSATB1 antibodies. Arrowheads point to SOX6$^+$/TH$^+$ neurons. (C) Images show neurons stained with anti-rbSATB1 and anti-mSOX6 antibodies. Arrowheads indicate TH neurons expressing SATB1 and SOX6. Arrowheads point to neurons SOX6$^+$, SATb1$^+$ and neurons SOX6$^+$/SATB1$^+$ (scale bar: 50μm).

4.2.2 SOX6$^+$ neurons present selective vulnerability to rotenone

As previously mentioned, mDA neurons located in the ventral tier of the SNc expressing SOX6 degenerate in PD patients, while VTA mDA neurons expressing OTX2 show resistance to MPTP in mice. To analyse the identity of the subpopulations of presumptive mDA neurons expressing SOX6 and OTX2, their vulnerability to the toxins causing parkinsonism in humans, MPTP and rotenone was assessed. First, cell viability was measured in IWP2 treated presumptive mDA neurons exposed to 100nM Rotenone

for 48 hours. Results showed that, in the presence of 100nM Rotenone, cell viability was reduced in neurons exposed to 0.5µM IWP2 (20% decrease) when compared with the untreated IWP2 control. However, this decrease was not significant. In the control and CHIR conditions exposed to 100nM rotenone, cell viability was not significantly decreased (10% reduction), when compared with the untreated counterparts (Figure 4.8).

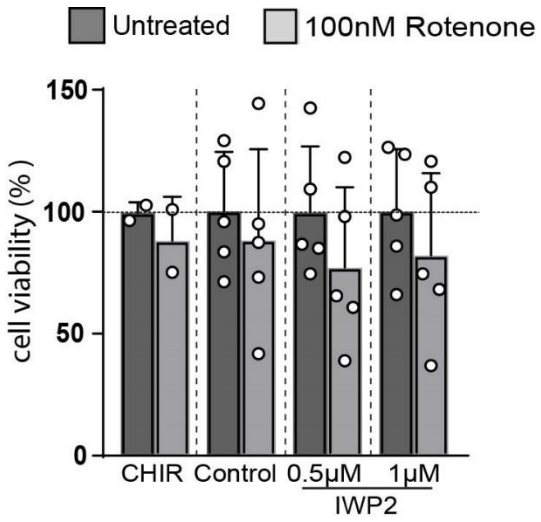

Figure 4.8 hESC derived mDA neurons (day 35) differentiated with IWP2 presented vulnerability when exposed to 100nM rotenone for 48 hours. Cell viability was measured in presumptive mDA neurons in the CHIR, Control, 0.5µM and 1µM IWP2 conditions treated with 100nM Rotenone. Cell viability in the rotenone treated neurons was compared to their untreated counterparts. Mean values ± SD; one-way ANOVA (Sidak); experimental replicates; n=2/5.

different concentrations of rotenone (50nM and 100nM) for 48 hours and to 50µM MPP^+ for 96 hours. Interestingly, *TH* levels were significantly reduced (2-fold decrease) in the 0.5µM IWP2 condition treated with 100nM rotenone in comparison to the IWP2 untreated condition. *TH* expression was not significantly decreased in 0.5µM IWP2 treated neurons exposed to 50nM rotenone. Neurons differentiated with 1µM IWP2 did not present a significant decrease of *TH* levels in any of the rotenone concentrations. Exposure to MPP^+ resulted in a 1.6-fold decrease of *TH* expression in both IWP2 conditions, when normalised to the untreated counterpart but the reduction was not significant. The control and CHIR conditions did not present a significant decrease in TH expression when exposed to rotenone or MPP^+ (Figure 4.9). These results suggested that neurons exposed to IWP2, containing $SOX6^+$neurons, were more sensitive to

100nM rotenone than the control and CHIR conditions, which were enriched with $OTX2^+$ neurons. Therefore, the next step was to analyse whether $TH^+/SOX6^+$ were selectively more vulnerable than $TH^+/OTX2^+$ neurons when exposed to 100nM rotenone.

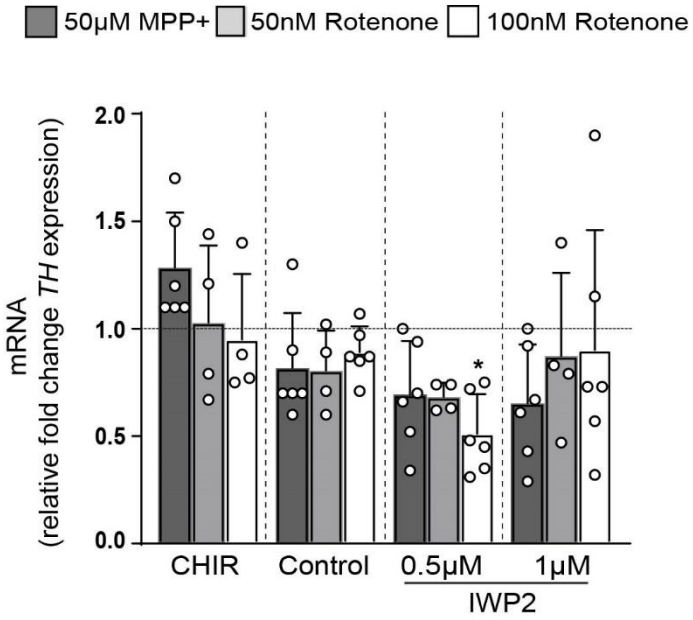

Figure 4.9 Presumptive mDA neurons differentiated with 0.5µM IWP2 are selectively vulnerable to rotenone. Relative *TH* mRNA levels in presumptive mDA neurons at day 35 were quantified by qPCR from the CHIR, control, 0.5µM and 1µM IWP2 conditions exposed to MPP^+ and rotenone were compared to their untreated counterpart (normalized to 1). Mean values ± SD; one-way ANOVA (Sidak); experimental replicates; n=4,6. *p<0.05.

Given that the most striking effect on TH expression was seen in neurons exposed to 100nM rotenone, SOX6 and OTX2 expression was studied by immunocytochemistry for $TH^+/SOX6^+$ neurons and $TH^+/OTX2^+$ neurons in the CHIR, control and 0.5µM IWP2 conditions (Figure 4.10 A and B). The percentages were obtained by normalising the rotenone treated with their untreated counterpart in the three different conditions. Quantifications for $TH^+/DAPI^+$ indicated that the number of TH neurons was 50% reduced in the 0.5µM IWP2 condition. Although it was not significant, the reduction was quite large. An increase in the number of replicates would probably make the result significant. The control and the CHIR condition did not present a decrease in the number of TH neurons (Figure 4.10 C). Similarly, the number of $TH^+/SOX6^+$ neurons in the IWP2 condition treated with rotenone was significantly decreased (50%) in comparison to its

untreated counterpart, while almost no reduction was observed for the $TH^+/OTX2^+$ neurons (Figure 4.10 A, B and D). The total number of DAPI neurons was quantified in all the conditions to determine that the decrease in TH^+ and $TH^+/SOX6^+$ neurons observed was not due to a reduction on the total number of cells. The number of $DAPI^+$ cells in the rotenone treated conditions did not present a decrease when compared to the untreated conditions (Figure 4.10 E). This is consistent with the fact that cell viability of the rotenone treated neurons is not significantly reduced (Figure 4.8). These results suggest that $TH^+/SOX6^+$ neurons obtained with the IWP treatment are more vulnerable than the $TH^+/OTX2^+$ neurons. All together the results indicate that $TH^+/SOX6^+$ presumptive mDA neurons and $TH^+/OTX2^+$ presumptive mDA neurons present a SN-like and a VTA-like phenotype, respectively.

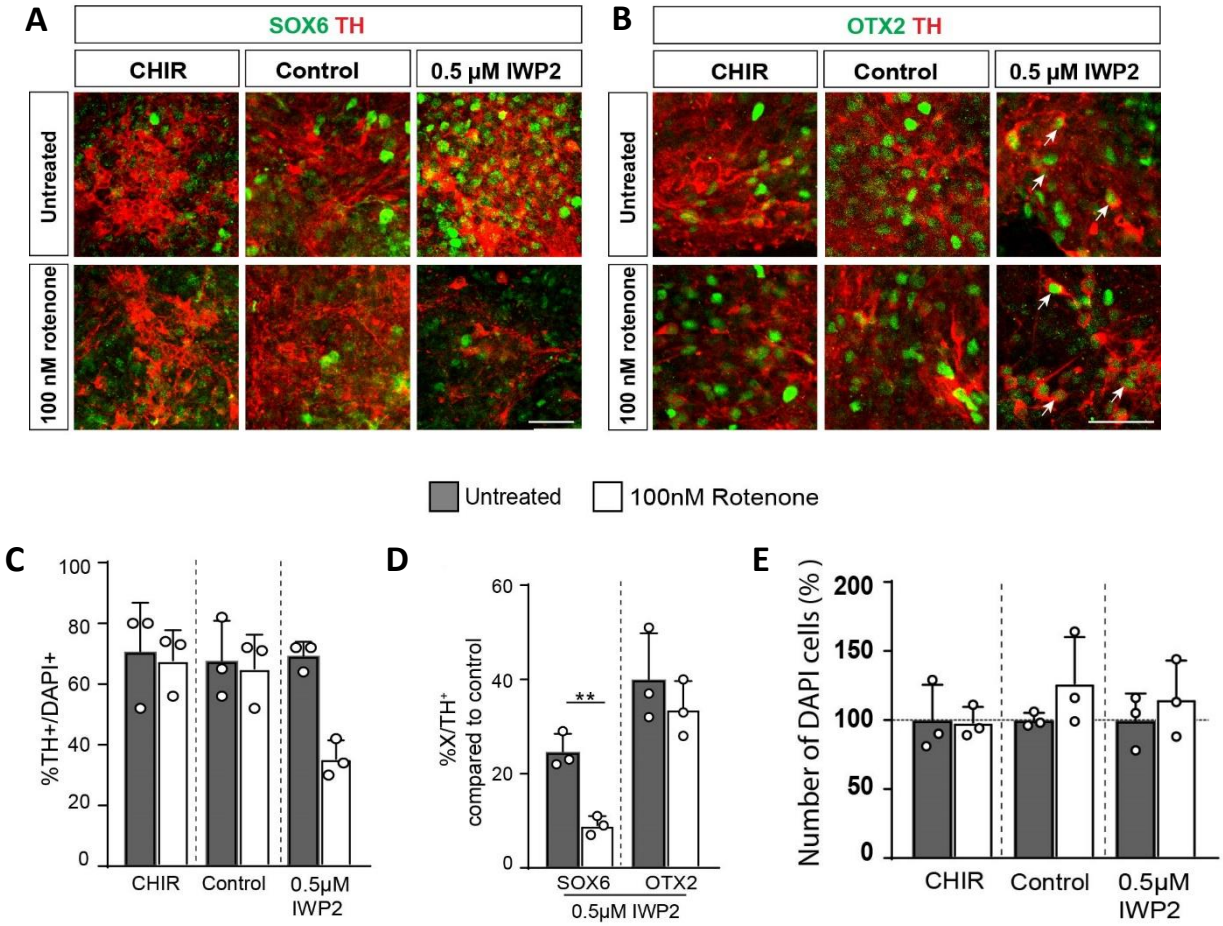

Figure 4.10 Presumptive mDA neurons TH$^+$/SOX6$^+$ at day 35 differentiated with IWP2 present selective vulnerability to rotenone. (A) Confocal micrographs of a monolayer of hESC derived neurons at day 35 in the CHIR, control and 0.5µM IWP2 conditions which were untreated and treated with 100nM rotenone. Images show neurons stained with anti-mTH and anti-rbSOX6. (scale bar: 50µm). (B) Confocal micrographs of a monolayer of hESC derived neurons at day 35 in the CHIR, control and 0.5µM IWP2 conditions which were untreated and treated with 100nM rotenone. Images show neurons stained with anti-mTH and anti-gOTX2. Arrows point to TH$^+$/OTX2$^+$ presumptive mDA neurons (scale bar: 50µm). (C) Quantification of TH$^+$/DAPI$^+$ neurons in the CHIR, control and 0.5µM IWP2 conditions when untreated and treated with 100nM rotenone; Mean values ± SD; Kruskal-Wallis (Dunn); experimental replicates; n=3. (D) Quantification of SOX6$^+$/TH$^+$ and OTX2$^+$/TH$^+$ neurons in the 0.5µM IWP2 condition when untreated and treated with 100nM rotenone. Mean values ± SD; repeated measures one-way ANOVA (Sidak); experimental replicates; n=3.**p<0.01. (E) Quantification of the total number of DAPI cells in the CHIR, control and 0.5µM IWP2 conditions when untreated and treated with 100nM rotenone; Mean values ± SD; repeated measures one-way ANOVA (Sidak); experimental replicates; n=3.

4.2.3 Is SOX6 an intrinsic determinant of SNc mDA neurons?

To explore whether SOX6 and OTX2 are intrinsic determinants of SNc and VTA mDA fate respectively, these transcription factors were overexpressed in early hESC derived mDA neurons. Neurons differentiated with Shh+purmorphine were infected with SOX6 (L-SOX6) and OTX2 (L-OTX2) lentiviruses after the accutase split around day 20. The control lentivirus (L-control) was an empty plasmid (Figure 4.11 A). Immunocytochemistry showed that the transcription factors were successfully overexpressed in presumptive mDA neurons, giving rise to enriched cultures of SOX6 or OTX2 presumptive mDA neurons. Interestingly, neurons transfected with L-control, expressed OTX2 but almost no SOX6 expression was detected (Figure 4.11 B).

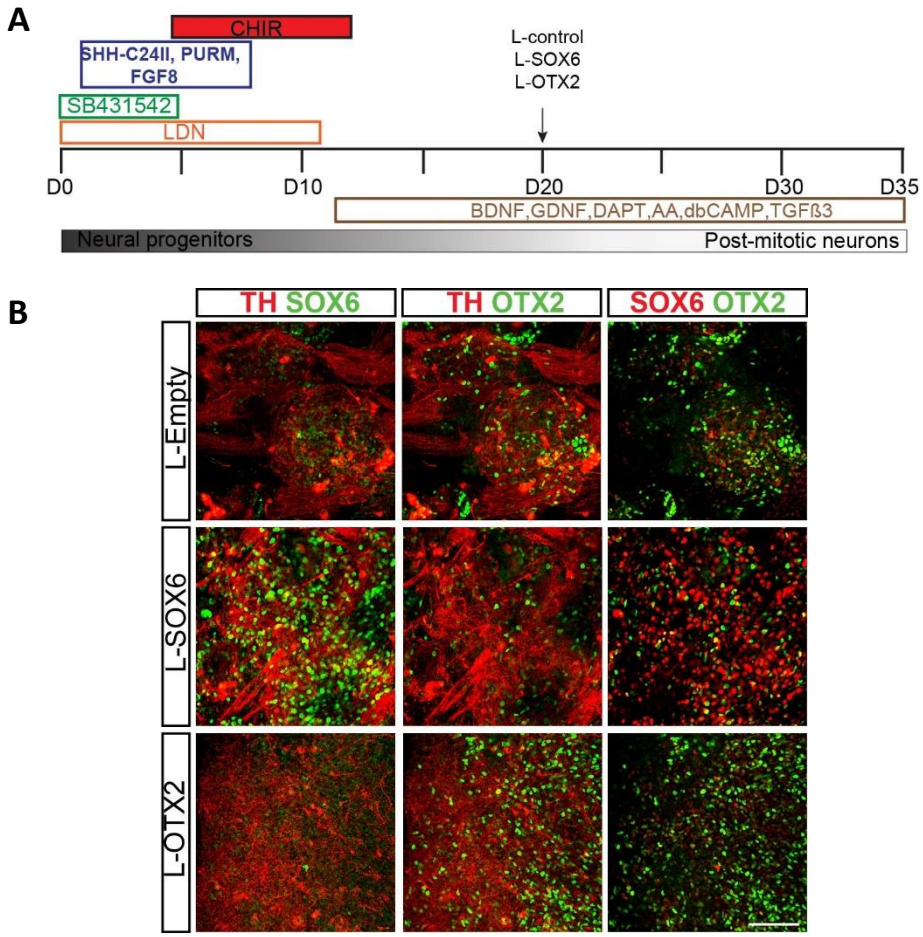

Figure 4.11 Late progenitors infected with L-SOX6 and L-OTX2 give rise to mDA neurons expressing SOX6 and OTX2, respectively at day 35. (A) Diagram illustrating the protocol used for the lentiviral infection with L-empty, L-SOX6 and L-OTX2. (B) Confocal micrographs of a monolayer of hESC derived neurons at day 35 transfected with lentivirus control, SOX6 and OTX2. Images show neurons stained with anti-mTH, anti-rbSOX6 and anti-gOTX2 antibodies (scale bar: 50µm).

Vulnerability of the lentiviral transfected mature presumptive mDA neurons was assessed by exposing them to 20µM and 50µM MPP^+ for 72 and 96 hours. Immunocytochemistry showed that TH neurons expressing SOX6 were vulnerable to MPP^+, while $TH^+/OTX2^+$ neurons were unaffected after treatment with 20µM MPP^+ (Figure 4.12 A). ATP levels were reduced (2-fold decrease) in presumptive mDA neurons transfected with L-SOX6 and treated with 50µM MPP^+, while exposure at 20µM MPP^+ resulted in a 1.5-fold reduction. In neurons transfected with the virus OTX2, ATP levels were slightly decreased (1.2-fold reduction) when exposed to 20µM MPP^+, while

exposure at 50µM MPP^+ resulted in almost 2-fold decrease. Neurons transfected with the control virus were unaffected when treated with the toxin (Figure 4.12 B).

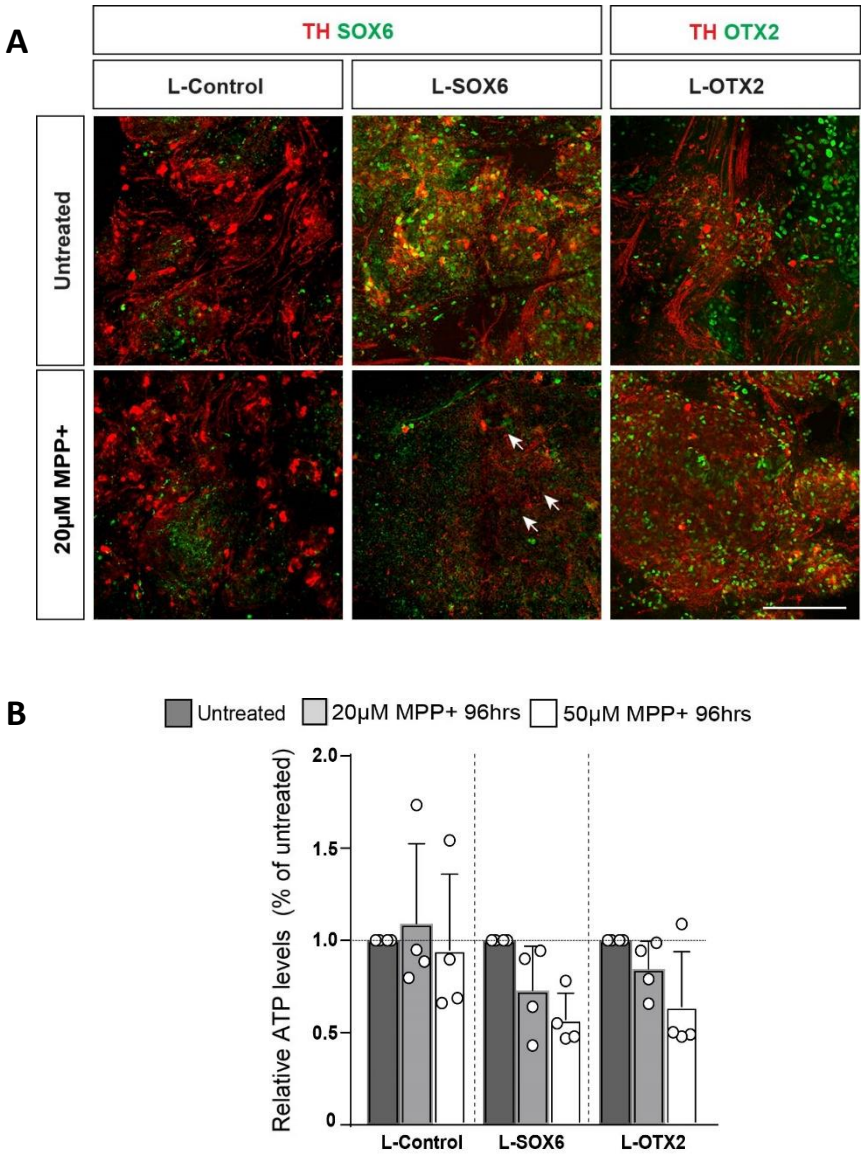

Figure 4.12 Presumptive mDA neurons L-SOX6 transduced present selective vulnerability when exposed to MPP^+ at day 35. (A) Confocal micrographs of a monolayer of hESC derived neurons at day 35 transfected with lentivirus control, SOX6 and OTX2 when exposed to MPP^+ for 72 hours. Images show neurons stained with anti-mTH, anti-rbSOX6 and anti-gOTX2 antibodies. Arrows point to regions displaying loss of $TH^+/SOX6^+$ neuron (scale bar: 50µm). (B) Measurement of ATP levels in L-control, L-SOX6 and L-OTX2 transduced neurons after exposure to MPP^+ for 96 hours. ATP levels in L-control, L-SOX6 and L-OTX2 transduced mDA neurons exposed to MPP^+ were compared to their untreated counterpart (normalized to 1). Mean values ± SD;Friedman test (Dunn); experimental replicates; n=4. *p<0.05

To study whether mitochondria dysfunction was observed in $TH^+/SOX6^+$ neurons when exposed to 50nM rotenone for 24 hours, levels of radical O_2^- in the mitochondria were analysed by using MitoSOX and quantified with flow cytometry in neurons transfected with L-control, L-SOX6 and L-OTX2. Results indicated that MitoSOX levels were significantly higher in the rotenone treated L-SOX6 neurons when compared to their untreated counterpart. Conversely, MitoSOX levels were unchanged in the L-control and L-OTX2 transfected neurons exposed to rotenone when compared to their untreated counterpart (Figure 4.13 A).

In addition, the vulnerability of lentiviral transfected neurons was evaluated by quantifying ATP levels following exposure to 50nM and 100nM rotenone for 24 hours. Relative ATP levels in L-SOX6 transfected presumptive mDA neurons exposed to 50nM and 100nM Rotenone (24 hours) were decreased 50% when compared with the untreated L-SOX6 transfected neurons. In contrast, no reduction in the ATP levels was observed in the L-control and L-OTX2 transfected neurons treated with 50nM and 100nM Rotenone in comparison to the untreated counterparts (Figure 4.13 B).

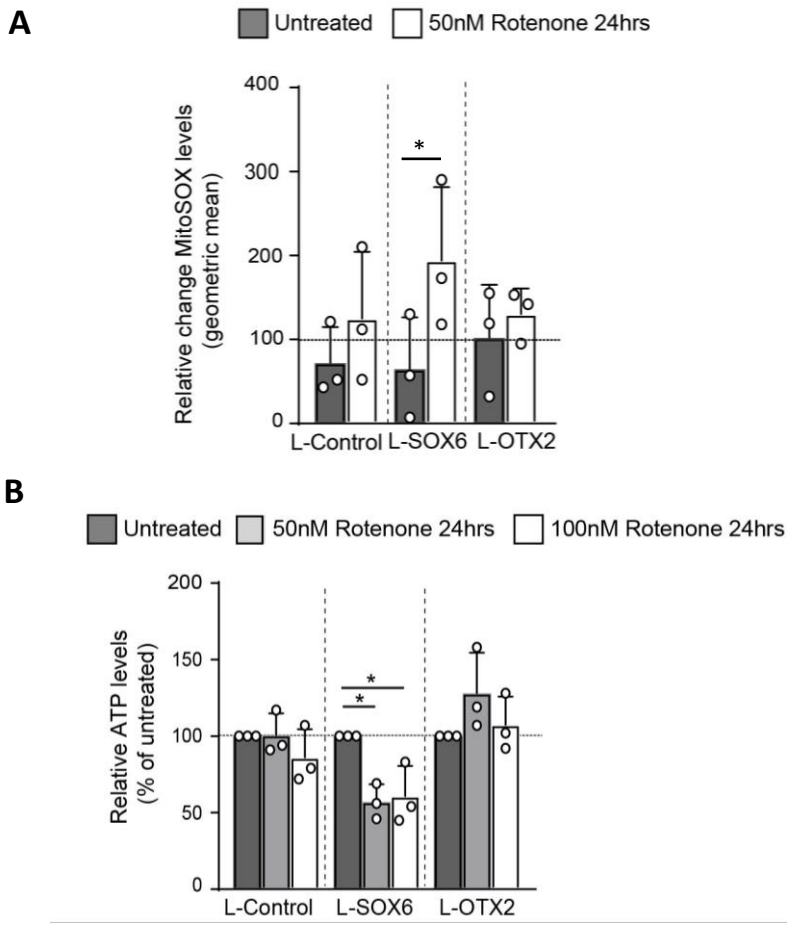

Figure 4.13 L-SOX6 infected neurons display selective vulnerability following exposure to 50nM and 100nM rotenone (24 hours). (A) Changes in MitoSOX fluorescence levels were measured with flow cytometry in L-control, L-SOX6 and L-OTX2 transduced neurons untreated and exposed to 50nM rotenone for 24 hours. The graph shows the geometric mean. Mean values ± SD; repeated measures one-way ANOVA (Sidak); experimental replicates; n=3. *p<0.05. (B) ATP levels were determined in L-control, L-SOX6 and L-OTX2 presumptive mDA neurons exposed to 50nM and 100nM at day 35. Mean values ± SD; one-way ANOVA (Sidak); experimental replicates; n=3/4. *p<0.05.

Overall, these results indicated that SOX6 transduced neurons presented mitochondrial dysfunction when exposed to toxins causing parkinsonism in humans, while OTX2 transduced presumptive mDA neurons were resistant to these compounds and the control neurons were unaffected. Although hESC derived mDA neurons SOX6^{+} present selective vulnerability to rotenone, it is unknown whether SOX6 is an intrinsic determinant of SNc mDA neurons. Therefore, protein expression in L-control, L-SOX6 and L-OTX2 transduced mDA neurons was studied by mass spectrometry.

Mass spectrometry was performed in collaboration with the University of Tours in France and I performed data analysis. Protein expression in L-SOX6 transfected mDA neurons was compared with protein expression in L-OTX2 transfected neurons to unveil differences in these two neuronal subpopulations caused by the overexpression of these TF. Another comparison was done between L-SOX6 and L-control transfected presumptive mDA neurons to determine whether the control population had a similar L-OTX2 transduced phenotype as initially suggested. Because studies determined that spectral counts of less than five are highly variable when using a low number of samples (Lundgren *et al.*, 2010), I only included proteins detected with an average normalised weighted spectra (NWS) count ≥5. Only results with a fold change of 1.6 or greater were considered. Western blots were performed by my postdoctoral colleague Dr. Clement Soleilhavoup. I included them to show that SOX6 and OTX2 expression was higher in the L-SOX6 and L-OTX2 infected mDA neurons, respectively (Figure 4.14 A and B).

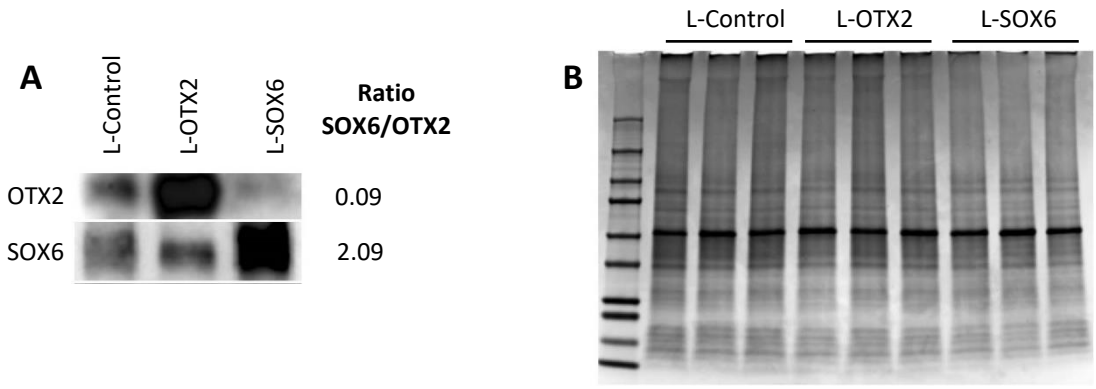

Figure 4.14 Validation of SOX6 and OTX2 expression in lentiviral transduced neurons. (A) Western blot analysis indicates that SOX6 and OTX2 are overexpressed in L-SOX6 and L-OTX2 transduced mDA neurons, respectively; technical replicates; (n=3). (B) Comassie blue staining.

Comparison between L-SOX6 and L-OTX2 transfected presumptive mDA neurons revealed that energy-related metabolism pathways such as glycolysis, gluconeogenesis, glucose and carbon metabolism were enriched in the L-SOX6 transfected hESC-derived neurons. In contrast, the pathway involved in processing unfolded proteins in the ER was upregulated in L-OTX2 transfected hESC-derived neurons (Figure 4.15 A). This suggests than in comparison with the L-OTX2 transduced mDA neurons, L-SOX6 infected presumptive mDA neurons have a higher metabolism requirement than the L-OTX2 transfected presumptive mDA neurons. In contrast, the L-OTX2 transfected presumptive mDA neurons have the unfolding protein response upregulated. Analysis of the proteins upregulated in the L-SOX6 versus the L-OTX2 transfected presumptive mDA neurons, revealed that five of the proteins upregulated (CRABP1, TPI1, ENO1, PRDX2 and LDHB) in the L-SOX6 transfected presumptive mDA neurons, were higher expressed in the SN when compared with the VTA mDA neurons in human (PRDX2; Allen Brain Atlas: https://human.brain-map.org/microarray/search) and mouse (CRABP1, TPI1, ENO1 and LDBH; Greene et al., 2005 and Protein atlas: https://www.proteinatlas.org/ENSG00000166426-CRABP1/brain). Similarly, two proteins (SERPINH1 and ATP12A) upregulated in the L-OTX2 transduced neurons, were higher expressed in the VTA when compared with the SN mDA neurons in human (SERPINH1; Allen Brain Atlas: https://human.brain-map.org/microarray/search) and rat (Greene, Dingledine and Greenamyre, 2005; Figure 4.15 B).

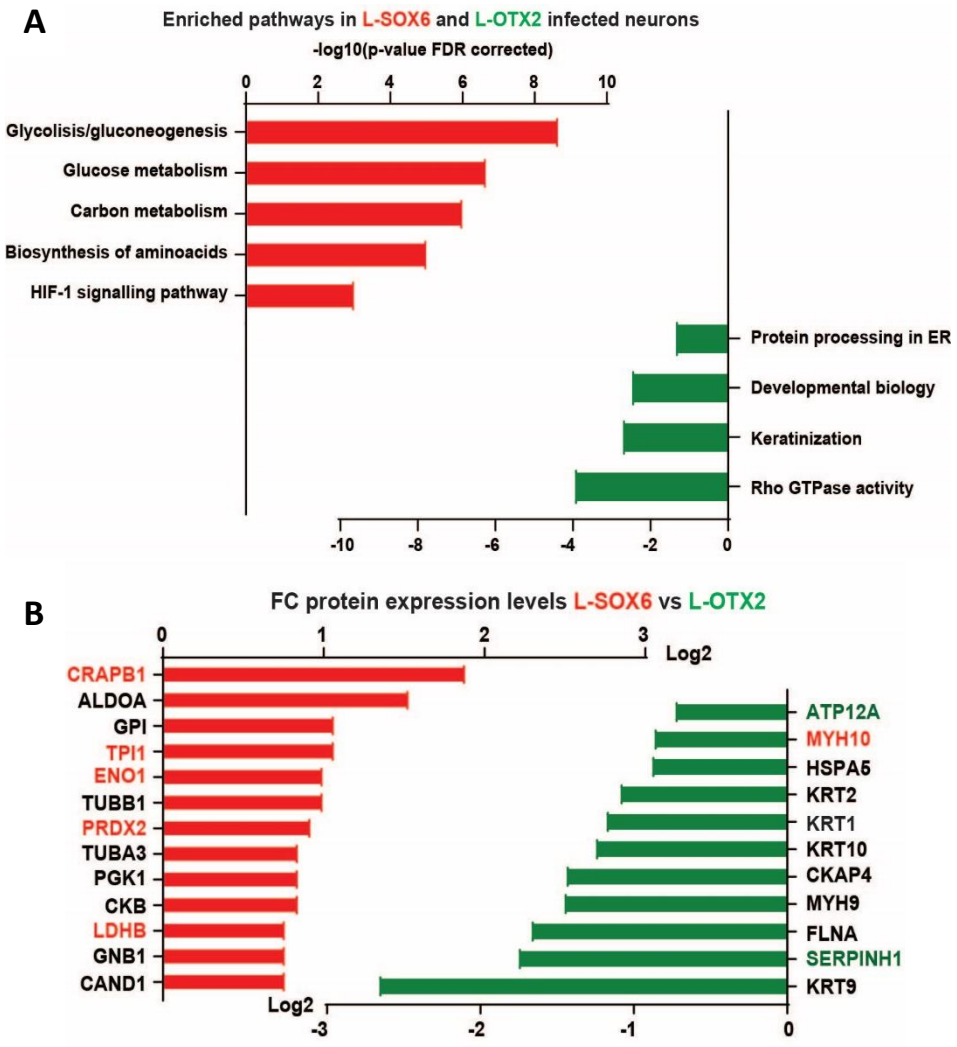

Figure 4.15 Overexpression of SOX6 in mDA neurons results in an enrichment of metabolic pathways in comparison with the mDA neurons L-OTX2 transfected. (A) Pathway enrichment analysis in the L-SOX6 versus the L-OTX2 infected presumptive mDA neurons. Red and green bars correspond to the proteins/pathways highly expressed in SOX6 and OTX2 transfected presumptive mDA neurons, respectively. Proteins in red and in green are higher expressed in SN and VTA mDA neurons, respectively. (B) Proteins differentially expressed when comparing SOX6 with OTX2 lentiviral transfected presumptive mDA neurons.

When looking at the comparison of L-SOX6 versus L-control infected presumptive mDA neurons, three of the four pathways upregulated in the L-OTX2 transduced neurons were also enriched in the L-control (ER unfold protein response, developmental biology and keratinization). This suggests that L-control transfected neurons have similar phenotype than the L-OTX2 neurons (Figure 4.16 A and B).

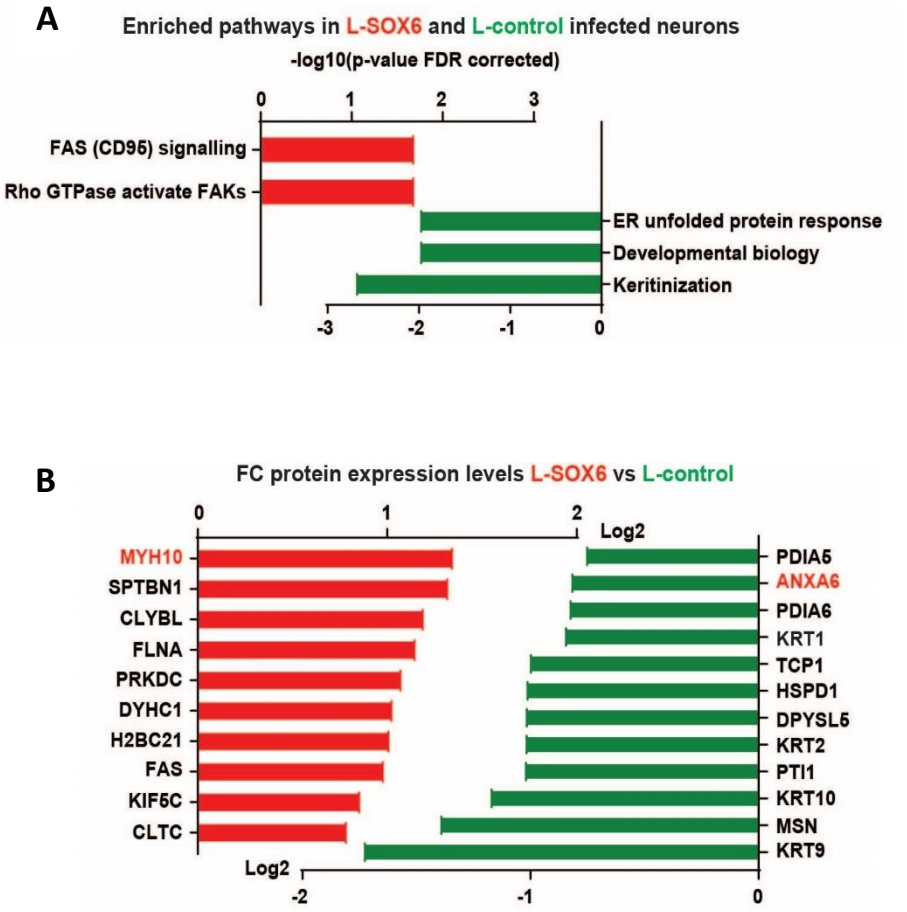

Figure 4.16 Control mDA neurons present a similar pathway enrichment to the OTX2 transduced mDA neurons when compared with the L-SOX6 infected neurons. (A) Pathways enriched in the L-SOX6 versus the L-control infected presumptive mDA neurons. Red and green bars correspond to the proteins/pathways highly expressed in L-SOX6 and L-control transfected presumptive mDA neurons, respectively. Proteins in red and in green are higher expressed in SN and VTA mDA neurons, respectively. (B) Proteins differentially expressed when comparing L-SOX6 with L-control transfected presumptive mDA neurons.

Because of the enrichment of metabolic pathways seen by mass spectrometry in the L-SOX6 transfected presumptive mDA neurons when compared with the L-OTX2 infected presumptive mDA neurons, metabolic rates of lentiviral transduced neurons were assessed by measuring the extracellular acidification rate (ECAR) with the Seahorse assay. Based on the previous mass spectrometry results, we would expect that the metabolic rate of L-SOX6 transduced neurons would be significantly higher than the metabolic rate of L-OTX2 transduced neurons. However, results showed that no

significant difference was seen in the ECAR measured between L-control, L-SOX6 and L-OTX2 transfected neurons (Figure 4.17).

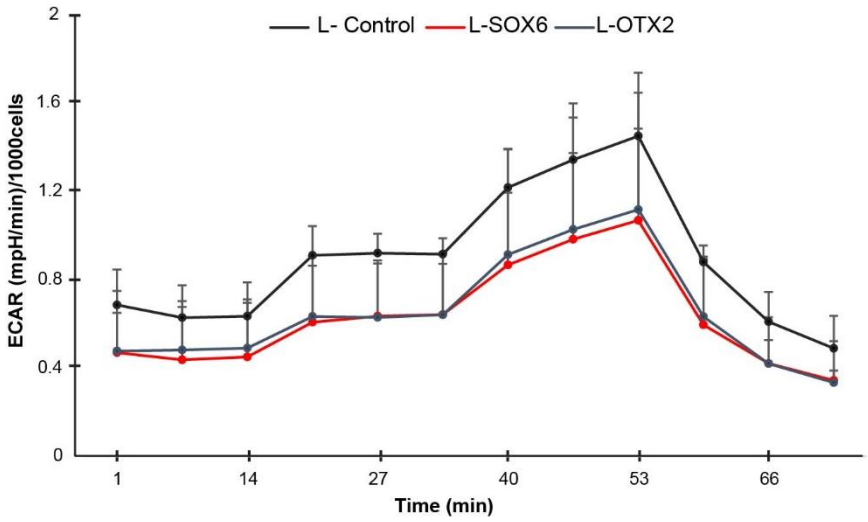

Figure 4.17 No significant difference in the extracellular acidification rate (ECAR) is observed between L-SOX6 and L-OTX2 transduced neurons. Measurement of the ECAR in lentiviral transduced presumptive mDA neurons at day 35 by using the Seahorse assay. ECAR values were normalised to the number of cells alive after the test. Mean values ± SD; repeated measures one-way ANOVA (Sidak); experimental replicates; n=3.

4.2.4 Can hESC-derived lentiviral transfected and IWP2 exposed neurons used for transplantation studies?

Transplantations with the hESC-derived IWP2 treated and lentiviral transfected neurons that I cultured in the laboratory were performed in rat striatum by the group of Dr. Mariah Lelos in the University of Cardiff. Analysis, after 6 weeks post-grafting, showed that the lentiviral transfected and IWP2 treated neurons were able to form grafts expressing TH (Figure 4.18 A, B, C, A', B' and C' and Figure 4.19 A, B, A' and B'). However, the IWP2 exposed neurons had a high proliferative rate (Figure 4.18 D and D'). In addition, SOX6 and OTX2 expression in the L-SOX6 and L-OTX2 grafts respectively was verified (Figure 4.19 C and D). These preliminary results demonstrate that IWP2 exposed neurons and lentiviral transduced neurons can be transplanted in the rat striatum and therefore they could be use in a future for transplantation studies.

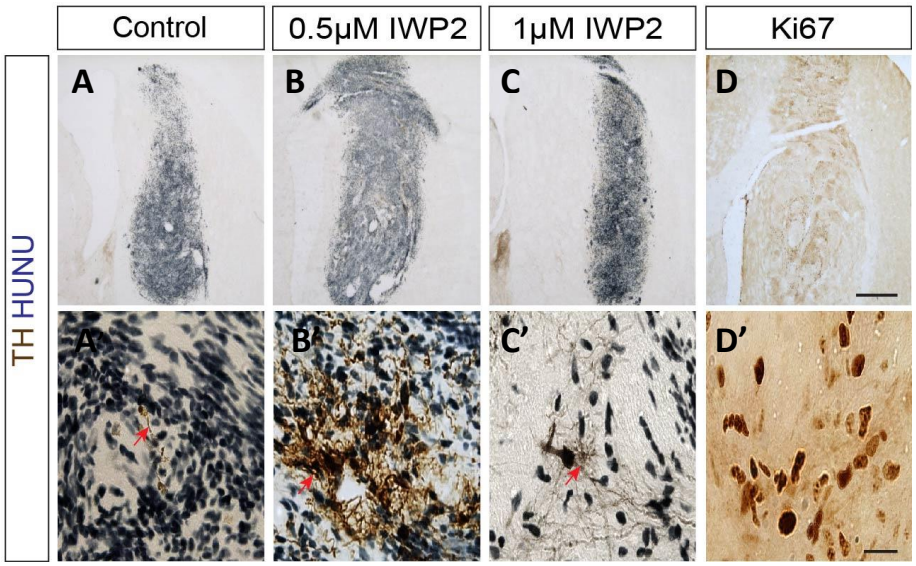

Figure 4.18 Transplantation study 6 weeks post-grafting of the IWP2 treated neurons. (A, B and C) Bright-field images of the grafts obtained with the control and IWP2 (0.5µM and 1µM) conditions. (A', B' and C') Bright-field images showing TH projections from the grafts. Red arrows indicate TH axonal innervations that are also positive for the human marker HUNU. (D and D') Bright-field images of proliferating cells. Pictures and staining were done by Charlotte Bridge.

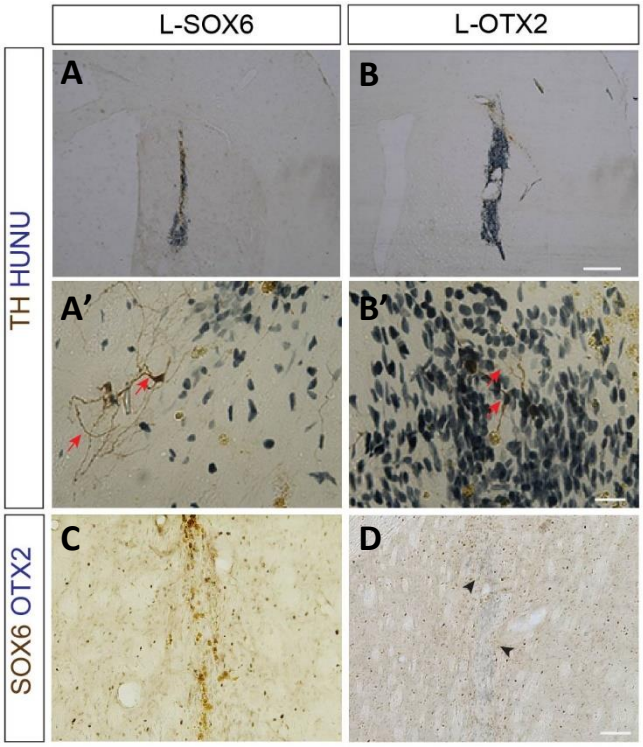

Figure 4.19 Transplantation study 6 post-grafting of the lentiviral transduced neurons. (A and B) Bright-field images of the grafts obtained with the L-SOX6 and L-OTX2 transfected neurons. (A' and B') Bright-field images of TH projections in the engrafted L-SOX6 and L-OTX2 transfected neurons. Red arrows point to TH axonal innervations. (C and D) Bright-field images of $SOX6^+$ and $OTX2^+$ neurons in engrafted L-SOX6 and L-OTX2 transfected neurons. Black arrows point to OTX2 expressing neurons. Pictures and staining were done by Charlotte Bridge.

4.3 Discussion

This chapter determined that the subpopulation of presumptive mDA neurons differentiated with low Wnt signalling levels and expressing SOX6 have a SNc-like phenotype while presumptive mDA neurons differentiated with high Wnt signalling levels and expressing OTX2 have a VTA-like phenotype. Indeed, $SOX6^+$ presumptive mDA neurons expressed SNc markers (SATB1, SOX6 and GIRK2) and as occurs *in vivo* showed vulnerability to the toxin rotenone causing Parkinson-like symptoms. In contrast, $OTX2^+$ neurons express VTA markers (CALB1 and OTX2) and are resistant to these compounds. In addition, this work revealed that SNc-like (with selective vulnerability to toxins) and VTA-like (resistance to toxins) phenotype can also be obtained when overexpressing SOX6 and OTX2 in presumptive mDA neurons, respectively. This suggests that SOX6

expression induces SNc fate in hESC derived mDA neurons, however there is not enough evidence to conclude that SOX6 acts as an intrinsic determinant of SNc mDA neurons.

Protocols differentiating hESC into mDA neurons with IWP2 and lentiviral transfection showed that, contrary to the $TH^+/OTX2^+$ neurons obtained, $TH^+/SOX6^+$ neurons generated with both protocols were vulnerable to toxins causing parkinsonism (MPP^+ and Rotenone). Neurons differentiated with IWP2 that were $SOX6^+/TH^+/SATB1^+$ showed selective vulnerability when analysed with immunocytochemistry. In addition, TH levels were significantly decreased in 0.5µM IWP2 treated presumptive mDA neurons when exposed to Rotenone and in 0.5µM and 1µM IWP2 treated presumptive mDA neurons when exposed to MPP^+ in comparison with the CHIR and control conditions. As described in chapter 3, the percentage of $SOX6^+/TH^+$ is 30%, meaning that cultures display other neuronal types. In fact, IWP2 addition induces the apparition of $SOX6^+/TH^-$ cells (data not shown). In the 1µM IWP2 condition, decrease in TH levels was not significant probably due to the population heterogeneity which tends to always be higher than in the 0.5µM IWP2 condition. As seen in the quantification of TH levels by qPCR, the control condition is more sensitive than the CHIR condition when exposed to the parkinsonism toxin rotenone. This might be explained by the fact that impairment in Wnt signalling causes the degeneration of dopaminergic neurons in *Drosophila* exposed to rotenone, suggesting that certain Wnt signalling levels are necessary for survival of dopaminergic neurons, especially in stress conditions (Stephano *et al.*, 2018). Therefore, hESC-derived mDA differentiated with CHIR (high Wnt signalling levels) are more resistant to toxins than the control condition (low Wnt signalling levels). Similarly, the IWP2 conditions (inhibition of Wnt signalling) are the most vulnerable to rotenone and MPP^+ since they are differentiated with the lowest Wnt signalling levels.

Mass spectrometry data obtained from L-control, L-SOX6 and L-OTX2 transfected mDA neurons revealed that in comparison with the OTX2 overexpressed presumptive mDA neurons, SOX6 lentiviral transduced presumptive mDA neurons have higher expression of proteins involved in energy metabolism (glycolysis, gluconeogenesis, carbon metabolism, biosynthesis of aminoacids). Interestingly, other genetic and proteomic studies found an enrichment of metabolic pathways in the SN of human and mouse (Chung *et al.*, 2005; Licker *et al.*, 2014). However, the results from the seahorse assay

showed no significant increase of ECAR levels in L-SOX6 transduced neurons when compared with the L-OTX2 transduced neurons. Therefore, although an enrichment of metabolic pathways has been observed by mass spectrometry in L-SOX6 neurons when compared with L-OTX2 neurons, L-SOX6 transfected neurons do not seem to be functionally more energetic. Given that an enrichment of metabolic pathways has not been seen in the L- SOX6 infected presumptive mDA neurons when compared to the L-control transfected neurons, it is not possible to conclude that SOX6 overexpression induces the expression of energy metabolism related proteins. Instead, an enrichment of ER stress pathway has been observed in the L-control and L-OTX2 in comparison with the L-SOX6 transfected presumptive mDA neurons. The chaperones HSPA5, PDIA5 and PDIA6 are downregulated in the L-SOX6 infected presumptive mDA neurons when compared with the L-OTX2 and L-control. Therefore, this work suggests that the vulnerability of $SOX6^+$ hESC-derived mDA could be due to a lower expression of chaperones such as HSPA5 that are important for unfolded protein response.

Late progenitors differentiated with the IWP2 and the lentiviral protocol were transplanted into rat lesioned striatum. After 6 weeks of transplantation brains were analysed and although neurons differentiated with both protocols produced grafts, neurons treated with IWP2 were highly proliferative, probably due to the heterogeneity of these cultures. Because of time constrains further experiments could not be performed, however it would be interesting to carry out functional studies with L-SOX6 and L-OTX2 infected presumptive mDA neurons. Since, L-SOX6 and L-OTX2 appear to have a SN-like and VTA-like phenotype, respectively, an amelioration of motor symptoms in transplants with $SOX6^+$ presumptive mDA neurons and an improvement of cognitive functions in transplants with $OTX2^+$ neurons would be expected.

Overall, these results suggested that in the ventral midbrain, the medial progenitor domain $Wnt^-/SOX6^+/CORIN^+/OTX2^-$ gives rise to SN-like mDA neurons ($SATB1^+/SOX6^+/GIRK2^+$) vulnerable to toxins causing parkinsonism. In contrast, the lateral progenitor domain $Wnt^+/SOX6^-/CORIN^-/OTX2^+$ generates VTA-like mDA neurons ($OTX2^+/CALB1^+$) resistant to these toxins (Figure 4.20). However, are mDA progenitors $SOX6^+/CORIN^+/OTX2^-$ giving rise to SN mDA neurons only? Or are other cellular populations arising from this medial domain? This will be investigated in the following

chapter by tracing SOX6 expressing progenitors in mice, to better investigate the role that SOX6 plays in the development of mDA neurons.

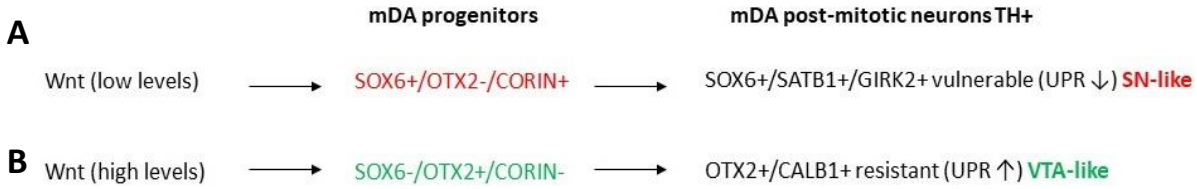

Figure 4.20 Schematic representation of how Wnt signalling modulation induces SN-like and VTA-like mDA neurons, respectively. (A) Low levels of Wnt signalling in the medial progenitor domain generate mDA neurons presenting a SN-like phenotype. (B) High levels of Wnt signalling in the lateral progenitor domain generate mDA neurons presenting a VTA-like phenotype. Red: medial progenitor domain. Green: lateral progenitor domain. UPR: Unfolded protein response.

Chapter 5

Tracing SOX6 to study the development of SN and VTA mDA neurons

Chapter 5 Tracing SOX6 to study the development of SN and VTA mDA neurons

5.1 Introduction

It has been already identified, in mouse, that the transcription factor (TF) Sox6 is involved the development of oligodendrocytes, cortical interneurons, chondrocytes and SNc mDA neurons (Lefebvre, Li and De Crombrugghe, 1998; Stolt *et al.*, 2006; Batista-Brito *et al.*, 2009; Panman *et al.*, 2014). In the ventral midbrain, Sox6 appears to be important for the development and maintenance of SNc mDA neurons by repressing certain VTA features. Progenitors that are medially located in the vMB express Sox6 and give rise to SNc mDA neurons which maintain Sox6 expression. Although loss of Sox6 expression does not impair the development of SNc neurons, differences were observed such as an increase and reduction in the number of SN neurons expressing Calb1 and Aldh1a1, respectively. Also, innervation to the dorsal-lateral striatum, the area where the SN projects, was remarkably less dense (Panman *et al.*, 2014). Based on the role that Sox6 and Otx2 play in the development of SNc and VTA mDA neurons in the mouse brain, respectively, Chapters 3 and 4 were focused on the determination of culturing conditions to generate distinct subpopulations of hESC derived mDA neurons $SOX6^{+}$ or $OTX2^{+}$ displaying SN-like or VTA-like characteristics, respectively. In addition, the link between SOX6 expression and selective vulnerability of SN mDA neurons was also studied. Chapter 5 further explores the role of Sox6 as an intrinsic determinant of SNc mDA neurons by using a $Sox6^{eGFP\text{-}Cre\text{-}ERT2}$ mouse line. In these mice, the eGFP-Cre-ERT2 cassette is inserted in the exon 8 of the *Sox6* gene being under control of an ATG codon. The presence of this cassette, blocks Sox6 expression and causes GFP expression in cells that are $Sox6^{+}$. Three objectives were addressed: 1. the use of GFP expression to trace the projections of Sox6 expressing neurons 2.crossing the $Sox6^{eGFP\text{-}Cre\text{-}ERT2}$($Sox6^{GFPCreRT}$) mouse line with a $ROSA^{LoxP\text{-}STOP\text{-}LoxP\text{-}LacZ}$($R26^{LacZ}$) mouse line for lineage tracing of Sox6

expressing progenitors over time and 3. Using the mouse line to further investigatethe linkage between Wnt, Corin and Sox6.

5.2 Characterisation of the *Sox6$^{eGFP\text{-}Cre\text{-}ERT2}$* mouse line

The company geneOnway developed a new *Sox6^{GFPCreRT}* mouse line. These mice have incorporated an eGFP-Cre-ERT2 cassette in exon 8 of the *Sox6* gene. In mice homozygous for this cassette, Sox6 expression is impaired and GFP is instead detected by immunohistochemistry. At E11.5, as previously observed in wild type mice (*Sox6$^{+/+}$*), Sox6 is medially expressed in the progenitor domain localised in the vMB and expression is detected (Figure 5.1 A, A' and A''). In heterozygous mice (*Sox6$^{eGFP\text{-}Cre\text{-}ERT2/+}$*) the medial progenitor domain in the vMB coexpresses GFP and Sox6 (Figure 5.1 B, B' and B''). Finally, in mutant mice (*Sox6$^{eGFP\text{-}Cre\text{-}ERT2/eGFP\text{-}Cre\text{-}ERT2}$*) GFP expression is medially localised and Sox6 is not detected (Figure 5.1 C, C' and C'').

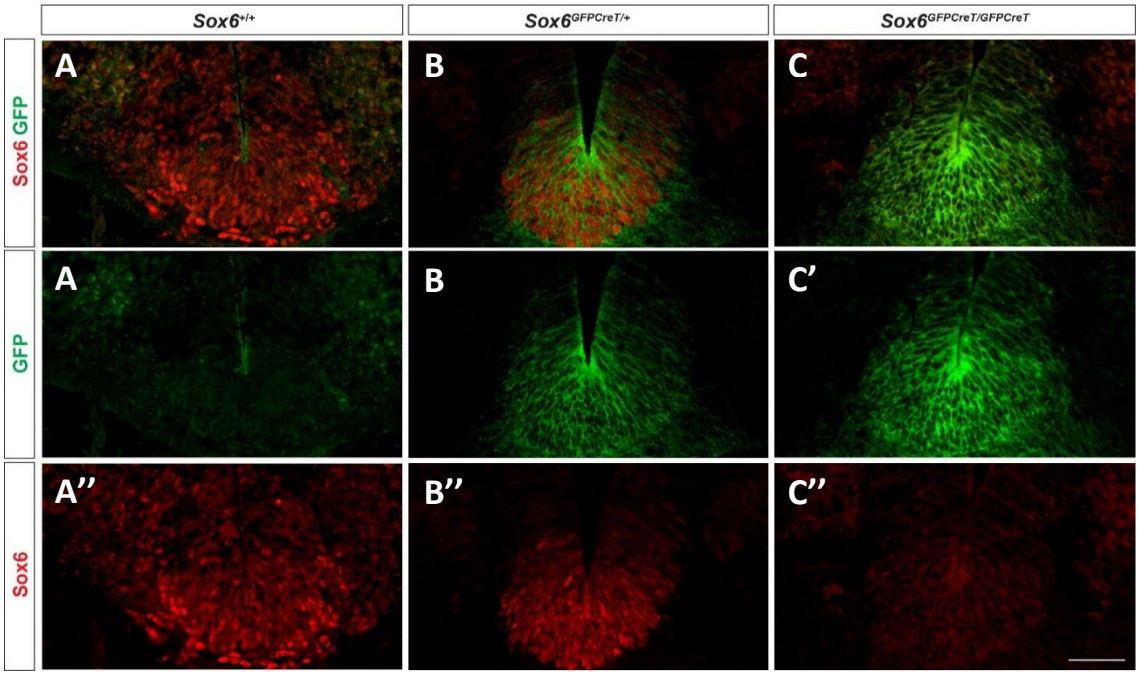

Figure 5.1 Characterisation of GFP expression in the vMB progenitor domain of wild-type (*Sox6$^{+/+}$*), heterozygous (*Sox6$^{eGFP\text{-}Cre\text{-}ERT2/+}$*) and homozygous (*Sox6$^{eGFP\text{-}Cre\text{-}ERT2/\ eGFP\text{-}Cre\text{-}ERT2}$*) mice at E11.5. (A to C'') Confocal micrographs of (A, A' and A'') wild-type (*Sox6$^{+/+}$*), (B, B' and B'') heterozygous (*Sox6$^{GFPCreT/+}$*) and (C, C' and C'') mutant (*Sox6$^{GFPCreT/GFPCreT}$*) mouse midbrain sections stained with anti-rbGFP and anti-gpSOX6. (Scale bar: 50µm).

Next, Foxa2 and Lmx1a immunohistochemistry analysis confirmed that GFP and Sox6 expressing progenitors localised in the vMB corresponded to the mDA progenitor

domain that gives rise to SNc and VTA mDA neurons. GFP expression colocalised with Lmx1a and Foxa2 expression in heterozygous and mutant mice (Figure 5.2 A- B''). The detection with antibodies of Foxa2 and Lmx1a was variable between the different mice at E11.5, probably due to the optimisation of fixation times. This is the reason why in Figure 5.2 B' and A'', Lmx1a and Foxa2 expression are weakly detected, respectively.

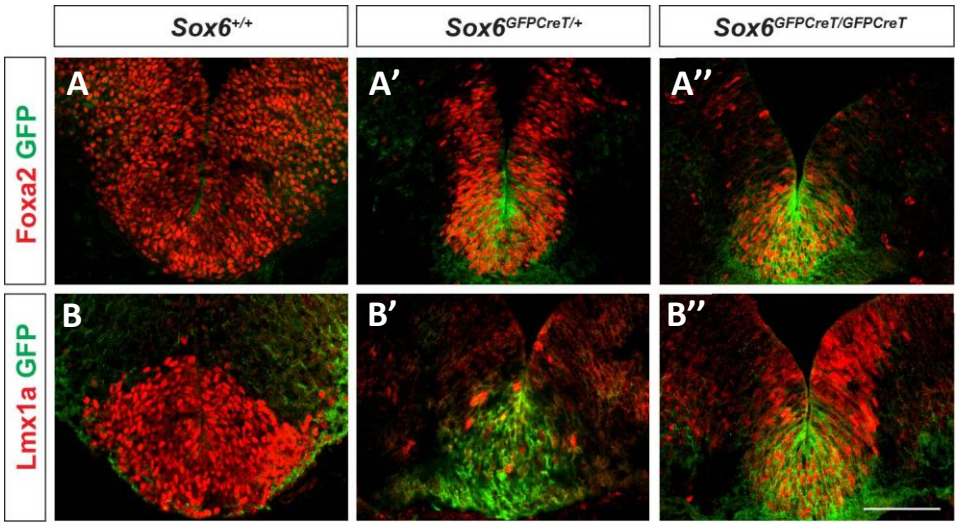

Figure 5.2 GFP expression colocalised with the mDA progenitor domain Foxa2$^+$ and Lmx1a$^+$ in heterozygous and mutant mice at E11.5.(A to B'') Confocal micrographs of (A and B) wild-type (*Sox6*$^{+/+}$), (A' and B') heterozygous (*Sox6*$^{GFPCreT/+}$) and (A'' and B'') mutant (*Sox6*$^{GFPCreT/GFPCreT}$) mouse midbrain sections. (A, A' and A'') Sections were stained with anti-rbGFP and anti gFOXA2. (B, B' and B'') Sections were stained with anti-rbLMX1a and anti-gGFP (scale bar: 50µm).

In mice at E18.5, co-expression between Sox6, GFP and TH was analysed. Similarly to the E11.5 mice, GFP expression colocalised with mDA neurons SOX6$^+$/TH$^+$. In wild type mice, GFP was not detected and Sox6 expression was mainly localised in SNc mDA neurons expressing TH (Figure 5.3 A, A' and A''). In heterozygous mice, TH$^+$/Sox6$^+$ mDA neurons showed GFP expression and, as expected, in mutant mice Sox6 was not detected in SNc mDA neurons which instead were TH$^+$ and GFP$^+$ (Figure 5.3 B, B', B'', C, C' and C'').

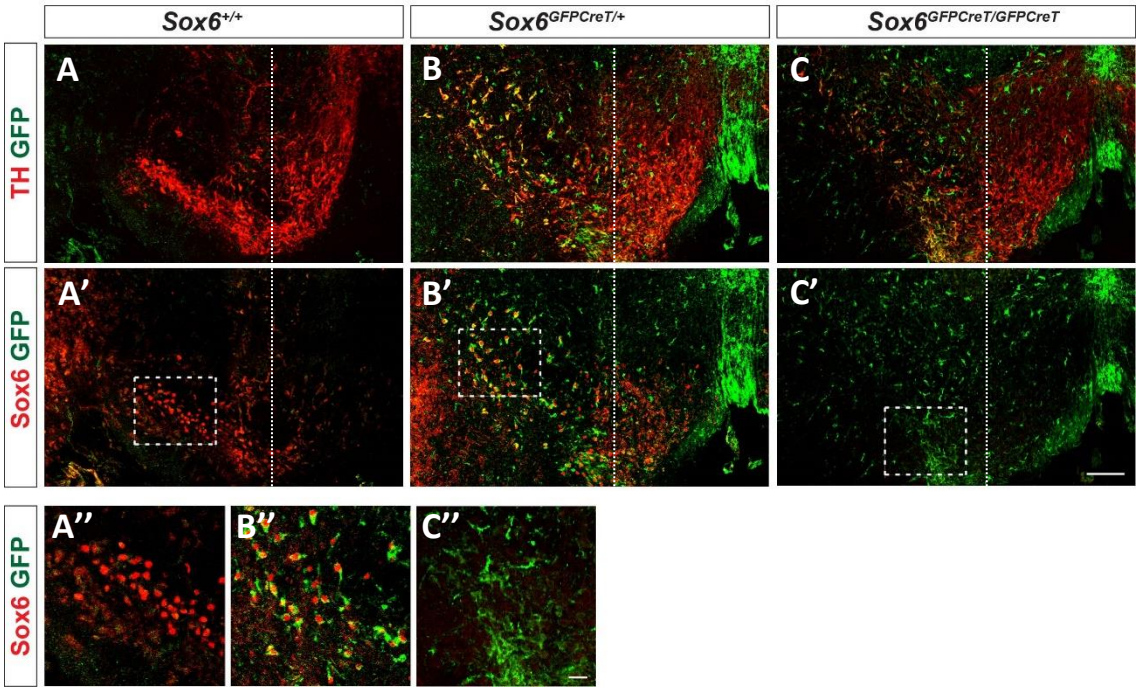

Figure 5.3 Characterisation of GFP expression in SNc and VTA mDA neurons of mice at E18.5. (A to C') Confocal micrographs of (A and A') wild-type (*Sox6*$^{+/+}$), (B and B') heterozygous (*Sox6*$^{GFPCreT/+}$) and (Cand C') mutant (*Sox6*$^{GFPCreT/GFPCreT}$) mouse midbrain sections stained with anti-rbGFP, anti-gpSOX6 and anti-shTH antibodies. (A'' to C'') Zoom of the section defined with a dashed square in the SNc of wild type (A''), heterozygous (B'') and mutant mice (C'') stained with anti-rbGFP, anti-gpSOX6 and anti-shTH antibodies. The dashed white line separates SNc (right) from VTA (left) mDA neurons (scale bar: 200µm).

One of the objectives was to trace the innervations of Sox6^{+} SNc mDA neurons by using GFP expression. At E15.5, GFP was studied in the diencephalon, where bundles of TH^{+} axons projected from the SNto the striatum (nigrostriatal pathway) and from the VTA to the limbic system (mesolimbic pathway). As previously observed, GFP colocalised with Sox6^{+}TH^{+} neurons but projections could not be traced by GFP immunohistochemistry (Figure 5.4 A, B, A' and B').

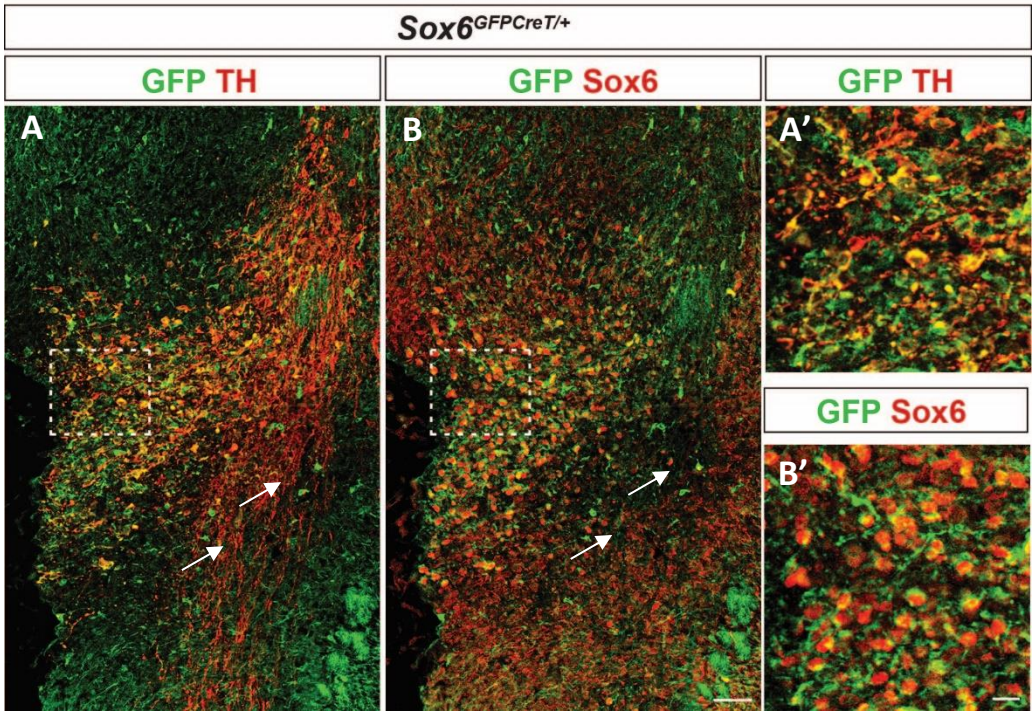

Figure 5.4 Immunohistochemical analysis of GFP expression in bundles of TH^+ axons in *Sox6*$^{eGFP\text{-}Cre\text{-}ERT2/+}$ mouse at E15.5. (A and B) Confocal micrographs of mouse diencephalon section stained with anti-rbGFP, anti-gpSOX6 and anti-shTH antibodies. (A' and B') Zoom of the section defined with a dashed square in A and B. Arrows indicate the absence of GFP expression in the bundles of TH^+ axons (scale bar: 100µm).

Interestingly, in heterozygous mice, $GFP^+/TH^-/Sox6^-$ neurons were intermingled with TH expressing neurons in the caudal linear and interfascicular nucleus in the VTA (Figure 5.5 A, B, C, D, C' and D'). This population appeared to be more abundant in the caudal than in the rostral VTA. Given that GFP could not be detected in the wild type mouse (see Figure 5.3 A and A'), the lack of Sox6 expression in this area, could be due to the lack of sensitivity of the antibody rather than a problem with GFP antibody background (Figure 5.5 B, D and D').

Although projections from Sox6 expressing mDA neurons could not be traced, the expression of GFP was located in progenitors and mDA neurons expressing Sox6. In addition, Sox6 and GFP expression were not detected in mutant and wild type mice, respectively. Overall, these results indicated that the mouse line is working as expected.

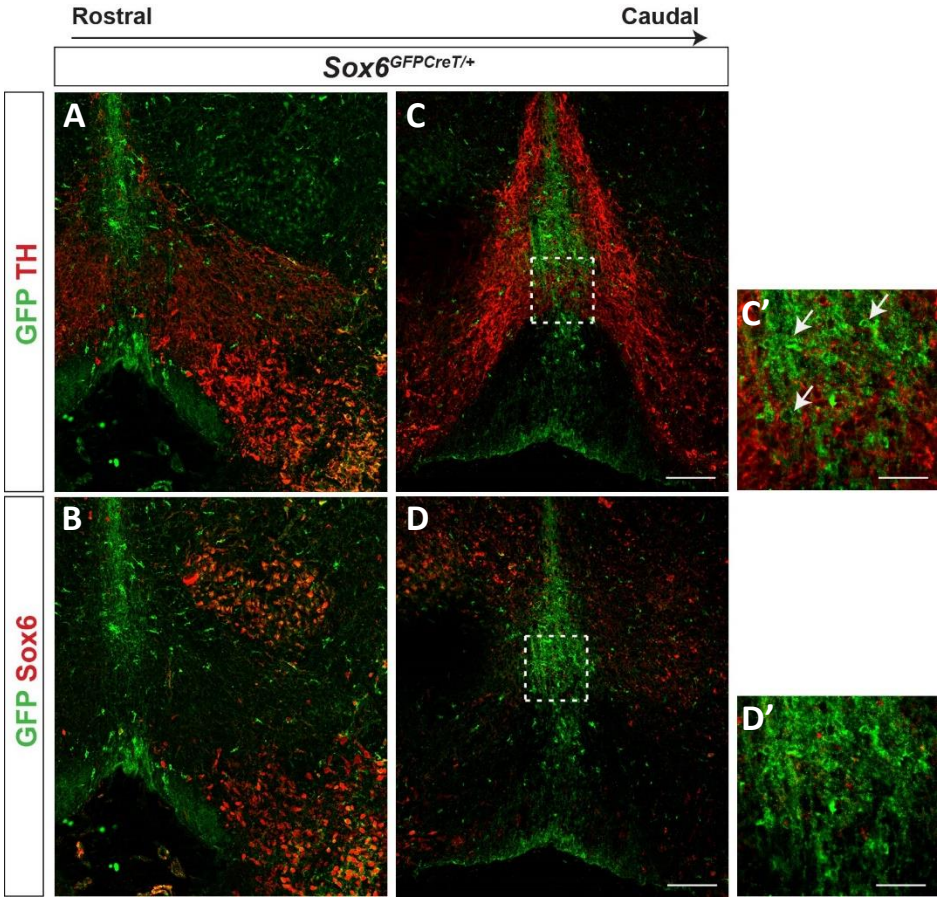

Figure 5.5 GFP expression was identified in a population of TH$^-$ neurons located in the caudal linear and the interfascicular nucleus in the VTA of a heterozygous mouse at E18.5. (A, B, C and D) Confocal micrographs of mouse rostral midbrain section (A and B) and caudal midbrain section (C and D) stained with anti-rbGFP, anti-gpSOX6 and anti-shTH antibodies. (C' and D') Zoom of the area defined with a dashed square show that GFP does not overlap with TH and Sox6. (Scale bar: 100µm). Arrows point to neurons that are GFP$^+$.

5.3 Tracing Sox6$^+$ progenitors with tamoxifen treatment

To trace Sox6$^+$ progenitors, tamoxifen was administrated in *Sox6*$^{GFPCreT/+}$ crossed with *R26*$^{lz/lz}$ mice at different time points. In mice *Sox6*$^{GFPCreT/+}$ *R26*$^{lz/lz}$, upon binding with tamoxifen, CreER is translocated into the nucleus of S*ox6* cells allowing *LacZ* to be constitutively expressed in all the progeny of Sox6$^+$/LacZ$^+$/GFP$^+$ cells. Given that CreER is translocated into the nucleus from 6 to 24 hours after mice have been exposed to tamoxifen, cells that express *Sox6* from 6 to 36 hours after tamoxifen exposure can be histochemically detected (Blaess *et al.*, 2011).

Mice exposed to tamoxifen for 2 consecutive days (E8.5+E9.5) were fixed at E11.5. Immunohistochemical analysis detected ß-galactosidase expression in the Sox6^{+} medial progenitor domain from the vMB which also expressed Lmx1a (Figure 5.6 A, B, C and D). However, in comparison with the number of Sox6 expressing progenitors, ß-galactosidase was weakly detected (Figure 5.6 B and D). This indicated that Sox6^{+} progenitors giving rise to SNc mDA neurons E9.5/E10.5.

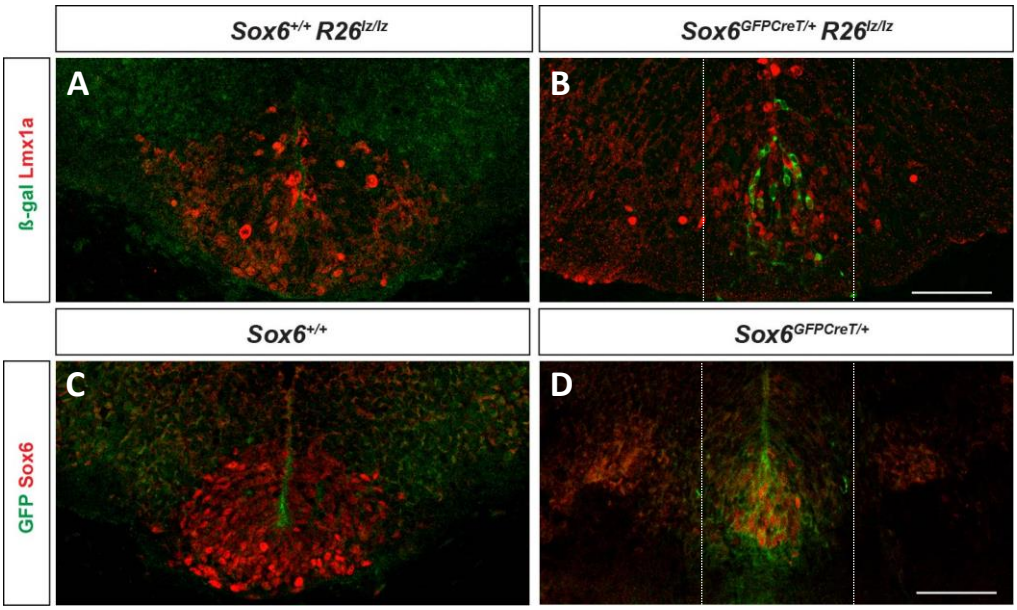

Figure 5.6 ß-galactosidase (ß-gal) is detected in the Sox6^{+} vMB progenitor domain medially located of E11.5 mice. (A and B) Confocal micrographs of mouse midbrain section from (A) wild type and (B) *Sox6$^{GFPCreT/+}$ R26$^{lz/lz}$* mice treated with tamoxifen at E8.5+E9.5. Sections were stained with anti-gβ-gal and anti-rbLmx1a antibodies. (C and D) Confocal micrographs of mouse midbrain section in (C) wild type and (D) *Sox6$^{GFPCreT/+}$ R26$^{lz/lz}$* treated with tamoxifen at E8.5+E9.5. Sections were stained with anti-rbGFP and anti-gpSox6 antibodies. Dashed lines separate the medial progenitor domain (inside) from the lateral progenitor domain (sides). (Scale bar: 50µm).

Next, mice were exposed to tamoxifen for 3 consecutive days (E8.5, E9.5 and E10.5) and were analysed at E18.5. Because Sox6 is involved in the development of cortical interneurons (Azim *et al.*, 2009; Batista-Brito *et al.*, 2009), ß-galactosidase expression was studied in the cortex of these animals.

As previously described by Azim et al., 2009, cortical interneurons were generated from progenitors in the pallial ventricular zone expressing Sox6 (Figure 5.7 A, B and B'). Similarly, ß-galactosidase expression was detected close to the striatum, in what seems to correspond to the medial ganglionic eminence (Figure 5.7 C, C', D and D'). Given that

most of the cells are labelled by ß-galactosidase, these results indicate that CreER efficiently translocates into the nucleus in cortical cells and this happens in areas that are expected to show Sox6 expression. In addition, the negative control (mice lacking CreER), do not exhibit ß-galactosidase (Figure 5.7 C and C').

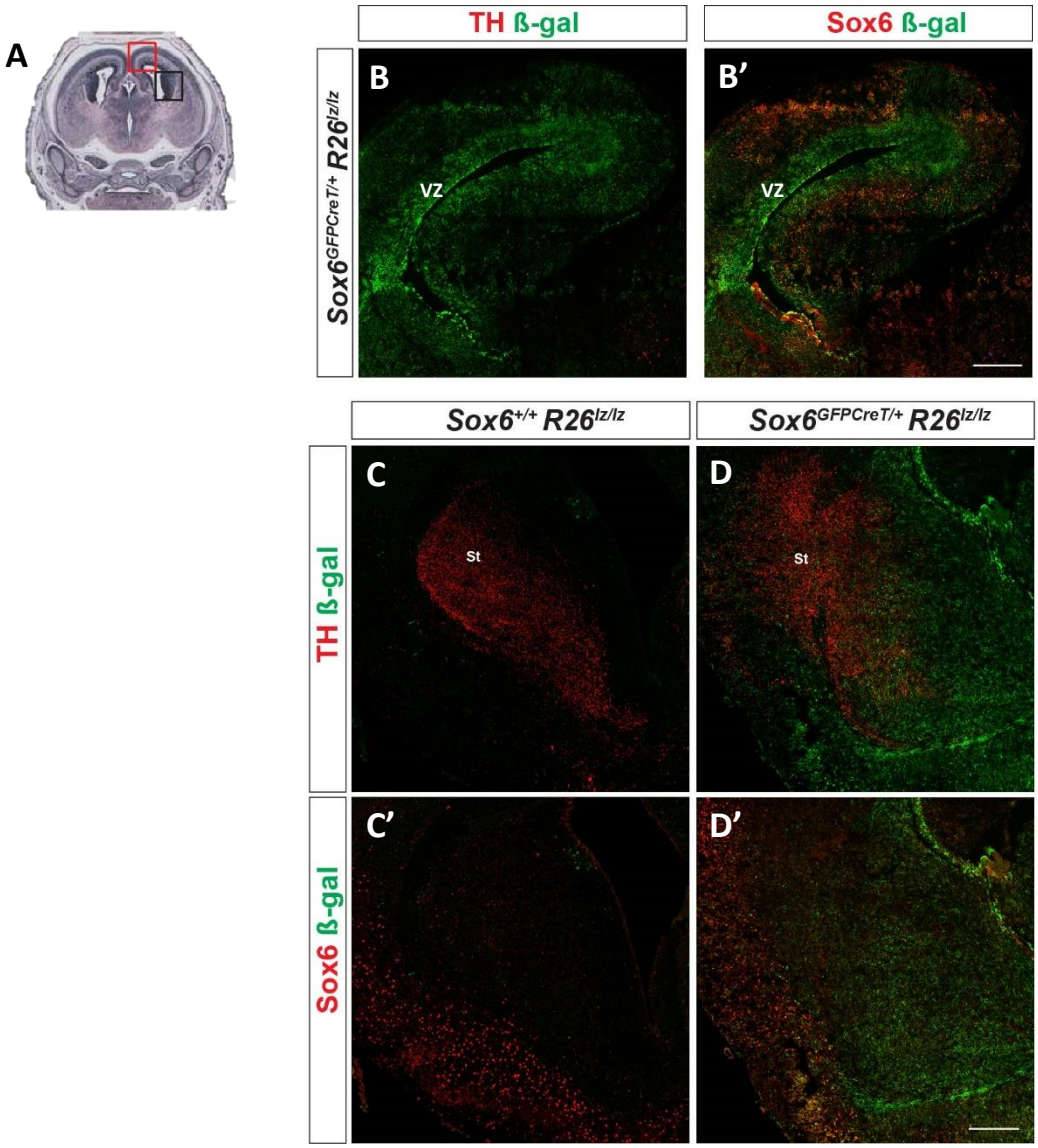

Figure 5.7 ß-galactosidase (ß-gal) is detected in the cortex of E18.5 mice. (A) Areas of the cortex analysed. Red square corresponds to B and B' and black square corresponds to C, C', D and D'. (B and B') Confocal micrographs of mouse cortex section from *Sox6*$^{GFPCreT/+}$ *R26*$^{lz/lz}$ mice treated with tamoxifen at E9.5+E10.5+E11.5. Sections were stained with anti-gβ-gal, anti-rbTH and anti-gpSox6 antibodies. ß-gal expression is identified in the pallial ventricular zone (VZ). (C to D') Confocal micrograph of mouse cortex section comprising the striatum (st) from (C and C') wild type mice and (D and D') *Sox6*$^{GFPCreT/+}$ *R26*$^{lz/lz}$ mice. Sections were stained with anti-gβ-gal, anti-rbTH and anti-gpSox6 antibodies. The projections from mDA neurons expressing TH are detected in the striatum (scale bars: 100µm).

The midbrain was studied in mice exposed for 3 consecutive days to tamoxifen at 2 timepoints: E8.5, E9.5 and E10.5 and at E10.5, E11.5 and E12.5. When analysing the VTA, a cell population TH^-/ß-gal^+ was detected in the caudal linear and interfascicular nucleus of heterozygous mice (*Sox6*$^{GFPCreT/+}$ *R26*$^{lz/lz}$) exposed to tamoxifen at the two timepoints. As expected, wild type mice (*Sox6*$^{+/+}$ *R26*$^{lz/lz}$) did not show ß-galactosidase expression (Figure 5.8 A,B,C,A',B' and C'). Interestingly, the expression of ß-galactosidase was higher in the caudal than the rostral VTA. In mice exposed to tamoxifen from E8.5 to E10.5, some scattered cells expressing ß-galactosidase were detected rostrally but most of them where located in the caudal VTA (Figure 5.8 B and B'). In mice exposed to tamoxifen from E10.5 to E12.5, ß-galactosidase was identified caudally, while no ß-galactosidase expression was detected in the rostral VTA (Figure 5.8 C and C'). This suggests that the caudal TH^-/ß-gal^+ neuronal population medially located in the VTA is generated from $Sox6^+$ progenitors early (probably around E8.5/E9.5), while the rostral TH^-/ß-gal^+ neuronal population medially located in the VTA is generated from $Sox6^+$ progenitors late (probably from E10.5). Although, Sox6 expression has not been detected in the TH^-/ß-gal^+ cells, this population might correspond to the previously detected GFP^+/TH^- cellular population (see Figure 5.5).

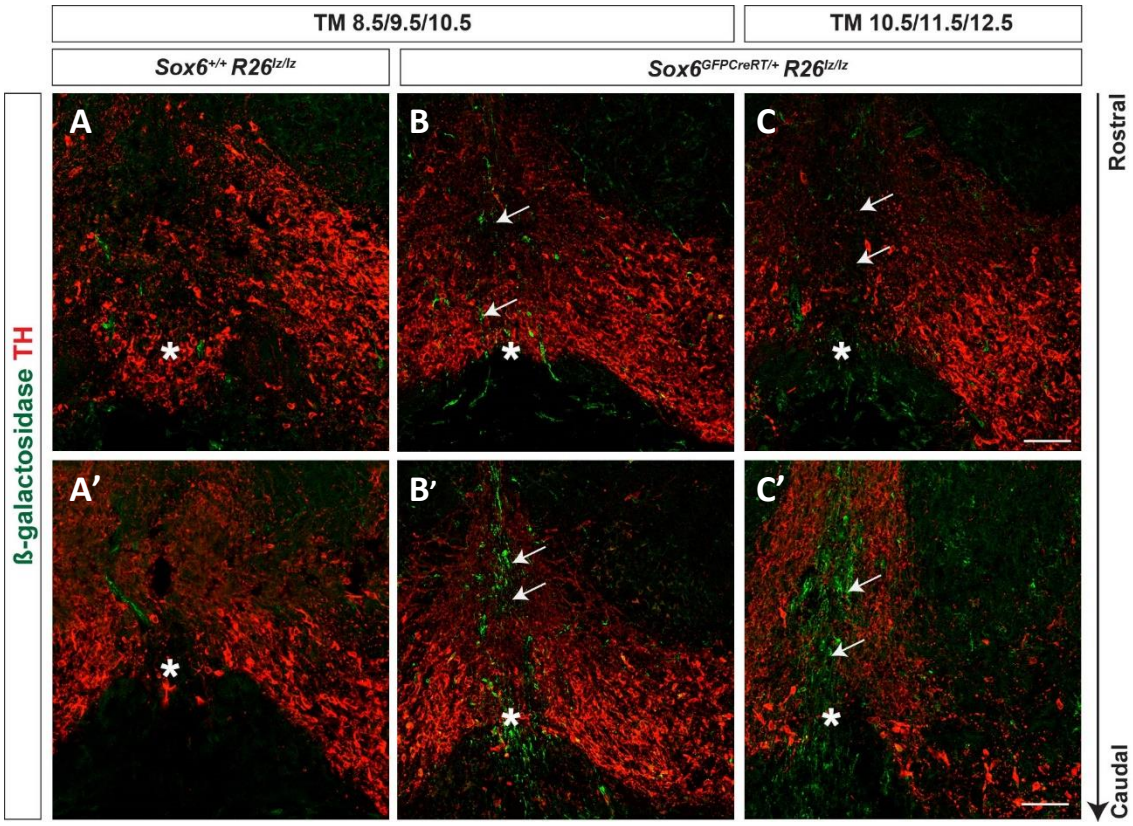

Figure 5.8 ß-galactosidase expression is identified in the caudal linear and interfascicular nucleus of the VTA in E18.5 mouse. (A, B, C, A, B' and C') Confocal micrographs of mouse VTA in the rostral midbrain section (A, B and C) and caudal midbrain section (A',B' and C'). (A and A') Sections were stained with anti-gß-gal and anti-rbTH antibodies in wild type (*Sox6*$^{+/+}$ *R26*$^{lz/lz}$) mouse exposed to tamoxifen at E8.5, E9.5 and E10.5 (TM E8.5/9.5/10.5). (B and B') Sections were stained with anti-gß-gal and anti-rbTH antibodies in *Sox6*$^{GFPCreT/+}$ *R26*$^{lz/lz}$ mouse exposed to tamoxifen at E8.5, E9.5 and E10.5 (TM E8.5/9.5/10.5). (C and C') Sections were stained with anti-gß-gal and anti-rbTH antibodies in *Sox6*$^{GFPCreT/+}$ *R26*$^{lz/lz}$ mouse exposed to tamoxifen at E10.5, E11.5 and E12.5 (TM E10.5/11.5/12.5).Sections were stained with anti-gß-gal and anti-rbTH antibodies in wild type (*Sox6*$^{+/+}$ *R26*$^{lz/lz}$) mouse *Sox6*$^{GFPCreT/+}$ *R26*$^{lz/lz}$ mice treated with tamoxifen at E9.5+E10.5+E11.5. Arrows point to TH^{-}/ß-gal^{+} neurons. Asterisk indicates the ventral midline. (Scale bar: 100µm).

SNc mDA neurons were analysed in mice exposed to tamoxifen for 3 consecutive days: tamoxifen at E8.5, E9.5 and E10.5 and at E10.5, E11.5 and E12.5 was done. As expected, SNc mDA neurons in wild type mice did not express ß-galactosidase (Figure 5.9 A , A' and Figure 5.10 A, A'). However, in heterozygous mice exposed to tamoxifen at two different timepoints, only a few scattered SNc mDA neurons were TH^{+}/Sox6^{+}/ß-gal^{+} (Figure 5.9 B, B', C, C' and Figure 5.10 B, B', C, C').

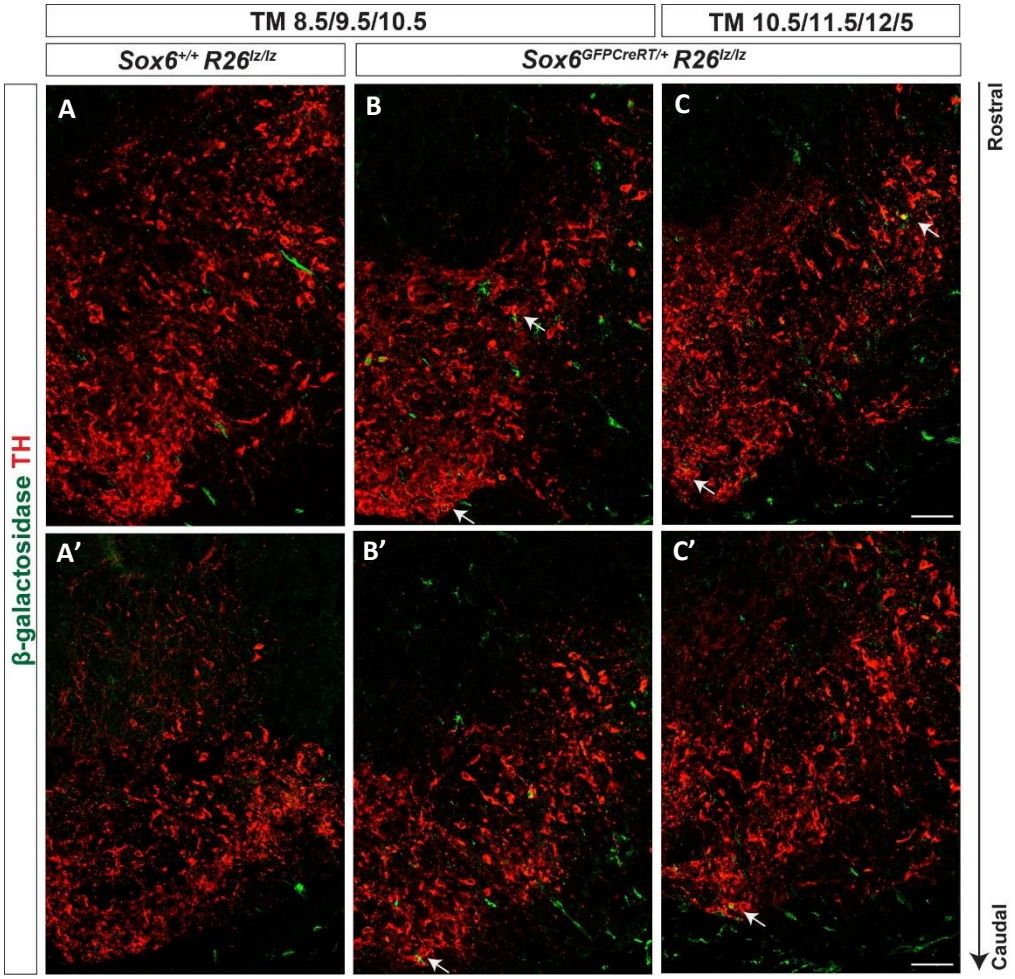

Figure 5.9 Some scattered SNc mDA neurons express ß-galactosidase in E18.5 mouse. (A,B,C,A',B' and C') Confocal micrographs of mouse SNc in the rostral midbrain section (A,B and C) and caudal midbrain section (A',B' and C'). (A and A') Sections were stained with anti-gβ-gal and anti-rbTH antibodies in wild type (*Sox6*$^{+/+}$ *R26*$^{lz/lz}$) mouse exposed to tamoxifen at E8.5, E9.5 and E10.5 (TM E8.5/9.5/10.5). (B and B') Sections were stained with anti-gβ-gal and anti-rbTH antibodies in *Sox6*$^{GFPCreT/+}$ *R26*$^{lz/lz}$ mouse exposed to tamoxifen at E8.5, E9.5 and E10.5 (TM E8.5/9.5/10.5). (C and C') Sections were stained with anti-gβ-gal and anti-rbTH antibodies in *Sox6*$^{GFPCreT/+}$ *R26*$^{lz/lz}$ mouse exposed to tamoxifen at E10.5, E11.5 and E12.5 (TM E10.5/11.5/12.5). Arrows point to TH^{+}/ß-gal^{+} neurons. (Scale bar: 100µm).

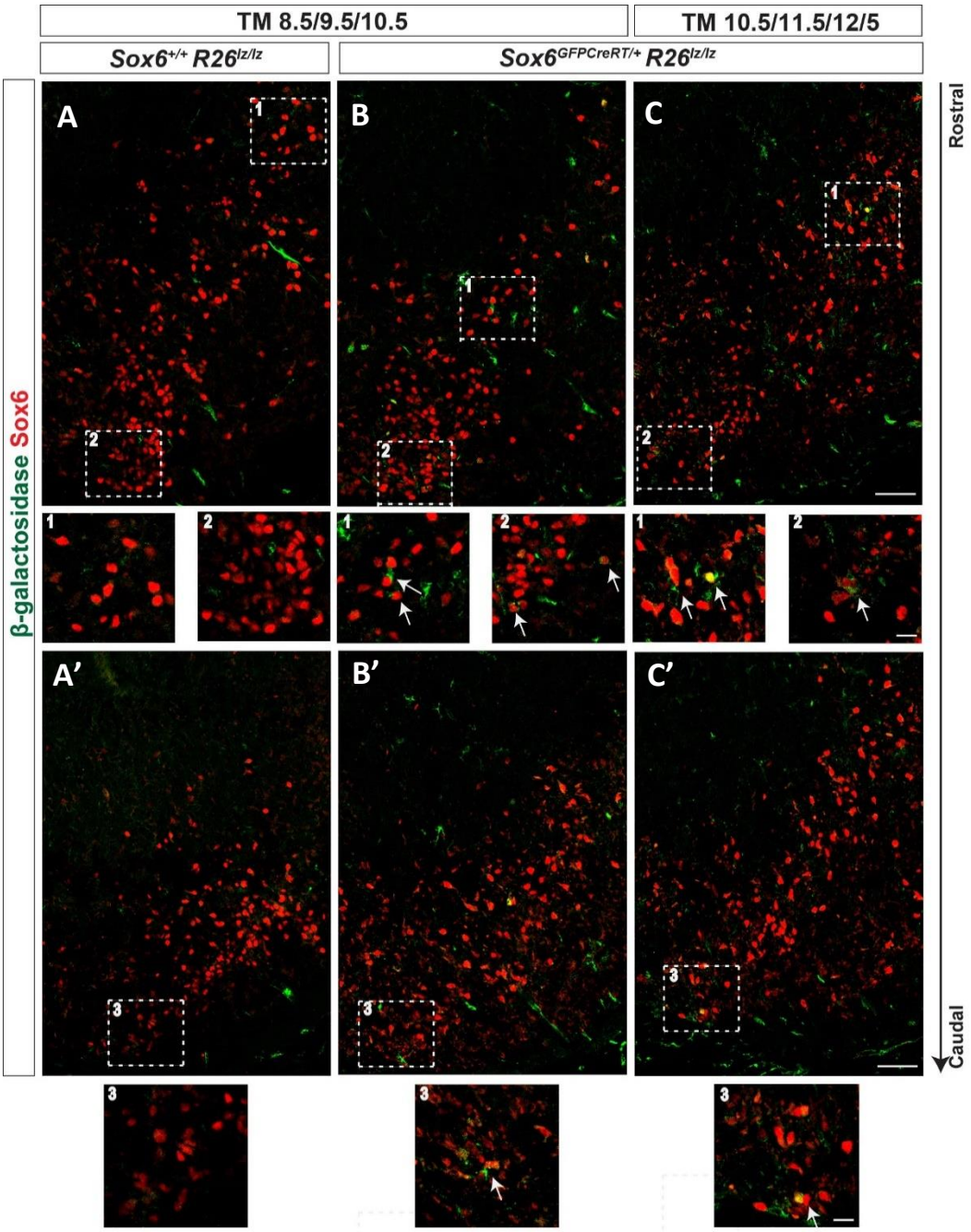

Figure 5.10 Detailed analysis of SNc mDA neurons coexpressing Sox6 and ß-galactosidase in the SNc of E18.5 mouse. (A, B, C, A',B' and C') Confocal micrographs of mouse SNc in the rostral midbrain section (A,B and C) and caudal midbrain section (A',B' and C'). (A and A') Sections were stained with anti-gß-gal and anti-gpSox6 antibodies in wild type (*Sox6*$^{+/+}$ *R26*$^{lz/lz}$) mouse exposed to tamoxifen at E8.5, E9.5 and E10.5 (TM E8.5/9.5/10.5). (B and B') Sections were stained with anti-gß-gal and anti-gpSox6 antibodies in *Sox6*$^{GFPCreT/+}$ *R26*$^{lz/lz}$ mouse exposed to tamoxifen at E8.5, E9.5 and E10.5 (TM E8.5/9.5/10.5). (C and C') Sections were stained with anti-gß-gal and anti-gpSox6 antibodies in *Sox6*$^{GFPCreT/+}$ *R26*$^{lz/lz}$ mouse exposed to tamoxifen at E10.5, E11.5 and E12.5 (TM E10.5/11.5/12.5). Zoom of the area defined with their corresponding numbered dashed square. Arrows point to TH^{+}/ß-gal^{+} neurons. (Scale bar: 100µm).

5.4 Investigation of marker expression in Sox6 knockout mice

As previously studied in Chapter 3, low Wnt signalling levels induced Sox6 and Corin expression. In this Chapter, the *Sox6*^{GFPCreT} mouse line was used to investigate the link between Wnt, Sox6 and Corin expression.

Former immunohistochemical analysis showed that Sox6 expression is impaired in *Sox6*$^{GFPCreT/GFPCreT}$ mice (see Figure 5.1). *In situ* hybridisation for *Corin* was done in progenitors of heterozygous (*Sox6*$^{GFPCreT/+}$) and mutant (*Sox6*$^{GFPCreT/GFPCreT}$) mice at E11.5. Results showed that no difference in *Corin* expression was observed when Sox6 expression was lost (Figure 5.11). Unfortunately, due to time constraints, *Axin2* expression, a downstream target of Wnt signalling whose levels are increased when the pathway is activated, could not be verified. This result suggests that *Corin* is not a downstream target of *Sox6*, as its expression pattern does not vary when *Sox6* expression is impaired.

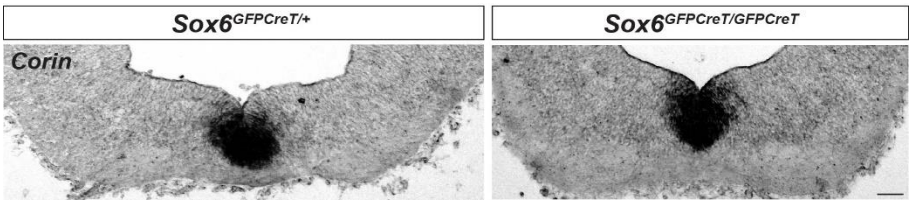

Figure 5.11 *Corin* gene expression is not changed when *Sox6* expression is lost. Bright field images of in-situ hybridisations for *Corin* performed in E11.5 mouse midbrain sections of heterozygous (*Sox6*$^{GFPCreT/+}$) and mutant (*Sox6*$^{GFPCreT/GFPCreT}$) mouse. (Scale bar: 200µm).

5.5 Discussion

In this Chapter, the *Sox6*^{GFPCreT} mouse line was characterised. As expected, GFP co-expressed with Sox6 in areas where this transcription factor was previously described to be expressed, such as the cortex and SNc mDA neurons. However, tracing of the Sox6^{+} mDA neuronal projections throughout GFP expression was not possible. This work also uncovered a population of GFP^{+}/TH^{-} cells in the caudal linear and interfascicular nucleus of the VTA, which could also be labelled by ß-galactosidase.

Interestingly, Cre-LoxP recombination appeared to be more efficient in the cortex and the cell population medially located in the VTA, than in the SNc mDA neurons,whereas ß-galactosidase was barely detected. Indeed, the efficiency of Cre-LoxP recombination *in vivo* mainly depends on three different parameters: the tamoxifen administration (which includes the dose and the route by which which it is administered), the level of Cre^{ERT2} expression and the chromatin structure and epigenetics of the floxed alleles (in this case of *LacZ*) (Jahn *et al.*, 2018). In the *Sox6*^{GFPCreT} line, tamoxifen administration was done via intraperitoneal injections, subcutaneous injections, and oral gavage. From all the methods of exposure, oral gavage offered the best results in this mouse line, as there were almost no miscarriages and the recombination was improved, particularly in the ventral midbrain. Changes in the concentration of tamoxifen did not seem to have an effect, however the recombination was more efficient when mice were exposed to tamoxifen for 3 days instead of 2 days. A difference in the levels of Cre^{ERT2} expression or in the chromatin structure and epigenetics of LacZ could explain the variation in ß-galactosidase expression in diverse areas of the brain (Soriano, 1999; Legue and Joyner, 2010). Indeed, GFP and Cre^{ERT} are under the control of the same *Sox6* promoter and GFP expression seems to be higher in the cortex and the cells located medially in the VTA than in SNc mDA neurons. This could suggest that Cre^{ERT} is more highly expressed in the cortex and the cells localised in the caudal linear and interfascicular nucleus of the VTA than in SNc mDA neurons, resulting in a better detection of ß-galactosidase in these regions of the brain. On the other hand, epigenetic modifications, and chromatin structure differences between SNc mDA neurons and the cortex or the VTA neuronal population could make the DNA containing Cre recognition sites in the SNc mDA

neurons less accessible, leading to almost no detection of ß-galactosidase in these neurons (Legue and Joyner, 2010).

The cell population identified in the caudal linear and interfascicular nucleus of the VTA, does not show Sox6 expression, but is GFP^+ and ß-galactosidase$^+$, suggesting that these cells are generated from the $Sox6^+$ progenitor domain and that they express Sox6 post-mitotically. It is possible that all the cell populations expressing Sox6 in the midbrain could not be identified using immunohistochemistry against Sox6. Moreover, it has been recently described that some mDA neurons located in the parabrachial pigmented nucleus of the VTA express Sox6, a subpopulation that has not been detected via immunohistochemistry (Poulin *et al.*, 2018). Due to time constraints, further analysis of this GFP^+/TH^- population could not be performed. Given that a big glutamatergic neuronal subpopulation medially located in the VTA is $Vglut2^+/TH^-$, it would be interesting to study Vglut2 expression in this cell subpopulation (Yamaguchi *et al.*, 2011; Morales and Margolis, 2017). Thus, if these cells would be $Vglut2^+$, the medial progenitor domain of the ventral midbrain expressing Sox6, would also be generating non dopaminergic glutamatergic neurons. This should not come as a surprise, as $Lmx1a^+$ mDA progenitors also give rise to non-dopaminergic neurons from the subthalamic nucleus lineage that express Vglut2 (Kee *et al.*, 2017).

The $Sox6^{GFPCreT}$ mouse line can also be used to identify possible Sox6 downstream targets in mutants having Sox6 impaired with the advantage that Sox6 expressing neurons can be traced throughout GFP expression. In this chapter *Corin* expression was analysed in the mDA progenitors of mutant E11.5 mice by in-situ hybridisation, but no change was observed when compared with the control. This could either be because *Corin* is not a downstream target of Sox6 or that Sox6 expression is compensated by its homologue Sox5, resulting in the unchanged *Corin* expression. Indeed, previous studies showed an expansion of Sox5 expression in cortical interneurons of $Sox6^{-/-}$ mice (Azim *et al.*, 2009). Therefore, Sox5 compensating for Sox6 expression and function in the midbrain, could be the reason why $Sox6^{GFPCreT/GFPCreT}$ and $Sox6^{-/-}$ mice do not present strong changes in the midbrain (Panman *et al.*, 2014). As previously mentioned, due to time constraints, Axin2, whose expression is induced following Wnt signalling activation,

could not be analysed. Nonetheless, if studied, its expression in *Sox6*$^{GFPCreT/GFPCreT}$ mice would likely remain unchanged since these mice do not present a strong phenotype.
It is difficult to conclude that Sox6 acts as an intrinsic determinant of SNc mDA neurons since the development of this neuronal population is not impaired in mice lacking Sox6 expression. Therefore, further analysis should be performed of Sox6 and Sox5 protein expression in order to understand the role that these TF play in the development of SNc mDA neurons.

Chapter 6

Discussion

Chapter 6 General discussion

6.1 Introduction

In this chapter I will discuss the implications of the results (Chapter 3, 4 and 5) on three important questions in the field: 1. Are protocols able to differentiate hESC into SNc mDA neurons? 2. What is the mechanism by which Wnt/ß-catenin signalling controls the development of SN and VTA mDA neurons? 3. Why is there selective vulnerability of different neuronal subpopulations in neurodegenerative diseases?

6.2 Mapping hESC-derived mDA neuronal subpopulations

Throughout the years, several protocols have been developed to differentiate hESC into mDA neurons. Protocols differentiating hESC into mDA neurons always start with the inhibition of the TGFβ signalling pathway mediators SMAD (required for the induction of the ectodermal fate through expression of BMP), promoting the development of the neuroectoderm. In addition, a strong activation of Shh and Wnt signalling is required However, platforms vary in the concentration of Wnt and Shh inductors they employ, the duration of Wnt and Shh activation and the starting day of the pathways activation (Kriks *et al.*, 2011; Kirkeby *et al.*, 2012; Kikuchi *et al.*, 2017; Nolbrant *et al.*, 2017).The platforms from Kriks et al., 2011, Kirkeby et al., 2012 and Nolbrant et al., 2017 have been the most successful protocols in generating functional hESC derived mDA neurons. The IWP2 platform developed in this thesis derives from the Kriks et al. protocol and the Nolbrant et al. protocol derives from the Kirkeby et al. system. To avoid the suppression of Shh signalling (Chung et al., 2009) and to allow the ventralisation of the cells, Wnt is induced two days later than Shh in the Kriks and the IWP2 protocols (Figure 6.1 A, B and C). In contrast, the Nolbrant and Kirkeby protocols differentiate mDA neurons by induction of Wnt and Shh signalling at the same time point. However, this system uses CHIR (a molecule that activates Wnt signalling) at lower concentrations (0.6µM-1µM) than the Kriks et al. protocol (3µM) (Kirkeby et al., 2012; Kriks et al., 2011). The use of concentrations higher than 1µM in the Nolbrant et al. protocol induces dorsal fate, contrary to the Kriks protocol where the midbrain fate is obtained. This could be

explained by the fact that Wnt signalling is activated too early. FGF8 is also added to caudalise the neurons and to obtain a midbrain rather than a forebrain fate (Figure 6.1 A and B) (Fasano *et al.*, 2010). Interestingly, the Nolbrant protocol adds FGF8 8 days later than all the other protocols including the IWP2 platform to generate caudal mDA neurons deriving from the caudal vMB progenitor domain. This platform is based on previous results, where the graft outcome was improved with hESC derived mDA neurons expressing caudal midbrain markers (Kirkeby *et al.*, 2017; Nolbrant *et al.*, 2017). In contrast, the IWP2 established platform, obtains more rostral mDA neuronal population derived from the rostro-medial vMB progenitor domain, because of neurons differentiated under low Shh (with the SAG) and low Wnt signalling levels (Figure 6.1 C).

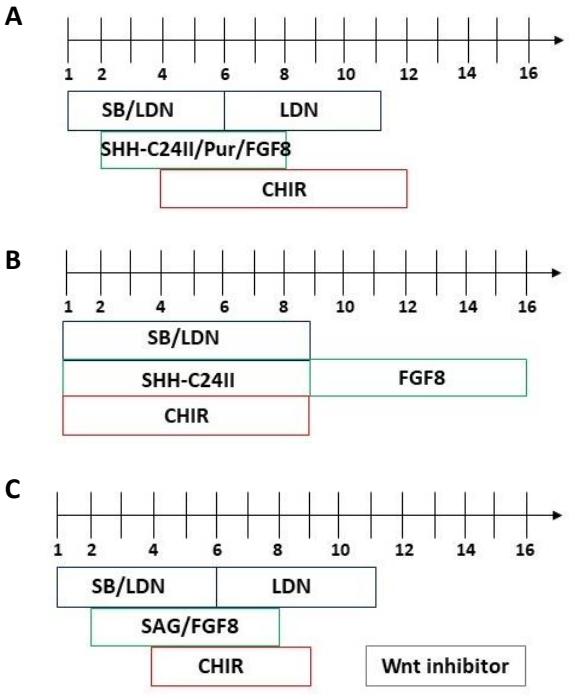

Figure 6.1 Diagrams illustrating the different protocols that differentiate hESC into mDA neurons. (A) Kriks et al., 2011 protocol. (B) Nolbrant et al., 2017 protocol. (C) IWP2 protocol. Note that the Wnt inhibitors used in this thesis are IWP2, XAV939, dkk1 and IWR1.

Platforms differentiating hESC into mDA neurons seek to obtain pure cultures of SNc mDA neurons so that they can be transplanted in PD patients having lost this neuronal population and improve motor impairments. Indeed, studies determined that SN neurons were crucial for motor impairment recovery in rats having a 6-OHDA-lesioned striatum. Transplantations in the lesioned striatum rats performed with vMB tissue

lacking SN (Pitx3 double mutants result in an absence of SN mDA neurons), resulted in grafts with a loss of $Girk2^+/Calb^-$ striatal projections. In addition, grafted rats with Pitx3 knockout tissue performed worse in motor function tests than the ones engrafted with Pitx3 heterozygous (Grealish *et al.*, 2010). Girk2 and Calbindin have been identified as SN and VTA mDA markers, respectively, and retrograde tracing in the dorso-lateral striatum labelled $Girk2^+/TH^+$ located in the periphery of the graft (Thompson *et al.*, 2005). Therefore, markers Girk2 and Calbindin are used to identify the identity of the transplanted hESC-derived mDA neurons in the lesioned striatum of rats (Kriks *et al.*, 2011; Kirkeby *et al.*, 2012; Kikuchi *et al.*, 2017; Nolbrant *et al.*, 2017). The mDA neurons generated with the Kriks, Kirkeby and Nolbrant protocol were engrafted successfully in the 6-OHDA-lesioned striatum of rats and their motor impairments were recovered as assessed by motor function tests. In addition, in the Kirkeby protocol amperometric measurements 18 weeks post-transplantation showed that neurons released dopamine and $Girk2^+/TH^+$ neurons were identified in the grafts of all the platforms (Table 6.1) (Kriks *et al.*, 2011; Kirkeby *et al.*, 2012; Nolbrant *et al.*, 2017). Although these neurons were successfully transplanted in the lesioned rat striatum and showed Girk2 expression, it is difficult to conclude that this neuronal population is SN. In fact, these protocols give rise to mDA neurons that are VTA-like (coexpressing OTX2 and TH). As previously mentioned, VTA mDA neurons show coexpression of OTX2 and TH in mouse and human brains (as observed in chapter 3) (Di Salvio *et al.*, 2010; Panman *et al.*, 2014; Poulin *et al.*, 2014; La Manno *et al.*, 2016). Moreover, the identity of grafted neurons depends on the environment where they are transplanted. For instance, peripheral neurons in the grafts tend to be $Girk2^+/TH^+$ and the ones in the core of the grafts are mainly $Calb^+/TH^+$. Although, the striatum tends to induce Girk2 expression in the periphery of the graft, when mDA neurons are transplanted in the nucleus accumbens, peripheral neurons from the graft are predominantly $Calb^+/TH^+$ (Fjodorova, Torres and Dunnett, 2017). Therefore, are these neurons expressing Girk2 or is it a consequence of the area of the striatum where they have been transplanted? Thus, it is necessary to further study the expression of other specific markers for SN and VTA mDA neurons. In fact, in human brain tissue Girk2 is expressed in all the SN mDA neurons (dorsal and ventral subpopulations) and strong Girk2 expression has also been detected in the

lateral VTA (adjacent to SN mDA neurons), a resistant neuronal subpopulation in PD patients (Reyes *et al.*, 2012). In contrast, in the IWP2 protocol, analysis of different markers (SATB1, SOX6, GIRK2 CALB and OTX2) was undertaken to identify the neuronal subpopulations obtained. One of the limitations of this protocol is that levels of mDA markers are decreased when compared with the other protocols (Table 6.1). In addition, although two different neuronal subpopulations are generated (SN-like $SATB1^+/SOX6^+/GIRK2^+/TH^+$ as well as a VTA-like $OTX2^+/CALBINDIN^+/TH^+$ sensitive and resistant to toxins, respectively), neuronal cultures are very heterogenous and $SOX6^+/TH^-$ neurons (data not shown) are obtained especially when exposed to high IWP2 concentrations. This could be the reason why, at early stages of transplantation studies there are too many proliferative cells in the grafts formed by IWP2 treated mDA neurons.

Protocol	Advantages	Limitations	Neuronal Subpopulation
Kriks et al., 2011 Kirkeby et al., 2012 Nolbrant et al., 2017	• Homogeneous population of mDA neurons • Recovery of motor impairments in mice with lesioned striatum	• No extensive marker analysis • VTA-like mDA neurons	• VTA-like ($OTX2^+/TH^+$)
IWP2 protocol	• 2 different neuronal mDA subpopulations: SN-like and VTA-like. • Selective vulnerability of the neuronal subpopulations.	• Heterogeneous neuronal culture. • Decreased levels of mDA markers when compared with the previous protocols.	• SN-like ($SATB1^+/SOX6^+/GIRK2/TH^+$) • VTA-like ($OTX2^+/CALB^+/TH^+$)

Table 6.1 Table comparing relevant protocols to differentiate hESC into mDA neurons with the IWP2 protocol.

As previously described in the introduction, molecular profiling mainly through RNA sequencing, of mDA neurons resulted in the identification and classification of new neuronal subpopulations in the SN and VTA (Poulin *et al.*, 2014, 2018; La Manno *et al.*, 2016; Tiklová *et al.*, 2019). The most vulnerable subpopulation of SNc mDA neurons (the ventral tier) in mouse and human expresses different markers such as SATB1, LMO3,

SOX6, ALDH1A1 and TH (Poulin *et al.*, 2014, 2018; Brichta *et al.*, 2015; La Manno *et al.*, 2016). Indeed, a similar phenotype has been observed in the stomach of mice, where SATB1 is also expressed in $SOX6^+/TH^+$ gastric neurons. Loss of SOX6 expression results in a decrease in the number of gastric TH^+ neurons and gastroparesis (reduction of gastric emptying), a phenomenon that has also been observed in PD patients (Memic *et al.*, 2018). In contrast, one of the resistant subpopulations in the mouse VTA shows expression of OTX2, ALDH1A1, CALBINDIN1 and TH (Poulin *et al.*, 2014, 2018; La Manno *et al.*, 2016). Even though further marker analysis should be done, the neuronal populations obtained in the published protocols can be classified as VTA-like. Similarly, $SOX6^+/TH^+$ and $OTX2^+/TH^+$ neuronal populations obtained in the IWP2 protocol can be classified as SNc-like and VTA-like, respectively.

A recent pre-clinical study, which has been approved for clinical trials in PD patients, on iPSC-derived mDA neurons was performed in mice and monkeys. Transplantations were successful in the lesioned striatum of these animals and safety analysis (epigenetic, toxicity, tumorgenicity) was extensively performed. However, no studies *in vitro* of the molecular identity of mature neurons or on the transplanted neurons appeared in the publication (Doi *et al.*, 2020). What is the fate of these neurons? Will this affect their projections and outcome in human brains? Given that human brain is more complex than rodent or primate brain, maybe an extensive study on the identity of mature neurons should also be performed before moving to the next step.

The knowledge of the mechanisms involved in the development of mDA neurons has grown enormously in the last few years. However, the role that signalling pathways and epigenetics play in mDA development is still poorly understood.

6.3 Role of Wnt signalling in the development of SNc mDA neurons: a possible mechanism

Wnt/ß-catenin is one of the most important signalling pathways involved in the development of mDA neurons, yet the mechanism is still unknown. As previously described, a hypothesis is that Wnt signalling is involved in the determination of the SN and VTA mDA fate. In mouse, Wnt/ß-catenin pathway is activated in the ventral-lateral mDA progenitor domain which will generate VTA mDA neurons, while it is repressed in the ventral-medial mDA progenitor domain which will give rise to SN mDA neurons. In addition, the investigations in this thesis of the *Sox6*$^{eGFP\text{-}Cre\text{-}ERT2}$ mouse line (chapter 5) suggest that the ventral-medial mDA progenitor domain gives rise to a subpopulation of Sox6^{+} neurons located medially in the VTA and that do not express TH. In this point of the discussion, I will propose a mechanism that could be used to explain the development of the two subpopulations of midbrain Sox6^{+} neurons located in the SNc and the medial VTA that have been described in chapter 5.

This research suggests that Wnt signalling inhibition induces SOX6 and CORIN expression in hESC-derived mDA progenitors. In the differentiation protocol different Wnt inhibitors were used and showed different efficiencies. Interestingly, inhibitors that suppressed Wnt/ß-catenin and non Wnt/ß-catenin pathways (IWP2 and DKK1) were more effective in comparison to the Wnt/ß-catenin tankyrase inhibitors such as XAV939 and IWR1 (which almost had no effect). This supports the fact that Wnt/ß-catenin and non Wnt/ß-catenin are involved in the development of mDA neurons as previously described (Andersson *et al.*, 2008, 2013). In addition, it suggests that Sox6 and Corin expression are controlled by both pathways. Indeed, DKK1 acts via the Wnt/PCP-Rac pathway, the one identified in the development of mDA neurons (Andersson *et al.*, 2008, 2013; Cha *et al.*, 2008).

Although, this thesis has not investigated the mechanism by which Wnt signalling repression induces Sox6 and Corin expression, a possible model explaining how Wnt defines the two different progenitor domains can be deduced from the results and published data (Figure 6.2). The fact that Corin and Sox6 coexpress in the medial mDA progenitor domain, that their expression is increased when Wnt signalling is inhibited

and that Corin expression is not modified in Sox6 knockout mice, indicates that Wnt signalling could act via Corin to control Sox6 expression. Even though no publications demonstrated a direct interaction of Corin and Wnt proteins, Corin is a transmembrane protein that contains two Frizzled-like CRD domains (Yan *et al.*, 1999). This suggests that Corin could interact with Wnts throughout the CRD domains. In the lateral vMB dopaminergic progenitor domain, an area with no Corin expression and giving rise to VTA mDA neurons, Wnt/ß-catenin would be activated by Wnt signalling at the correct developmental stage. This would result in the expression of Otx2 and subsequent repression of Sox6 (Chung *et al.*, 2009; Panman *et al.*, 2014). In the medial vMB dopaminergic progenitor domain, an area with Corin expression and giving rise to SNc mDA neurons, interaction of Wnt with Corin could result in the inhibition of the Wnt/ß-catenin pathway promoting Sox6 and downregulating Otx2 expression. In turn, Sox6 could inhibit ß-catenin as *in vitro* studies demonstrated that Sox6 represses ß-catenin expression by physically interacting with it (Figure 6.2 (Iguchi *et al.*, 2007).

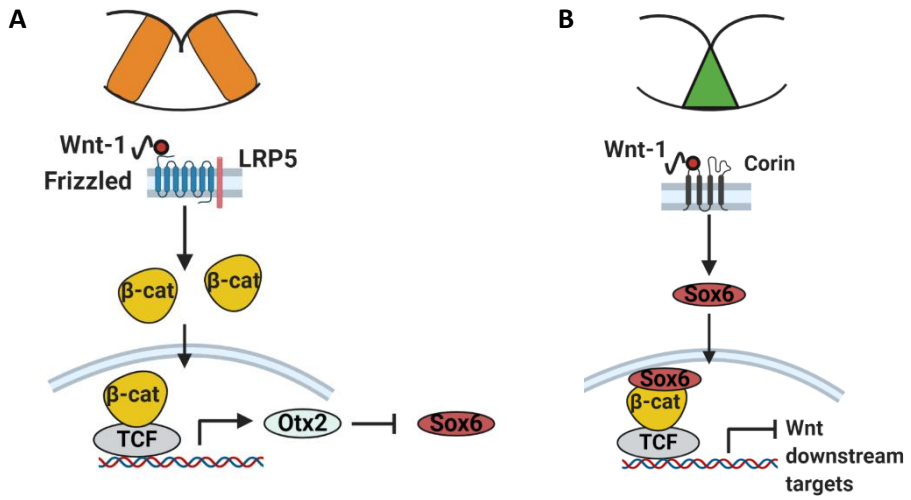

Figure 6.2 Diagram illustrating a possible Wnt/ß-catenin mechanism for the determination of the SN and VTA mDA fate. (A) In the ventral-lateral mDA progenitor domain Wnt/ß-catenin pathway is activated and Otx2 is expressed. (B) In the ventral-medial mDA progenitor domain Wnt-1 recognises Corin, Sox6 is induced and in turn represses Wnt signalling by binding to ß-catenin. Orange bands and the green triangle represent the ventral-lateral and the ventral-medial mDA progenitor domains, respectively. ß-catenin (ß-cat).

Results in chapter 4 suggest that hESC derived $Sox6^+/TH^+$ mDA neurons (SNc-like), derived from the ventral-medial mDA progenitor domain, are more sensitive to MPP^+ or

Rotenone than the $Otx2^+/TH^+$ (VTA-like), derived from the ventral-lateral mDA progenitor domain. The selective vulnerability of SNc mDA neurons cause the motor impairments observed in PD patients, however the reasons behind this phenomenon are still unknown. Thus, a better understanding of the mechanisms that orchestrate the development of mDA neurons is key to decipher the determinants involved in the selective vulnerability of neuronal subpopulations.

6.4 Why is there selective vulnerability of different neuronal subpopulations in neurodegenerative diseases?

As previously described, PD patients present motor impairments due to the degeneration of SNc mDA neurons. Although VTA mDA neurons are developmentally related to SNc mDA neurons, they remain relatively spared until the late stages of the disease. Indeed, selective neuronal vulnerability is not a unique characteristic of PD. It is a common feature in diverse late age onset neurodegenerative disorders such as Alzheimer's disease (AD), Amyotrophic lateral sclerosis (ALS) or Huntington's disease (HD). The reason behind why some neuronal populations are more prone to degenerate in the different diseases is still unknown.

Energy demand, Ca^{2+} homeostasis and differences in the unfolded protein response (UPR) pathway are shared mechanisms identified in these neuronal populations that can explain their vulnerability. This suggests that common pathways are involved in the selective vulnerability of diverse neuronal subpopulations in neurodegenerative diseases. Indeed, TFs involved in the development of these neurons could be key in the regulation of these pathways. Some hypothesis state that vulnerable neuronal populations possess long axonal arborisations and have high energy demands making them more susceptible to mitochondrial stress such as SNc mDA neurons. (Pacelli *et al.*, 2015). Similarly, a bioinformatic model proposed that the higher the energy needed for a neuronal subpopulation, the more vulnerable this population will be. It predicts that, fast fatigable (FF) motor neurons, the vulnerable neuronal subpopulation in ALS, consumes a significantly higher quantity of ATP than the slow (S) motor neurons, a population that is relatively spared in the late stages of ALS. In fact, FF motor neurons

present a bigger soma, bigger axon size and have more neuromuscular terminals than S motor neurons (LeMasson, Przedborski and Abbott, 2014). Accumulation of intracellular Ca^{2+} is associated with the vulnerability of neuronal subpopulations. SNc mDA neurons are autonomous pacemakers dependent on Ca_v1-Ca^{2+} channels displaying high intracellular Ca^{2+} oscillations (Chan *et al.*, 2007). Once in the cytoplasm Ca^{2+} can easily interact with other proteins enhancing mitochondrial stress since their Ca^{2+} buffer capacity is minimal (Foehring *et al.*, 2009; Guzman *et al.*, 2009, 2010). Indeed, SNc mDA neurons present low levels of Ca^{2+} buffer proteins like Calbindin 1, which is highly present in the resistant VTA mDA neurons (Poulin *et al.*, 2018). Similarly, the hippocampal neuronal subpopulation CA1 and the layer II of the entorhinal cortex neurons degenerate in AD. *In vitro* data suggests that human foetal cortical neurons exposed to ß-amyloid peptides, displayed neurotoxicity dependent on calcium (Mattson *et al.*, 1992). In mice developing age related accumulation of ß-amyloid peptide the detection of an increase in the numbers of Ca_v1-Ca^{2+} channels over time in the vulnerable CA1 but not in the resistant CA3 hippocampal neuronal subpopulation was detected (Wang and Mattson, 2014). UPR signalling activation can have a damaging or a beneficial effect depending on the disease or the neuronal population. In $SOD1^{G93A}$ ALS mouse models, the ER cochaperone SIL1 expression was low in the vulnerable FF motor neurons and high in the resistant S motor neurons. Its overexpression reduced cellular stress, while its loss accelerated ER stress (Filézac De L'Etang *et al.*, 2015). Likewise, mass spectrometry data (chapter 4) detected that the expression of the chaperone HSPA5 was higher in SOX6 (vulnerable) overexpressed neurons than in OTX2 overexpressed neurons (resistant). The vulnerability or resistance of neuronal subpopulations in different neurodegenerative diseases results from a combination of multiple aspects (metabolism, protein expression, signalling pathways). TF involved in the determination of neuronal fate play a crucial role in the definition of a neuronal subpopulation. For instance, SOX6 and OTX2 could regulate pathways and the expression of proteins leading to the generation of vulnerable and resistant mDA neurons, respectively. SOX6 could downregulate the expression of the chaperone HSPA5, as its levels were also downregulated in SOX6 overexpressed erythroid cells (Barbarani *et al.*, 2017). In addition, L-SOX6 transfected neurons had enrichment of the

glycolysis pathway when compared with the L-OTX2 transfected neurons. Given that OTX2 can regulate certain glycolytic enzymes through its binding, this TF could also downregulate proteins involved in glycolysis leading to neurons less glycolytically active (Lu *et al.*, 2017). Other TF involved in the development of motor neurons or pyramidal neurons in the hippocampus have been identified. For example, the expression of the TF factor Phoxa2 was sufficient to generate mouse ESC derived oculomotor neurons, a resistant subpopulation in ALS, that were highly resilient to ALS-like excitotoxicity with high levels of Ca^{2+} buffering proteins (Allodi *et al.*, 2019). In addition, the TF factor Zbtb20 was identified as being key for the development of mouse CA1 pyramidal neurons (vulnerable in AD). Loss of Zbtb20 resulted in the reduction of the levels of CA1 markers (Xie *et al.*, 2010). Thus, further analysis of the mechanisms employed by TFs involved in fate determination of neuronal subpopulations would help to understand why they degenerate and to explore possible new therapeutic avenues for neurodegenerative diseases.

6.5 Conclusions

In conclusion this thesis demonstrates that:

1. A hESC platform that generates different mDA neuronal subpopulations can be established. This suggests that more extensive analysis of the identity of the hESC-derived mDA neuronal subpopulations generated in the published protocols is required to claim that they are SNc mDA neurons.
2. Wnt signalling could induce SNc mDA neuronal fate and the development of a subpopulation of $SOX6^{+}$ neurons located medially in the VTA through the induction of SOX6 and CORIN expression.
3. SOX6 and OTX2 could play a role in the vulnerability and resistant of SNc and VTA mDA neurons, respectively, by regulating the UPR pathway.

6.6 Future work

There are two important points in this thesis that should be further explored. Firstly, the mechanism by which Wnt signalling induces Sox6 and Corin expression. Secondly, a

better study of the identity of $SOX6^+/TH^+$ and $OTX2^+/TH^+$ neuronal subpopulations should be performed.

In the section 6.3 of the discussion chapter, a model to understand the mechanism by which Wnt signalling induces Corin and Sox6 expression has been proposed. In this model, Corin induces Sox6 expression and functions as a receptor for Wnt signalling. In turn, Sox6 interacts with ß-catenin inhibiting Wnt signalling downstream targets. To validate this hypothesis the expression of Sox6 should be studied in $Corin^{-/-}$ E11.5 mice with in-situ hybridisation and immunohistochemistry. Thus, if Corin activates Sox6 expression, no detection of Sox6 or reduction of Sox6 levels in the ventral-medial progenitor domain of the midbrain should be expected. Similarly, if Corin inhibits Wnt signalling throughout Sox6 expression, expression of Wnt signalling downstream targets such as Axin2 should be detected in the medial progenitor domain of the vMB in Corin knockout mice. This would indicate that loss of Corin expression results in the loss or reduction of Sox6 levels and subsequently in the expansion of Wnt signalling from the lateral progenitor domain to the medial progenitor domain in the vMB. Otx2 expression would also probably expand to the medial progenitor domain of the vMB.

The Wnt signalling established protocol, gave rise to a heterogeneous neuronal population with a percentage of them being $SOX6^+/TH^+$ and $OTX2^+/TH^+$. The identity of these populations was studied by immunocytochemistry and qPCR. Therefore, RNA single cell sequencing would be the best option to further identify these neuronal subpopulations. RNA single cell sequencing would be performed at the progenitor stage (day 13) and in mature neurons (day 35) of the CHIR, control and IWP2 conditions. With this technique we would be able to identify whether all the $SOX6^+/TH^+$ and $OTX2^+/TH^+$ are the same neuronal subpopulation or they express different markers. What would be expected is that the $SOX6^+/TH^+$ would be SN-like ($SATB1^+$, $GIRK2^+$ and $CALB1^-$ among other markers) while the $OTX2^+/TH^+$ would be VTA-like ($CALB^+$ in addition to other markers). Also, other neuronal populations would be detected such as the $SOX6^+/TH^-$ cells that are generated in some cultures. Overall, neurons in the CHIR and control conditions would be mainly VTA-like, while neurons in the IWP2 conditions would contain more diverse neuronal populations with a percentage of them being SN-like.

Appendix

Appendix Full size western blots analyses in lentiviral transduced neurons.

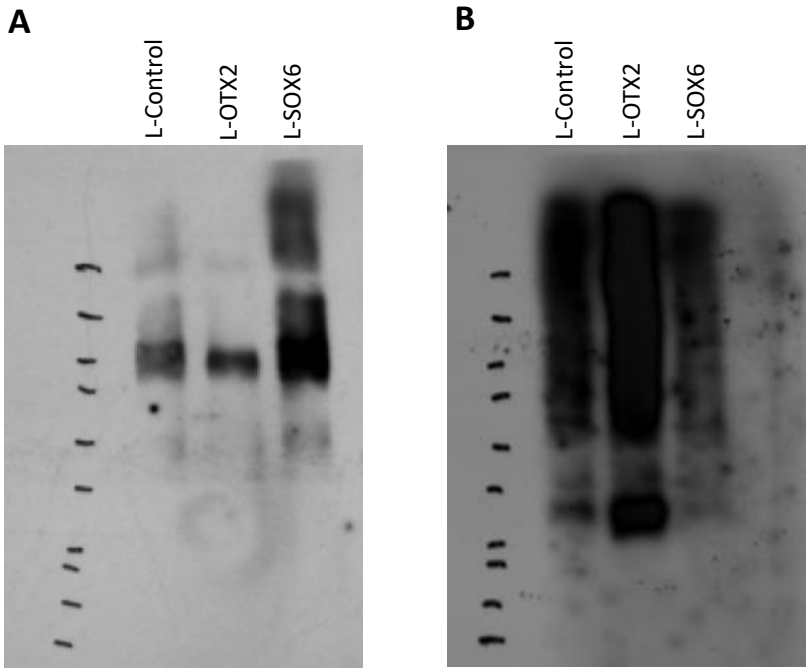

Figure appendix 1 Full-size western blot analyses of SOX6 and OTX2 expression in hESC-derived mDA lentiviral transduced neurons at day 35. (A) Western blot analysis of SOX6 in hESC-derived mDA neurons transduced with L-control, L-OTX2 and L-SOX6. (B) Western blot analysis of OTX2 in hESC-derived mDA neurons transduced with L-control, L-OTX2 and L-SOX6.

References

Albéri, L., Sgadò, P. and Simon, H. H. (2004) 'Engrailed genes are cell-autonomously required to prevent apoptosis in mesencephalic dopaminergic neurons', *Development*, 131(13), pp. 3229–3236. doi: 10.1242/dev.01128.

Allodi, I. *et al.* (2019) 'Modeling motor neuron resilience in ALS using sStem cells', *Stem Cell Reports*. ElsevierCompany., 12(6), pp. 1329–1341. doi: 10.1016/j.stemcr.2019.04.009.

Amit, S. *et al.* (2002) 'Axin-mediated CKI phosphorylation of beta-catenin at Ser45: a molecular switch for the Wnt pathway', *Genes and Development*, 16, pp. 1066–1076. doi: 10.1101/gad.230302.somal.

Anderegg, A. *et al.* (2013) 'An Lmx1b-miR135a2 regulatory circuit modulates Wnt1/Wnt signaling and determines the size of the midbrain dopaminergic progenitor pool', *PLoS Genetics*, 9(12), pp. 1–22. doi: 10.1371/journal.pgen.1003973.

Andersson, E. *et al.* (2006) 'Development of the mesencephalic dopaminergic neuron system is compromised in the absence of neurogenin 2', *Development*, 133(3), pp. 507–516. doi: 10.1242/dev.02224.

Andersson, Elisabet *et al.* (2006) 'Identification of intrinsic determinants of midbrain dopamine neurons', *Cell*, 124(2), pp. 393–405. doi: 10.1016/j.cell.2005.10.037.

Andersson, E. R. *et al.* (2008) 'Wnt5a regulates ventral midbrain morphogenesis and the development of A9-A10 dopaminergic cells in vivo', *PLoS ONE*, 3(10), pp. 1–14. doi: 10.1371/journal.pone.0003517.

Andersson, E. R. *et al.* (2013) 'Wnt5a cooperates with canonical Wnts to generate midbrain dopaminergic neurons in vivo and in stem cells', *Proceedings of the National Academy of Sciences of the United States of America*, 110(7), pp. 602–610. doi: 10.1073/pnas.1208524110.

Azim, E. *et al.* (2009) 'SOX6 controls dorsal progenitor identity and interneuron diversity during neocortical development', *Nature Neuroscience*. Nature Publishing Group, 12(10), pp. 1238–1247. doi: 10.1038/nn.2387.

Bachiller, D. *et al.* (2000) 'The organizer factors Chordin and Noggin are required for mouse forebrain development', *Nature*, 403(6770), pp. 658–661. doi: 10.1038/35001072.

Bafico, A. *et al.* (2001) 'Novel mechanism of Wnt signalling inhibition mediated by Dickkopf-1 interaction with LRP6/Arrow', *Nature Cell Biology*, 3(7), pp. 683–686. doi: 10.1038/35083081.

Blaess, S. *et al.* (2011) 'Temporal-spatial changes in Sonic Hedgehog expression and signaling reveal different potentials of ventral mesencephalic progenitors to populate distinct ventral midbrain nuclei', *Neural Development*, 6(1). doi: 10.1186/1749-8104-6-29.

Barbarani, G. *et al.* (2017) 'Unravelling pathways downstream Sox6 induction in K562 erythroid cells by proteomic analysis', *Scientific Reports*, 7(14088), pp. 1–13. doi: 10.1038/s41598-017-14336-6.

Barres, B. A. (2008) 'The mystery and magic of glia: a perspective on their roles in health and disease', *Neuron*. Elsevier Inc., 60(3), pp. 430–440. doi: 10.1016/j.neuron.2008.10.013.

Batista-Brito, R. *et al.* (2009) 'The Cell-Intrinsic Requirement of Sox6 for Cortical Interneuron Development', *Neuron*, 63(4), pp. 466–481. doi: 10.1016/j.neuron.2009.08.005.

Bentivoglio, M. and Morelli, M. (2005) 'The organization and circuits of mesencephalic dopaminergic neurons and the distribution of dopamine receptors in the brain', in Dunnett, S. B. et al. (eds) *Handbook of Chemical Neuroanatomy*, pp. 1–107. doi: 10.1016/S0924-8196(05)80005-3.

Bertler, Å. and Rosengren, E. (1959) 'Occurrence and distribution of dopamine in brain and other tissues', *Experientia*, 15(1), pp. 10–11. doi: 10.1007/BF02157069.

Bertocchini, F. and Stern, C. D. (2002) 'The hypoblast of the chick embryo positions the primitive streak by antagonizing nodal signaling', *Developmental Cell*, 3(5), pp. 735–744. doi: 10.1016/S1534-5807(02)00318-0.

Betarbet, R. *et al.* (2000) 'Chronic systemic pesticide exposure reproduces features of Parkinson's disease', *Nature Neuroscience*, 3(12), pp. 1301–1306. doi: 10.1038/81834.

Bhanot, P. *et al.* (1996) 'A new member of the frizzled family from Drosophila functions as a Wingless receptor identified . We show here that cultured Drosophila cells transfected with a novel member of the', *Nature*, 382, pp. 225–230.

Bitgood, M. J., Shen, L. and McMahon, A. P. (1996) 'Sertoli cell signaling by Desert hedgehog regulates the male germline', *Current Biology*, 6(3), pp. 298–304. doi: 10.1016/S0960-9822(02)00480-3.

Bonilla, S. *et al.* (2008) 'Identification of midbrain floor plate radial glia-like cells as dopaminergic progenitors', *Glia*, 56(8), pp. 809–820. doi: 10.1002/glia.20654.

Bowles, J., Schepers, G. and Koopman, P. (2000) 'Phylogeny of the SOX family of developmental transcription factors based on sequence and structural indicators', *Developmental Biology*, 227(2), pp. 239–255. doi: 10.1006/dbio.2000.9883.

Braak, H., Rüb, U., *et al.* (2003) 'Idiopathic Parkinson's disease: possible routes by which vulnerable neuronal types may be subject to neuroinvasion by an unknown pathogen', *Journal of Neural Transmission*, 110(5), pp. 517–536. doi: 10.1007/s00702-002-0808-2.

Braak, H., Del Tredici, K., *et al.* (2003) 'Staging of brain pathology related to sporadic Parkinson's disease', *Neurobiology of Aging*, 24(2), pp. 197–211. doi: 10.1016/S0197-4580(02)00065-9.

Brichta, L. *et al.* (2015) 'Identification of neurodegenerative factors using translatome-regulatory network analysis', *Nature Neuroscience*, 18(9), pp. 1325–1333. doi: 10.1038/nn.4070.

Broccoli, V., Boncinelli, E. and Wurst, W. (1999) 'The caudal limit of Otx2 expression positions the isthmic organizer', *Nature*, 401(6749), pp. 164–168. doi: 10.1038/43670.

Brons, I. G. M. *et al.* (2007) 'Derivation of pluripotent epiblast stem cells from mammalian embryos', *Nature*, 448(7150), pp. 191–195. doi: 10.1038/nature05950.

Cajanek, L. *et al.* (2013) 'Tiam1 regulates the Wnt/Dvl/Rac1 signaling pathway and the differentiation of midbrain dopaminergic neurons', *Molecular and Cellular Biology*, 33(1), pp. 59–70. doi: 10.1128/mcb.00745-12.

Carlsson, A. and Waldeck, B. (1958) 'A fluorimetric method for the determination of dopamine (3-Hydroxytyramine.)', *Acta Physiologica Scandinavica*, 44, pp. 293–298.

Caspary, T., Larkins, C. E. and Anderson, K. V. (2007) 'The Graded Response to Sonic Hedgehog Depends on Cilia Architecture', *Developmental Cell*, 12(5), pp. 767–778. doi: 10.1016/j.devcel.2007.03.004.

Castelo-Branco, G. *et al.* (2003) 'Differential regulation of midbrain dopaminergic neuron development by Wnt-1, Wnt-3a, and Wnt-5a', *Proceedings of the National Academy of Sciences of the United States of America*, 100(22), pp. 12747–12752. doi: 10.1073/pnas.1534900100.

Cavallo, R. A. *et al.* (1998) 'Drosophila Tcf and Groucho interact to repress Wingless signalling activity', *Nature*, 395, pp. 604–608. doi: 10.1038/255242a0.

Cha, S. W. *et al.* (2008) 'Wnt5a and Wnt11 interact in a maternal Dkk1-regulated fashion to activate both canonical and non-canonical signaling in Xenopus axis formation', *Development*, 135(22), pp. 3719–3729. doi: 10.1242/dev.029025.

Chamoun, Z. *et al.* (2001) 'Skinny Hedgehog, an Acyltransferase required for palmitoylation and activity of the Hedgehog signal', *Science*, 293(5537), pp. 2080–2084.

Chan, C. S. *et al.* (2007) '"Rejuvenation" protects neurons in mouse models of Parkinson's disease', *Nature*, 447(7148), pp. 1081–1086. doi: 10.1038/nature05865.

Chartier-Harlin, M. C. *et al.* (2004) 'α-synuclein locus duplication as a cause of familial Parkinson's disease', *Lancet*, 364(9440), pp. 1167–1169. doi: 10.1016/S0140-6736(04)17103-1.

Chen, B. *et al.* (2009) 'Small molecule-mediated disruption of Wnt-dependent signaling in tissue regeneration and cancer', *Nature Chemical Biology*, 5(2), pp. 100–107. doi: 10.1038/nchembio.137.Small.

Chen, X. *et al.* (2011) 'Processing and turnover of the Hedgehog protein in the endoplasmic reticulum', *Journal of Cell Biology*, 192(5), pp. 825–838. doi: 10.1083/jcb.201008090.

Chen, G. *et al.* (2011) 'Chemically defined conditions for human iPSC derivation and culture', *Nature Methods*, 8(5), pp. 424–429. doi: 10.1038/nmeth.1593.

Chi, C. L. *et al.* (2003) 'The isthmic organizer signal FGF8 is required for cell survival in the prospective midbrain and cerebellum', *Development*, 130(12), pp. 2633–2644. doi: 10.1242/dev.00487.

Chung, C. Y. *et al.* (2005) 'Cell type-specific gene expression of midbrain dopaminergic neurons reveals molecules involved in their vulnerability and protection', *Hum Mol Genet.*, 14(13), pp. 1709–1725. doi: 10.1093/hmg/ddi178.Cell.

Chung, S., Leung, A., Han, B., *et al.* (2009) 'Wnt1-lmx1a forms a novel autoregulatory loop and controls midbrain dopaminergic differentiation synergistically with the SHH-FOXA2 pathway', *Cell Stem Cell*, 5(6), pp. 646–658. doi: 10.1016/j.stem.2009.09.015.Wnt1-lmx1a.

Dahlstrom, A. and Fuxe, K. (1965) 'Evidence for the existence of monoamine-containing neurons in the central nervous system', *Acta Physiologica Scandinavica*, 62(232), pp. 5–52.

Dai, P. *et al.* (1999) 'Sonic hedgehog-induced activation of the Gli1 promoter is mediated by GLI3', *Journal of Biological Chemistry*, 274(12), pp. 8143–8152. doi: 10.1074/jbc.274.12.8143.

Daniels, D. L. and Weis, W. I. (2005) 'β-catenin directly displaces Groucho/TLE repressors from Tcf/Lef in Wnt-mediated transcription activation', *Nature Structural and Molecular Biology*, 12(4), pp. 364–371. doi: 10.1038/nsmb912.

Deutch, A. Y. *et al.* (1988) 'Telencephalic Projections of the A8 Dopamine Cell Group', *Annals of the New York Academy of Sciences*, 537(1), pp. 27–50. doi: 10.1111/j.1749-6632.1988.tb42095.x.

Devine, M. J. *et al.* (2011) 'Parkinson's disease induced pluripotent stem cells with triplication of the α-synuclein locus', *Nature Communications*. Nature Publishing Group, 2(1), pp. 410–440. doi: 10.1038/ncomms1453.

Ding, S., Wei, W. and Zhou, F. M. (2011) 'Molecular and functional differences in voltage-activated sodium currents between GABA projection neurons and dopamine neurons in the substantia nigra', *Journal of Neurophysiology*, 106(6), pp. 3019–3034. doi: 10.1152/jn.00305.2011.

Di Salvio, M. *et al.* (2010) 'Otx2 controls neuron subtype identity in ventral tegmental area and antagonizes vulnerability to MPTP', *Nature Neuroscience*. Nature Publishing Group, 13(12), pp. 1481–1489. doi: 10.1038/nn.2661.

Doi, D. *et al.* (2020) 'Pre-clinical study of induced pluripotent stem cell-derived dopaminergic progenitor cells for Parkinson's disease', *Nature Communications*. Springer US, 11(1). doi: 10.1038/s41467-020-17165-w.

Echelard, Y. *et al.* (1993) 'Sonic hedgehog, a member of a family of putative signaling molecules, is implicated in the regulation of CNS polarity', *Cell*, 75(7), pp. 1417–1430. doi: 10.1016/0092-8674(93)90627-3.

Falck, B. *et al.* (1962) 'Fluorescence of Catechol Amines and Related Compounds Condensed With Formaldehyde', *Journal of Histochemistry & Cytochemistry*, 10(3), pp. 348–354. doi: 10.1177/10.3.348.

Fasano, C. A. *et al.* (2010) 'Efficient derivation of functional floor plate tissue from human embryonic stem cells', *Cell Stem Cell*, 6(4), pp. 336–347. doi: 10.1016/j.stem.2010.03.001.

Fedi, P. *et al.* (1999) 'Isolation and biochemical characterization of the human Dkk-1 homologue, a novel inhibitor of mammalian Wnt signaling', *Journal of Biological Chemistry*, 274(27), pp. 19465–19472. doi: 10.1074/jbc.274.27.19465.

Filézac De L'Etang, A. *et al.* (2015) 'Marinesco-Sjögren syndrome protein SIL1 regulates motor neuron subtype-selective ER stress in ALS', *Nature Neuroscience*, 18(2), pp. 227–238. doi: 10.1038/nn.3903.

Fjodorova, M., Torres, E. M. and Dunnett, S. B. (2017) 'Transplantation site influences the phenotypic differentiation of dopamine neurons in ventral mesencephalic grafts in Parkinsonian rats', *Experimental Neurology*. The Authors, 291, pp. 8–19. doi: 10.1016/j.expneurol.2017.01.010.

Foehring, R. C. *et al.* (2009) 'Endogenous calcium buffering capacity of substantia nigral dopamine neurons', *Journal of Neurophysiology*, 102(4), pp. 2326–2333. doi: 10.1152/jn.00038.2009.

Freeman, T. B. *et al.* (1991) 'Development of dopaminergic neurons in the human substantia nigra', *Experimental Neurology*, 113(3), pp. 344–353. doi: 10.1016/0014-4886(91)90025-8.

Friling, S. *et al.* (2009) 'Efficient production of mesencephalic dopamine neurons by Lmxla expression in embryonic stem cells', *Proceedings of the National Academy of Sciences of the United States of America*, 106(18), pp. 7613–7618. doi: 10.1073/pnas.0902396106.

Gasbarri, A. *et al.* (1996) 'The projections of the retrorubral field A8 to the hippocampal formation in the rat', *Experimental Brain Research*, 112(2), pp. 244–252. doi: 10.1007/BF00227643.

Gilbert, S. F. and Barresi, M. J. (2016) 'Birds and mammals', in *Developmental Biology*. 11th edn. Sinauer associates, pp. 391–401.

Glinka, A. *et al.* (1998) 'Dickkopf-1 is a member of a new family of secreted proteins and functions in head induction', *Nature*, 391(6665), pp. 357–362. doi: 10.1038/34848.

Goldstein, B. *et al.* (2006) 'Wnt signals can function as positional cues in establishing cell polarity', *Developmental Cell*, 10(3), pp. 391–396. doi: 10.1016/j.devcel.2005.12.016.

González-Hernández, T. and Rodríguez, M. (2000) 'Compartmental organization and chemical profile of dopaminergic and GABAergic neurons in the substantia nigra of the rat', *Journal of Comparative Neurology*, 421(1), pp. 107–135. doi: 10.1002/(SICI)1096-9861(20000522)421:1<107::AID-CNE7>3.0.CO;2-F.

Grealish, S. *et al.* (2010) 'The A9 dopamine neuron component in grafts of ventral mesencephalon is an important determinant for recovery of motor function in a rat model of Parkinson's disease', *Brain*, 133(2), pp. 482–495. doi: 10.1093/brain/awp328.

Greene, J. G., Dingledine, R. and Greenamyre, J. T. (2005) 'Gene expression profiling of rat midbrain dopamine neurons: Implications for selective vulnerability in parkinsonism', *Neurobiology of Disease*, 18(1), pp. 19–31. doi: 10.1016/j.nbd.2004.10.003.

Gross, J. C. *et al.* (2012) 'Active Wnt proteins are secreted on exosomes', *Nature Cell Biology*. Nature Publishing Group, 14(10), pp. 1036–1045. doi: 10.1038/ncb2574.

Habas, R., Kato, Y. and He, X. (2001) 'Wnt/Frizzled activation of Rho regulates vertebrate gastrulation and requires a novel formin homology protein Daam1', *Cell*, 107(7), pp. 843–854. doi: 10.1016/S0092-8674(01)00614-6.

Hagell, P. *et al.* (2002) 'Dyskinesias following neural transplantation in parkinson's disease', *Nature Neuroscience*, 5(7), pp. 627–628. doi: 10.1038/nn863.

Guzman, J. N. *et al.* (2009) 'Robust pacemaking in substantia nigra dopaminergic neurons', *Journal of Neuroscience*, 29(35), pp. 11011–11019. doi: 10.1523/JNEUROSCI.2519-09.2009.

Guzman, J. N. *et al.* (2010) 'Oxidant stress evoked by pacemaking in dopaminergic neurons is attenuated by DJ-1', *Nature*, 468(7324), pp. 696–700. doi: 10.1038/nature09536.

Halliday, G. M. *et al.* (2006) 'Evidence for specific phases in the development of human neuromelanin', *Journal of neural transmission*, 113(6), pp. 721–728. doi: 10.1007/s00702-006-0449-y.

Hermann, A. *et al.* (1997) 'Beta-catenin is a target for the ubiquitin-proteasome pathway', *The EMBO Journal*, 16(13), pp. 3797–3804. doi: 10.20886/jsek.2011.8.2.148-164.

Huang, S. M. A. *et al.* (2009) 'Tankyrase inhibition stabilizes axin and antagonizes Wnt signalling', *Nature*. Nature Publishing Group, 461(7264), pp. 614–620. doi: 10.1038/nature08356.

Huang, T. *et al.* (2011) 'Nuclear factor of activated T cells (NFAT) proteins repress canonical Wnt signaling via its interaction with dishevelled (Dvl) protein and participate in regulating neural progenitor cell proliferation and differentiation', *Journal of Biological Chemistry*, 286(43), pp. 37399–37405. doi: 10.1074/jbc.M111.251165.

Huggins, I. J. *et al.* (2017) 'The WNT target SP5 negatively regulates WNT transcriptional programs in human pluripotent stem cells', *Nature Communications*. Springer US, 8(1034), pp. 1–14. doi: 10.1038/s41467-017-01203-1.

Iguchi, H. *et al.* (2007) 'SOX6 suppresses cyclin D1 promoter activity by interacting with β-catenin and histone deacetylase 1, and its down-regulation induces pancreatic β-cell proliferation', *Journal of Biological Chemistry*, 282(26), pp. 19052–19061. doi: 10.1074/jbc.M700460200.

Janda, C. Y. *et al.* (2012) 'Structural basis of Wnt recognition by Frizzled', *Science*, 337(6090), pp. 59–64. doi: 10.1126/science.1222879.Structural.

Janda, C. Y. *et al.* (2017) 'Surrogate Wnt agonists that phenocopy canonical Wnt and β-catenin signalling', *Nature*. Nature Publishing Group, 545(7653), pp. 234–237. doi: 10.1038/nature22306.

Jeong, Y. and Epstein, D. J. (2003) 'Distinct regulators of Shh transcription in the floor plate and notochord indicate separate origins for these tissues in the mouse node', *Development*, 130(16), pp. 3891–3902. doi: 10.1242/dev.00590.

Jahn, H. M. *et al.* (2018) 'Refined protocols of tamoxifen injection for inducible DNA recombination in mouse astroglia', *Scientific Reports*. Springer US, 8(1), pp. 1–11. doi: 10.1038/s41598-018-24085-9.

Jho, E. *et al.* (2002) 'Wnt / β -Catenin / Tcf signaling induces the transcription of Axin2 , a negative regulator of the signaling pathway', *Molecular and Cellular Biology*, 22(4), pp. 1172–1183. doi: 10.1128/MCB.22.4.1172.

Joksimovic, M. *et al.* (2009) 'Wnt antagonism of Shh facilitates midbrain floor plate neurogenesis', *Nature Neuroscience*, 12(2), pp. 125–131. doi: 10.1038/nn.2243.

Kalia, L. V. and Lang, A. E. (2015) 'Parkinson's disease', *The Lancet*. Elsevier Ltd, 386(9996), pp. 896–912. doi: 10.1016/S0140-6736(14)61393-3.

Kandel, E. *et al.* (2012a) 'Neurotransmitters', in Kandel, E. et al. (eds) *Principles of neural science*. McGrawHill, pp. 289–306.

Kandel, E. *et al.* (2012b) 'The cells of the nervous system', in Kandel, E. et al. (eds) *Principles of neural science*. McGrawHill, pp. 88–96.

Kee, N. *et al.* (2017) 'Single-cell analysis reveals a close relationship between differentiating dopamine and subthalamic nucleus neuronal lineages', *Cell Stem Cell*, 20(1), pp. 29–40. doi: 10.1016/j.stem.2016.10.003.

Kikuchi, T. *et al.* (2017) 'Human iPS cell-derived dopaminergic neurons function in a primate Parkinson's disease model', *Nature*. Nature Publishing Group, 548(7669), pp. 592–596. doi: 10.1038/nature23664.

Kim, C. H. *et al.* (2000) 'Repressor activity of headless/Tcf3 is essential for vertebrate head formation', *Nature*, 407(6806), pp. 913–916. doi: 10.1038/35038097.

Kim, S. *et al.* (2019) 'Transneuronal propagation of pathologic α-synuclein from the gut to the brain models Parkinson's disease', *Neuron*. Elsevier Inc., 103(4), pp. 627–641. doi: 10.1016/j.neuron.2019.05.035.

Kirkeby, A. *et al.* (2012) 'Generation of Regionally Specified Neural Progenitors and Functional Neurons from Human Embryonic Stem Cells under Defined Conditions', *Cell Reports*. The Authors, 1(6), pp. 703–714. doi: 10.1016/j.celrep.2012.04.009.

Kirkeby, A. *et al.* (2017) 'Predictive markers guide differentiation to improve graft outcome in clinical translation of hESC-Based therapy for Parkinson's disease', *Cell Stem Cell*. Elsevier Inc., 20(1), pp. 135–148. doi: 10.1016/j.stem.2016.09.004.

Kitada, T. *et al.* (1998) 'Mutations in the parkin gene cause autosomal recessive juvenile parkinsonism', *Nature*, 392, pp. 605–608.

Kitajima, K. *et al.* (2013) 'Wnt signaling regulates left-right axis formation in the node of mouse embryos', *Developmental Biology*. Elsevier, 380(2), pp. 222–232. doi: 10.1016/j.ydbio.2013.05.011.

Kordower, J. H. *et al.* (2013) 'Disease duration and the integrity of the nigrostriatal system in Parkinson's disease', *Brain*, 136(8), pp. 2419–2431. doi: 10.1093/brain/awt192.

Korkut, C. *et al.* (2009) 'Trans-synaptic transmission of vesicular Wnt signals through Evi/Wntless', *Cell*. Elsevier Ltd, 139(2), pp. 393–404. doi: 10.1016/j.cell.2009.07.051.

Kovacs, G. G. *et al.* (2012) 'An antibody with high reactivity for disease-associated α-synuclein reveals extensive brain pathology', *Acta Neuropathologica*, 124(1), pp. 37–50. doi: 10.1007/s00401-012-0964-x.

Kriks, S. *et al.* (2011) 'Dopamine neurons derived from human ES cells efficiently engraft in animal models of Parkinson's disease', *Nature*. Nature Publishing Group, 480(7378), pp. 547–551. doi: 10.1038/nature10648.

von Krosigk, M. *et al.* (1992) 'Synaptic organization of gabaergic inputs from the striatum and the globus pallidus onto neurons in the substantia nigra and retrorubral field which project to the medullary reticular formation', *Neuroscience*, 50(3), pp. 531–549. doi: 10.1016/0306-4522(92)90445-8.

Krupnik, V. E. *et al.* (1999) 'Functional and structural diversity of the human Dickkopf gene family', *Gene*, 238(2), pp. 301–313. doi: 10.1016/S0378-1119(99)00365-0.

Kühl, M. *et al.* (2000) 'Ca2+/calmodulin-dependent protein kinase II is stimulated by Wnt and Frizzled homologs and promotes ventral cell fates in Xenopus', *Journal of Biological Chemistry*, 275(17), pp. 12701–12711. doi: 10.1074/jbc.275.17.12701.

Lee, J. J. *et al.* (1994) 'Autoproteolysis in hedgehog protein biogenesis', *Science*, 266(5190), pp. 1528–1537. doi: 10.1126/science.7985023.

Lefebvre, V., Li, P. and De Crombrugghe, B. (1998) 'A new long form of Sox5 (L-Sox5), Sox6 and Sox9 are coexpressed in chondrogenesis and cooperatively activate the type II collagen gene', *EMBO Journal*, 17(19), pp. 5718–5733. doi: 10.1093/emboj/17.19.5718.

LeMasson, G., Przedborski, S. and Abbott, L. F. (2014) 'A computational model of motor neuron degeneration', *Neuron*. Elsevier Inc., 83(4), pp. 975–988. doi: 10.1016/j.neuron.2014.07.001.

Licker, V. *et al.* (2014) 'Proteomic analysis of human substantia nigra identifies novel candidates involved in parkinson's disease pathogenesis', *Proteomics*, 14(6), pp. 784–794. doi: 10.1002/pmic.201300342.

Liu, C. *et al.* (1999) 'b-Trcp couples b-catenin phosphorylation-degradation and regulates Xenopus axis formation', *Proceedings of the National Academy of Sciences of the United States of America*, 96, pp. 6273–6278.

Liu, C. *et al.* (2002) 'Control of beta-catenin phosphorylation/degradation by a dual-kinase mechanism', *Cell*, 108, pp. 837–847. doi: 10.1016/S0092-8674(02)00685-2.

La Manno, G. *et al.* (2016) 'Molecular diversity of midbrain development in mouse, human and stem cells', *Cell*, 167, pp. 566–580.

Legue, E. and Joyner, A. L. (2010) 'Genetic fate mapping using site-specific recombinases', *Methods Enzyomology*, 477(5), pp. 153–181. doi: 10.1016/j.physbeh.2017.03.040.

Lefebvre, V., Li, P. and De Crombrugghe, B. (1998) 'A new long form of Sox5 (L-Sox5), Sox6 and Sox9 are coexpressed in chondrogenesis and cooperatively activate the type II collagen gene', *EMBO Journal*, 17(19), pp. 5718–5733. doi: 10.1093/emboj/17.19.5718.

Lu, Y. *et al.* (2017) 'OTX2 expression contributes to proliferation and progression in Myc-amplified medulloblastoma', *American Journal of Cancer Research*, 7(3), pp. 647–656.

Lundgren, D. H. *et al.* (2010) 'Role of spectral counting in quantitative proteomics', *Expert Review of Proteomics*, 7(1), pp. 39–53. doi: 10.1586/epr.09.69.

Mao, B. *et al.* (2001) 'LDL-receptor-related protein 6 is a receptor for Dickkopf proteins', *Nature*, 411, pp. 321–325.

Martí, E. *et al.* (1995) 'Distribution of Sonic hedgehog peptides in the developing chick and mouse embryo', *Development*, 121(8), pp. 2537–2547.

Matsumoto, M. and Hikosaka, O. (2009) 'Two types of dopamine neuron distinctly convey positive and negative motivational signals', *Nature*. Nature Publishing Group, 459(7248), pp. 837–841. doi: 10.1038/nature08028.

Mattson, M. P. *et al.* (1992) 'β-Amyloid peptides destabilize calcium homeostasis and render human cortical neurons vulnerable to excitotoxicity', *Journal of Neuroscience*, 12(2), pp. 376–389. doi: 10.1523/jneurosci.12-02-00376.1992.

Mavromatakis, Y. E. *et al.* (2011) 'Foxa1 and Foxa2 positively and negatively regulate Shh signalling to specify ventral midbrain progenitor identity', *Mechanisms of Development*. Elsevier Ireland Ltd, 128(1–2), pp. 90–103. doi: 10.1016/j.mod.2010.11.002.

McMahon, A. P. and Bradley, A. (1990) 'The Wnt-1 (int-1) proto-oncogene is required for development of a large region of the mouse brain', *Cell*, 62(6), pp. 1073–1085. doi: 10.1016/0092-8674(90)90385-R.

McRitchie, D. A., Hardman, C. D. and Halliday, G. M. (1996) 'Cytoarchitectural distribution of calcium binding proteins in midbrain dopaminergic regions of rats and humans', *Journal of Comparative Neurology*, 364(1), pp. 121–150. doi: 10.1002/(SICI)1096-9861(19960101)364:1<121::AID-CNE11>3.0.CO;2-1.

Memic, F. *et al.* (2018) 'Transcription and Signaling Regulators in Developing Neuronal Subtypes of Mouse and Human Enteric Nervous System', *Gastroenterology*, 154(3), pp. 624–636. doi: 10.1053/j.gastro.2017.10.005.

Mendez, I. *et al.* (2005) 'Cell type analysis of functional fetal dopamine cell suspension transplants in the striatum and substantia nigra of patients with Parkinson's disease', *Brain*, 128(7), pp. 1498–1510. doi: 10.1093/brain/awh510.

Metzakopian, E. *et al.* (2012) 'Genome-wide characterization of Foxa2 targets reveals upregulation of floor plate genes and repression of ventrolateral genes in midbrain dopaminergic progenitors', *Development (Cambridge)*, 139(14), pp. 2625–2634. doi: 10.1242/dev.081034.

Mikels, A. J. and Nusse, R. (2006) 'Purified Wnt5a protein activates or inhibits β-catenin-TCF signaling depending on receptor context', *PLoS Biology*, 4(4), pp. 570–582. doi: 10.1371/journal.pbio.0040115.

Millet, S. *et al.* (1999) 'A role for Gbx2 in repression of Otx2 and positioning the mid/hindbrain organizer', *Nature*, 401, pp. 161–164.

Morales, M. and Margolis, E. B. (2017) 'Ventral tegmental area: cellular heterogeneity, connectivity and behaviour', *Nature Reviews Neuroscience*, 18(2), pp. 73–85. doi: 10.1038/nrn.2016.165.

Nair-Roberts, R. G. *et al.* (2008) 'Stereological estimates of dopaminergic, GABAergic and glutamatergic neurons in the ventral tegmental area, substantia nigra and retrorubral field in the rat', *Neuroscience*. IBRO, 152(4), pp. 1024–1031. doi: 10.1016/j.neuroscience.2008.01.046.

Neal, A. P. and Guilarte, T. R. (2013) 'Mechanisms of lead and manganese neurotoxicity', *Toxicology research*, 2(1), pp. 99–114. doi: 10.1038/jid.2014.371.

Nolbrant, S. *et al.* (2017) 'Generation of high-purity human ventral midbrain dopaminergic progenitors for in vitro maturation and intracerebral transplantation', *Nature Protocols*. Nature Publishing Group, 12(9), pp. 1962–1979. doi: 10.1038/nprot.2017.078.

Nordström, U., Jessell, T. M. and Edlund, T. (2002) 'Progressive induction of caudal neural character by graded Wnt signaling', *Nature Neuroscience*, 5(6), pp. 525–532. doi: 10.1038/nn854.

Nouri, N. *et al.* (2015) 'Excessive Wnt/beta-catenin signaling promotes midbrain floor plate neurogenesis, but results in vacillating dopamine progenitors', *Molecular and Cellular Neuroscience*. Elsevier Inc., 68, pp. 131–142. doi: 10.1016/j.mcn.2015.07.002.

Nusse, R. (2001) 'An ancient cluster of Wnt paralogues', *Trends in genetics*, 17(8), p. 443. doi: 10.1016/S0168-9525(01)02434-9.

Nusslein-Volhard, C. and Wieschaus, E. (1980) 'Mutations affecting segment number and polarity in Drosophila', *Nature*, 287, pp. 795–801.

Ono, Y. *et al.* (2007) 'Differences in neurogenic potential in floor plate cells along an anteroposterior location: midbrain dopaminergic neurons originate from mesencephalic floor plate cells', *Development*, 134(17), pp. 3213–3225. doi: 10.1242/dev.02879.

Pacelli, C. *et al.* (2015) 'Elevated mitochondrial bioenergetics and axonal arborization size are key contributors to the vulnerability of dopamine neurons', *Current Biology*, 25(18), pp. 2349–2360. doi: 10.1016/j.cub.2015.07.050.

Pan, Y. *et al.* (2006) 'Sonic hedgehog Signaling Regulates Gli2 Transcriptional Activity by Suppressing Its Processing and Degradation', *Molecular and Cellular Biology*, 26(9), pp. 3365–3377. doi: 10.1128/mcb.26.9.3365-3377.2006.

Panman, L. *et al.* (2014) 'Sox6 and Otx2 control the specification of substantia nigra and ventral tegmental area dopamine neurons', *Cell Reports*. The Authors, 8(4), pp. 1018–1025. doi: 10.1016/j.celrep.2014.07.016.

Patten, I. *et al.* (2003) 'Distinct modes of floor plate induction in the chick embryo', *Development*, 130(20), pp. 4809–4821. doi: 10.1242/dev.00694.

Pepinsky, R. B. *et al.* (1998) 'Identification of a palmitic acid-modified form of human Sonic hedgehog', *Journal of Biological Chemistry*, 273(22), pp. 14037–14045. doi: 10.1074/jbc.273.22.14037.

Peters, C. *et al.* (2004) 'The cholesterol membrane anchor of the Hedgehog protein confers stable membrane association to lipid-modified proteins', *Proceedings of the National Academy of Sciences of the United States of America*, 101(23), pp. 8531–8536. doi: 10.1073/pnas.0308449101.

Placzek, M. and Briscoe, J. (2005) 'The floor plate: Multiple cells, multiple signals', *Nature Reviews Neuroscience*, 6(3), pp. 230–240. doi: 10.1038/nrn1628.

Porter, J. A. *et al.* (1995) 'The product of hedgehog autoproteolytic cleavage active in local and long-range signalling', *Nature*, 374, pp. 363–366. doi: 10.1038/nature00943.

Porter, J. A. *et al.* (1996) 'Hedgehog patterning activity: Role of a lipophilic modification mediated by the carboxy-terminal autoprocessing domain', *Cell*, 86(1), pp. 21–34. doi: 10.1016/S0092-8674(00)80074-4.

Porter, J. A., Young, K. E. and Beachy, P. A. (1996) 'Cholesterol Modification of Hedgehog Signaling Proteins in Animal Development', *Science*, 274(5285), pp. 255–259.

Poulin, J. F. *et al.* (2014) 'Defining midbrain dopaminergic neuron diversity by single-cell gene expression profiling', *Cell Reports*. The Authors, 9(3), pp. 930–943. doi: 10.1016/j.celrep.2014.10.008.

Poulin, J. F. *et al.* (2018) 'Mapping projections of molecularly defined dopamine neuron subtypes using intersectional genetic approaches', *Nature Neuroscience*. Springer US, 21(9), pp. 1260–1271. doi: 10.1038/s41593-018-0203-4.

Pourhaghighi, R. *et al.* (2020) 'BraInMap elucidates the macromolecular connectivity landscape of mammalian brain', *Cell Systems*. Elsevier Inc., 10(4), pp. 333-350.e14. doi: 10.1016/j.cels.2020.03.003.

Prakash, N. *et al.* (2006) 'A Wnt1-regulated genetic network controls the identity and fate of midbrain-dopaminergic progenitors in vivo', *Development*, 133(1), pp. 89–98. doi: 10.1242/dev.02181.

Przedborski, S. and Vila, M. (2001) 'MPTP: A review of its mechanisms of neurotoxicity', *Clinical Neuroscience Research*, 1(6), pp. 407–418. doi: 10.1016/S1566-2772(01)00019-6.

Reyes, S. *et al.* (2012) 'GIRK2 expression in dopamine neurons of the substantia nigra and ventral tegmental area', *Journal of Comparative Neurology*, 520(12), pp. 2591–2607. doi: 10.1002/cne.23051.

Richards, C. D., Shiroyama, T. and Kitai, S. T. (1997) 'Electrophysiological and immunocytochemical characterization of GABA and dopamine neurons in the substantia nigra of the rat', *Neuroscience*, 80(2), pp. 545–557. doi: 10.1016/S0306-4522(97)00093-6.

Riessland, M. *et al.* (2019) 'Loss of SATB1 induces p21-dependent cellular senescence in post-mitotic dopaminergic neurons', *Cell Stem Cell*. Elsevier Inc., 25(4), pp. 514–530. doi: 10.1016/j.stem.2019.08.013.

Rios-Esteves, J. and Resh, M. D. (2013) 'Stearoyl CoA Desaturase Is Required to Produce Active, Lipid-Modified Wnt Proteins', *Cell Reports*. The Authors, 4(6), pp. 1072–1081. doi: 10.1016/j.celrep.2013.08.027.

Root, D. H. *et al.* (2014) 'Single rodent mesohabenular axons release glutamate and GABA', *Nature Neuroscience*, 17(11), pp. 1543–1551. doi: 10.1038/nn.3823.

Root, D. H. *et al.* (2016) 'Glutamate neurons are intermixed with midbrain dopamine neurons in nonhuman primates and humans', *Scientific reports*. Nature Publishing Group, 6(April), p. 30615. doi: 10.1038/srep30615.

Rosso, S. B. *et al.* (2005) 'Wnt signaling through Dishevelled, Rac and JNK regulates dendritic development', *Nature Neuroscience*, 8(1), pp. 34–42. doi: 10.1038/nn1374.

Di Salvio, M. *et al.* (2010) 'Otx2 controls neuron subtype identity in ventral tegmental area and antagonizes vulnerability to MPTP', *Nature Neuroscience*. Nature Publishing Group, 13(12), pp. 1481–1489. doi: 10.1038/nn.2661.

Sampson, T. R. *et al.* (2016) 'Gut microbiota regulate motor deficits and neuroinflammation in a model of Parkinson's disease', *Cell*. Elsevier, 167(6), pp. 1469–1480. doi: 10.1016/j.cell.2016.11.018.

Saneyoshi, T. *et al.* (2002) 'The wnt/calcium pathway activates NF-AT and promotes ventral cell fate in Xenopus embryos', *Nature*, 417(6886), pp. 295–299. doi: 10.1038/417295a.

Schepers, G. E., Teasdale, R. D. and Koopman, P. (2002) 'Twenty pairs of Sox: Extent, homology, and nomenclature of the mouse and human Sox transcription factor gene families', *Developmental Cell*, 3(2), pp. 167–170. doi: 10.1016/S1534-5807(02)00223-X.

Scott, O. *et al.* (2014) 'Global developmental delay, progressive relapsing-remitting parkinsonism, and spinal syrinx in a child with SOX6 mutation', *Journal of Child Neurology*, 29(11), pp. 1–4. doi: 10.1177/0883073813514134.

Seifert, J. R. K. and Mlodzik, M. (2007) 'Frizzled/PCP signalling: a conserved mechanism regulating cell polarity and directed motility', *Nature Reviews Genetics*, 8(2), pp. 126–138. doi: 10.1038/nrg2042.

Sheldahl, L. C. *et al.* (1999) 'Protein kinase C is differentially stimulated by Wnt and Frizzled homologs in a G-protein-dependent manner', *Current Biology*, 9(13), pp. 695–698. doi: 10.1016/S0960-9822(99)80310-8.

Shi, Y., Kirwan, P. and Livesey, F. J. (2012) 'Directed differentiation of human pluripotent stem cells to cerebral cortex neurons and neural networks', *Nature Protocols*, 7(10), pp. 1836–1846. doi: 10.1038/nprot.2012.116.

Simon, H. H. *et al.* (2001) 'Fate of midbrain dopaminergic neurons controlled by the engrailed genes', *Journal of Neuroscience*, 21(9), pp. 3126–3134. doi: 10.1523/jneurosci.21-09-03126.2001.

Singleton, A. B. *et al.* (2003) 'α-Synuclein locus triplication causes Parkinson's Disease', *Science*, 302(5646), pp. 841–841. doi: 10.1126/science.1090278.

Slusarski, D. C. *et al.* (1997) 'Modulation of embryonic intracellular Ca2+ signaling by Wnt-5A', *Developmental Biology*, 182(1), pp. 114–120. doi: 10.1006/dbio.1996.8463.

Slusarski, D. C., Corces, V. G. and Moon, R. T. (1997) 'Interaction of Wnt and a Frizzled homologue triggers G-protein-linked phosphatidylinositol signalling', *Nature*, 390(6658), pp. 410–413. doi: 10.1038/37138.

Smidt, M. P. *et al.* (2000) 'A second independent pathway for development of mesencephalic dopaminergic neurons requires Lmx1b', *Nature Neuroscience*, 3(4), pp. 337–341. doi: 10.1038/73902.

Smidt, M. P. *et al.* (2004) 'Early developmental failure of substantia nigra dopamine neurons in mice lacking the homeodomain gene Pitx3', *Development*, 131(5), pp. 1145–1155. doi: 10.1242/dev.01022.

Smits, S. M. *et al.* (2003) 'Involvement of Nurr1 in specifying the neurotransmitter identity of ventral midbrain dopaminergic neurons', *European Journal of Neuroscience*, 18(7), pp. 1731–1738. doi: 10.1046/j.1460-9568.2003.02885.x.

Sommer, A. *et al.* (2018) 'Th17 lymphocytes induce neuronal cell death in a human iPSC-based model of Parkinson's disease', *Cell Stem Cell*, 23(1), pp. 123–131. doi: 10.1016/j.stem.2018.06.015.

Soriano, P. (1999) 'Generalized lacZ expression with the ROSA26 Cre reporter strain', *Nature Genetics*, 21(1), pp. 70–71. doi: 10.1038/5007.

Stamatakis, A. M. *et al.* (2013) 'A unique population of ventral tegmental area neurons inhibits the lateral habenula to promote reward', *Neuron*. Elsevier Inc., 80(4), pp. 1039–1053. doi: 10.1016/j.neuron.2013.08.023.

Stamos, J. L. *et al.* (2014) 'Structural basis of GSK-3 inhibition by N-terminal phosphorylation and by the Wnt receptor LRP6', *eLife*, (3), pp. 1–22. doi: 10.7554/eLife.01998.

Stark, K. *et al.* (1994) 'Epithelial transformation of metanephric mesenchyme in the developing kidney regulated by Wnt-4', *Nature*, 372(6507), pp. 679–683. doi: 10.1038/372679a0.

Stephano, F. *et al.* (2018) 'Impaired Wnt signaling in dopamine containing neurons is associated with pathogenesis in a rotenone triggered Drosophila Parkinson's disease model', *Scientific Reports*. Springer US, 8(1), pp. 1–11. doi: 10.1038/s41598-018-20836-w.

Stolt, C. C. *et al.* (2006) 'SoxD Proteins Influence Multiple Stages of Oligodendrocyte Development and Modulate SoxE Protein Function', *Developmental Cell*, 11(5), pp. 697–709. doi: 10.1016/j.devcel.2006.08.011.

Stott, S. R. W. and Ang, S.-L. (2013) 'The generation of midbrain dopaminergic neurons', in Rubenstein, J. L. R. and Rakic, P. (eds) *Patterning and cell type specification in the developing CNS and PNS: comprehensive developmental neruoscience*, pp. 435–453. doi: 10.1016/B978-0-12-397265-1.00022-8.

Streit, A. *et al.* (2000) 'Initiation of neural induction by FGF signalling before gastrulation', *Nature*, 406(6791), pp. 74–78. doi: 10.1038/35017617.

Stuber, G. D. *et al.* (2010) 'Dopaminergic terminals in the nucleus accumbens but not the dorsal striatum corelease glutamate', *Journal of Neuroscience*, 30(24), pp. 8229–8233. doi: 10.1523/JNEUROSCI.1754-10.2010.

Sunmonu, N. A. *et al.* (2011) 'Gbx2 and Fgf8 are sequentially required for formation of the midbrain-hindbrain compartment boundary', *Development*, 138(4), pp. 725–734. doi: 10.1242/dev.055665.

Surmeier, D. J., Obeso, J. A. and Halliday, G. M. (2017) 'Selective neuronal vulnerability in Parkinson disease', *Nature Reviews Neuroscience*, 18(2), pp. 101–113. doi: 10.1038/nrn.2016.178.

Szczepny, A., Hime, G. R. and Loveland, K. L. (2006) 'Expression of hedgehog signalling components in adult mouse testis', *Developmental Dynamics*, 235(11), pp. 3063–3070. doi: 10.1002/dvdy.20931.

Takada, R. *et al.* (2006) 'Monounsaturated Fatty Acid Modification of Wnt Protein: Its Role in Wnt Secretion', *Developmental Cell*, 11(6), pp. 791–801. doi: 10.1016/j.devcel.2006.10.003.

Takahashi, K. *et al.* (2007) 'Induction of Pluripotent Stem Cells from Adult Human Fibroblasts by Defined Factors', *Cell*, 131(5), pp. 861–872. doi: 10.1016/j.cell.2007.11.019.

Takahashi, K. and Yamanaka, S. (2006) 'Induction of Pluripotent Stem Cells from Mouse Embryonic and Adult Fibroblast Cultures by Defined Factors', *Cell*, 126(4), pp. 663–676. doi: 10.1016/j.cell.2006.07.024.

Tamai, K. *et al.* (2004) 'A mechanism for Wnt coreceptor activation', *Molecular Cell*, 13(1), pp. 149–156. doi: 10.1016/S1097-2765(03)00484-2.

Tanaka, K., Kitagawa, Y. and Kadowaki, T. (2002) 'Drosophila segment polarity gene product porcupine stimulates the posttranslational N-glycosylation of wingless in the endoplasmic reticulum', *Journal of Biological Chemistry*, 277(15), pp. 12816–12823. doi: 10.1074/jbc.M200187200.

Tang, M. *et al.* (2010) 'Interactions of Wnt/β-catenin signaling and sonic hedgehog regulate the neurogenesis of ventral midbrain dopamine neurons', *Journal of Neuroscience*, 30(27), pp. 9280–9291. doi: 10.1523/JNEUROSCI.0860-10.2010.

Tasic, B. *et al.* (2016) 'Adult mouse cortical cell taxonomy revealed by single cell transcriptomics', *Nature Neuroscience*, 19(2), pp. 335–346. doi: 10.1038/nn.4216.

Tauriello, D. V. F. *et al.* (2012) 'Wnt/β-catenin signaling requires interaction of the Dishevelled DEP domain and C terminus with a discontinuous motif in Frizzled', *Proceedings of the National Academy of Sciences of the United States of America*, 109(14), pp. 812–820. doi: 10.1073/pnas.1114802109.

Tetsu, O. and McCormick, F. (1999) 'β-catenin regulates expression of cyclin D1 in colon carcinoma cells', *Nature*, 398(6726), pp. 422–426. doi: 10.1038/18884.

Thompson, L. *et al.* (2005) 'Identification of dopaminergic neurons of nigral and ventral tegmental area subtypes in grafts of fetal ventral mesencephalon based on cell morphology, protein expression, and efferent projections', *Journal of Neuroscience*, 25(27), pp. 6467–6477. doi: 10.1523/JNEUROSCI.1676-05.2005.

Thompson, L. H., Kirik, D. and Björklund, A. (2008) 'Non-dopaminergic neurons in ventral mesencephalic transplants make widespread axonal connections in the host brain', *Experimental Neurology*, 213(1), pp. 220–228. doi: 10.1016/j.expneurol.2008.06.005.

Thomson, J. A. *et al.* (1998) 'Embryonic stem cell lines derived from human blastocysts', *Science*, 282(5391), pp. 1145–1147. doi: 10.1126/science.282.5391.1145.

Tiklová, K. *et al.* (2019) 'Single-cell RNA sequencing reveals midbrain dopamine neuron diversity emerging during mouse brain development', *Nature Communications*. Springer US, 10(1), pp. 1–12. doi: 10.1038/s41467-019-08453-1.

Tsumori, T. *et al.* (2010) 'Central amygdaloid axon terminals are in contact with retrorubral field neurons that project to the parvicellular reticular formation of the medulla oblongata in the rat', *Brain Research*. Elsevier B.V., 1306, pp. 18–28. doi: 10.1016/j.brainres.2009.09.118.

Tukachinsky, H. *et al.* (2012) 'Dispatched and Scube Mediate the Efficient Secretion of the Cholesterol-Modified Hedgehog Ligand', *Cell Reports*, 2(2), pp. 308–320. doi: 10.1016/j.celrep.2012.07.010.

Tukachinsky, H., Lopez, L. V. and Salic, A. (2010) 'A mechanism for vertebrate Hedgehog signaling: Recruitment to cilia and dissociation of SuFu-Gli protein complexes', *Journal of Cell Biology*, 191(2), pp. 415–428. doi: 10.1083/jcb.201004108.

Usoskin, D. *et al.* (2015) 'Unbiased classification of sensory neuron types by large-scale single-cell RNA sequencing', *Nature Neuroscience*. Nature Publishing Group, 18(1), pp. 145–153. doi: 10.1038/nn.3881.

Vaquerizas, J. M. *et al.* (2009) 'A census of human transcription factors: Function, expression and evolution', *Nature Reviews Genetics*, 10(4), pp. 252–263. doi: 10.1038/nrg2538.

Vaswani, A. R. *et al.* (2019) 'Correct setup of the substantia nigra requires Reelin-mediated fast, laterally-directed migration of dopaminergic neurons', *eLife*, 8, pp. 1–34. doi: 10.7554/eLife.41623.

Vinson, C. R. and Adler, P. N. (1987) 'Directional non-cell autonomy and the transmission of polarity information by the frizzled gene of Drosophila', *Nature*, 329, pp. 549–551.

Vortkamp, A. *et al.* (1996) 'Regulation of rate of cartilage differentiation by Indian Hedgehog and PTH-related protein', *Science*, 273(5275), pp. 613–622. doi: 10.1126/science.273.5275.613.

Wang, B., Fallon, J. F. and Beachy, P. A. (2000) 'Hedgehog-Regulated Processing of Gli3 Produces an Anterior / Posterior Repressor Gradient in the Developing Vertebrate Limb University of Wisconsin at Madison', *Cell*, 100, pp. 423–434.

Wang, Y. and Mattson, M. P. (2014) 'L-type Ca2+ currents at CA1 synapses, but not CA3 or dentate granule neuron synapses, are increased in 3xTgAD mice in an age-dependent manner', *Neurobiology of Aging*, 35(1), pp. 88–95. doi: 10.1038/jid.2014.371.

Wassarman, K. M. *et al.* (1997) 'Specification of the anterior hindbrain and establishment of a normal mid/hindbrain organizer is dependent on Gbx2 gene function', *Development*, 124(15), pp. 2923–2934.

Willert, K. *et al.* (2003) 'Wnt proteins are lipid-modified and can act as stem cell growth factors', *Nature*, 423(6938), pp. 448–452. doi: 10.1038/nature01611.

Wilson, P. A. and Hemmati-Brivanlou, A. (1995) 'Induction of epidermis and inhibition of neural fate by Bmp-4', *Nature*, 376(6538), pp. 331–333. doi: 10.1038/376331a0.

Wu, W. *et al.* (2000) 'Mutual antagonism between dickkopf1 and dickkopf2 regulates Wnt/β-catenin signalling', *Current Biology*, 10(24), pp. 1611–1614. doi: 10.1016/S0960-9822(00)00868-X.

Xie, Z. *et al.* (2010) 'Zbtb20 is essential for the specification of CA1 field identity in the developing hippocampus', *Proceedings of the National Academy of Sciences of the United States of America*, 107(14), pp. 6510–6515. doi: 10.1073/pnas.0912315107.

Yamaguchi, T. *et al.* (2011) 'Mesocorticolimbic glutamatergic pathway', *Journal of Neuroscience*, 31(23), pp. 8476–8490. doi: 10.1523/JNEUROSCI.1598-11.2011.

Yamaguchi, T., Wang, H. L. and Morales, M. (2013) 'Glutamate neurons in the substantia nigra compacta and retrorubral field', *European Journal of Neuroscience*, 38(11), pp. 3602–3610. doi: 10.1111/ejn.12359.

Yan, D. *et al.* (2001) 'Elevated expression of axin2 and hnkd mRNA provides evidence that Wnt/β-catenin signaling is activated in human colon tumors', *Proceedings of the National Academy of Sciences of the United States of America*, 98(26), pp. 14973–14978. doi: 10.1073/pnas.261574498.

Ye, W. *et al.* (1998) 'FGF and Shh signals control dopaminergic and serotonergic cell fate in the anterior neural plate', *Cell*, 93(5), pp. 755–766. doi: 10.1016/S0092-8674(00)81437-3.

Yelnik, J. *et al.* (1987) 'Golgi study of the primate substantia nigra. Quantitative morphology and typology of nigral neurons', *The journal of comparative neurology*, 265, pp. 455–472.

Zeisel, A. *et al.* (2018) 'Molecular architecture of the mouse nervous system', *Cell*, 174(4), pp. 999-1014.e22. doi: 10.1016/j.cell.2018.06.021.

Zimprich, A. *et al.* (2004) 'Mutations in LRRK2 cause autosomal-dominant Parkinsonism with pleomorphic pathology', *Neuron*, 44, pp. 601–607.

Zinzen, R. P. *et al.* (2009) 'Combinatorial binding predicts spatio-temporal cis-regulatory activity', *Nature*. Nature Publishing Group, 462(7269), pp. 65–70. doi: 10.1038/nature08531.